University of Strathclyde

Department of Electronic and Electrical Engineering

A NOVEL CONFIGURATION OF ALL-OPTICAL DIFFERENTIAL PROTECTION SCHEME

MUHAMMAD NASIR

A thesis presented in fulfilment of the
requirements for the degree of

Doctor of Philosophy

2020

Signed : *Muhnasir*

Date   : 17 / 04 / 2020

In the name of Allah the Merciful

All the praise is due to Allah

This thesis is dedicated to my beloved parents and my family

Acknowledgements

Abstract

Advantages of the optical current sensing techniques have stimulated the development of the optical differential protection schemes for busbar protection. However, these optical differential schemes adopt mixed optical-numerical processes that use a platform based on modern numerical/microprocessor protection schemes. Therefore, opportunities to improve these mixed optical-numerical protection schemes still exist. This thesis proposes a novel configuration to perform an optical differential protection scheme that is implemented using a designed arrangement of basic optical components. In this design, the inherent operational functionality of the current differential connection is realised in the optical domain with a designed configuration of optical components. Due to the purely optical nature of the scheme, the need for complex numerical processing, which consists of direct digitisation of the output from individual sensors followed by digital signal processing within the relay, is eliminated. Therefore, the designed scheme could minimize the differential protection complexity while retaining the quality of the differential scheme. Moreover, it has also the potential for a significant reduction in the protection operating time. To verify and validate the optical configuration, one model is proposed, but simulated with different components and validated by simulation and experiment. The simulation results show that, firstly, the proposed scheme is verified, and both of the model and configurations are correct. Secondly, the proposed optical system which uses the polarization-maintaining optical fibre as fibre links has successfully met the protection performance objectives with respect to sensitivity (dependability), security, and speed of operation. Furthermore, a prototype of the proposed scheme has been constructed, and the obtained empirical data further validated the outcome from the simulation models. The validation by the empirical data provided, first, the proposed arrangement of the optical components were correctly configured, and the models of the optical components were correctly represented. Second, the experimental data have been successfully predicted by the simulation models. Finally, the proposed scheme prototype achieved good discrimination necessary for protection purposes.

List of Contents

List of Figures

List of Tables

Chapter 1. Introduction

1.1. Background

Power system protection is an essential component in electric power system operation in order to ensure safe operation of a power system. The protection system objective is to detect an abnormal condition and takes appropriate action to ensure that the faulty components are isolated from the rest of the system immediately, and thus, the impact of the fault is minimised [1],[2]. The protection objective can be met by fulfilling the protection requirements: sensitivity, selectivity, speed and reliability.

The protection system is designed with several capabilities: detection and measurement, comparison, evaluation and decision making. Thus, the protection systems elements consist of four main types of equipment (primary system measurement, protection relay, circuit breaker and DC supply), and also some additional components [3],[4].

A busbar is one of the most critical power system elements since it has role as the connecting point of a variety of elements such as generator, transformer, transmission line, and loads [5]. Faults at a busbar will endanger the continuity of power supply, may damage the equipment, and jeopardise system stability. Therefore, the busbar has to be equipped with fast and reliable protection scheme. A differential scheme is the most common form of protection applied to a busbar in practice [6],[7],[8].

A current transformers (CT) is a component of power system protection used to supply the protection system with replicas of power system currents scaled-down to a standard level for protection and measurement devices. Conventional, iron core CTs have been in power systems service for more than a century [9],[10],[11]. Since conventional CTs are based on electromagnetic coupling with iron core design, they suffer from measurement accuracy issues resulting from the existence of the magnetizing current [12],[13]. This can be worsened by saturation which can cause significant current measurement errors [14],[15], potentially leading to erroneous relay operation [16],[17] and false tripping of the circuit breakers (CB) [18],[19],[20]. The effects are

1

particularly significant in busbar protection applications [21] as many CTs are often connected in parallel and thus increasing the influence of the magnetising current.

In existing practice the saturation effects of the conventional current transformers can be minimized in several ways, such as: keeping the secondary burden as low as possible, using a higher specification CTs such as CT with a better quality of the iron core in order to cope with the anticipated high fault currents [22], and applying CTs with a higher accuracy class [23],[24],[25]. In most situations these solutions provide an acceptable CT performance for protection purposes. However, they still may present certain economic difficulties due to the use a better quality of the iron core and a higher accuracy class of CT and technical issue because it is not completely eliminate the saturation problem. Moreover, dedicated algorithms have been introduced in numerical protection relays to detect CT saturation in order to mitigate their adverse effects on protection operation. Such methods include magnetization curve method [26], utilisation of neural networks [27], adaptive protection [28], mathematical morphology [29], and many others.

The best alternative to avoid saturation problems is utilization of a current measurement approach without ferrous core such as linear coupler [30], Rogowski coil [31],[32],[33] or Hall Effect transducer [34]. However, these current transducers have a disadvantage that only small amount of current can be drawn from the output. The most recent current measurement techniques use optical current sensing methods. Based on the sensing mechanism employed and materials used, the optical current sensors can be categorized in four groups: hybrid sensors, magnetic force sensors, bulk optic sensors, and all-fibre sensors [35]. Moreover, among these sensors, the Fibre Bragg grating (FBG) [36],[37] or Faraday effect [38] ,[39],[40] principles are applied. The Faraday effect is a magneto-optic phenomenon due to interaction between optical material and electromagnetic wave polarization that is observed in transmission. In the Faraday effect, a rotation of the polarisation plane is in proportion to the magnetic field *B*. Therefore, an optical sensor that measures the magnetic field *B* can be developed by utilizing this Faraday effect. However, some factors should be considered because it can distort the Faraday rotation along the light propagation such as birefringence effect in fibre optic, and temperature.

The optical sensing methods are still in development, however, they are very promising for high voltage applications, protection systems in particular, due to absence of saturation effects, inherent electrical isolation, immunity against electromagnetic interferences, low power consumption, small size, and light weight.

1.2. Problem Statement

The significant and inherent advantages of the optical current sensing techniques have stimulated the development of the optical differential protection schemes for busbar protection in this thesis. A number of the optical sensing technology based differential protection schemes have been researched and developed which implement the fibre Bragg grating (FBG) [41],[42],[43],[44]. Other techniques in the optical differential protection schemes exploit a range of optical sensors based on the magneto-optic Faraday effect [45],[46],[47]. These existing optical differential schemes adopt a modern numerical/microprocessor protection platform. Since the electric currents are measured by optical current transducers, digitized, and analysed using dedicated numerical algorithms, such schemes could be named as "mixed optical-numerical protection". They involve two-step processes. The first step, is the conversion of the measured currents from analogue to optical modulation that is performed by the optical current transducers/sensors. The second step is a substitution process into protection scheme algorithms. These processes translate the optical signals into digital values which are then used by an algorithm within a numerical relay to implement a given protection relaying scheme.

This thesis proposes a novel method of performing an optical differential protection scheme that is implemented using a designed arrangement of basic optical devices without the need for complex numerical processing. Therefore, it could be termed as "**all-optical differential protection**". The designed arrangement means that the protection scheme utilises a designed configuration of basic optical components such as linear polarizers, polarized light source including Faraday rotators as optical current sensors, and optical photo receiver. Using this designed arrangement, the inherent operational functionality of the current differential connection is realised in the optical domain. Due to maintain the optical domain process in the protection scheme, the

arrangement is key aspects that must be done carefully by a simple series connection of basic optical components that consist of a matching pair of polarisers and combined with optical current sensors. Therefore, it becomes a main feature that distinguishes it from the mixed optical-numerical protection scheme.

As a consequence of the design, it is intended to minimize the differential protection complexity while retaining the quality of the differential scheme. Due to the purely optical nature of the scheme, the need for direct digitisation of the output from individual sensors followed by digital signal processing within the relay is eliminated. For this reason, the proposed scheme has the potential for significant reduction of the protection operating time.

The problem statements of this thesis are formulated as follows:

a. How to develop a new configuration of optical busbar differential protection scheme which implements optical current measurement techniques and basic optical components that will operate according to the principles of a circulating current differential protection?
b. How to perform protection performance assessment in efficient and systematic manner?
c. How to make a designed prototype and build a prototype of the proposed optical busbar differential protection scheme in order to carry out the laboratory experimental validation?

1.3. Thesis Objectives

The principal objective of this research is to design, simulate, construct and experimentally validate a novel all-optical busbar differential protection scheme. Therefore, detailed objectives of the thesis are:

1. Review and theoretical evaluation of the conventional circulating current differential protection and the existing optical differential protection scheme including the existing conventional and optical methods of current sensing.

This objective became a starting point and a framework for a new design development in optical differential busbar protection scheme.

2. Design development of a new configuration of optical devices which will operate according to the principles of a differential protection scheme. This second objective is intended to address a creating of a new optical configuration that performs differential protection function by utilising the measured current in the optical domain. The new configuration is adopted from the conventional differential protection which performs its function using the current in analogue domain.

3. Development of the modelling approach to accurately represent the characteristics of basic optical components that are utilised in the all-optical busbar differential protection scheme for computer simulations. This will enable software based systematic verification and initial validation of the protection scheme performance.

4. Detailed design, component selection and fabrication of the fully functioning laboratory prototype of the proposed all-optical busbar differential protection scheme.

5. Laboratory test based experimental validation of the developed scheme prototype.

1.4. Thesis contribution to knowledge

This thesis makes a number of contributions to knowledge both on the theoretical and practical levels. The thesis contributions can be identified into four aspects which are:

1. Propose a new configuration
2. Model representation of the new configuration
3. Simulate the new configuration in the computer program
4. Laboratory experiment including laboratory work to create a prototype detailed design and to make the prototype for testing and validation.

Those contributions can be summarised as follows:

(a) A new configuration of optical differential protection scheme has been created. This configuration utilises all-optical devices i.e. polarisers, fibre optic cable, and specially designed optical current sensors. This novel configuration is termed in this thesis as "all-optical differential protection scheme".

(b) Development of the modelling approach for representing optical components such as polariser, optical current sensor, fibre optic cable, and polarised light, based on Jones formalization.

(c) Development of the simulation methodology for the purposes of design and performance assessment of the optical protection schemes. These detailed simulations are utilised to inform the development of the physical prototype and also to quantify the system characteristics such as performance.

(d) Laboratory work comprises several steps such as the detailed design of the optical differential protection component, building the optical protection prototype and testing the prototype to collect experimental data.

The following publications directly resulted from the research presented in this thesis:

- M. Nasir, A. Dysko, P. Niewczas, G. Fusiek, "All-optical busbar differential protection scheme for electric power systeme", 13rd IET International Conference on Developments in Power Systems Protection (DPSP), Edinburgh, 2016.

- M. Nasir, A. Dysko, P. Niewczas, C. Booth, P. Orr, G. Fusiek, "Power System Differential Protection Based on Optical Current Measurement", 48th International Universities' Power Engineering Conference, Dublin, 2013.

1.5. Thesis Outline

This thesis is divided into seven major chapters as follows:

Chapter 2 introduces the fundamentals of power system protection. It includes power system protection objectives, design criteria, key characteristics and components. The main protection types are described with the emphasis on differential protection principles, as well as the requirements related to busbar differential protection. It also highlights the limitations of the conventional current transformer, trends of protection

relays and modern digital substations. Some alternatives to avoid the conventional CT limitations by utilization of a totally different CT construction without ferrous core are described. Optical current transducers are identified as one of the possible candidates to be applied in the optical differential protection scheme.

Chapter 3 describes several optical principles such as electromagnetic wave equation, polarized light waves, Fresnel's equation, light propagation in optical crystal, Jones principle, and Jones Cartesian matrices transformation. Several well-known models of the polarized light and optical devices are also explained. It also reveals optical methods for measuring voltage and current in power system including properties of some crystals for sensor head.

Chapter 4 presents a new concept of all-optical differential protection scheme incorporating the Faraday magneto optical current sensor. This concept involves the generic steps of conducting design and problem formulation process, as well as the optical current sensor design. The proposed differential scheme, which consists of optical devices to perform a function analogous to circulating current differential protection, is explained in terms of fundamental design requirements and development process of optical differential protection scheme. The configuration of all-optical busbar differential protection scheme is then modelled using simple Jones matrix representation in which optical transmission links between each device are assumed as an ideal transmission medium. The chapter also includes a theoretical proof of the operating principle of the proposed novel all-optical differential protection scheme.

Chapter 5 explains the modelling and computer based simulation of the proposed novel all-optical differential protection scheme. It discusses optical devices model using Jones complex matrix for representing polarisers, Faraday optic current sensors, and fibre optic links. Power system faults and optical systems simulation scenarios are explained. Five alternative model configurations of the proposed all-optical differential protection are created and tested in simulation, i.e. from the ideal model to the complex (i.e. most realistic) model. The simulation based exercise quantifies the capability of the scheme to meet the main protection system objectives i.e. sensitivity/dependability, stability/security and speed.

Chapter 6 presents the prototype developing process and laboratory experiment. It comprises the scheme prototype development process, as well as selection of the required components for the proposed differential protection. Setting up the experiment's equipment and creating the testing procedures are also revealed. The results are aimed to confirm the validity of the simulation model, i.e. the correct representation and arrangement of the optical devices.

Finally, **chapter 7** concludes the thesis, summarises the key outcomes and highlights potential future avenues of this research.

1.6. References for chapter 1

[1]   Alstom, *Network Protection & Automation Guide*, 2011 ed.: Alstom Grid, 2011.

[2]   C. R. Mason. (1956). *The Art & Science of Protective Relaying*.

[3]   IEE, *Power system protection 1: Principles and components* vol. 1. London: Institution of Electrical Engineers - London, 1995.

[4]   P. M. Anderson, *Power System Protection*: Wiley, 1998.

[5]   Alstom. (01/06/2013). *COSI-CT LC/LCD Low Ratio Optical Curent Transformers*. Available: http://www.nxtphase.com/

[6]   AIEE-EEI, "Bus Protection," *Transactions of the American Institute of Electrical Engineers,* vol. 58, pp. 206-212, 1939.

[7]   S. E. Zocholl and D. Costello, "Application guidelines for microprocessor-based, high-impedance bus differential relays," in *2009 62nd Annual Conference for Protective Relay Engineers*, 2009, pp. 451-468.

[8]   R. M. Smith, W. K. Sonnemann, and G. B. Dodds, "Considerations in Applying Ratio Differential Relays for Bus Protection," *Transactions of the American Institute of Electrical Engineers,* vol. 58, pp. 243-252, 1939.

[9]   K. L. Curtis, "The current transformer," *Proceedings of the American Institute of Electrical Engineers,* vol. 25, pp. 707-718, 1906.

[10]   P. C. Morganthaler, "Current transformers," *Proceedings of the American Institute of Electrical Engineers,* vol. 29, pp. 10-14, 1910.

[11]   W. Schossig. (2007, 11 Oct 2008) History of Protection. *PAC World Magazine*. Available:

https://www.pacw.org/fileadmin/doc/AutumnIssue07/history_autumn07.pdf

[12]   A. C. Schwager and V. A. Treat, "Shaping of Magnetization Curves and the Zero Error Current Transformer," *Transactions of the American Institute of Electrical Engineers,* vol. 52, pp. 45-52, 1933.

[13]   L. F. Blume, G. Camilli, S. B. Farnham, and H. A. Peterson, "Transformer magnetizing inrush currents and influence on system operation," *Transactions of the American Institute of Electrical Engineers,* vol. 63, pp. 366-375, 1944.

[14]   F. S. Rothe and C. Concordia, "Transient Characteristics or Current Transformers During Faults-II," *Transactions of the American Institute of Electrical Engineers,* vol. 66, pp. 731-734, 1947.

[15]   IEEE, "Transient response of current transformers," *IEEE Transactions on Power Apparatus and Systems,* vol. 96, pp. 1809-1814, 1977.

[16]   H. T. Seeley, "The effect of current-transformer residual magnetism on balanced-current or differential relays," *Electrical Engineering,* vol. 62, pp. 164-168, 1943.

[17]   R. A. B. Ferreira and F. A. R. Filho, "Current transformers saturation and its implications in protective differential schemes detection and operation decision using wavelet transform and Artificial Neural Networks," in *13th International Conference on Development in Power System Protection 2016 (DPSP)*, 2016, pp. 1-6.

[18]   J. L. Blackburn, *Protective relaying : principles and applications*, 3rd ed.. ed. Boca Raton, FL: Boca Raton, FL : CRC Press, 2007.

[19]   O. P. Dahal, S. M. Brahma, S. J. Ranade, and R. J. Malahowski, "Investigation of various options to avoid false tripping of a primary distribution feeder: Part I - modeling and analysis," in *North American Power Symposium 2010*, 2010, pp. 1-6.

[20]   A. Hargrave, M. J. Thompson, and B. Heilman, "Beyond the knee point: A practical guide to CT saturation," in *2018 71st Annual Conference for Protective Relay Engineers (CPRE)*, 2018, pp. 1-23.

[21] R. A. Pfuntner, "Current transformers near high-current busses," *Electrical Engineering,* vol. 70, pp. 1077-1077, 1951.

[22] W. J. Smolinski, "Design Considerations in the Application of Current Transformers for Protective Relaying Purposes," *IEEE Transactions on Power Apparatus and Systems,* vol. PAS-92, pp. 1329-1336, 1973.

[23] "IEEE Standard Requirements for Instrument Transformers," *IEEE Std C57.13-2016 (Revision of IEEE Std C57.13-2008),* pp. 1-96, 2016.

[24] IEEE, "IEEE Guide for Protective Relay Applications to Power System Buses," *IEEE Std C37.234-2009,* pp. C1-115, 2009.

[25] L. F. Kennedy and A. T. Sinks, "New current transformer for bus differential protection," *Electrical Engineering,* vol. 60, pp. 1180-1187, 1941.

[26] Y. C. Kang, J. K. Park, S. H. Kang, A. T. Johns, and R. K. Aggarwal, "An algorithm for compensating secondary currents of current transformers," *IEEE Transactions on Power Delivery,* vol. 12, pp. 116-124, 1997.

[27] D. C. Yu, J. C. Cummins, Z. Wang, Y. Hong-Jun, L. A. Kojovic, and D. Stone, "Neural network for current transformer saturation correction," in *1999 IEEE Transmission and Distribution Conference (Cat. No. 99CH36333)*, 1999, pp. 441-446 vol.1.

[28] R. A. Allah, "Adaptive busbar differential relaying scheme during saturation period of current transformers based on alienation concept," *IET Generation, Transmission & Distribution,* vol. 10, pp. 3803-3815, 2016.

[29] T. Y. Ji, Q. He, M. J. Shi, M. S. Li, and Q. H. Wu, "CT saturation detection and compensation using mathematical morphology and linear regression," in *2016 IEEE Innovative Smart Grid Technologies - Asia (ISGT-Asia)*, 2016, pp. 1054-1059.

[30] E. L. Harder, E. H. Klemmer, W. K. Sonnemann, and E. C. Wentz, "Linear couplers for bus protection," *Electrical Engineering,* vol. 61, pp. 241-248, 1942.

[31] IEEE, "IEEE Guide for the Application of Rogowski Coils Used for Protective Relaying Purposes," *IEEE Std C37.235-2007,* pp. c1-45, 2008.

[32] IEEE, "Practical Aspect of Rogowski Coil Applications to Relaying," *IEEE Special Report,* pp. c1-72, 2010.

[33] P. Orr, P. Niewczas, C. Booth, G. Fusiek, A. Dyśko, F. Kawano, T. Nishida, and P. Beaumont, "An Optically-Interrogated Rogowski Coil for Passive, Multiplexable Current Measurement," *IEEE Sensors Journal,* vol. 13, pp. 2053-2054, 2013.

[34] L. Cristaldi, A. Ferrero, M. Lazzaroni, and R. Ottoboni, "A linearisation method for commercial Hall-Effect current transducers," in *Proceedings of the 17th IEEE Instrumentation and Measurement Technology Conference [Cat. No. 00CH37066]* vol. 3, ed, 2000, pp. 1220-1225 vol.3.

[35] IEEE, "Optical current transducers for power systems: a review," *Power Delivery, IEEE Transactions on,* vol. 9, pp. 1778-1788, 1994.

[36] L. Dziuda, G. Fusiek, P. Niewczas, G. M. Burt, and J. R. McDonald, "Laboratory evaluation of the hybrid fiber-optic current sensor," *Sensors and Actuators A: Physical,* vol. 136, pp. 184-190, 2007.

[37] R. B. Amin Moghadas, Mehdi Shadaram, "An Innovative Fibre Bragg Grating Sensor Capable of Fault Detection in Radial power Systems," presented at the 4th Annual IEEE System Conference 2010, 2010.

[38] P. Niewczas, "Implementation of a Faraday Effect based Optical Current Transducer using digital signal processing techniques," Thesis [Ph. D.] -- University of Strathclyde, 2000., 2000.

[39] M. H. Samimi, A. A. S. Akmal, H. Mohseni, and J. Jadidian, "Open-Core Optical Current Transducer: Modeling and Experiment," *IEEE Transactions on Power Delivery,* vol. 31, pp. 2028-2035, 2016.

[40] K. Bohnert, P. Gabus, and B. H, "Fiber-Optic Current and Voltage Sensor for High-Voltage Substations," in *16th International conference on Optical Fiber Sensors*, 2003, p. 3.

[41] G. Fusiek, P. Orr, H. Wang, and P. Niewczas, "All-optical differential current detection technique for unit protection applications," in *2013 IEEE International Instrumentation and Measurement Technology Conference (I2MTC)*, 2013, pp. 1214-1217.

[42] G. Fusiek, P. Orr, and P. Niewczas, "Reliability of an all-optical differential current detection technique during environmental temperature perturbations," in *IEEE SENSORS 2014 Proceedings*, 2014, pp. 1121-1124.

[43]   P. Orr, G. Fusiek, P. Niewczas, C. D. Booth, A. Dysko, F. Kawano, T. Nishida, and P. Beaumont, "Distributed Photonic Instrumentation for Power System Protection and Control," *Instrumentation and Measurement, IEEE Transactions on,* vol. 64, pp. 19-26, 2015.

[44]   D. Tzelepis, A. Dyśko, G. Fusiek, J. Nelson, P. Niewczas, D. Vozikis, P. Orr, N. Gordon, and C. D. Booth, "Single-Ended Differential Protection in MTDC Networks Using Optical Sensors," *IEEE Transactions on Power Delivery,* vol. 32, pp. 1605-1615, 2017.

[45]   Y. C. Kang, S. H. Kang, and P. A. Crossley, "A busbar differential protection relay immune to the effects of CT saturation," in *Developments in Power System Protection, 2004. Eighth IEE International Conference on*, 2004, pp. 391-394 Vol.1.

[46]   Y. C. Kang, S. H. Kang, and P. A. Crossley, "Design, evaluation and implementation of a busbar differential protection relay immune to the effects of current transformer saturation," *Generation, Transmission and Distribution, IEE Proceedings-,* vol. 151, pp. 305-312, 2004.

[47]   H. Y. Li and P. A. Crossly, "Design and evaluation of a current differential protection scheme incorporating a fiber optical current sensor," in *Power Engineering Society Summer Meeting, 2000. IEEE*, 2000, pp. 1396-1400 vol. 3.

Chapter 2. Power System Protection: Principles and Methods

2.1. Introduction

This chapter reviews several principles and method of power system protection. The chapter starts with the aims and objectives of protection system. It is then followed by protection system design requirements and reliability aspects in terms of dependability and security. Components of protection system are introduced and followed by a more detailed review of conventional iron core voltage and current transformers. Then basic principles of the circulating current differential protection are also revealed with special emphasis on the requirements of a busbar differential protection. Finally, the limitations and most recent trends in power system protection are reviewed.

2.2. Power system protection

2.2.1. The needs of protection system

An electrical power system that usually consists of generating units, transmission system and distribution network is designed and managed to operate continuously delivering electric power to end users. Generating and supplying electrical energy to every connected load without any interruption is the fundamental purpose of any electrical power system. However, there is no guarantee that the power system is free from disturbances, failures, breakdowns or faults at all times. Such events, when they occur, may cause disruption of the system normal operation.

Since it is not economical to design a system to withstand all possible system condition, the alternative is to design a protective system that can quickly detect an abnormal condition and take appropriate action to ensure that the faulty components are isolated from the rest of the system, and thus, the impact of the fault is minimised. The type of action that should be taken depends on the type of protective device and

specifics of the abnormal condition observed by the device. Therefore, the existence of the protection system in a power system is a crucial, safety critical requirement.

The protection systems that exist today are only able to detect and react after the occurrence a fault in the system. It would certainly be better if the protective devices could predict the occurrence of fault. However, there are no such devices as accurately predicting an instant of a fault with high level of confidence is not possible. Therefore, protection systems must rely on the response principle where the operation of protection system components occurs after an incident (e.g. a fault) has taken place [1],[2].

2.2.2. Objectives of protection system

The primary objective of protection system is to detect any occurrences of a fault and to remove (isolate) any faulted elements of power system as soon as possible from the rest of power system. The fault clearance is achieved by isolating the faulted part through the opening of the associated circuit breakers (CBs). This action must be taken to prevent the spread of the fault effects, to maintain system stability, and to allow continuing operation of the rest of the power system [3, 4].

The secondary objective of the protection system is to minimize damage and repair cost when a fault occurs. Besides its role as a safeguard for equipment and apparatus, even more importantly, it ensures safety of personnel.

The last objective is to provide information about type and location of the fault in power system. This information is required by engineers and technicians in order to accelerate the power system recovery.

2.2.3. Main and backup protection, and protection zones

Main protection is the protection system that becomes the first line of defence against system faults and operates first to isolate the fault by opening the associated CBs. Therefore, the CB(s) should be located at the point(s) of connection of each power system element in order to have the ability to physically isolate the faulted element from the rest of the system [5-7].

Backup protection is the protection system that operates only when the main protection fails to perform its duty. The primary and backup protection systems should be selectively coordinated to meet the protection requirements. Backup protection clears the faulted equipment by re-tripping the primary CBs or by tripping CBs in adjacent zones. As a consequence of tripping the CBs of adjacent zones, wider area of the power system is removed from service. Backup protection consists of two types which are local and remote backup. The local backup protection is located and assigned to operate when the fault occurs within the zone, and trips either the primary CB, or CBs in adjacent zones. Remote backup protection is located in adjacent zones and generally only trips CBs in the adjacent zone(s).

Each element of power system is grouped into a predefined area known as protection zone in order to provide a full coverage for protection purposes. In this way, the power system consists of many protection zones that are overlapping to avoid any blind spot (an area without protection coverage). The main protection operates for any fault occurring within the protection zone by tripping the associated CBs in order to remove the faulty part (faulty zone).

With regard to protection zone arrangement, protection systems can be categorised as either a unit protection or non-unit protection scheme. Unit protection scheme is designed to operate only for short circuits within the predefined zone and never operate for short circuits outside its zone. On the other hand, a non-unit protection has no clearly defined operation zone but covers a non-specifically defined area and can operate for faults outside of its main zone. The coverage (reach) of non-unit protection schemes is determined by the relay settings.

2.3. Power system protection design

2.3.1. Protection system design criteria (requirements)

In order to meet the protection objectives, the protection system should meet the minimum of four design criteria (protection requirements): sensitivity, selectivity, speed, and reliability [5-8].

2.3.1.1. Sensitivity

Sensitivity is the ability of protection system to identify the fault related quantity that exceed a detection threshold (nominal pickup) without mistaking it for normal operation quantity. Such fault quantities cause a protective action when they exceed the pre-set threshold. Therefore, the sensitivity term is used when referring to the minimum operating level of relays such as current, voltage, power, etc. In older generation electromechanical relays, the sensitivity was limited by device design because it was depended on the sensitivity of the measuring movement and was measured by its volt-ampere consumption to initiate operation. On the other hand, with modern digital and numerical relays, the sensitivity is rarely limited by the device design but by its application and the parameters of instrument transformers (i.e. CTs and VTs). Therefore, the modern relays have better sensitivity than electromechanical relays. When the main protection on the faulted zone fails, the back-up protection also must be sensitive to detect the fault in the remote parts of the power system.

2.3.1.2. Selectivity

Selectivity (discrimination) is the capability of the protection system to operate only the closest protection devices, including the nearest CB, in order to remove the faulty component. This protection strategy is intended to minimize system disruption and to avoid any further damage to the system. It also means that the protection system is required to isolate the section of the faulted zone by tripping only the appropriate CBs and allow the healthy parts of the network to remain in operation. Discrimination as a property of selective tripping is obtained when a minimum amount of equipment is removed from service during the process of fault isolation. Discrimination can be achieved by two general methods: time grading and application of unit-type protection.

2.3.1.3. Speed (operating time)

High speed of protection system operation is required to reduce the damage to equipment in the faulted zone, minimise the risk of system instability, and even mitigate loss of synchronism which could lead to power system blackout. The speed of operation is related to the critical clearing time (CCT) when faults occur in the power system. However, an excessively fast protection may result in undesired

disconnection during the transient faults which, in some cases, can also destabilise the system.

2.3.1.4. Reliability

It is practically and economically unfeasible to design an electric power system that has capability to withstand all possible equipment failures and abnormal operating conditions. Therefore, electric power systems must utilize highly reliable protection systems that can promptly detect abnormal conditions and take appropriate actions to ensure isolation of faults. In addition to utilization of highly reliable equipment, certain level of redundancy is also needed in order to achieve the high reliability requirements of protection system. There is a difference between redundancy and back-up protection. A redundant protection is a second (or third) system that has essentially similar performance to the primary protection, while a back-up protection provides a lower degree of performance such as lower speed or selectivity [9],[10].

In general, reliability denotes the ability of protection system to perform the function consistently under stated conditions for a specified period of time. The reliability of protection system is measured by the degree of certainty that protection system will perform correctly (dependably) together the assurance against incorrect operation (termed also as protection security). Therefore, from that definition of reliability of protection system, it consists of two particular aspects: dependability and security.

Furthermore, dependability is the degree of certainty that a protection system (or a relay) will operate correctly. Security is defined as the measure of the certainty the protection system will not operate incorrectly during normal operation conditions or for faults outside of their protection zone.

Based on the security definition that is associated with unit protection scheme, the protection system should remain stable and refrain from operation under any conditions external to the protected zone such as through faults and load currents. Examples of power system conditions that require high level of protection system security are: direct motor start-up and the transformer inrush current.

2.3.1.5. Other attributes: simplicity and economics considerations

In addition to the previous four design criteria, another protection system attribute is simplicity of design which is closely associated with reliability. As a rule of thumb, a simpler protection system with lesser number of relays, circuits and contacts will maintain better reliability. It is because a complicated protection scheme requires many more inter-related components to operate correctly. Such schemes also tend to create difficulties (e.g. due to human error) in settings, maintenance, and repair. The primary factors that influence the reliability of a protection system are: simplicity of relay design, high quality of manufacture, correctness of scheme design and installation, and good maintenance and supervision.

Although economic considerations are different from the previous five technical requirements, this non-technical aspect must be included in the design requirements of a protection system. The reasons are that the economic aspect has a direct effect on the protection objective which is to minimize damage and repair cost (outage cost). It is also linked to the enhanced performance of protection system because higher performance usually means higher cost. Moreover, it has a direct contribution to the whole design of the power system that covers equipment cost (capital investment), protection costs, and outage cost (operation and maintenance cost). Therefore, it is important to optimize the design requirements by conducting a comprehensive analysis including economics and engineering analysis in order to achieve the best compromise between the capital investment, protection and outage cost.

2.3.2. Reliability: dependability versus security and redundancy

Dependability corresponds to the degree of certainty that a protection system operates correctly when required and at the designed speed for a fault within the protected zone. On the other hand, security relates to the degree of certainty that a protection system will prevent incorrect operation or faster than designed with regards to external faults and normal operating conditions [11-14]. The dependability and security are two aspects of the reliability that are contrary each other. Increasing dependability by increasing the sensitivity of fault detection will lead to a reduction in the level of security and vice versa, reducing dependability will increase security.

Moreover, in order to increase one aspect of reliability without compromising the other, the possible solution can be achieved by designing protection system with adequate redundancy. In other words, when the reliability level of a single device arrangement is still unacceptable because it is below the reliability requirement, a reliability improvement can be achieved by adding a redundant system that operates independently to the primary protection. A simple redundant system consists in duplication of the primary protection while a sophisticated redundant system is a combination of relays from the same or different manufacturer with specific arrangements. Therefore, the redundant system plays important role for the reliability of protection system [13, 14].

The redundancy of equipment (or device) is intended to minimize single component failure that could provide a desired balance between the dependability and security. For example, implementation of multiple protection schemes in order to protect a certain protection zone where the tripping signal of each protection schemes are configured in several different ways. The common configuration methods are series, parallel and mixed series-parallel configuration [15],[16].

The series configuration requires that all protection relays in the scheme send a tripping signal in order to execute a tripping operation. As a consequence, this method increases the security of protection system because it prevents mal-operation. Example of the series configurations is 'two-out-of-two' arrangements. For the parallel configuration, only one protection relay in the schemes is required to send tripping signal in order to generate a tripping operation. Hence the result of the parallel configuration (e.g. 'one-out-of-two' arrangement) will increase the dependability because it prevents failure to operate due to an undetected fault by one of the protection methods.

Whereas for a mixed series-parallel configuration with 'two-out-of-three' arrangement, it has better performance from the previous configuration because it provides both reliability of tripping and security against unwanted tripping. The 'two-out-of-three' arrangement or voting scheme requires three main protections and is usually implemented for special protection schemes (SPS) [17, 18] and vital EHV transmission lines, the existence of which, has direct effect on overall stability of the

system. Three main protections of different manufacturers for transmission line are used for the reliability reasons, in addition to other backup systems [19].

To summarize, higher speed and selectivity means higher cost and complexity, while higher selectivity allows higher speed. Dependability is generally proportional to sensitivity and speed, whereas the security is generally proportional to selectivity. Higher sensitivity and higher speed could ensure higher degree of the protection dependability. However, higher protection sensitivity usually causes reduction in protection security. The high speed protection could mitigate the equipment damage and instability but it may reduce the protection security and the protection coordination (selectivity). These problematic tasks can be solved by compromising and matching the protection requirements among the dependability, security, sensitivity, selectivity and speed. Therefore, the redundancy is one of the best options to achieve the desired solution.

2.4. Components of protection system

In order to fulfil the protection system objective, the protection system has various components including sensing elements, relays with an intelligent control system, tripping and switching apparatus, DC supply, and some additional components.

The operation sequences of protection system components are described as follows. First of all, the protection relay receives the relay operating quantities from instrument transformers or other devices. In the next step, the relay evaluates the operating quantities and decides either to operate or not to operate. Finally, only when the relay operates, it then generates a tripping signal as the relay output decision. Schematic wiring of protection system and their components are illustrated in Figure 2.1 [6].
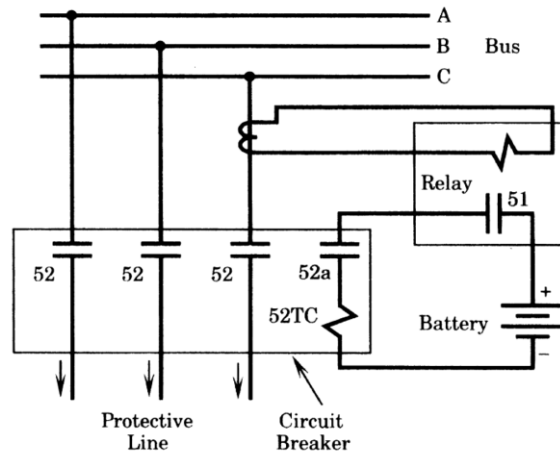
Figure 2.1   Schematic wiring of relay and CB trip circuit [6]

Brief explanation of the protection system components [2-8]:

1. Instrument transformers – this equipment includes current transformers (CTs) and voltage transformers (VTs) that are used to provide information related to power system condition to protection relays.

2. Protection relays – It is the heart of protective system because it has intelligent (logical) abilities such as detection, comparison, evaluation and decision making. Based on relay classification [20], relays which are associated with protection could be divided into two main groups. The relays in the first group are often termed "comparators" because their function is to compare electrical quantities. This relay type is designed to operate when it detects or measures abnormal conditions. The second group is known as auxiliary relays which are designed to connect the auxiliary circuits. The auxiliary relays are operated by the measuring relay (comparator) contacts in order to close (or open) further contacts with higher current ratings.

3. Circuit Breaker (CB) – CBs must be safely used in normal and fault conditions to connect and disconnect both normal operating currents as well as fault currents. CB is required to perform three duties:

   a.   It must be capable of opening the faulty circuit and breaking the fault current.

   b.   It must be capable of being closed on to a fault.

21

c. It must be capable of carrying fault current for a short time while another breaker is clearing the fault.

Therefore, CB has to have three ratings: breaking capacity, making capacity and short time capacity. For the purpose of removing a fault from the power system, one or more CBs are required in conjunction with the protection relays. A simple CB operating mechanism is as follows, a CB trip coil is energized when it receives the trip signal from the protection relay and associated control circuit. Then, it releases a latch and a quick opening operation of CB main contacts due to the stored energy in the closing spring. The time intervals between each event in CB operating mechanism are very short, a few electrical cycles (tens of milliseconds). The relay output contact is wired in series with the CB trip-coil and the DC-battery, see Figure (2.1). The DC-battery supplies energy to the CB trip coil for its operation. Thus, when the relay operates, the CB trip coil quickly separates the CB main contacts.

4. DC supply– DC supply is required for the relays (protection relays, monitoring relays, reclosing relays, and regulating relays), CB operating mechanism, and auxiliary relays that are related to tripping operation. They are also utilized for communication facilities, indicating devices (signal, lamp and alarm) and other auxiliaries. A complete DC supply unit contains a number of battery cells and the charging units in order to maintain the batteries ampere-hour capacity. The battery accumulates energy during the availability period of AC supply and discharges energy when the protection system operates. By considering situations when a power system faults or total failure of incoming power occurs, the stored DC power in batteries is the best reliable alternative to provide power to all concerned protection relay circuits and the CBs operation for removing and restoring the situation. Therefore, separate and independent DC supplies are normally provided for the protection relays and CBs to ensure higher reliability.

Some additional elements of the protection system are communication channel, monitoring and supervision, indication devices, cable (wiring), terminals and test link where they are not shown in the previous schematic diagram. Some of these additional elements are needed in some cases. The brief description of the additional elements as follows:

5. Communication channel (communications facilities) – these facilities are used to communicate messages, exchange measured data, monitoring/supervision, protection signalling and inter-tripping. Some unit protection schemes require a communication link (protection signalling) between the relays at distant locations in order to perform the protective function. These communications links are also required when a CB is commanded in remote operation as a consequence of a local event (inter-tripping) or other defined action such blocking the trip signal. There are many types of communications facilities such as private pilots, rented pilots or channels, power line carrier (line traps and HF capacitor coupler), radio channels and optical fibre communication links.

6. Monitoring and supervision (self-monitoring/supervision) – in the older generation of protection system technology these features are available through auxiliary relay control circuits that provide information regarding failures in the trip circuit, CB operating mechanism, CT and VT. However, in the recent numerical relay technology, these features are already included in the relay (known as self-monitoring/supervision). Besides providing the already mentioned benefits, these features are a "watchdog" for the relay itself, for trip circuit supervision, and VT supervision because it can detect no voltage output when a VT fuse is blown out. When a watchdog alarm goes off, an urgent repair works must be carried out promptly to prevent protection system failure should a fault occur at that time.

7. Other additional components include indication devices, cables (wiring), terminals and test links.

2.5. Conventional voltage and current transformers

The conventional voltage and current transformers are intended to provide a scaled down replica of primary voltage and current, respectively, from transmission levels down to a suitable level for protective relays. As a consequence of reducing the electrical quantities in magnitude the protection relays can be designed as relatively small and inexpensive devices. Both instrument transformers also provide insulation of the low voltage relay equipment from the high voltage power system.

In application of current and voltage transformers, several requirements should be considered in order to achieve proper performance and selection [7, 21, 22]. These requirements cover the following: ratio in terms of primary to secondary currents or voltages, accuracy, impulse level, connections, type and class of insulation, continuous thermal current rating, short-time thermal and mechanical current ratings, mechanical and electrical construction, and service conditions.

In low primary voltage (or low current) applications voltage and current transformers often cannot be easily distinguished due to similarity in size. However, they can be recognized by their connection to the power system. The primary winding of voltage transformers is connected in shunt to the power system, while the current transformers are connected in the series.

2.5.1. Voltage transformers

The purpose of voltage transforming devices is to continuously derive a voltage supply of 110V from high voltage source. The maximum output power of voltage transformers (VT) is typically 300 VA. The VT's typical construction for primary voltages up to 33 kV is a single three-phase unit (Figure 2.2.a) [2], while for higher voltages there are usually three single-phase units in order to maintain phase isolation (Figure 2.2.b) [23].

In terms of their construction voltage transforming devices can be grouped as follows:
1. Wound-type VT (Electromagnetic two winding transformer)
2. Cascade voltage transformer
3. Capacitor voltage transformer (CVT) with an electromagnetic unit
4. Coupling capacitor voltage divider (CCVD) or coupling capacitor voltage transformer (CCVT).

The wound-type VT is similar to a small power transformer that has primary and secondary windings on a common core. Due to increasing system voltage levels, the electromagnetic two wound type VTs with a single primary winding become inefficient and obsolete because of the size and insulation problems that tend to increase the cost at disproportionate rate.

(a). MV instrument transformer	(b). HV instrument transformer

Figure 2.2   Typical voltage transformers CT [23]

One of the solutions to this problem is the cascade VT as shown in Figure 2.3 [2], which has several separate stages of primary winding connected in series in order to form a multi-stage primary winding VT. Another solution is a CVT as displayed in Figure 2.4 [2], where the secondary voltage is taken from the secondary winding of a conventional wound-type transformer while the primary winding is connected to a stack of primary capacitor divider at a lower tapping across to the earth. This CVT is often more economic due to size reduction than a VT because the wound primary of conventional two winding VT type is superseded by a mixed configuration of the capacitor dividers and a small wound VT.
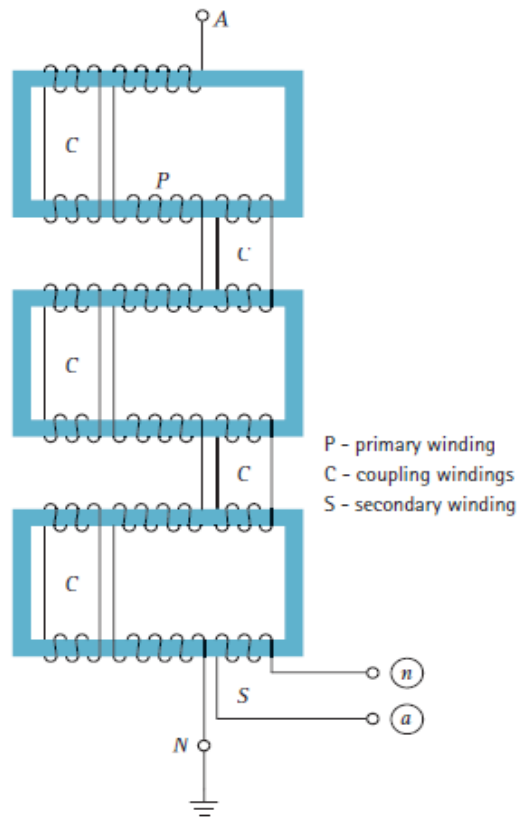
Figure 2.3   Schematic diagram of typical cascade VT [2]
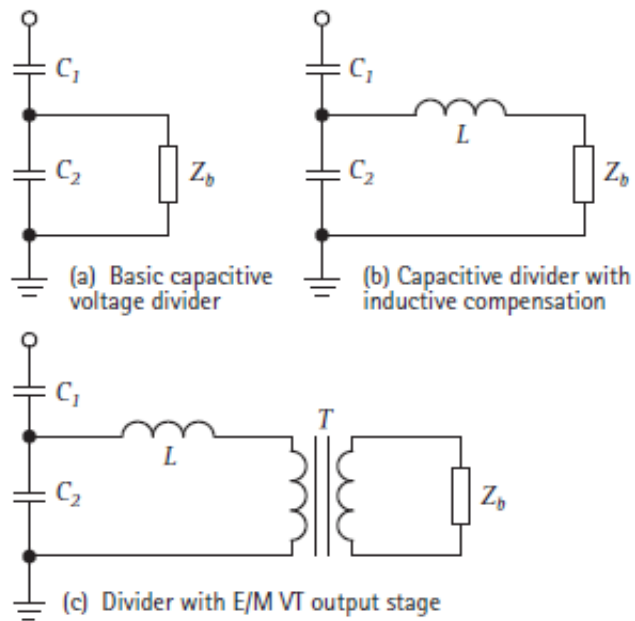
Figure 2.4   Schematic diagram of capacitor voltage transformer [2]

Due to the use of capacitance dividers in the CVT, the equivalent source impedance is capacitive. Therefore, to obtain the voltage output like the conventional VT, a tuned inductor must be connected in series with the lower capacitor in order to correct the phase angle error of the secondary voltage at normal frequency.

The last VT construction type is coupling capacitor voltage divider (CCVD). The capacitor divider is utilized to replace the tuned circuit in the previous design in order to give a better transient response performance. Moreover, the output circuit is associated with a pre-amplified signal converter and voltage amplifier to provide the correct voltage and power levels for relay equipment. These circuit and device combinations substitute the reactor and wound transformer unit of the conventional CVT. Another improvement is an addition of the specific circuit arrangement to facilitate the dual purpose functions, i.e. voltage measurement and as injection channels for high frequency power line carrier (PLC) protection schemes. Therefore, the CCVD is more suitable for use with high speed forms of protection.

2.5.2. Current transformers

The current transformers typically consist of a ferrous material core and two windings (primary and secondary). Based on the number of turns on the primary side, CTs can be grouped in two major types: single turn (bar) primary and multi-turn wound-primary[1]. However, based on the construction models, there are four common types of CTs: wound CT, bar CT, window CT, and bushing CT. Current transformer images can be shown in Figure 2.5 and Figure 2.6 [24].

a. Wound type   b. Window type
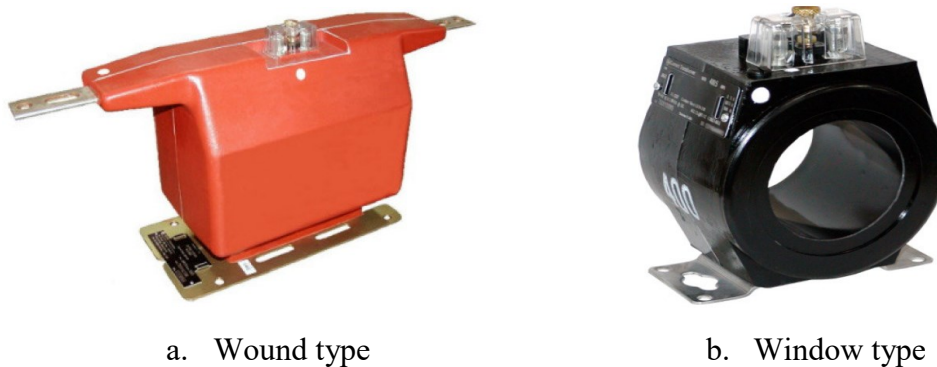
Figure 2.5   Current transformer: a. wound type, b. window type [24]

Figure 2.6   High voltage current transformer [24]

A main criterion in selecting a correct CT ratio is the maximum and continuous load current of power system and current rating of the connected apparatus such as relays and instruments. Since the load current will generate the corresponding secondary current that flows through the relay circuits all the time, this continuous current value should be matched with the rated current of the relay. In conjunction with the previous consideration, the protective relays are usually designed for a certain nominal load current (5A or 1A) and this value must not be exceeded for extended periods of time. Thus, the CT should be selected to provide approximately either 5A or 1A at normal loading conditions that corresponds to the standard output of the current transformer.

CT accuracy relates to how close the secondary current wave resembles the primary current wave. Since the current wave consists both of the wave amplitude and phase difference, hence the CT accuracy is defined based on these two components. The CT accuracy depends on two construction parameters which are the cross section area of the ferrous core and the number of turns in the secondary winding.

The greater cross section area of the ferrous core causes better accuracy due to more flux can be developed before the core saturation occurs. Better accuracy can also be achieved by increasing the number of secondary turns because the smaller flux is required to force the secondary current through the relay. As the CT is used to

transform the currents at both nominal load and fault current levels, CT accuracy should cover both levels [7].

There are two different types of CT characteristics, namely a metering CT and a protective CT. The metering CTs are required to operate with high accuracy in the range of normal operating current which is typically in the interval of 10% to 120% of the rated current. Above this interval the metering CTs are expected to saturate. The benefit of CT saturation in this case is that it protects the instruments connected to the secondary winding. The protective CTs, on the other hand, are intended to operate under fault conditions, therefore, they are required to function at currents significantly above the nominal rating and must retain a reasonable accuracy up to the highest expected fault current to ensure the correct operation of protection system.

Due to different intended functions, the magnetizing characteristics of protective CTs stretch over a much wider range of currents as shown in Figure 2.7 [8],[25]. In other words, the operating range of a metering CT is usually located in the region of ankle point of the protective CT. Hence the protective CTs have working points far below the knee point which is in the ankle point region of excitation characteristic when it operates close to the normal rated current. Therefore, the CT will not saturate easily during high fault current. In order to achieve the characteristic without saturation problem, the protective CT's core should have larger cross-section area. However, increasing the cross-section area also means that the cost of protective CTs is higher. To maintain the cost and size within reasonable levels, the material of the CT core must be selected from the best quality iron characterised by high saturation level such as grain oriented steels [4].
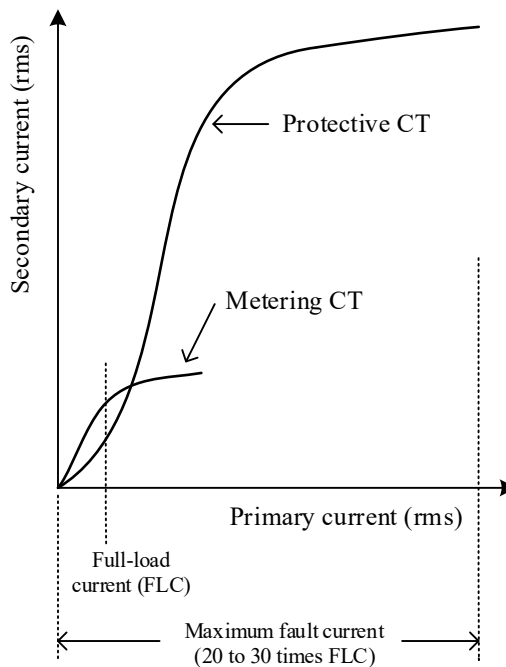
Figure 2.7   Protective CT versus measurement CT [8],[25]

In existing practice the saturation effects of the conventional current transformers can be minimized in several ways, such as:

- Keeping the secondary burden as low as possible
- Using a higher specification CTs such as CT with a better quality of the iron core in order to cope with the anticipated high fault currents [18]
- Applying CTs with a higher accuracy class [19],[20],[21].
- Introducing dedicated algorithms in numerical protection relays to detect CT saturation in order to mitigate their adverse effects on protection operation. Such methods include magnetization curve method [22], utilisation of neural networks [23], adaptive protection [24], mathematical morphology [25], and many others.

In similar sense, when applying busbar differential protections, the CT saturation have to be considered. To deal with this problem, several methods have been introduced in literatures. The methods can be classified as: using elements or devices, such as harmonic current restraint [26], applying computer techniques, such as saturation

detection algorithms [27],[28],[29],[30],[31],[32] and a combination of device and software, such as CT saturation countermeasure element (CTSCE) that consists of a waveform discriminating element (WDE) and a starting element (SE) [33],[34]. Some algorithms prevent relay operation during CT saturation. Therefore, these may result in unnecessary longer trip times of the protection system.

2.6. Protection relays and differential protection methods

2.6.1. Protection relays

The fundamental element of a protection relay is a fault detecting and decision making unit that is often termed as *basic unit*. These basic units can be categorized as electromechanical units, sequence networks, solid-state units, logic circuits, integrated circuits, and microprocessor devices (termed as intelligent electronic devices – IEDs) [20],[26]. These basic units in cooperation with any necessary logic networks and auxiliary units are arranged to establish a protection scheme. The basic units could be utilized to determine the protection operating principles. Protective relays are classified either by the monitored variable or by the performed function. The existing common relay types with their operating principles can be summarised as follows [12]:

1. **Overcurrent relay** (OCR) – this relay type operates (or picks up) when it senses a current that exceeds the setting value. A few OCR variants are defined based on their time characteristic: instantaneous, independent definite time, inverse definite minimum time (IDMT).

2. **Differential relay** – a differential relay responds to the difference between incoming and outgoing currents associated with the protected zone. The current difference is measured by the relay and when it is sufficiently high, it causes the relay to operate. Differential relays are commonly applied in busbar, generator, and transformer protection.

3. **Directional relay** – a relay that responds to the relative phase angle difference of a current phasor with respect to another current or voltage reference.

4. **Distance relay** – a generic term covering those forms of protective relays in which the response to the input quantities is primarily a function of the electrical distance between the relay location and the fault point.

5. **Pilot protection relay** – a form of line protection that uses a communication channel as a means of comparing electrical quantities at the opposite terminals of the line.

2.6.2. Differential relay

Differential protection scheme is widely utilized in power system protection because it provides good discrimination and simplicity. In order to explain the differential protection scheme, a test power system is shown in Figure 2.8. Fault conditions that are obtained from the test system will be used to demonstrate both the conventional circulating current and the novel optical type differential protection developed in this thesis.
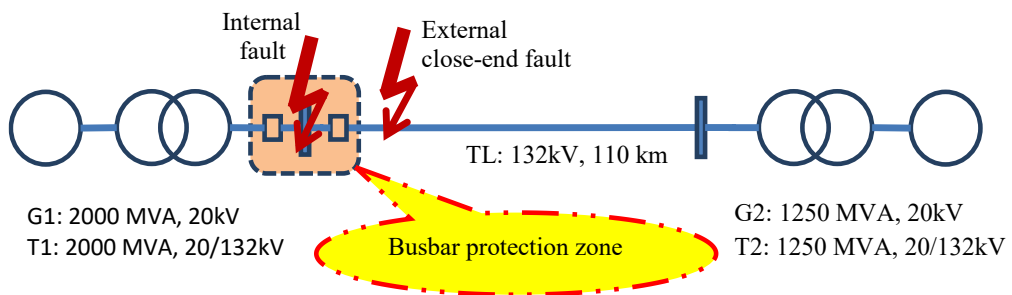
Figure 2.8   Power system model for optical differential protection scheme

When analysis performance of differential protection, two fundamental types of fault conditions are always considered, i.e. internal faults and external faults as depicted in Figure 2.8. A normal operation is considered having similar characteristics to the external fault in terms of current flow direction but with much lower current amplitude. These two fault conditions are considered in assessing the dependability (internal faults) and security (external faults) of differential protection.

2.6.3. Principle of circulating current differential protection

In order to illustrate the differential protection operating principle, a simple circulating current busbar protection is used [2, 6]. The busbar section in Figure 2.8 is drawn in more details to include the secondary circuit with differential protection relay as shown in Figure 2.9.

a. Principle of differential protection

b. External fault   c. Internal fault
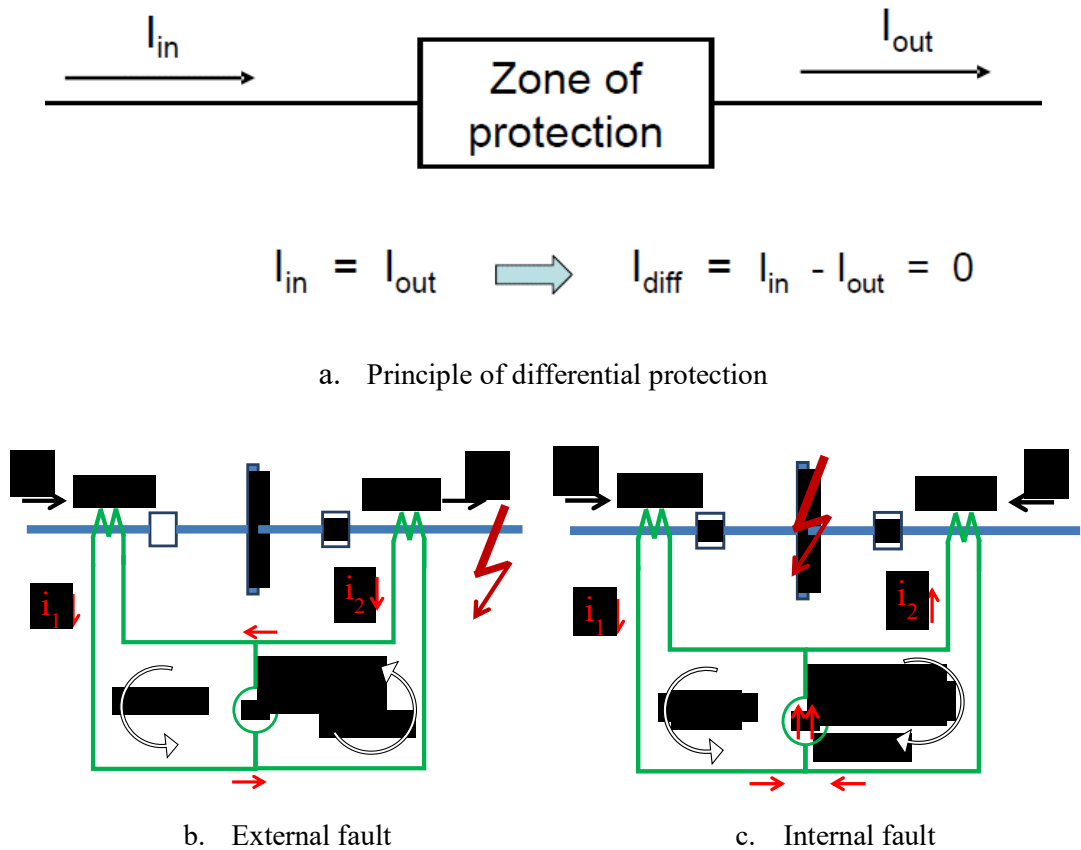
Figure 2.9 Circulating current differential protection principle.

Kirchhoff's current law states that the directed sum of currents in any node of the network is equal to zero. The Kirchhoff's current law is written as:

$$\sum_{k=1}^{n} I_k = 0 \qquad (2.2)$$

where I_k is the electric current in k-th branch, n is total number of branches (circuits) with current flowing towards (or from) the node. By inference the Kirchhoff's current law states that the sum of currents entering a given node must be equal to the currents leaving that node at any given time.

When applied to the busbar section shown in Figure 2.9, the Kirchhoff's current law states that the directed sum of currents in the healthy junction point is equal to zero. The Kirchhoff's current law is then translated into the principle which governs the differential protection scheme as follows:

$$I_{diff} = \left| \sum_{k=1}^{n} I_k \right| \tag{2.2}$$

When the sum of currents (I_{diff}) is not equal to zero, it is an indication of a fault occurrence in that section. For example, when external fault occurs outside of the busbar protection zone as depicted in Figure 2.9.a, the sum up of all directed currents in equation (2.2) is zero and could be written as:

$$I_{diff} = |I_1 + I_2| = 0$$

Otherwise, for internal fault, the directed current sum up is greater than zero and is expressed as:

$$I_{diff} = |I_1 + I_2| > 0$$

Apart from a busbar section mentioned above, other electric power system equipment such as transformer, generator, and motor as well as a section of transmission/distribution line can also be protected by the differential protection based on the same principle.

Moreover, to achieve the correct value of electric current summation in a busbar differential protection, all current transformers (CT) should have identical CTs in terms of magnetisation characteristic, turns ratio and burden, must be parallel connected and the measurements fully surrounding the protected zone. For an ideal CT condition, the sum of all currents would be zero under normal (no fault) condition

in the protection zone. Otherwise, the current sum unequal to zero would indicate existence of a fault in the protected element. These statements form the foundations of the differential protection scheme and expressed in (2.3).

$$\left.\begin{aligned} i_{diff} &= |\textstyle\sum_{k=1}^{n} i_k| \, ; \\ \textit{Normal operation: } i_{diff} &= 0 \, ; \\ \textit{Fault indication: } i_{diff} &> 0 \end{aligned}\right\} \tag{2.3}$$

However, in order to cover any non-ideal CT characteristic, relay threshold setting ($i_{setting}$) of the differential protection is typically used. The differential relay principle is still unchanged even though the relay setting has been added. In general, the differential relay only generates trip signal if the differential current is greater than the relay setting [2, 6, 27]. Therefore, the statements in equation (2.3) can be rewritten using the relay threshold setting instead of zero as:

$$\left.\begin{aligned} i_{diff} &= |\textstyle\sum_{k=1}^{n} i_k| \, ; \\ \textit{No trip is generated, if: } i_{diff} &\leq i_{setting} \, ; \\ \textit{Trip is generated, if: } i_{diff} &> i_{setting} \end{aligned}\right\} \tag{2.4}$$

where i_{diff} is the differential current in the relay branch, and $i_{setting}$ is a relay threshold setting.

The basic method to prevent a mal-operation of differential relay due to a mismatch current (often termed as spill current) is a proper selection of the relay setting. To determine the setting relay, the mismatch currents have to be calculated by taking several power system conditions into account such as maximum load current, maximum through fault, and minimum in-zone fault. Therefore, the relay setting should be determined according to the following key points as guidelines:

1) It must be greater than the mismatch current at the following conditions:
   a) Maximum load under normal system operation, and
   b) Maximum through fault current.
2) It has to be lower than the differential current at minimum in-zone fault.

However, when the mismatch current increases, raising the relay setting is not always the best solution, as it may significantly decrease the sensitivity of the relay. The

solution used in practice is the application of certain differential scheme modifications such as high impedance differential protections, or percentage differential relay biasing [5, 7, 11, 27-29].

2.6.4. High impedance and low impedance in the circulating current scheme

This section explains two methods which are high impedance and low impedance busbar differential protection schemes to deal with the CT saturation problem. The high impedance method is revealed in the first explanation as follows.

In the previous section, the iron-cored current transformers were assumed that is perfect and the secondary currents are exact replicas of the line currents. However, in a practical situation, the case is different when the faulted high current is flowing to the faulted point just outside the busbar protection zone. As a consequence, the faulted high current is likely to saturate the CT in the faulted line, whereas the unfaulty lines will carry smaller currents and their current transformers will experience either no saturation or varying degrees of saturation, depending on the total current flowing in the lines. The CT saturation has the effect of lowering or short circuit the exciting impedance, therefore, the shunt impedance becomes zero and the CT can produce no output. This condition is represented by a short circuit using broken line, across the exciting impedance as shown in Figure 2.10 [6]. It should be noted that this condition is not similar to a physical short circuit, because it is behind the winding resistance.
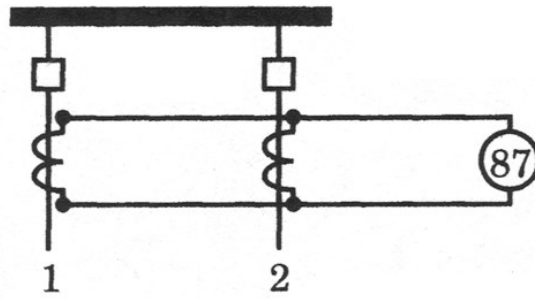
(a) Physical circuit.
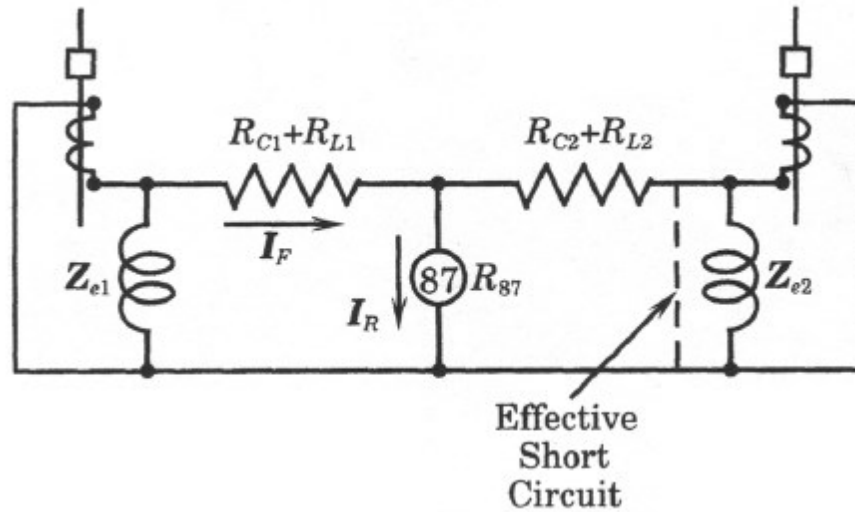
(b) Equivalent circuit.

Figure 2.10 CT saturation effect on the CT 2 [6].

Based on the equivalent circuit in Figure 2.10, the magnetizing impedance for CT 2 is effectively a short circuit. As a result, no current flows in the secondary of CT 2. The fault current I_F flowing in CT 1 divides inversely with the parallel impedances to give a relay current of

$$I_R = \frac{R_{CT2} + R_{L2}}{R_{87} + R_{CT2} + R_{L2}} I_F \tag{2.5}$$

Where R_{CT2} = secondary resistance of CT 2

R_{L2} = secondary lead resistance of CT 2

R_{87} = resistance of differential relay

If R_{87} is small, I_R will approximate to I_F, which is unacceptable because the relay will trip for this external fault with CT 2 saturated. On the other hand, If R_{87} is large, I_R is reduced. Equation (2.5) can be written in simple way, but with little error as follows:

$$I_R = \frac{R_{CT2} + R_{L2}}{R_{87} + R_{CT2} + R_{L2}} I_F \tag{2.6}$$

It is clear that, by increasing R_{87}, the spill current I_R can be reduced below any specified relay setting. R_{87} is frequently increased by the addition of a series-connected resistor which is known as the stabilising resistor.

The other method is a low impedance application for busbar differential protection scheme. The relay impedance usually is much smaller as the saturated CT impedance that will cause the majority of the differential current flowing through the relay and creating a false operation on saturation. To overcome this problem, the low impedance principal introduces a restraint quantity which basically determines how much current is going through the protection zone. When the higher the through current flows, the higher of the differential current is caused by the inaccuracy of the current transformers. The differential relays will build the restraint value differently depend on the relay designs. Therefore, it is important to know how the specific relay derives the restraint value when applying settings to the relay.

The most common restraint value is the summation of the feeder current amplitude (not vector) or the maximum of the feeder currents. Most differential protective relays are using the percentage restraint characteristic. The pick up value for the differential current will be a percentage of the restrain current value. The characteristic works in a way that it raises the pick up value of the differential pick up in proportion to the error assumed and expressed as the restraint current. The percentage differential elements compare a differential current (operating current) with a restraining current. The differential current I_{Diff} and restraining current I_{Res} are generally expressed as:

$$I_{Diff} = |i_1 + i_2| \tag{2.7}$$

$$I_{Res} = \frac{(|i_1| + |i_2|)}{2} \tag{2.8}$$

The typical ratio differential protection characteristic is depicted in Figure 2.11 [6].
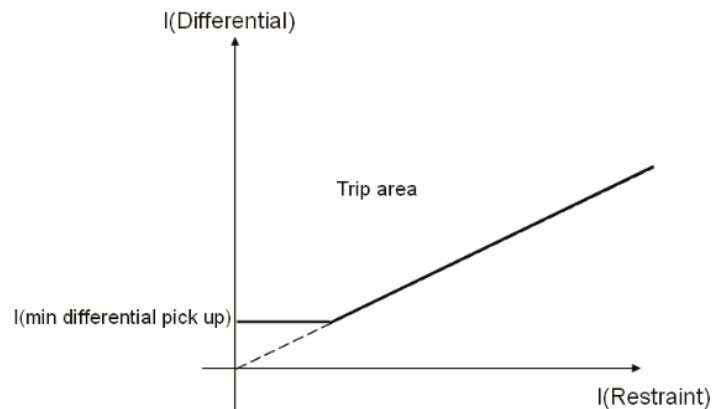
Figure 2.11 Percentage restraint characteristic.

2.6.5. Requirements of busbar differential protection

Although busbar faults are infrequent, they have serious consequences. The direct consequences of faults are excessive voltage drop, overheating, mechanical stress, and potential equipment damage. Additionally, the indirect consequence is the loss of supply on the faulted busbar and all connected feeders due to the protection trip action. Therefore, in order to minimise these consequences, the main busbar protection requirements are as follows [30]:

1. Security/stability – stable operation for external faults.
2. Reliability/selectivity – any internal fault has to be detected by the relay and should operate with 100% selectivity.
3. Speed – a fast operating time is required to minimize the impact of high fault current on busbar and other grid elements such as CBs, lines and transformers.
4. Sensitivity.

Design of busbar protection should comply with all of the above requirements. Thus, the design has to accommodate the best compromise between reliability, sensitivity, speed, security and cost.

2.7. Review of protection system: limitation and trends

Busbar in power systems is very critical elements because they have function as the point of junction of many circuits such as generation sources, transmission lines, inter-bus transformer, and loads. Power systems faults located on or near the busbar tend to have very high magnitude currents. Hence, it can cause severe damage to any elements of power system [29, 36]. Moreover, the structure of power systems are more complex due to the high penetration distributed generations and the implemented new technology for maintaining power system integrity. These conditions have also contribution to rise the fault currents. Therefore, a high-speed bus protection is often required to limit the damage on equipment and system stability or to maintain service to as much load as possible. However, this high-speed clearing must be balanced against the need for security. Tripping incorrectly for an external fault may cause large outages, and jeopardize power system stability. Thus, the busbar protection emphasis on the essential requirements of speed and stable operation.

Differential protection schemes are applied for high voltage busbar in the power system because they are the most sensitive and reliable method for protecting a busbar. Failure-to-trip on an internal fault, as well as false tripping of a busbar during load service, or in case of an external fault, both have disastrous effects on the stability of power systems.

The challenge of busbar differential protection is the issue of false differential current due to CT saturation and mismatch ratio. The high fault magnitudes increase the possibility of CT saturation during external faults close to the busbar, and CT saturation increases the possibility of an incorrect operation of the protection systems. Other issues are the technology trends in the electric power system and the protection systems. These issues are explained in the following sub-section.

2.7.1. Limitations of conventional current measurement

Magnetic saturation phenomenon in CTs due to the use of ferrous materials as CT's core is one of the main limitations of the conventional CTs. The saturation process is initiated by the creation of high flux density in the iron core that can be caused by

several factors such as high fault currents with or without a dc offset, residual flux, high secondary burden, or a combination of these factors. The saturation occurs when the flux density exceeds the design limits of the CT core. As a result, accuracy of the CT becomes poor because the secondary current is lower in magnitude than the value expected from the nominal ratio of the CT. Another undesirable effect is the introduction of harmonic components into the output current that may cause a distortion as displayed in Figure 2.12 [29, 31]. This, in turn, can potentially affect the protection relay performance.
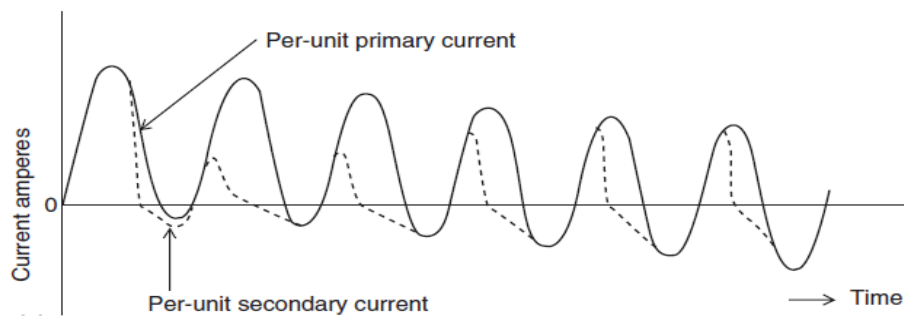
a. Large resistive burden
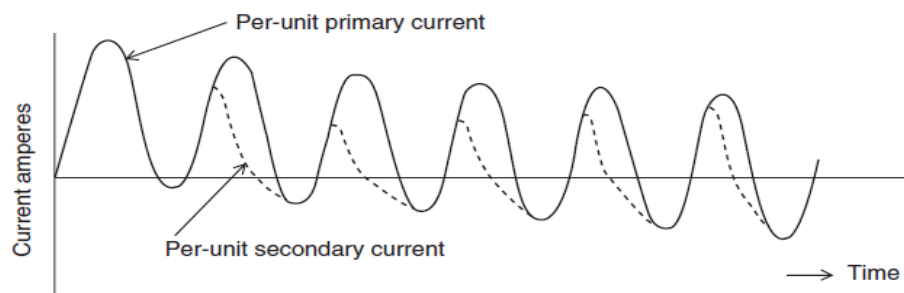
b. Small resistive burden

Figure 2.12   Distortion in CT secondary current due to saturation effect: a. large resistive burden; b. small resistive burden [29, 31]

Although the output current error exists in saturated CTs at faults conditions, during the first few cycles the CT may still give reasonable output before it completely saturates. In many cases, such output can be sufficient for relaying purposes depending

on the applied protection scheme. Therefore, there are protection relays which can tolerate distorted CT output to some extent by using advanced signal processing techniques to compensate for (or filer out) the distortions [31, 32].

However, beyond the few cycles following the fault, the saturation has a significant impact on the CT accuracy. During these periods, the CTs fail to deliver a true reproduction of primary current that may cause undesirable protection system operation which falls into the following categories: excessive trip delay, fail to trip, or false trip (unnecessary operation) [32, 33].

The CT saturation can lead to variety of serious, protection performance related issues. For example, an overcurrent relay with inverse time current characteristic may trip with additional delay due to shrinkage of the current input to the relay. As a consequence of the delayed tripping, a large portion of distribution systems may lose power supply because the protection relays may operate without the selective coordination.

Another effect of saturated CTs is that the tripping may not occur (failure to trip) because the sufficient current for tripping is unavailable in an instantaneous overcurrent relay. In that condition, the back-up protection will operate after an extended time delay by opening the CB in the adjacent zone. As a consequence, also this type of event would result in a more extensive outage because, e.g. disconnecting the entire busbar. Under most severe situation an essential busbar may be tripped connecting a generating unit or equipment which may lead to system instability or a blackout.

Furthermore, another consequence of saturated CTs is a false trip. A circulating current differential relays may falsely trip on through faults condition when one of the CTs saturates. Saturation of one CT will not reproduce the expected balancing current while the other CT could provide the expected current. The current difference from the CTs may result in an unwanted operation of the differential relay for a fault beyond its protected zone.

There are several practical options to minimize saturation effects of the conventional current transformers. Firstly, the quality of the iron core and its saturation

characteristics should be selected to cope with the anticipated high fault currents. Secondly, the secondary burden should be kept as low as possible. Although these solutions do not completely eliminate the saturation problem, in most situation they provide an acceptable CTs performance for protection purposes.

Another alternative that is promising to avoid the CT saturation problems is utilization of a different CT construction without ferrous a core. Some CT manufacturers have developed alternative designs such as air-gap CT, linear coupler, Rogowski coil, hybrid optical and pure optical current transducer [34]. From the time when CT was the first invented and implemented in power system protection in 1898 until the relatively recent invention of a new design optical current transducer (OCT), it has been a long development process spanning across more than a century [35, 36]. The OCT techniques are considered to be implemented in this thesis.

Second limitation of the conventional instrument transformer is limited measurement bandwidth.

Other potential problems of the conventional instrument transformers may result from size, weight, and insulation requirements. Increasing the power system generating and transfer capacity requires a bigger CT size CT while increasing system voltage requires a better insulation and suitable dimensional design. It will result the massive CT's structures that ultimately consume high cost.

2.7.2. Trends of protection relays

The need of protection system capable of automatically opening a CB to isolate a faulted section was introduced in the early 20th century [35]. Since the most popular technologies at that time were based on the electromechanical principles, the protection relays were also manufactured using electromechanical components. Electromechanical relay designs lasted almost for a century, and especially, the attracted armature relay types are still used in the system due to a significant advantage in terms of dependability.

Due to the new technology trends, the protection relays have evolved successively from electromechanical relays to static relay forms (1960), then changed into digital

relay configurations (1980), and finally into numerical (microprocessor) relay architectures (1984) [37, 38]. Compared to the first generation electromechanical relays, the technology has changed rapidly from the static (second generation) to microprocessor based relays (fourth generation) only in thirty years.

Despite many changes in the relay hardware design, the operating principles and characteristics of the electromechanical relays are still applied in many relay types today. Each technology-based development has brought some additional advantages such as the reduction in relay dimension, flexibility in the settings, and improvements in functionality.

The most significant achievement that only exists in the fourth generation relays is availability of several advanced functions and features covering enhanced protection, supervision, monitoring, measurement, data recording, diagnosis, communication, etc. Another achievement of the fourth generation is a shifting design from 'one relay per case' into single multi-function relay. It was common in the first three relay generations to use the term 'one relay per case' where a single relay was an item of hardware housed in a separate case. To obtain several protective functions in previous generations, a large number of relays had to be arranged and electrically wired together. However, in the last generation, in most cases it is possible to utilise a single multi-function relay which may be comprised of multiple high power microprocessors to deliver the required computational performance for executing simultaneously multiple protective algorithms in real time.

The most recent technology trend driven by the information and communication technology (ICT) is substation automation using IEC 61850 standard that will lead to power utility automation system [39]. This trend has a significant influence on the relay development in terms of functionality and performance. Some description of this trend will be explained in the following section 2.7.3 on modern digital substation.

Another potential influence of the ICT trends is the changing nature of power system protection that will include not only detecting abnormal system conditions and taking predetermined actions to isolate the faulted elements, but also cover several additional functions such as monitoring, communication, and control. The protection schemes in

this trend are also intended to have more functions by making corrective actions to mitigate the consequences of the abnormal conditions, to preserve system integrity, and to provide acceptable system performance [40-42]. Thus, it is expected that the recent trend will drive towards new designs and role of protection system that is very different from the design of conventional protection system.

2.7.3. Modern digital substation

In traditional substations, the CBs, CTs, VTs and protection relays are electrically wired together using copper cables. Technology developments have driven the invention of new protection equipment and apparatus with some advanced features which take advantage of modern digital technology, communications and standards. These developments will lead to new substation architectures known as substation automation systems.

The automation system architectures of the modern digital substation are based on the IEC 61850 standard as shown in Figure 2.13 [39],[43-45]. This IEC regulation covers communication standard between devices in the substation, and related system requirements. The modern digital substations consist of several key components and elements which include [45-49]:

- Intelligent electronic devices (IED) – substation protective devices.
- Station and process bus – the communication bus for exchanging signals between two levels. Station bus is for the bay level IED and station control, while process bus is for the bay level IED and system equipment, devices and transducers.
- GPS time clock – precise time synchronisation of all devices in the substation as well as synchronisation at different locations.
- Merging units – collect signals from equipment and transducers as well as interfacing to the bay level.
- Instrument transformer (CTs and VTs), CBs and other field sensors.
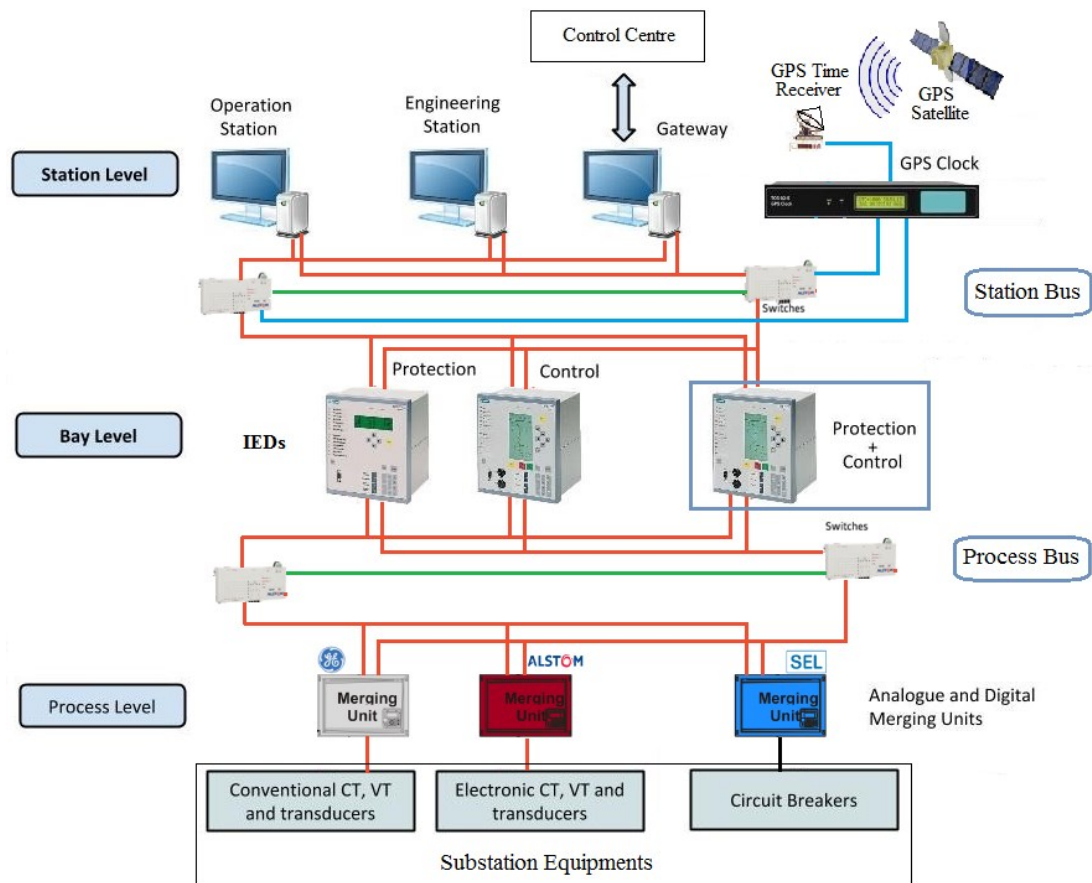
Figure 2.13   Simplified architecture of substation automation system [39],[43-45]

Installations of the modern protection equipment in the traditional substations have created a mixture of conventional and non-conventional technology. Since the modern digital substations utilise simple connection methods using fibre-optic communication media, integration of mixed technologies requires interfacing devices (merging units) between the traditional analogue signals, and the digital protection and control IEDs at the bay level.

The substation automation system offers numerous benefits over the traditional substation with conventional arrangements that are listed below [50]:

- Easier, safer, and simpler installation (reduce cost of copper cabling)
- Easy and fast maintenance
- better EMC performance and isolation of circuits
- Better reliability (redundant system in station and process bus)

- High measurement accuracy, supervision and data record
- Interoperability of devices from different manufacturers
- Increased performance with fast data transfer.

Although substation automation system offers many benefits, there are some barriers in their implementation such as the stakeholders still rely on the conventional substation technology because it has been proven in operation for many years. Other barriers include the lack of proven implementation of substation automation system. Since the substation automation system is completely changing the substation architectures that are radically different from the conventional substation. Therefore, a proven implementation of the substation automation is needed in order to challenge stakeholders' paradigm, to build their confidence, and to gain practical experience in the area of power utility automation.

2.8. Summary

This chapter discussed the basic principles and methods of power system protection. Various requirements of protection system were explained in detail. Components of protection system were presented including detailed description of voltage and current transformers. Moreover, circulating current differential protection and some requirements related to busbar differential protection were also revealed. Review of protection system also included limitation of conventional CTs, protection relay trends, and modern digital substations.

The key points of this chapter are the CT saturation issue and busbar protection scheme. For future trend in the power system protection, the optical current sensors could be a potential solution for substituting the old fashioned ferrous core CT in order to overcome the CT saturation issue. In line to the optical current sensor development, optical methods are investigated to create a new optical busbar differential protection scheme. This new optical protection scheme is intended to be a protection solution in order to meet the requirements of busbar protection for the future power system trends.

The following chapter will provide reviews on optics topic and optical methods for current measurement and the next two chapter will investigate on optical configuration of busbar differential protection scheme.

2.9. References for chapter 2

[1]   IEE, *Power system protection 1: Principles and components* vol. 1. London: Institution of Electrical Engineers - London, 1995.

[2]   Alstom, Ed., *Network Protection & Automation Guide*. London: Alstom Grid, 2011, p.^pp. Pages.

[3]   C. R. Mason. *The Art & Science of Protective Relaying*.

[4]   IEE, *Power System Protection* vol. 1. London: Institution of Electrical Engineers, 1995.

[5]   S. H. Horowitz, *Power System Relaying 3e*, 2008.

[6]   P. M. Anderson. (1999). *Power System Protection*.

[7]   IEEE. (2001). *IEEE Recomended Practice for Protection and Coordination of Industrial and Commercial Power Systems*.

[8]   Y. G. Paithankar and S. R. Bhide, *Fundamentals of Power Systems Protection*, Second ed. ed. New Delhi: PHI Learning Private Limited, 2012.

[9]   S. Ward, B. Gwyn, G. Antonova, and et-al, "Redundancy considerations for protective relaying systems," in *2010 63rd Annual Conference for Protective Relay Engineers*, 2010, pp. 1-10.

[10]   ABB. *Power System Protection, 8.13 Backup protection*. Available: https://library.e.abb.com/public/d1ef27cd5e3e586fc125795f004356ff/DAHandbook_Section_08p13_Backup_Protection_757293_ENa.pdf

[11]   W. A. Elmore, *Protective relaying theory and applications [internet resource]*, 2nd ed., rev. and expanded. ed. New York: New York : Marcel Dekker, 2004.

[12]   IEEE, "IEEE Standard Definitions for Power Switchgear," *IEEE Std C37.100-1992,* p. 0_1, 1992.

[13]   NERC. (2008). *Protection System Reliability - Redundancy of Protection System Elements* [Technical paper]. Available: http://www.nerc.com/docs/pc/spctf/Redundancy_Tech_Ref_1-14-09.pdf

[14]   IEEE. (2007). *IEEE Recomended Practice for the Design of Reliable Industrial and Commercial Power Systems*.

[15]   IEEE, "Redundancy considerations for protective relaying systems," 2010.

[16]   J. Sykes, V. Madani, J. Burger, M. Adamiak, and W. Premerlani, "Reliabilty of protection systems (what are the real concerns)," in *Protective Relay Engineers, 2010 63rd Annual Conference for*, 2010, pp. 1-16.

[17]   M. Zima. (2002, 6 June 2001). Special Protection Schemes in Electric Power Systems - Literature Survey. 22. Available: http://e-collection.library.ethz.ch/eserv/eth:25263/eth-25263-01.pdf

[18]   NERC. (2015, Proposed Definition of "Special Protection System" *NERC*. Available:
http://www.nerc.com/pa/Stand/Prjct201005_3RmdialActnSchmsPhase3ofPrt
ctnSystmsDL/Proposed_SPS_Definition_11232015_final.pdf

[19]   IEEE, "IEEE Guide for Protective Relay Applications to Transmission Lines," *IEEE Std C37.113-1999,* pp. 1-113, 2000.

[20]   W. A. Elmore, *Protective Relaying [electronic resource] : Theory and Applications*, 2nd ed.. ed. Hoboken: Hoboken : Taylor and Francis, 2003.

[21]   IEEE. (1978). *IEEE Standard Requirements for Instrument Transformers*.

[22]   IEEE, "IEEE Standard Requirements for Instrument Transformers," *IEEE Std C57.13-2008 (Revision of IEEE Std C57.13-1993),* pp. c1-82, 2008.

[23]   ABB, "ABB Product - Instrument Transformers," Zurich, Switzerland2017.

[24]   Siemens, "Siemens Product - Instrument Transformers," 2018.

[25]   B. Ravindranath and M. Chander, *Power System Protection and Switchgear*: Wiley Eastern Limited, 1977.

[26]   R. L. Alexander, "Intelligent electronic device (IED) technology SCADA and 3O metering," in *2002 Rural Electric Power Conference. Papers Presented at the 46th Annual Conference (Cat. No. 02CH37360)*, 2002, pp. C6-1.

[27]   J. Holbach, "Comparison between high impedance and low impedance bus differential protection," in *Power Systems Conference, 2009. PSC '09.*, 2009, pp. 1-16.

[28] W. Schossig. (2008) Introduction to the History of Differential Protection. *PAC World Magazine*. Available: https://www.pacw.org/fileadmin/doc/SummerIssue08/history_summer08.pdf

[29] J. L. Blackburn, *Protective relaying : principles and applications*, 3rd ed.. ed. Boca Raton, FL: Boca Raton, FL : CRC Press, 2007.

[30] IEEE, "IEEE Guide for Protective Relay Applications to Power System Buses," *IEEE Std C37.234-2009,* pp. C1-115, 2009.

[31] IEEE, "Transient response of current transformers," *IEEE Transactions on Power Apparatus and Systems,* vol. 96, pp. 1809-1814, 1977.

[32] A. Y. Wu, "The Analysis of Current Transformer Transient Response and Its Effect on Current Relay Performance," *IEEE Transactions on Industry Applications,* vol. IA-21, pp. 793-802, 1985.

[33] J. R. Linders, C. W. Barnett, J. W. Chadwick, P. R. Drum, K. J. Khunkhun, W. C. Kotheimer, P. A. Kotos, D. W. Smaha, J. W. Walton, P. B. Winston, and S. E. Zocholl, "Relay performance considerations with low-ratio CTs and high-fault currents," *IEEE Transactions on Industry Applications,* vol. 31, pp. 392-404, 1995.

[34] IEEE, "Optical current transducers for power systems: a review," *Power Delivery, IEEE Transactions on,* vol. 9, pp. 1778-1788, 1994.

[35] W. Schossig. (2007, 11 Oct 2008) History of Protection. *PAC World Magazine*. Available:
https://www.pacw.org/fileadmin/doc/AutumnIssue07/history_autumn07.pdf

[36] Alstom. (01/06/2013). *COSI-CT LC/LCD Low Ratio Optical Curent Transformers*. Available: http://www.nxtphase.com/

[37] M. Begovic, D. Novosel, and M. Milisavljevic, "Trends in power system protection and control," in *Systems Sciences, 1999. HICSS-32. Proceedings of the 32nd Annual Hawaii International Conference on*, 1999, p. 8 pp.

[38] L. P. Cavero and J. W. Chadwick, "Trends in power system protection and control systems," in *Developments in Power System Protection, 2001, Seventh International Conference on (IEE)*, 2001, pp. 442-445.

[39] ABB, "ABB Review Special Report IEC 61850," Zurich, Switzerland, ABB Technical Journal, August 2010 (2010).

[40]   IEEE, "Application Considerations of IEC 61850/UCA 2 for Substation Ethernet Local Area Network Communication for Protection and Control," 2005.

[41]   J. Bertsch, C. Carnal, D. Karlson, J. McDaniel, and V. Khoi, "Wide-Area Protection and Power System Utilization," *Proceedings of the IEEE,* vol. 93, pp. 997-1003, 2005.

[42]   S. Skok, *System integrity protection scheme based on PMU technology*: Institution of Engineering and Technology, 2016.

[43]   M. Kanabar. (2011). *Investigating Performance and Reliability of Process Bus Networks for Digital Protective Relaying*.

[44]   T. S. Sidhu, M. G. Kanabar, and P. P. Parikh, "Implementation Issues with IEC 61850 Based Substation Automation Systems " presented at the Fifteenth National Power Systems Conference (NPSC), Bombay, 2008.

[45]   IEEE, "Centralized Substation Protection and Control," 2015.

[46]   Y. Rangelov, N. Nikolaev, and M. Ivanova, "The IEC 61850 standard ; Communication networks and automation systems from an electrical engineering point of view," in *2016 19th International Symposium on Electrical Apparatus and Technologies (SIELA)*, 2016, pp. 1-4.

[47]   A. Apostolov and D. Tholomier, "Impact of IEC 61850 on Power System Protection," in *2006 IEEE PES Power Systems Conference and Exposition*, 2006, pp. 1053-1058.

[48]   S. Brahma, "Advancements in Centralized Protection and Control Within a Substation," *IEEE Transactions on Power Delivery,* vol. 31, pp. 1945-1952, 2016.

[49]   M. Adamiak, D. Baigent, and R. Mackiewicz. (2014). *IEC 61850 Communication Networks and Systems In Substations: An Overview for Users*. Available: http://www.gegridsolutions.com/multilin/journals/issues/spring09/iec61850.pdf and http://www.ucaiug.org/Meetings/CIGRE_2014/USB%20Promo%20Content/GE%20Digital%20Energy/Whitepapers/IEC%2061850%20Communication%20Networks%20and%20Systems%20in%20Substations.pdf

[50]   S. Meier and S. Kunsman. (2016). *Protection and Control System Impacts from The Digital World*. Available: http://new.abb.com/substation-automation/systems/whitepapers/protection-and-control-system-impacts-from-the-digital-world?elqTrackId=9ef19e246405455dbaf0991e92db8432&elqaid=716&elqat=2

Chapter 3. Optics and Optical Methods of Current and Voltage Measurement

3.1. Introduction

This chapter presents an overview of principles and methods related to optics and optical sensing of both voltage and current. The chapter is started with optics section in which the main optical principles such as polarized light waves, Fresnel's equation and vector transformation are explained. It is then followed by the description of the propagation of polarized light in optical crystal, Jones principle, and Jones Cartesian matrices transformation. Polarized light models are revealed and followed by a more detailed description of the optical device's model using matrix representation. In optical measurement techniques section, optical methods for measuring voltage and current in power system are explained including properties of some crystals used for sensor heads. Last section reviews on all-optical differential protection scheme.

3.2. Optics and polarized light

3.2.1. Electromagnetic waves

The harmonic variations of the electric and magnetic fields are always perpendicular to one another and to the direction of propagation given by k, as plotted by the orthogonal set of axes in Figure 3.1 [1].
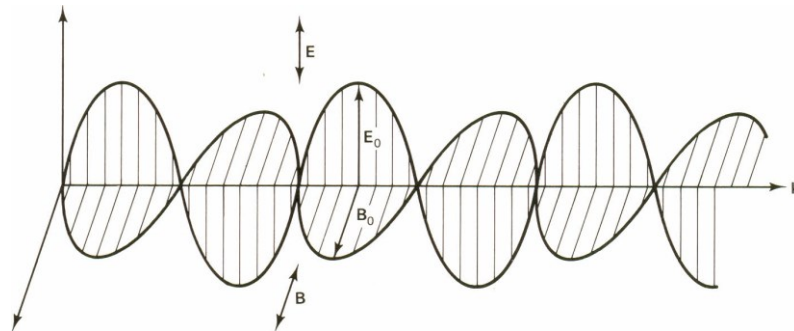
Figure 3.1   Electromagnetic wave [1]

These variations can be described by the harmonic wave equation in the form [1],[2]

$$\mathbf{E} = \widetilde{\mathbf{E}}e^{i(\mathbf{k}.\mathbf{r}-\omega t)} \tag{3.1a}$$

$$\mathbf{B} = \widetilde{\mathbf{B}}e^{i(\mathbf{k}.\mathbf{r}-\omega t)} \tag{3.1b}$$

where $\mathbf{E}$ and $\mathbf{B}$ represent the electric and magnetic fields, respectively, and $\widetilde{\mathbf{E}}$ and $\widetilde{\mathbf{B}}$ are their amplitudes. From electromagnetic theory, the relation of the field amplitudes is given by equation (3.2)

$$E_0 = c\, B_0 \tag{3.2}$$

For a specified time and place, equation (3.2) can be rewritten as

$$E = c\, B \tag{3.3}$$

The transferred power of electromagnetic wave per unit area, S, is calculated as:

$$S = \epsilon_0 c^2 EB \tag{3.4}$$

Since the vectors $\mathbf{E}$ and $\mathbf{B}$ are orthogonal, the cross product of them will have the same direction as the wave propagation. Therefore, the transferred power S can be written as in equation (3.5) and S is also called the Poynting vector.

$$\mathbf{S} = \epsilon_0 c^2 \mathbf{E} \times \mathbf{B} \tag{3.5}$$

The time average of delivered power per unit area (irradiance), E_e, is

$$E_e = \langle |\mathbf{S}| \rangle = \epsilon_0 c^2 \langle E_0 B_0\, sin^2(\mathbf{k} \cdot \mathbf{r} \pm \omega t) \rangle \tag{3.6}$$

Since the average of the functions $sin^2\theta$ and $cos^2\theta$ over a period is easily shown to be exactly ½, equation (3.6) for the case of free space can be expressed as

$$\begin{aligned} E_e &= \frac{1}{2}\epsilon_0 c^2 E_0 B_0 \\ E_e &= \frac{1}{2}\epsilon_0 c\, E_0{}^2 \\ E_e &= \frac{1}{2}\left(\frac{c}{\mu_0}\right) B_0{}^2 \end{aligned} \tag{3.7}$$

The alternative forms of equation (3.7) is equation (3.8) [3] which is applied to a medium of refractive index n if ϵ_0 is replaced by ϵ/n^2 and c is replaced by velocity $= {}^c/_n$.

$$E_e = \frac{1}{2}\epsilon\, v^2 E_0 B_0$$
$$E_e = \frac{1}{2}\frac{\epsilon}{n}\, v\, E_0{}^2 \qquad\qquad (3.8)$$
$$E_e = \frac{1}{2}\left(\frac{v/n}{\mu_0}\right) B_0{}^2$$

3.2.2. Polarized Light Waves

The electric vector of a linearly polarized wave of a uniform transverse electric (TE) travelling plane wave varies with position r and time t is represented by

$$E(r,t) = [\tilde{E}\cos\,(\omega t - k.r)]\hat{u} \qquad\qquad (3.9)$$

where $\hat{u}$ is a unit vector in the direction of the linear polarization, orthogonal to the direction of wave propagation that is given by the constant *wave vector* k [4, 5]. $\tilde{E}$ is amplitude of the oscillation which is independent of r and t. In order to describe the uniform TE (transverse-electric) plane wave in arbitrary polarization (linearly or elliptically), equation (3.9) can be generalized to become

$$E(r,t) = [\tilde{E}\cos\,(\omega t - k.r + \delta)]\hat{u} + [\widetilde{E'}\cos\,(\omega t - k\cdot r + \delta')]\hat{u}', \qquad (3.10)$$

$$\hat{u}\cdot\hat{u} = \hat{u}'\cdot\hat{u}' = 1, \qquad \hat{u}\cdot\hat{u}' = \hat{u}\cdot k = \hat{u}'\cdot k = 0$$

$\hat{u}$ and $\hat{u}'$ are two orthogonal unit vectors in the wave-front along the electric vector that is resolved into components of amplitudes $\tilde{E}$ and $\widetilde{E'}$ and phases δ and δ', respectively.

3.2.2.1. Description of uniform transverse electric (TE) plane wave

Suppose the wave in equation (3.10) that is assumed propagating along the positive direction of the z-axis of a xyz orthogonal, right-handed, and Cartesian coordinate

system, the unit vector $\hat{\boldsymbol{u}}$ and $\hat{\boldsymbol{u}}'$ are chosen parallel to the positive direction of x and y axes. As a consequence, equation (3.10) becomes

$$\boldsymbol{E}(z,t) = \left[\tilde{E}_x \cos\left(\omega t - \frac{2\pi}{\lambda}z + \delta_x\right)\right]\hat{\boldsymbol{x}} + \left[\tilde{E}_y \cos\left(\omega t - \frac{2\pi}{\lambda}z + \delta_y\right)\right]\hat{\boldsymbol{y}} \qquad (3.11)$$

In equation (3.11) $\tilde{E}_x$ and $\tilde{E}_y$ are amplitudes of oscillation of the electric-field component along x and y axes, and δ_x and δ_y represent the respective phases of these oscillations. $\hat{\boldsymbol{x}}$ and $\hat{\boldsymbol{y}}$ are unit vectors in the positive direction of the x and y axes.

Since considering the application of wave polarization and its modification by an optical device, the full representation of the wave in equation (3.11) is verbose. Therefore, a more concise mathematical description for the wave is needed as outlined by the following sequence of steps [4],[6]:

1. Once the fixed unit vectors $\hat{x}$ and $\hat{y}$ of the linearly polarized components of the wave have been chosen, there is no need to hold theses unit vectors in the mathematical representation. This can be achieved by grouping the scalar components in the form of 2x1 column vector (matrix) $\boldsymbol{E}$ as follows:

$$\boldsymbol{E}(z,t) = \begin{bmatrix} \tilde{E}_x \cos\left(\omega t - \frac{2\pi}{\lambda}z + \delta_x\right) \\ \tilde{E}_y \cos\left(\omega t - \frac{2\pi}{\lambda}z + \delta_y\right) \end{bmatrix} \qquad (3.12)$$

2. The temporal information of the wave can also be suppressed because the field components at all points in space for a monochromatic field are known to oscillate sinusoidal with time at the same frequency. Equation (3.12) can be replaced by (3.13).

$$\boldsymbol{E}(z) = e^{-j\frac{2\pi}{\lambda}z} \begin{bmatrix} \tilde{E}_x\, e^{j\delta_x} \\ \tilde{E}_y\, e^{j\delta_y} \end{bmatrix} \qquad (3.13)$$

3. The spatial information of the wave can be omitted by considering the fields over one fixed transverse plane. The intended mathematical description of a uniform TE plane wave is achieved when z=0 is substituted in equation (3.13) as follows

$$E(0) = \begin{bmatrix} \tilde{E}_x\, e^{j\delta_x} \\ \tilde{E}_y\, e^{j\delta_y} \end{bmatrix} \tag{3.14}$$

The vector $E(0)$ of equation (3.14) is the desired concise expression of a single plane wave that is known as *monochromatic, uniform and transverse electric*. This vector is also termed **Jones vector** of the wave with simple expression

$$E = \begin{bmatrix} E_x \\ E_y \end{bmatrix} \tag{3.15}$$

where

$$E_x = |E_x| e^{j\delta_x}, \quad E_y = |E_y| e^{j\delta_y} \tag{3.16}$$

3.2.2.2. Wave intensity

Intensity of an optical wave I is simply expressed as the sum of the squared amplitudes of the component oscillations along two mutually orthogonal directions [7]. This statement could be written as

$$I = |E_x|^2 + |E_y|^2 \tag{3.17}$$

or

$$I = E_x^* E_x + E_y^* E_y \tag{3.18}$$

In a more compact form, intensity I can be obtained by pre-multiplying the Jones vector E of equation (3.15) by its Hermitian adjoint E^*

$$I = E^* E \tag{3.19}$$

3.2.3. Coordinate transformation due to rotation effect

Rotation concept in physics is frequently understood as a coordinate transformation. There are two types of coordinate transformations as displayed in Figure 3.2 which are passive and active transformations [8],[9],[10].
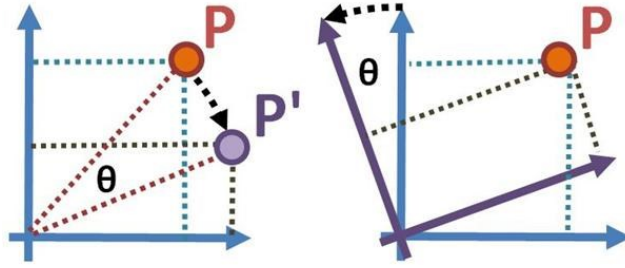
Figure 3.2   Active transformation (left) and passive transformation (right).

- The passive transformation refers to description of the same object in two different coordinate systems. The initial object (vector) is left unchanged, while the coordinate system and its basis object (vectors) are rotated. Thus, this transformation rotates the basis while keeping the (object) vector fixed. The matrix transformation of a vector corresponding to counter clockwise rotation by the angle θ is given by:

$$R_{passive} = R(\theta) = \begin{pmatrix} \cos\theta & \sin\theta \\ -\sin\theta & \cos\theta \end{pmatrix} \tag{3.21}$$

- The active transformation is a transformation of one or more objects with respect to the same coordinate system. This transformation rotates a vector in a fixed basis. The rotation matrix to achieve clockwise rotation of the vector by the angle θ is given by:

$$R_{active} = Rot(\theta) = \begin{pmatrix} \cos\theta & -\sin\theta \\ \sin\theta & \cos\theta \end{pmatrix} \tag{3.22}$$

The passive transformation will be applied in the following section, while the active transformation will be used in an optical current sensor representation.

3.2.4. Jones vector transformation under the effect of a coordinate rotation

The complex Jones vector in equation (3.15) is dependent upon the choice of the x and y coordinate-axes in the plane of the wave-front. When the coordinate system is rotated, the complex Jones vector representation is also changed accordingly.
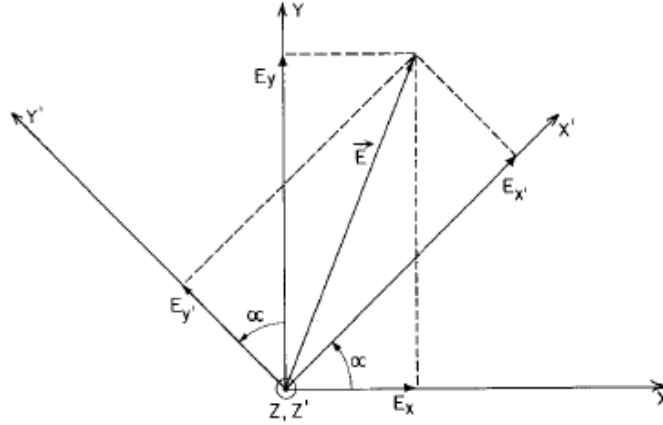
Figure 3.3   Revolution of the electric vector E along two non-coincident coordinate systems (x, y) and (x', y') [4]

Referring to Figure 3.3 [4], suppose $x'y'z'$ is a new coordinate system of the old xyz coordinate system whose z'-axis is coincident with the z-axis. By using the projections of the electric-field vector E along the old coordinate axes and the new coordinate axes, these projections are interrelated using matrix transformation in equation (3.21) and expressed [4]:

$$\begin{bmatrix} E_{x'} \\ E_{y'} \end{bmatrix} = \begin{bmatrix} \cos \alpha & \sin \alpha \\ -\sin \alpha & \cos \alpha \end{bmatrix} \begin{bmatrix} E_x \\ E_y \end{bmatrix} \tag{3.23a}$$

or more concisely,

$$E_{x',y'} = R(\alpha) \, E_{x,y} \tag{3.23b}$$

3.2.5. Fresnel's Equation

Fresnel equations describe the fraction of incident energy transmitted or reflected at a plane surface. Figure 3.4 shows a light beam at point P on a plane interface (the xy-plane) and the resulting reflected and refracted beams [1].
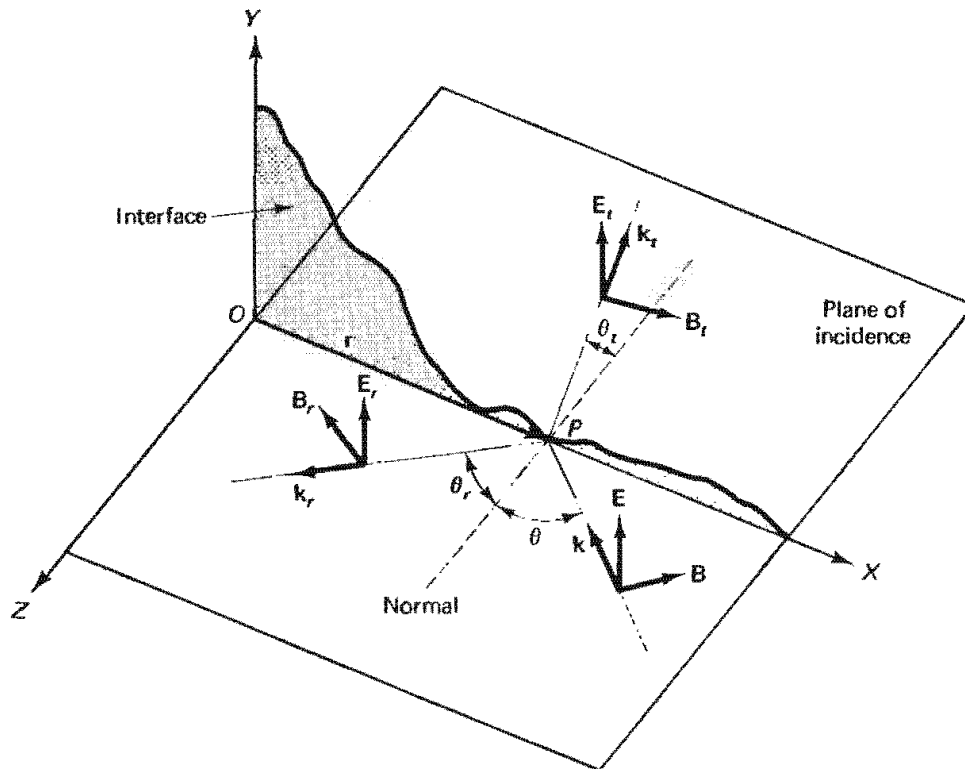
Figure 3.4   Defining diagram for incident, reflected, and transmitted beams at the XY plane interface when the electric field is perpendicular to the plane of incidence (TE mode) [1]

In terms of the choices made for the direction of E in Figure 3.4 [1], the requirements for the electric field and the corresponding magnetic fields for transverse electric (TE) mode, respectively, are

$$\text{TE:} \begin{cases} \boldsymbol{E}_{TE} + \boldsymbol{E}_{r-TE} = \boldsymbol{E}_{t-TE} \\ \boldsymbol{B}_{TE} \cos\theta - \boldsymbol{B}_{r-TE} \cos\theta = \boldsymbol{B}_{t-TE} \cos\theta_t \end{cases} \tag{3.24}$$

Using the similar manner and Figure 3.5 [1] for transverse magnetic (TM) mode, analogous to equation (3.24) is

$$\text{TM}: \begin{cases} \boldsymbol{B} + \boldsymbol{B}_{r-TM} = \boldsymbol{B}_{t-TM} \\ -\boldsymbol{E}_{TM} \cos\theta + \boldsymbol{E}_{r-TM} \cos\theta = -\boldsymbol{E}_{t-TM} \cos\theta_t \end{cases} \qquad (3.25)$$
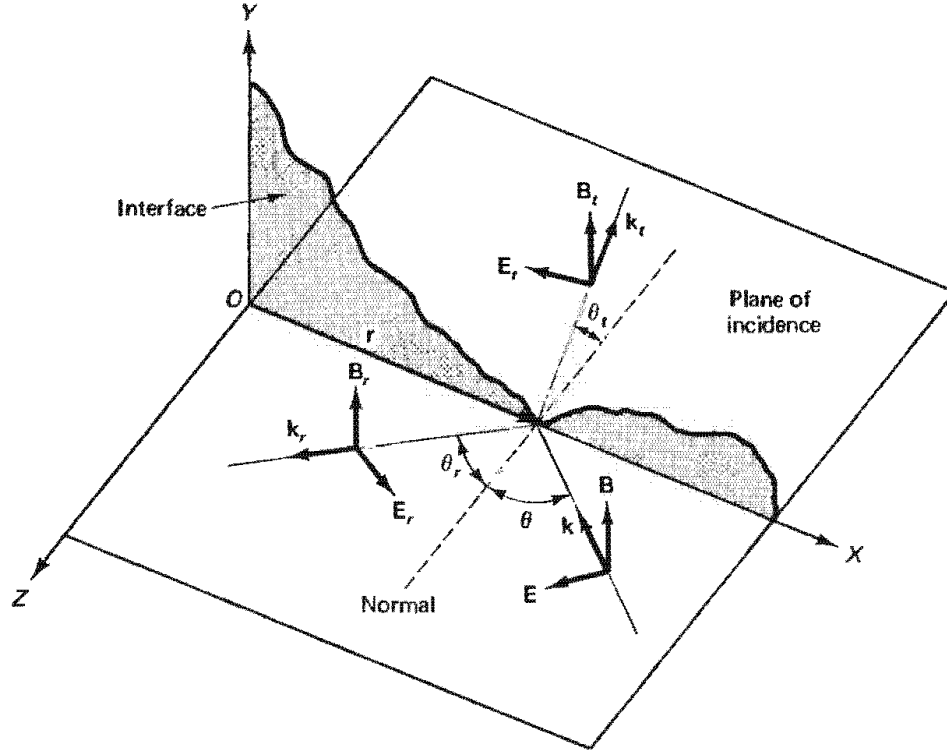
Figure 3.5   Defining diagram for incident, reflected, and transmitted beams at the XY plane interface when the magnetic field is perpendicular to the plane of incidence (TM mode) [1]

The magnetic fields of equation (3.24) and (3.25) can be expressed in terms of electric fields by the relationship

$$\boldsymbol{E} = v\boldsymbol{B} = \left(\frac{c}{n}\right)\boldsymbol{B} \qquad (3.26)$$

Writing the index of refraction for incident and refracting media as n_1 and n_2, respectively, equation (3.24) and (3.25) can be rewritten:

$$\text{TE}: \begin{cases} \boldsymbol{E}_{TE} + \boldsymbol{E}_{r-TE} = \boldsymbol{E}_{t-TE} & (3.27a) \\ \\ n_1\boldsymbol{E}_{TE} \cos\theta - n_1\boldsymbol{E}_{r-TE} \cos\theta = n_2\boldsymbol{E}_{t-TE} \cos\theta_t & (3.27b) \end{cases}$$

$$\textbf{TM}: \begin{cases} n_1 \boldsymbol{E}_{TM} + n_1 \boldsymbol{E}_{r-TM} = n_2 \boldsymbol{E}_{t-TM} & (3.28a) \\ \\ -\boldsymbol{E}_{TM} \cos\theta + \boldsymbol{E}_{r-TM} \cos\theta = -\boldsymbol{E}_{t-TM} \cos\theta_t & (3.28b) \end{cases}$$

First step, eliminating $\boldsymbol{E}_t$ from each pair of equations and solving for the *reflection coefficient* $r = \boldsymbol{E}_r/\boldsymbol{E}$, and introducing a *relative refractive index* $n \equiv n_2/n_1$ give:

$$\textbf{TE}: \quad r_{TE} = \frac{\boldsymbol{E}_{r-TE}}{\boldsymbol{E}_{TE}} = \frac{\cos\theta - n\cos\theta_t}{\cos\theta + n\cos\theta_t} \tag{3.29}$$

$$\textbf{TM}: \quad r_{TM} = \frac{\boldsymbol{E}_{r-TM}}{\boldsymbol{E}_{TM}} = \frac{n\cos\theta - \cos\theta_t}{n\cos\theta + \cos\theta_t} \tag{3.30}$$

Since n and θ_t are related to θ based on Snell's law i.e. $\sin\theta = n\sin\theta_t$, therefore θ_t could be eliminated using

$$n\cos\theta_t = n\sqrt{1 - \sin^2\theta_t} = \sqrt{n^2 - \sin^2\theta} \tag{3.31}$$

The results are

$$\textbf{TE}: \quad r_{TE} = \frac{\boldsymbol{E}_{r-TE}}{\boldsymbol{E}_{TE}} = \frac{\cos\theta - \sqrt{n^2 - \sin^2\theta}}{\cos\theta + \sqrt{n^2 - \sin^2\theta}} \tag{3.32}$$

$$\textbf{TM}: \quad r_{TM} = \frac{\boldsymbol{E}_{r-TM}}{\boldsymbol{E}_{TM}} = \frac{n^2\cos\theta - \sqrt{n^2 - \sin^2\theta}}{n^2\cos\theta + \sqrt{n^2 - \sin^2\theta}} \tag{3.33}$$

Second step, eliminating $\boldsymbol{E}_r$ instead of $\boldsymbol{E}_t$ in equation (3.27) and (3.28), similar steps lead to the following equations describing the *transmission coefficient, $t = \boldsymbol{E}_t/\boldsymbol{E}$*:

$$\textbf{TE}: \quad t_{TE} = \frac{\boldsymbol{E}_{t-TE}}{\boldsymbol{E}_{TE}} = \frac{2\cos\theta}{\cos\theta + \sqrt{n^2 - \sin^2\theta}} \tag{3.34}$$

$$\textbf{TM}: \quad t_{TM} = \frac{\boldsymbol{E}_{t-TM}}{\boldsymbol{E}_{TM}} = \frac{2n\cos\theta}{n^2\cos\theta + \sqrt{n^2 - \sin^2\theta}} \tag{3.35}$$

Equation (3.34) and (3.35) can also be found more quickly by using equation (3.27a) and (3.28a) which written in the form

$$\textbf{TE}: \qquad t_{TE} = r_{TE} + 1 \qquad\qquad (3.36)$$

$$\textbf{TM}: \qquad n\, t_{TM} = r_{TM} + 1 \qquad\qquad (3.37)$$

Equation (3.32) to (3.35) are the Fresnel equations, giving reflection and transmission coefficients, the ratio of both reflected and transmitted E-field amplitude to the incident E-field amplitude.

3.3. Propagation of polarized light through polarizing optical devices

The concept of polarized light that propagates through polarizing optical devices is the basis for the proposed configuration of all-optical differential protection scheme. In this scheme, a polarized light beam propagates through a series of successive optical devices. A detailed description of the mathematical formulation is presented in the following four sub-sections.

3.3.1. Basic concept of polarizing optical devices model

In this section, the polarization modifying interaction between the polarized light and the polarizing optical component is explained. In this interaction, the following assumptions are made [4]:

1) The light beam is approximated by a uniform TE infinite plane wave that may be either monochromatic or quasi-monochromatic.
2) The interaction between an incident beam and an optical device is linear and frequency-conserving. This excludes some effects such as non-linear optical effects, inelastic light scattering of Raman or Brillouin type and allied effects.
3) Only the external (terminal) properties of an optical device or an optical system are emphasized, with less attention paid to the details of the internal polarization-modifying processes that are responsible for such terminal behavior.

3.3.2. Jones Principle

Jones principle is a formal system for analysing both the light and optical material interaction as shown in Figure 3.6. It provides an efficient method for describing the

polarized light and propagation of the electric field through several polarizing components at the amplitude level [6]. When the polarized wave incident $\boldsymbol{E}_i$ propagates in a single polarizing optical system J, one or more modified TE exiting waves $\boldsymbol{E}_o$ are emerged from the optical system. This Jones formalization is constrained in equation (3.38)

$$\boldsymbol{E_o} \;=\; J\,\boldsymbol{E_i} \tag{3.38}$$
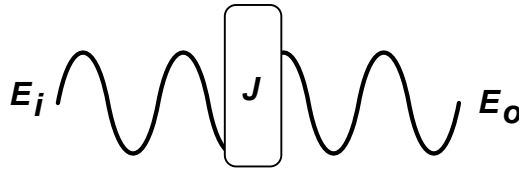
Figure 3.6   Interaction of polarized light and optical component J

Because the polarized light is utilized as the transverse wave carrier in the proposed optical differential protection scheme (including the optical current sensor), it brings a consequence that the polarized light has to be modelled in terms of its two linear orthogonal polarizations. Therefore, the polarized light $\boldsymbol{E}$ could be represented by the two elements vector horizontal (E_x) and vertical (E_y) to describe its state of polarization (SOP). As result, the use of a **[2x1]** column matrix is a suitable representation.

Moreover, since $\boldsymbol{E}_i$ consists of two-element vector E_{ix} and E_{iy}, the modified emerging wave $\boldsymbol{E}_o$ also contains two element vector E_{ox} and E_{oy}. In the absence of non-linearity and other frequency-changing processes, the pair of oscillations E_{ox} and E_{oy} at the output of the optical system is related to the pair of oscillations E_{ix} and E_{iy} at the input of the optical system and can be described by the linear equations (3.39).

$$E_{ox} \;=\; J_{11}\,E_{ix} + J_{12}\,E_{iy} \tag{3.39a}$$
$$E_{oy} \;=\; J_{21}\,E_{ix} + J_{22}\,E_{iy} \tag{3.39b}$$

These equations can be combined in a matrix form (3.40)

$$\begin{bmatrix} E_{ox} \\ E_{oy} \end{bmatrix} = \begin{bmatrix} J_{11} & J_{12} \\ J_{21} & J_{22} \end{bmatrix} \begin{bmatrix} E_{ix} \\ E_{iy} \end{bmatrix} \qquad (3.40)$$

The equation (3.40) expresses a fundamental step of the lanes-matrix formulation based on the Jones principle in [11-17] and some other research publications [4, 18-20].

3.3.3. Jones Principle for successive series of optical devices

When a polarizing optical system consists of a series of optical devices (as shown in Figure 3.7), the cumulative effect of multiple optical devices can be determined by a simple multiplication of the matrices where output of the first device becomes input for the next device and so on [11],[21]. This principle is expressed by equation (3.41)

$$\boldsymbol{E_o} = J_m J_{m-1} \quad \cdots \quad J_2 J_1 \boldsymbol{E_i} \qquad (3.41)$$

where $\boldsymbol{E_o}$ and $\boldsymbol{E_i}$ are matrices representing polarized output and input light respectively, m is a number of optical components in the path, $J_m, J_{m-1}, \ldots, J_2 J_1$ are matrices representative of the material that introduces an optical polarizing effect. This equation is called Jones formalization for optical devices connected in series.
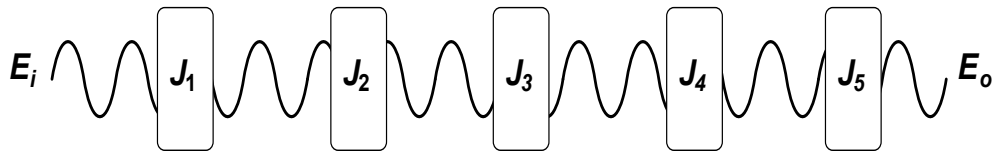
Figure 3.7   Jones formalism with successive optical components in series

3.3.4. Transformation of the Jones Matrix under the effect of a Cartesian coordinate rotation

In the previous section, the electric vectors of the incident $\boldsymbol{E_i}$ and outgoing $\boldsymbol{E_o}$ waves of an optical system in equations (3.41) are referred to the Cartesian coordinate systems. These Cartesian coordinate systems are the same for all optical systems, and

therefore, they can be directly linked together without any coordinate system transformations.

A general approach should be explained to deal with successive optical system problems when the second (other) device is rotated to a different angle and the axes does not match the coordinate system. Therefore, a new coordinate system is needed due to the effect of a coordinate rotation. Suppose the input coordinate system is rotated around the incident wave-vector k with an angle α counter-clockwise when looking against k, and let, at the same time, the output coordinate system is also rotated by the same angle in the same sense. The effect of this rotation according to equation (3.23) is to transform $\boldsymbol{E}_i \rightarrow R(\alpha)\boldsymbol{E}_i$ and $\boldsymbol{E}_o \rightarrow R(\alpha)\boldsymbol{E}_o$ [4, 21].

A procedure of finding this general approach could be explained as follows. Multiplying of equation (3.38) by $R(\alpha)$ gives

$$R(\alpha) \, \boldsymbol{E}_o = R(\alpha) \, J \, \boldsymbol{E}_i \qquad (3.42)$$

and using the fact that $R(-\alpha) \, R(\alpha) = I$ (identity matrix), it can be rewritten

$$[R(\alpha) \, \boldsymbol{E}_o] = [R(\alpha) \, J R(-\alpha)] \, [\, R(\alpha)\boldsymbol{E}_i] \qquad (3.43)$$

Equation (3.43) shows that the effect of rotating both input and output coordinate systems by the same angle α corresponds to transform the Cartesian Jones matrix according to

$$J_{new} = [R(\alpha) \, J_{old} \, R(-\alpha)] \qquad (3.44)$$

J_{old} and J_{new} represent Jones matrices of the optical system before and after the rotation, respectively.

3.4. Polarized light and optical devices models

The propagation of light through polarizing optical systems employing Jones matrix representation will be examined. The explanation will be focused on perfect models of the polarized light and optical devices that contribute to entire model in the optical busbar differential protection scheme.

3.4.1. Perfect representation of the polarized light

A simplified model of the polarized light as expressed in equation (3.15) could be used to describe the state of polarization. The Jones vector for horizontally linearly polarized light is simply $\begin{bmatrix} 1 \\ 0 \end{bmatrix}$. This simplified form is the *normalized* form of the vector. The general matrix representation for a linearly polarized light that has angle α with respect to *x*-axis is

$$E = \begin{bmatrix} \cos \alpha \\ \sin \alpha \end{bmatrix} \tag{3.45}$$

The general form of Jones matrix $E = \begin{bmatrix} E_x \\ E_y \end{bmatrix}$. The ideal representation is achieved by replacing E_x or E_y with a fixed value.

3.4.2. Perfect optical devices model by Jones matrix representation

Perfect model for the three optical devices representation are:

- Polariser

The perfect polariser matrices [3, 4] are

$$J_{PV} = \begin{bmatrix} 0 & 0 \\ 0 & 1 \end{bmatrix}, \text{ a linear polariser, TA vertical} \tag{3.46}$$

and

$$J_{PH} = \begin{bmatrix} 1 & 0 \\ 0 & 0 \end{bmatrix}, \text{ a linear polariser, TA horizontal} \tag{3.47}$$

- Optical current sensor

The perfect optical current sensor matrix can be stated [3, 4]

$$J_{OCS} = \begin{bmatrix} \cos \beta & -\sin \beta \\ \sin \beta & \cos \beta \end{bmatrix}, \text{ rotator by angle } + \beta \tag{3.48}$$

- Free propagation

The Jones matrix for the free propagation isotropic medium is expressed

$$J_I = \begin{bmatrix} 1 & 0 \\ 0 & 1 \end{bmatrix} \qquad (3.49)$$

3.4.3. Optical device modelling by complex function representation

Each optical device in the proposed configuration of all optical differential protection scheme should be modelled in order to conduct a simulation [22]. The optical devices will be modelled using complex functions of Jones matrix to provide a realistic representation.

To represent the optical devices, the interaction between the incident wave and the optical system is described by the Jones formalization as in equation (3.15). In that equation, the [2x2] matrix J of the optical device and its elements J_{ij}, are complex functions [6],[23],[24]. Therefore, the Jones matrix J is a function of [4]:

1) Frequency or wavelength of the incident wave;
2) Type and characteristic of optical device under consideration;
3) Orientation of the system with respect to the incident wave vector;
4) Location of the input and output reference coordinate planes $z = 0$ and $z' = 0$, respectively;
5) Azimuthal orientation of the input and output transverse coordinate axes (x, y) and (x', y'), around the incident and the outgoing wave vectors, respectively; and
6) The particular outgoing plane wave, if more than one such wave is generated as a result of the interaction between the incident wave and the optical system.

Basic models of the transmission type optical devices are described independently for each optical device. The basic models cover [4],[3],[25]:

1. Isotropic retardation (phase-plate) model
2. Absorbance (absorption) model
3. Dichroic model
4. Birefringence model
5. Faraday effect model

Although the basic models of the optical devices only considered as an independent single model, they could describe behaviour of the optical device. The mathematical representation using complex function by Jones formulation becomes very useful when two or more models have a contribution at the same time in an optical device.

In order to represent the fundamental optical device models, some variables are defined as follows:

c is the speed of light in the vacuum,

d is the section thickness of the medium.

k is the extinction coefficient of the medium.

k_e is the extraordinary extinction coefficients of the medium for the linearly polarized light parallel to the transmission axis.

k_o is the ordinary extinction coefficients of the medium for the linearly polarized light perpendicular to the transmission axis.

λ is a vacuum wavelength of the linearly polarized wave that passes through a section of the medium,

n is a *refractive* index of the medium,

n_e is the extraordinary refractive indices of the medium.

n_o is the ordinary refractive indices of the medium.

$(n_e - n_o)$ is commonly called the birefringence of the medium

n_x is the slow axis refractive indices of the medium.

n_y is the fast axis refractive indices of the medium.

θ denotes the magnitude of rotation of the axis of the polarization state per unit path length in the medium.

The above symbols will be used in the following sections when describing optical device models.

3.4.3.1. Isotropic retarder model

The first basic optical device is isotropic retarder behaviour. A simple [2x2] Jones matrix J which describes free propagation of a plane wave of light over a distance d without encountering any interaction is given by equation (3.50) [4].

$$\begin{bmatrix} E_{ox} \\ E_{oy} \end{bmatrix} = \begin{bmatrix} e^{-j\frac{2\pi}{\lambda}nd} & 0 \\ 0 & e^{-j\frac{2\pi}{\lambda}nd} \end{bmatrix} \begin{bmatrix} E_{ix} \\ E_{iy} \end{bmatrix} \tag{3.50}$$

This equation expresses the simple fact that the polarized light, whose vacuum wavelength is λ has been retarded by $\frac{2\pi}{\lambda}nd$.

The optical device in this case is a plane-parallel section of an isotropic medium of refractive index n through which the plane wave is freely propagating. The input and output coordinate systems (x, y) and (x', y') coincide with the bounding planes and are aligned in parallel as depicted in Figure 3.8.
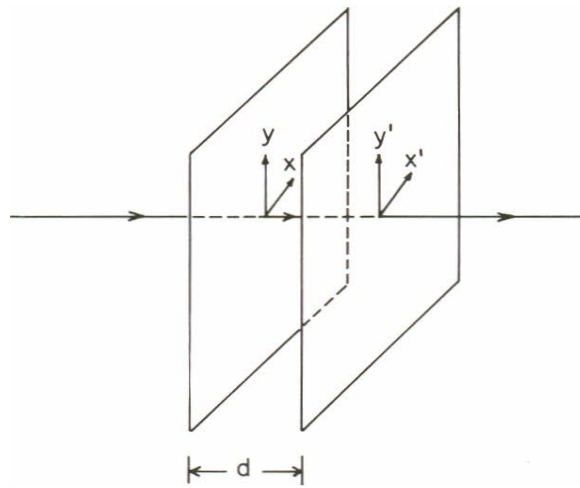
Figure 3.8   A plane-parallel section of an isotropic medium [4]

The Jones matrix for this first polarizing optical device which is called an isotropic retarder (or phase-plate) can be written as

$$\boldsymbol{J_{b1}} = \begin{bmatrix} e^{-j\frac{2\pi}{\lambda}nd} & 0 \\ 0 & e^{-j\frac{2\pi}{\lambda}nd} \end{bmatrix} \tag{3.51}$$

3.4.3.2. Isotropic refraction and absorption model

Second behavioural model of the optical device is an isotropic retarder and absorber. For this model, a section of medium with thickness d acts as an isotropic retarder and absorber which means that the medium has characteristics both isotropically-refracting

and isotropically-absorbing at the same time. As a result, a linearly polarized plane wave is retarded and attenuated after travelling a distance d by an amount that is independent of the direction of propagation or the state of wave polarization. The Jones matrix representation for this medium is

$$J_{b2} = \begin{bmatrix} e^{-j\frac{2\pi}{\lambda}(n-jk)d} & 0 \\ 0 & e^{-j\frac{2\pi}{\lambda}(n-jk)d} \end{bmatrix} \qquad (3.52)$$

This Jones matrix is simply obtained from the isotropic retarder equation (3.51) by including the complex index of refraction $(n - jk)$ in place of the real index of refraction n and where k is called the extinction coefficient of the medium.

3.4.3.3. Linearly birefringence model

The third behavioural model of an optical device is a birefringence behaviour which occurs when the medium is not isotropic but rather uniaxially linearly birefringent. The wave is propagating through the medium in two orthogonal propagation directions, either perpendicular or parallel with respect to the optic axis of this medium as shown in Figure 3.9 [26].
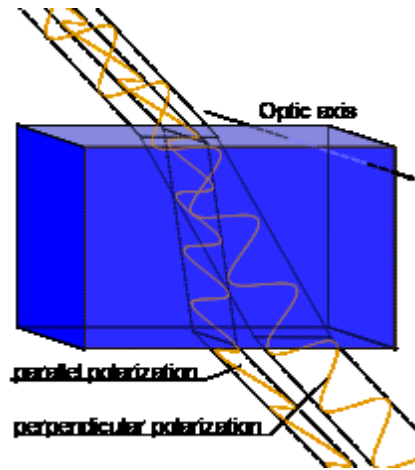
Figure 3.9   A birefringent medium behaviour with a polarized light [26]

On one hand, when the wave is linearly polarized and propagating in the perpendicular direction to the optic axis, the wave will experience a refractive index n_o and will travel at a speed c/n_o. On the other hand, when the wave is linearly polarized and

travelling in parallel to the optic axis, the wave will experience a different specific refractive index n_e and will travel at a speed c/n_e, where c is the speed of light in vacuum. Both n_o and n_e are commonly known as the ordinary and the extraordinary refractive indices of the medium, respectively. When the transverse electric vector of the wave has components both parallel (x) and perpendicular (y) to the optic axis, the effect of wave propagation through a distance d is expressed by

$$\boldsymbol{J_{b3}} = \begin{bmatrix} e^{-j\frac{2\pi}{\lambda}\, n_e\, d} & 0 \\ 0 & e^{-j\frac{2\pi}{\lambda}\, n_o\, d} \end{bmatrix} \tag{3.53}$$

The quantity $(n_e - n_o)$ is commonly called the birefringence of the medium. The wave travels faster or slower depending if it is linearly polarized along the direction of lower or higher refractive index, respectively. Therefore, if $n_e < n_o$ (known as negative birefringence), the x axis of the optic axis is called the fast axis of the linear retarder and the y axis is called its slow axis. On the other hand, if $n_e > n_o$ (positive birefringence), the x and y axes become the slow and fast axes, respectively [27].

3.4.3.4. Dichroic (linear partial polariser) model

Fourth model of the optical device represents dichroic behaviour. The dichroic medium acts as a linear partial polarizer. The term partial polarizer is used because incident of unpolarised light on this device will be transmitted as partially polarized light. When a linearly-polarized wave travels in perpendicular direction to the transmission axis (absorption), the wave will be attenuated in amounts which depend on the direction of the vibration of the transverse electric field with respect to the transmission axis (optic axis). Thus, the absorption is maximum if the vibration direction is parallel to the transmission axis and the absorption is minimum if the vibration direction is perpendicular to the transmission axis as depicted in Figure 3.10.
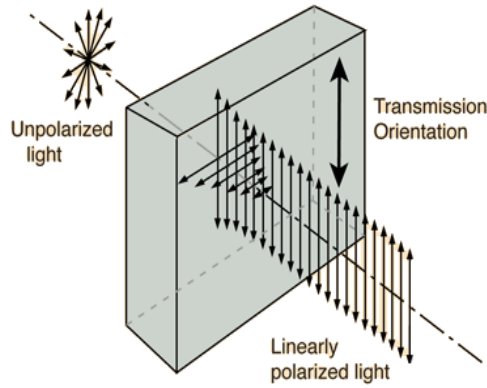
Figure 3.10　A dichroic medium behaviour when encountered by polarized light

The Jones matrix of *the dichroic* medium can be expressed as in equation (3.54)

$$\boldsymbol{J_{b4}} = e^{-j\frac{2\pi}{\lambda}nd} \begin{bmatrix} e^{-\frac{2\pi}{\lambda}dk_e} & 0 \\ 0 & e^{-\frac{2\pi}{\lambda}dk_o} \end{bmatrix} \tag{3.54}$$

3.4.3.5. Faraday effect model

The last model of the polarizing optical device is optical rotation behaviour which is known as Faraday Effect. The Faraday Effect model of polarizing optical medium is illustrated in Figure 3.11 [28].
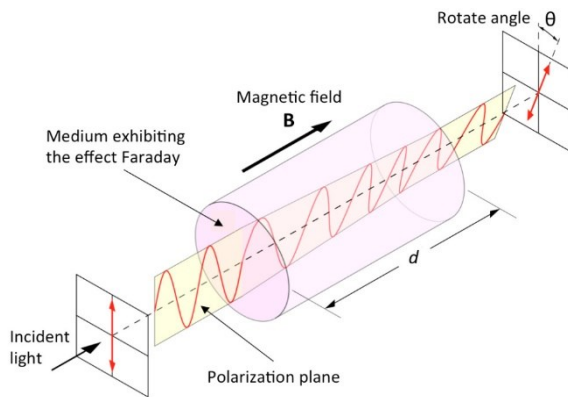
Figure 3.11　Medium exhibiting an optical rotation (Faraday Effect) [28]

The Faraday effect is encountered when polarized light propagates through an optical current sensor such as terbium gallium garnet (TGG). In this case, linearly polarized

light remains linearly polarized as the light travel through the medium but the direction of the vibration of the electric vector rotates uniformly and continuously with distance. The expression of the Faraday Effect in the Jones matrix as follows:

$$J_{b5} = e^{-j\frac{2\pi}{\lambda}nd} \begin{bmatrix} cos\,\theta & -sin\,\theta \\ sin\,\theta & cos\,\theta \end{bmatrix} \tag{3.55}$$

where the multiplicative scalar outside this matrix corresponds to an overall phase delay, with n representing an "average" index of refraction.

3.5. Optical measurement techniques

Optical voltage and current measurement techniques could overcome the intrinsic drawbacks of the conventional technologies due to their light weight, small size, and broad response of frequency bandwidth, high accuracy and electromagnetic interference immunity. Therefore, the optical measurement techniques have become interesting subject because it is suitable alternatives for high voltage sensing. The optical measurement techniques consist of several methods which are fibre Bragg grating (FBG) and polarimetric methods.

3.5.1. Fibre Bragg grating (FBG) method

Optical fibre sensors exploiting the fibre Bragg grating (FBG) method have been intensively researched [29],[30] and developed in the past few years due to its application in a variety of fields including electric power industry [31].

FBGs are formed by exposing the core of a photosensitive, single mode, germane-silicate fibre to two intersecting beams of a coherent UV light. This exposure introduces a periodic modulation of the refractive index of the core in particular region [32]. When the FBG encounter a multi-wavelength signal, a single wavelength that meets the Bragg condition in equation (3.56) is reflected back while the other wavelengths are transmitted through the fibre.

$$\lambda_B = 2\,n_{eff}\,\Lambda \tag{3.56}$$

In this equation, the Bragg wavelength λ_B is the reflected back signal, n_{eff} is the effective refractive index of the fibre core and Λ is the spacing between the gratings.

The FBG sensors have a number of distinguishing advantages [30]. Firstly, small size, the sensors can be directly written into the fibre without changing the fibre diameter. This technique makes them compatible with a wide range of situations where small diameter probes are essential, such as in advanced composite materials for strain mapping, or the human body for temperature profiling. Secondly, low cost, they can be mass produced at low cost, making them potentially competitive with conventional electrical sensors. Thirdly, robust, the FBG sensors can give an absolute measurement because they are insensitive to fluctuations in the irradiance of the illuminating source, as the information is usually obtained by detecting the wavelength shift induced by the measurand. Fourthly, quasi-distributed measurement, a number of sensing elements can be distributed along a fibre path and interrogated at a single location by series multiplexing techniques [30],[33].

Application of the FBG sensors in electric power system have been reported for measurement of voltage [34],[35, 36], current [37],[38] and fault detection [39],[40]. To measure these electrical quantities, the FBG technology is attached to a certain magnetic material such as piezoelectric [41] magnetostrictive material [39], terfenol-D [40]. An example of the FBG bonded to a multilayer piezoelectric stack as a hybrid voltage sensor, while the current sensor utilizes a small current transformer monitored by a dedicated voltage sensor is shown in Figure 3.12 [33].
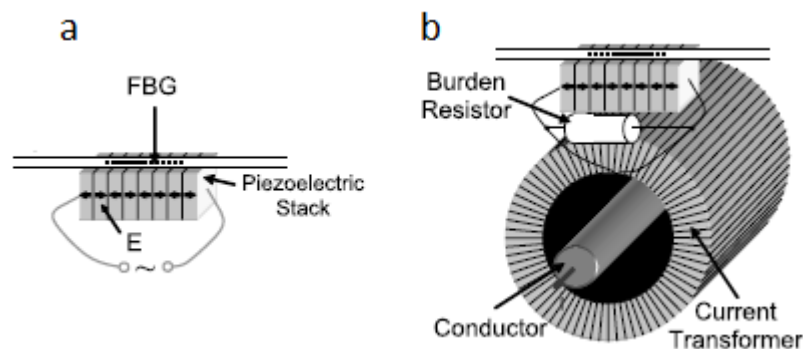
Figure 3.12   Typical FBG sensors: a. Voltage sensor, b. Current sensor [33]

A typical architecture of an FBG sensor scheme is displayed in Figure 3.13 [33]. Light from a laser source is guided by fibre to a group of serially-multiplexed FBGs. Reflections from all FBGs are returned via a coupler to the interrogating unit, at which the peak reflected wavelength from each sensor is extracted.
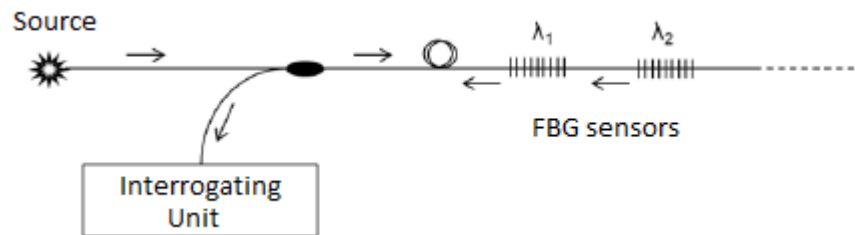
Figure 3.13   Typical FBG measurement scheme illustrating the multiplexed and reflection-mode topology. λ_1 and λ_2 are peak reflected wavelength [33]

The FBG sensors configurations need to be bonded onto the magnetic material by the use of epoxy adhesive (loading effect) which will reduce the magnetostrictive effect of the sensing material. Other problems of the magnetostrictive sensing elements are that the presence of the sensor can modify the magnetic field to be measured, and the output of the sensor can be varied by the field generated by other current [42].

3.5.2. Polarimetric methods

3.5.2.1. Optical voltage measurement

Optical voltage sensing device is developed based on electro-optic effect which exhibits birefringence behaviour when a certain optically isotropic material is placed in an electric field. The electro-optic effect consists of two phenomena which are Kerr effect and Pockels effect. [1, 43-45] [46].

Although the electro-optic effect consists of two phenomena, the Pockels effect is preferred for voltage sensing because it has a linear effect, while Kerr effect has a quadratic dependence [21, 44, 45],[47]. Therefore, the most common of optical voltage measurement device is a sensor based on Pockels effect.

In order to explain the existence of those two phenomena in the optical materials, a centre of symmetry (inversion symmetry) of materials have important role [1, 44]. Centre of symmetry exist at a point if there is no change in atomic arrangement when each atom that is stated as a vector $\boldsymbol{r}$ away from the point is replaced by one $-\boldsymbol{r}$ away. If a material has inversion symmetry, reversing electric field $\boldsymbol{E}$ should not change any physical properties of that material.

An example in the one-dimensional case, if a material has no inversion symmetry, application of an electric field to this material produces a change in the refraction index of

$$\Delta n_1 = \boldsymbol{r}E. \tag{3.57a}$$

where $\boldsymbol{r}$ is a constant characterizing of the linear electro optic effect. Reversing the applied field $\boldsymbol{E}$, it then yield

$$\Delta n_2 = -\boldsymbol{r}E. \tag{3.57b}$$

It is seen for the material without centre of symmetry that value of equation (3.57a) and (3.57b) is different i.e. $\Delta n_1 \neq \Delta n_2$. However, if the material has an inversion symmetry, $\Delta n_1 = \Delta n_2$ which implies $\boldsymbol{r} = -\boldsymbol{r}$. This can only be true for $\boldsymbol{r} = 0$. As a result, for the materials that have inversion symmetry, for example a liquid, reversing the electric field should not change any physical properties in that material.

In order to express the relation between polarization of medium and the applied electric field E, the refractive index relationship can be written [1], [47]:

$$\frac{1}{n^2} = \frac{1}{n_o^2} + \boldsymbol{r}E + \boldsymbol{R}E^2 \tag{3.58}$$

where, n_0 is a normal refractive index in the case without applied field, $\boldsymbol{r}$ and $\boldsymbol{R}$ respectively are the linear and quadratic electro-optic coefficients. It is assumed that there is no other effect that can modify n.

The Pockels and Kerr effects do not appear simultaneously, but one effect becomes dominant depending on the symmetry and the electrical-polarization structure of the material. Therefore, the Kerr electro-optic effect is displayed by materials with

inversion symmetry, whereas in materials with no inversion symmetry, the dominant interaction is the Pockels effect. The Pockels effect is expected to appear in solid materials and the Kerr effect mainly in liquid materials.

Other expression of the refractive index and the applied electric field E, the refractive index n for each orthogonal component of the optical polarization can be stated using a power series with respect to an applied electric field E [48]:

$$\frac{1}{n^2} = \frac{1}{n_o^2} + rE + RE^2 \tag{3.59}$$

where n_0 is a normal refractive index that is determined in the case without applied field, a and b are the coefficients for the electro-optic effect, and E is an applied electric field. The second term in the right-hand side of (3.59) shows a linear relationship with the electric field that corresponding to the Pockels effect which is a linear electro-optic effect. The third term shows a square dependence corresponding to the Kerr effect (a quadratic electro-optic effect). The higher order terms above E^3 have small contribution to the refractive index.

Some applications of electro-optic crystal using Pockels effect as the measurement devices have been investigated [49-54].

A schematic diagram of the voltage measurement is shown in Figure 3.14 [49]. An incident light is converted to linearly polarised light by a polariser. Then the linearly polarized light is changed to circularly polarised light using a quarter wave plate. The transmitted light passes through a Pockels crystal that has electrodes on both sides. These electrodes are connected to a voltage source hence cause electric field in the direction of the light beam. Due to the Pockels effect, the transmitted light which is the state of polarisation (SOP) of light changes from circular to elliptical. The result of phase retardation in the Pockels crystal is linearly proportional to the magnitude of the electric field. The light emitted from the crystal is then passed through an analyser in order to convert the polarisation modulated light to amplitude modulated light. Finally, the light output is converted to an electrical signal using a photo detector.
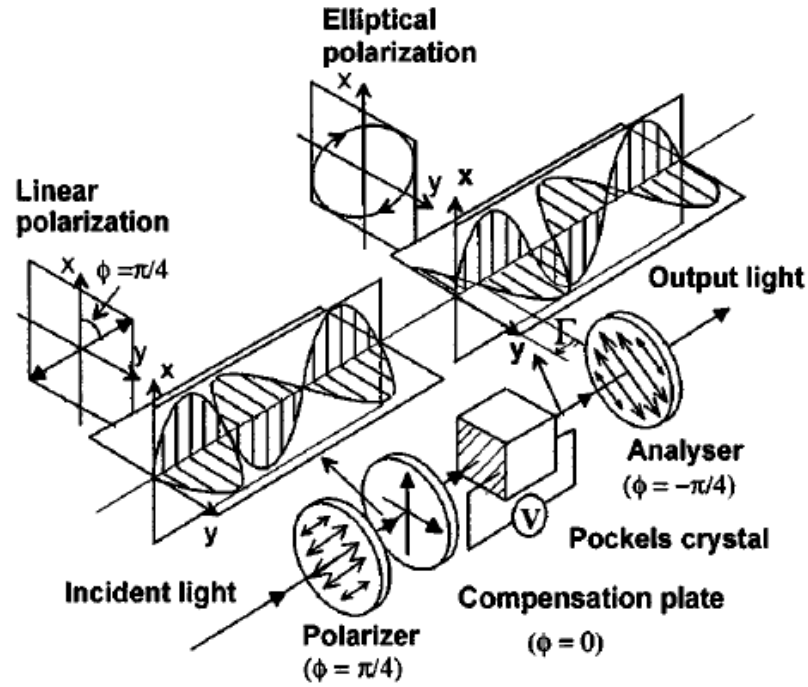
Figure 3.14 Optical voltage measurement using Pockels effect [49]

The optical power P of light emerging from the voltage sensor using Pockels effect [55] is given by

$$P = P_0 \left(1 + m \right) \tag{3.60}$$

$$m = \pi \frac{V}{V_\pi} \cdot f(V) \tag{3.61}$$

$$f(V) = \frac{\sin \{g(V)\}}{g(V)} \tag{3.62}$$

$$g(V) = \sqrt{\left(\pi \frac{V}{V_\pi} \right)^2 + (2\theta_{RP}d)^2} \tag{3.63}$$

where V is the voltage applied on the Pockels crystal, V_π is the half-wave voltage, and θ_{RP} is the optical rotary power of the crystal.

The relationship between applied voltage V and optical power P is shown in Figure 3.15 [55]. If the applied voltage is AC, the output signal consists of AC and DC

components where the AC component overlaid on the DC component. The AC to DC ratio is called the modulation index and it is equal to m as in (3.61). When applied voltage is lower than V_π, modulation index is approximately proportional to the applied voltage [55],[56].
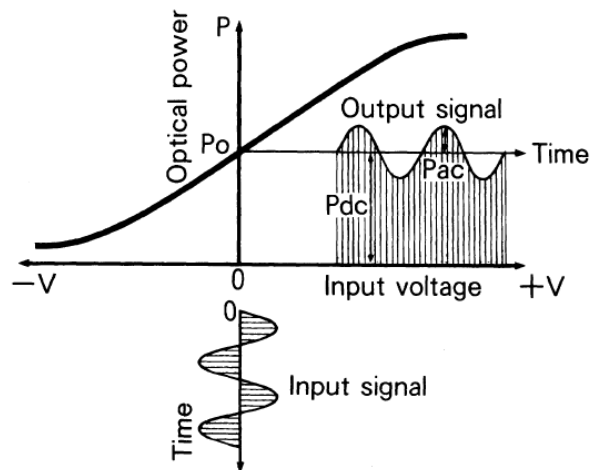
Figure 3.15   Characteristics of Optical voltage measurement using Pockels effect [55]

Regarding the applied electric field to propagation direction of the beam, the optical voltage sensors could be divided into longitudinal and transverse Pockels cell types. The sensor that is described above is called a longitudinal effect device because the applied electric field is in the same direction with the propagation of the beam device [53, 57-59] . Another example of the longitudinal Pockels cell is shown in Figure 3.16a [41]. This device uses cylindrical ring electrodes. The electrodes are separated by very uniform across the effective aperture of the cell.

As for transverse pocket cell is illustrated in Figure 3.16b [41], the applied field of the cell is normal to the direction of beam propagation. In this case, the field electrodes do not interface with the beam and the retardation (or phase difference), which is proportional to the electric field multiplied by the crystal length, can be increased by the use of longer crystals [60-64].
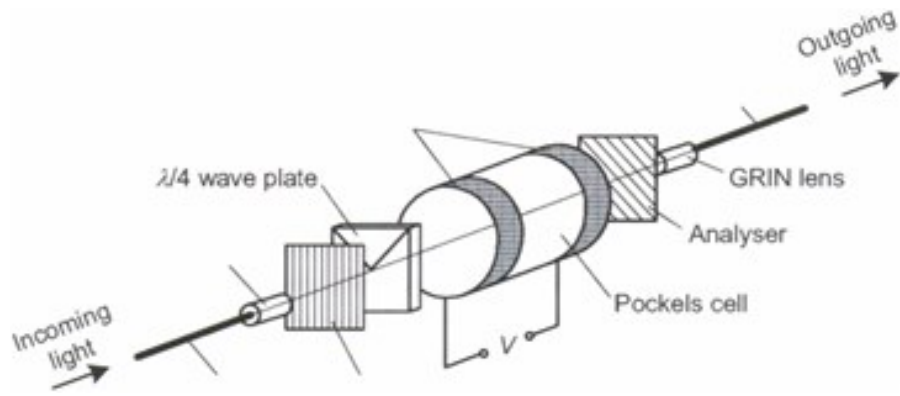
a. Longitudinal Pockels cell
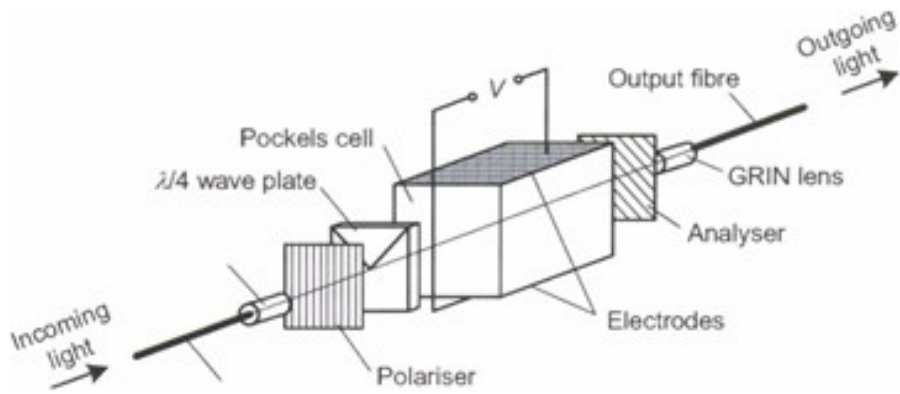
b. Transverse Pockels cell

Figure 3.16   Voltage sensor with different types Pockels cell: a. cylindrical, ring-electrode longitudinal cell, b. transverse electro-optic cell [41]

Many crystals exhibit the electro-optic effect such as $LiTaO_3$ (lithium tantalate), $LiNbO_3$ (lithium niobate), $Bi_{12}SiO_{20}$, $Bi_{12}GeO_{20}$, and $Bi_4Ge_3O_{12}$ [41, 48, 65-69]. These materials have some problems associated with them that will be described below.

First crystal group, lithium tantalate and lithium niobate crystals have natural birefringence and pyroelectricity. Due to the natural birefringence has temperature dependent characteristics, the sensor utilizing such materials will also have a temperature dependent response. Moreover, the pyroelectricity effect in the crystal is temperature dependent. As result, when the temperature of the crystal changes, electric charges are generated on the end surfaces of the crystals. As consequence, this generates additional electric field in the crystals and become a source of errors.

Second crystal group, $Bi_{12}SiO_{20}$ (BSO), $Bi_{12}GeO_{20}$ (BGO) have neither natural birefringence nor pyroelectricity. As result, the sensors using BSO and do not show any temperature dependence based on the natural birefringence and the pyroelectricity effect. Therefore, when these crystals are utilised in sensing, higher accuracy can be achieved. However, BSO and BGO have the optical activity that causes optical rotary power. As consequence, sensitivity of the sensor is a complicated function of propagating distance of light in the crystal and is difficult to adjust.

Third crystal group, $Bi_4Ge_3O_{12}$ has neither natural birefringence and pyroelectricity nor optical activity. Therefore, the sensor using this crystal has no temperature dependence due to natural birefringence and pyroelectricity. It can also be formed in transverse mode of modulation and its sensitivity can be easily adjusted with changing length of the crystals. Due to a lower relative dielectric constant of $Bi_4Ge_3O_{12}$ than other crystal in the two previous group, the disturbance of the electric field is lower for this crystal. As a result, $Bi_4Ge_3O_{12}$ seems to be the most suitable electro-optic crystal that can be utilized in an optical voltage or electric field sensor. However, any of these sensors are vulnerable to vibration effect as they are essentially light intensity encoded devices incorporating with analyser [48, 53].

3.5.2.2. Optical current sensing

Optical systems for high voltage current measurements that is known as optical current transducer have been developed in early 1970s when several different approaches were well documented [70-72],[73]. The optical current transducers have several advantages over the conventional CT due to their small size, light weight, low cost, absence of ferromagnetic resonance problems, large linear measurement range, broad response frequency bandwidth and electromagnetic interference immunity [74, 75],[76].

A fundamental difference between optical current measurements and conventional CTs is in the signal power involved. The secondary signal of a conventional CT has a power level of several watts, whereas the power in an optical current measurement is only a few micro watts (μW). In general, the current being measured in an optical current measurement is represented as modulated light.

The most common optical technique for current sensing is polarimetric method which is based on the Faraday rotation effect that is exhibited by magneto-optic crystals. This method has been reported in literatures [77-82].

Crystal materials for the head of optical current sensor could be diamagnetic, paramagnetic or ferromagnetic crystals [74] such as optical glass MOC-series [83], SF-6 glass [84], or Terbium Gallium Garnet (TGG) crystal [85, 86]. These magneto optic crystals become an actively optical medium when it is under magnetic field effect. If a linearly polarized light incident $\mathbf{E_i}$ passes through the actively optical medium, simultaneously the direction of the polarized light state emerging $\mathbf{E_o}$ is rotated parallel to the light propagation direction in proportion to the magnetic field $\mathbf{H}$ as displayed in Figure 3.17 [28].
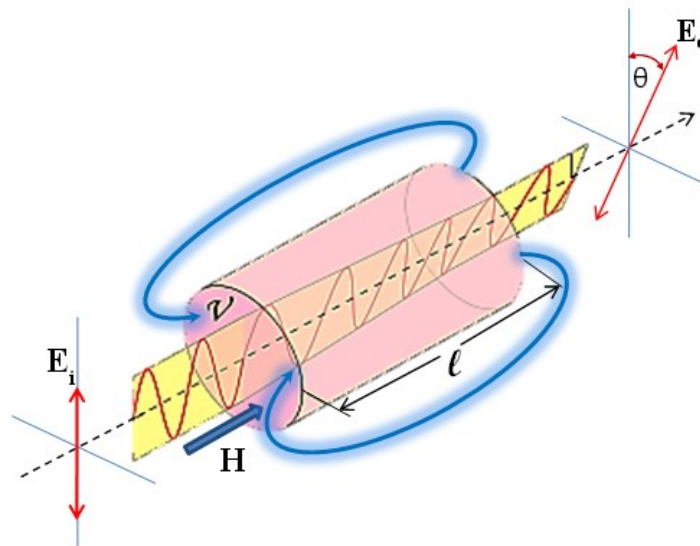
Figure 3.17   Faraday magneto-optic effect

In term of a quantitative relationship, the rotation angle of the polarized light θ is proportional to the magnetic field $\boldsymbol{H}$ and the cosine of angle between the direction of the magnetic field and the direction of the light propagation. This statement is described by Becquerel's formula which is well known as the Faraday effect [44, 87]:

$$\theta = V\,\mu \int_0^L \boldsymbol{H}\, dl \qquad (3.64)$$

where, V is the material Verdet constant related to material characteristics, wavelength, and temperature; μ is the permeability of the magneto-optic material; $\boldsymbol{H}$ is magnetic field; and dl is the path element of Faraday magneto-optic material. If the magnetic field $\boldsymbol{H}$ is uniform over the length of crystal, the rotation θ can be written as

$$\theta = V\,\mu\,\boldsymbol{H}\,L \qquad (3.65)$$

or

$$\theta = V\,\boldsymbol{B}\,L \qquad (3.66)$$

where L is the length of the Faraday sensor.

A conclusion can be derived from equation (3.65) and also supported by reference [44] that the polarized light rotation effect in non-magnetic optical medium has a linear relationship with the crystal Verdet constant and the external magnetic field strength.

A typical arrangement of optical components in a Faraday sensor is shown in Figure 3.18 [41]. A light beam is generated from the light source then passing to a Faraday magneto-optic crystal via a section of fibre optic, a GRIN lens collimator and a first polariser (a polariser) [73],[88]. When a magnetic field is applied as the effect of the current flowing, the linearly polarized light is rotated by an angle θ proportional to the applied field. Usually, but not universally, a second polariser (termed an analyser) is arranged at angle α of 45° with respect to the polariser in order to maximise the sensitivity of the sensor response. The light output is passed to a photo detector via a GRIN lens collimator and output fibre. The photo detector is utilized to translate modulated light into optical power modulation.
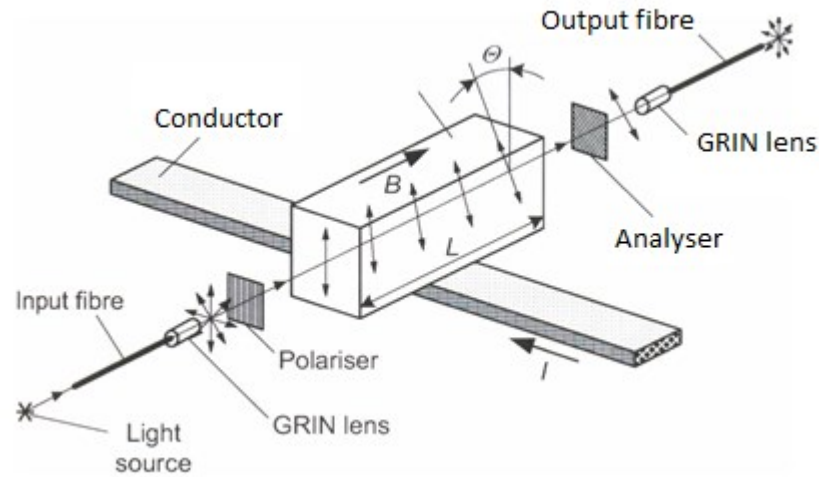
Figure 3.18   Arrangement of optical component in a Faraday sensor [41]

Various transducer designs have been proposed. The designs are classified into several major classes of transducer. Type 1 is a magnetic concentrator with optical measurement. In this design, a magnetic circuit surrounds the conductor; the magnetic field inside the magnetic core is optically measured in an air gap, as displayed in Figure 3.19a [79]. Using this approach, the sensing element is placed in a flux concentrator which amplifies the magnetic field passing through the Faraday magneto optic crystal [79, 89, 90].

Type 2 is a bulk optic type sensor [42, 91, 92] that is illustrated in Figure 3.19b [79]. In this type, a square-shaped sensing element is a closed optical path surrounding the conductor that is formed by four sensing arms and three reflection corners. The reflection corners are totally reflecting the linear polarised light beam.

The benefit of this type is mechanically stiffer. Therefore, mechanical and thermal gradients, vibrations and other external noises in the bulk optic material are very small. Another advantage is a more sensitive measurement without detrimental reflection problems. The bulk optic devices are produced in several shapes such as triangular, square and   ring-shaped sensing elements. However, they are generally difficult to manufacture and are relatively big and heavy.

Type 3 is optical fibre sensor [73, 93-95] where the optical path is inside a fibre that can be wound around the current carrying conductor with an arbitrary number of turs in order to achieve the desired sensitivity as shown in in Figure 3.19c [79].
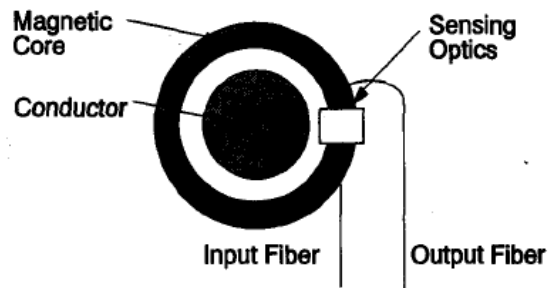
a. Magnetic concentrator with optical measurement
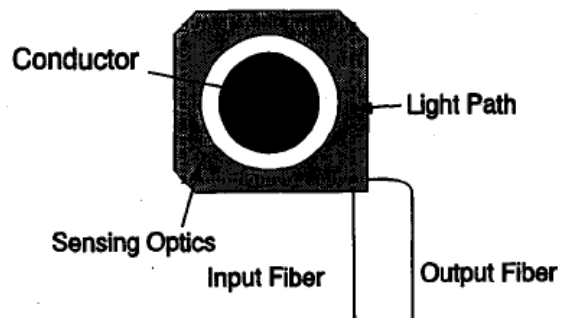
b. Magnetic concentrator with optical measurement
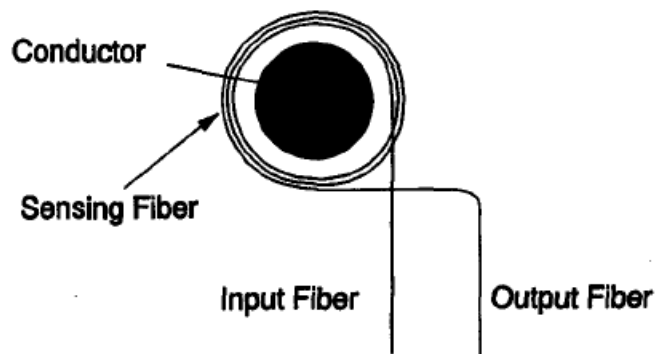
c. Magnetic concentrator with optical measurement

Figure 3.19   Several type of optical current transducer design [79]

In order to increase sensitivity of the sensor, it is required to employ the high value of the Verdet constant, especially when relatively a small current-induced magnetic field are expected to be measured. Therefore, the most common magneto optic glasses for the sensor heads of optical current transducers are SF-glasses, Hoya FR-5 glass, optical glass MOC-series, rare-earth doped material, yttrium iron garnet (YIG) and bismuth substituted YIG, and terbium iron garnet (TIG), terbium gallium garnet (TGG) crystal [74, 96]. In order to classify the optical material, several available optic materials those are aforementioned may be classified into three groups [97],[98]:

1. Diamagnetic doped glasses and paramagnetic ion-doped glasses.
2. Ferromagnetic materials.
3. Rare earth garnet.

In the first group, the diamagnetic doped glasses contain high concentrations of ions which give rise to large Verdet constants. Other materials which have the largest Verdet constants in this group are rare-earth glasses, i.e. paramagnetic ion-doped glasses. The most commonly used materials from this first group are Schott glass SF6 and SF series [84, 97], Hoya FR-5 glass [99], optical glass MOC-series [83], and rare-earth doped material [100].

Second group is rare earth iron garnet and substituting some element into a rare-earth iron garnet crystal. The most available commercial crystals from this group are yttrium iron garnet (YIG) that is known as pure YIG. In general, the Verdet constant of a YIG material is two to three orders of magnitude larger than that for typical diamagnetic glasses in the first group [101],[102]. This material exhibits relatively high Verdet constant and low optical loss at 1550 nm. However, the material exhibit temperature dependence of the Verdet constant and, therefore, current transducers exploiting this material would require temperature compensation. In order to improve the YIG performance, substituting some elements into a YIG crystal, for instance, bismuth (Bi) produce Bi-YIG which have higher Verdet constant and better temperature coefficient [103, 104],[105]. Moreover, addition of terbium (Tb), for example in iron garnet to create terbium iron garnet (TIG), will decrease the temperature dependence that makes better performances [106],[107],[108].

Last group, rare-earth garnet, such as terbium gallium garnet (TGG) crystal is an optimum material for Faraday devices due to a combination of excellent properties such as large Verdet constant, low optical losses, high thermal conductivity and high laser damage threshold [109]. The combination of these factors make TGG better suited to high average power applications. The principal limiting factor is thermally induced beam distortion. Beam distortion is less for TGG than Tb-doped glasses under the same power loading level.

Moreover, comparing to materials in the second group as shown in Table 3.1 [110], TGG is superior to terbium-doped glasses because TGG has twice the Verdet constant of a terbium-doped glass. Thermal conductivity of crystalline TGG is an order of magnitude greater than a typical glass. The optical losses are lower for TGG than Tb-doped glasses [46].

Table 3-1 Comparison of TGG & Tb-Doped Glass Properties @ 1064 nm

	TGG	Tb-Glass	
Verdet Constant, V:			
@1064 nm	-40	-20	$Rad. T^{-1}. m^{-1}$
@ 632 nm	-134	-70	$Rad. T^{-1}. m^{-1}$
Absorption Coefficient, α	0.0015	0.003	cm^{-1}
Thermal Conductivity	7.4	0.7	$W. m^{-1}. K^{-1}$
Refractive index, n	1.95	–	–
Nonlinear Index, n_2	8.0	2.45	$10^{-13} esu$
Figure of Merit, V/α	27	7	–
Figure of Merit, V/n_2	5	8	–

Based on the mentioned explanation above, this thesis focuses on the optical polarimetric method in order to realise an optical busbar differential protection scheme.

3.6. The state of art in all-optical differential protection scheme

Electric current measurement based on optical method have been developed in the 1970s and 1980s. Following development of optical sensing method in electric current measurement, investigation of optical application for protection schemes have also taken place. The use of optical protection scheme to protect elements of the electric power system have been reported. The first effort was utilisation of optical fibre as an alternative communication link for protection and teleprotection of differential relaying on short transmission line [111]. Other effort was an investigation of differential protection with fibre optic current sensors (FOCS) [112] and also a future design of differential based on IEC 61850 [113]. In these reports, the protection schemes apply the mixed optical-numerical techniques which are a combination of an optical method for current measurement with modern micro-processor relays. The mixed optical-numerical is actually an indirect method for differential current by summation process in digital form of the electric currents that are translated from optical form. Other characteristic of the protection scheme are the use of time-consuming encoding and decoding at each terminal, and a dedicated optical fibre communications link.

The optical protection scheme that rely on the optical sensing methods for a current differential protection scheme is documented in [114]. However, this design still use the dedicated communication link.

A different approach that utilises all-optical technique to implement the all-optical differential protection scheme is presented in [115],[116],[117],[33]. This all-optical protection scheme is achieved by distributed optical sensing method in conjunction with interrogation technique at single location.

The recent optical differential busbar protection schemes that are commercially offered in the market rely on a typical design based on indirect method of optical summing process in the modern numerical/microprocessor-based components. In these schemes, they involve two-step processes. The first step, the electric currents are measured by optical current transducers or optical current sensors. The process in this step is a

conversion of the measured currents from analogue to optical modulation that is performed by the optical current transducers/sensors.

The second step is translating and substituting processes. The optical signals in the first step are translated into digital values. Then, it is substituted into a differential protection scheme algorithm. Thus, the measured currents are digitized and send it to a dedicated numerical processing which is the busbar differential algorithm (routine) in order to be applied for a given differential protection relaying scheme. Therefore, this scheme could be named as "mixed optical-numerical protection".

The most recent technique in the all-optical protection scheme is introduced in [118], where the technique utilises distributed optical current sensing, differential protection principle and sensor interrogation at single point. However, this techniques is for the HVDC transmission network and using the FBG sensors. Therefore, this thesis proposes a new configuration of all-optical differential protection scheme for the AC power system utilising polarimetric optical current sensing method.

Some advantages of the all optical differential scheme could overcome the CT saturation problem in the traditional circulating current scheme because it utilizes the optical current sensors (OCT) without iron core component such as in the old fashioned CT. Since the optical feature exists in the OCT as part of the all optical differential scheme, it could be inferenced that all optical schemes could combine the advantages of high impedance circulating current and low impedance method (percentage differential protection scheme).

Other benefit of the all optical differential scheme is a fast operation due to the utilization of a laser light in this scheme without the use of a complex numerical processing. In addition, the direct summation method also contributes for the fast operation because it works in the optical domain without a process that required the optical to digital conversion components.

3.7. Summary

In this chapter, theoretical optics have been introduced. Various principles of optics and polarized light were presented in details. Interaction between polarized light and polarizing optical material by considering the optical material orientation were explained using Jones matrix formalization. Moreover, modelling of polarized light and optical devices using Jones matrices were presented. A review of optical method for both voltage and current measurements including properties of crystal materials were also described. The state of art in all-optical differential protection scheme was reviewed. Next chapter will discuss conceptual design and modelling of proposed configuration of all-optical differential protection scheme developed during the course of this PhD.

3.8. References for chapter 3

[1]   F. L. Pedrotti, *Introduction to optics*: Englewood Cliffs, N.J. : Prentice-Hall, 1987.

[2]   E. Hecht, *Optics*: Harlow : Pearson Education Limited, 2013.

[3]   F. L. Pedrotti, L. S. Pedrotti, and L. M. Pedrotti, *Introduction to Optics*: Pearson Prentice Hall, 2007.

[4]   R. M. A. Azzam, Bashara, N. M, *Ellipsometry and Polarized Light*. Amsterdam: Elsevier Science BV, 1987.

[5]   H. Tompkins and E. A. Irene, *Handbook of Ellipsometry*: Elsevier Science, 2013.

[6]   R. C. Jones, "A New Calculus for the Treatment of Optical Systems: I. Description and Discussion of the Calculus," *Journal of the Optical Society of America,* vol. 31, pp. 488-493, 1941/07/01 1941.

[7]   D. Goldstein and D. H. Goldstein, *Polarized Light, Revised and Expanded*: CRC Press, 2003.

[8]   E. Kreyszig, *Advanced engineering mathematics*, 10th ed., International student version.. ed. Hoboken, N.J. : Chichester: Hoboken, N.J. : Wiley Chichester : John Wiley distributor, 2011.

[9]   B. Hague, *An introduction to vector analysis for physicists and engineers*, 5th ed.. ed. Methuen: Methuen, 1961.

[10]   J. Vince, *Vector analysis for computer graphics [internet resource]*. London: London : Springer, 2007.

[11]   R. C. Jones, "New Calculus for the treatment of Optical Systems: I. Description and Discussion of Calculus," *Journal of the Optical Society of America,* vol. 31, p. 6, 1941.

[12]   R. C. H. Jones, H. Jr, "New Calculus for the treatment of Optical Systems: II. Proof of Three General Equivalence Theorems," *Journal of the Optical Society of America,* vol. 31, p. 7, 1941.

[13]   R. C. Jones, "New Calculus for the treatment of Optical Systems: III. The Sohncke Theory of Optical Activity," *Journal of the Optical Society of America,* vol. 31, p. 4, 1941.

[14]   R. C. Jones, "New Calculus for the treatment of Optical Systems: IV. -," *Journal of the Optical Society of America,* vol. 31, p. 8, 1941.

[15]   R. C. Jones, "A new calculus for the treatment of optical systems V A more general formulation, and description of another calculus," vol. 37.

[16]   R. C. Jones, "A new calculus for the treatment of optical systems VI Experimental determination of the matrix," vol. 37.

[17]   R. C. Jones, "A New Calculus for the Treatment of Optical Systems VII Properties of the N-Matrices," vol. 38.

[18]   A. J. Rogers, *Polarization in optical fibers*: Norwood, MA : Artech House, 2008.

[19]   G. Herbert, *Handbook of optical systems*: Weinheim ; Great Britain : Wiley-VCH, 2005.

[20]   Y. Hasegawa, Y. Ichikawa, H. Katsukawa, N. Tanaka, and Y. Sakurai, "Development of a new type of optical transducer for measuring fault current," *Power Delivery, IEEE Transactions on,* vol. 9, pp. 1245-1252, 1994.

[21]   C. A. Dimarzio, *Optics for engineers*: Boca Raton, FL : CRC Press, 2012.

[22]   A. M. Law, "How to Build Valid and Credible Simulation Models," in *the IEEE Winter Simulation Conference*, 2008, p. 9.

[23] H. Hurwitz and R. C. Jones, "A New Calculus for the Treatment of Optical Systems: II. Proof of Three General Equivalence Theorems," *Journal of the Optical Society of America,* vol. 31, pp. 493-499, 1941/07/01 1941.

[24] R. C. Jones, "A New Calculus for the Treatment of Optical Systems: III. The Sohncke Theory of Optical Activity," *Journal of the Optical Society of America,* vol. 31, pp. 500-503, 1941/07/01 1941.

[25] A. Yariv, *Optical waves in crystals : propagation and control of laser radiation*. New York: New York : Wiley, 1984.

[26] F. M. Zernike, *Applied nonlinear optics*: Wiley-interscience, 1973.

[27] C. L. Xianyun Ma, "A method to eliminate birefringence of a magneto-optic AC current transducer with glass ring sensor head," *IEEE Trans. on Power Delivery,* vol. 13, p. 5, 1998.

[28] M. Aerssens, A. Gusarov, B. Brichard, V. Massaut, Me, x, P. gret, and M. Wuilpart, "Faraday effect based optical fiber current sensor for tokamaks," in *Advancements in Nuclear Instrumentation Measurement Methods and their Applications (ANIMMA), 2011 2nd International Conference on*, 2011, pp. 1-6.

[29] A. D. Kersey and M. J. Marrone, "Fiber Bragg Grating High-Magnetic-Field Probe," in *The Tenth International Conference on Optical Fibre Sensors*, 1994, pp. 53-56.

[30] Y.-J. Rao, "Review Article: In-fibre Bragg grating sensors," *Measurement Science Technology,* vol. 8, pp. 355-375, 1997.

[31] Y. J. Rao, "Recent progress in applications of in-fibre Bragg grating sensors," *Optics and Lasers in Engineering,* vol. 31, pp. 297-324, 1999.

[32] K. T. V. Grattan and T. Sun, "Fiber optic sensor technology: an overview," *Sensors and Actuators A: Physical,* vol. 82, pp. 40-61, 2000.

[33] P. Orr, G. Fusiek, P. Niewczas, C. D. Booth, A. Dysko, F. Kawano, T. Nishida, and P. Beaumont, "Distributed Photonic Instrumentation for Power System Protection and Control," *Instrumentation and Measurement, IEEE Transactions on,* vol. 64, pp. 19-26, 2015.

[34] L. Dziuda, P. Niewczas, G. Fusiek, and J. M. McDonald, "Hibrid fiber optic voltage sensor for remote monitoring of electrical submersible pump motors," *Optical Engineering,* vol. 44, p. 6, 2005.

[35] P. Niewczas, L. Dziuda, G. Fusiek, and J. R. McDonald, "Design and evaluation of a preprototype hybrid fiber-optic voltage sensor for a remotely interrogated condition monitoring system," *Instrumentation and Measurement, IEEE Transactions on,* vol. 54, pp. 1560-1564, 2005.

[36] L. Dziuda, G. Fusiek, P. Niewczas, G. M. Burt, and J. R. McDonald, "Laboratory evaluation of the hybrid fiber-optic current sensor," *Sensors and Actuators A: Physical,* vol. 136, pp. 184-190, 2007.

[37] D. Reilly, A. J. Willshire, G. Fusiek, P. Niewczas, and J. R. McDonald, "A Fiber-Bragg-Grating-Based Sensor for Simultaneous AC Current and Temperature Measurement," *IEEE Sensors Journal,* vol. 6, pp. 1539-1542, 2006.

[38] L. Dziuda, P. Niewczas, and J. R. McDonald, "Hybrid fiber-optic current sensor for remote monitoring of electrical submersible plant," in *Sensors, 2005 IEEE,* 2005, p. 4 pp.

[39] K. B. Chiu T. Law, David C. Yu, "Fiber-Optics-Based Fault Detection in Power Systems," *IEEE Trans. on Power Delivery,* vol. 23, p. 9, 2008.

[40] R. B. Amin Moghadas, Mehdi Shadaram, "An Innovative Fibre Bragg Grating Sensor Capable of Fault Detection in Radial power Systems," presented at the 4th Annual IEEE System Conference 2010, 2010.

[41] Ł. Dziuda, "Novel approaches to hybrid voltage and current sensing for condition monitoring of remotely operated electrical plant," Thesis [Ph. D] -- University of Strathclyde, 2007., 2007.

[42] Y. N. Ning, Z. P. Wang, A. W. Palmer, K. T. V. Grattan, and D. A. Jackson, "Recent progress in optical current sensing techniques," *Review of Scientific Instruments,* vol. 66, pp. 3097-3111, 1995.

[43] I. S. Zheludev, "Electro-optical Effects in Crystals," *Soviet Physics Uspekhi,* vol. 9, p. 97, 1966.

[44] R. D. Guenther, *Modern optics*: New York : Wiley, 1990.

[45] A. Lipson, *Optical physics*: Cambridge : Cambridge University Press, 2011.

[46] M. N. Ediger and R. W. Waynant, *Electro-optics handbook*. New York: New York : McGraw-Hill, 1994.

[47] B. E. A. Saleh, *Fundamentals of photonics*. New York: New York : Wiley, 1991.

[48] K. Hidaka, "Progress in Japan of space charge field measurement in gaseous dielectrics using a Pockels sensor," *IEEE Electrical Insulation Magazine,* vol. 12, pp. 17-28, 1996.

[49] J. C. Santos, M. C. Taplamacioglu, and K. Hidaka, "Pockels high-voltage measurement system," *IEEE Transactions on Power Delivery,* vol. 15, pp. 8-13, 2000.

[50] H. Li, L. Cui, Z. Lin, L. Li, and C. Zhang, "An Analysis on the Optimization of Closed-Loop Detection Method for Optical Voltage Sensor Based on Pockels Effect," *Journal of Lightwave Technology,* vol. 32, pp. 1006-1013, 2014.

[51] H. Li, L. Cui, Z. Lin, L. Li, R. Wang, and C. Zhang, "Signal Detection for Optical AC and DC Voltage Sensors Based on Pockels Effect," *IEEE Sensors Journal,* vol. 13, pp. 2245-2252, 2013.

[52] Y. N. Zhao, G. Q. Zhang, Z. Z. Guo, S. Cheng, Z. G. Ma, and S. W. Li, "Application of Pockels Electro-Optic Effect in Voltage Transducer," in *2012 Symposium on Photonics and Optoelectronics*, 2012, pp. 1-6.

[53] A. Kumada and K. Hidaka, "Directly High-Voltage Measuring System Based on Pockels Effect," *IEEE Transactions on Power Delivery,* vol. 28, pp. 1306-1313, 2013.

[54] M. Passard, C. Barthod, M. Fortin, C. Galez, and J. Bouillot, "Design and optimization of a low-frequency electric field sensor using Pockels effect," *IEEE Transactions on Instrumentation and Measurement,* vol. 50, pp. 1053-1058, 2001.

[55] T. Mitsui, K. Hosoe, H. Usami, and S. Miyamoto, "Development of Fiber-Optic Voltage Sensors and Magnetic-Field Sensors," *IEEE Transactions on Power Delivery,* vol. 2, pp. 87-93, 1987.

[56] X. Jiang and F. y, "A method for measuring the transverse half-wave voltage of LiNbO$_3$," in *CSQRWC 2012*, 2012, pp. 180-182.

[57]   F. Long, J. Zhang, C. Xie, and Z. Yuan, "Application of the Pockels Effect to High Voltage Measurement," in *2007 8th International Conference on Electronic Measurement and Instruments*, 2007, pp. 4-495-4-499.

[58]   R. Xie and Q. Xu, "Comparison of 2D & 3D models for simulations of electric-field in OVS," in *2015 12th IEEE International Conference on Electronic Measurement & Instruments (ICEMI)*, 2015, pp. 589-593.

[59]   S. H. Han and J. W. Wu, "Measurement of the linear electro-optic effect in chiral nonlinear optical crystal," in *Lasers and Electro-Optics, 1999. CLEO/Pacific Rim '99. The Pacific Rim Conference on*, 1999, pp. 869-870 vol.3.

[60]   F. Pan, X. Xiao, Y. Xu, and S. Ren, "Optical AC Voltage Sensor Based on Two Bi4 Ge3 O12 Crystals," *IEEE Transactions on Instrumentation and Measurement,* vol. 61, pp. 1125-1129, 2012.

[61]   L. Changsheng, C. Xiang, and T. Yoshino, "Measurement of AC electric power based on dual transverse Pockels effect," *IEEE Transactions on Instrumentation and Measurement,* vol. 50, pp. 1375-1380, 2001.

[62]   H. Miyashita and Y. Fujii, "Measurement of current, voltage and power using single quartz crystal," in *2002 15th Optical Fiber Sensors Conference Technical Digest. OFS 2002(Cat. No.02EX533)*, 2002, pp. 491-494 vol.1.

[63]   F. Pan, X. Xiao, Y. Xu, and S. Ren, "An Optical AC Voltage Sensor Based on the Transverse Pockels Effect," *Sensors (Basel, Switzerland),* vol. 11, pp. 6593-6602, 2011.

[64]   G. Gaborit, L. Gillette, F. Lecoche, L. Duvillaret, A. Grau, and G. Schmitt, "Contactless real-time voltage monitoring of multi-conductors cables with electro-optic sensor," in *2014 IEEE Electrical Insulation Conference (EIC)*, 2014, pp. 147-151.

[65]   P. Yakymyshyn, A. Fekete, S. Lee, D. Romalo, F. Rahmatian, and C. Yakymyshyn, "Characterization of a bismuth germanate electric field sensor," in *Conference on Lasers and Electro-Optics (CLEO 2000). Technical Digest. Postconference Edition. TOPS Vol.39 (IEEE Cat. No.00CH37088)*, 2000, p. 309.

[66] K. Osamu and K. Kazuhiko, "Electro-Optical Effect of Bi4 Ge3 O12 Crystals for Optical Voltage Sensors," *Japanese Journal of Applied Physics,* vol. 32, p. 4288, 1993.

[67] P. A. Williams, A. H. Rose, K. S. Lee, D. C. Conrad, G. W. Day, and P. D. Hale, "Optical, thermo-optic, electro-optic, and photoelastic properties of bismuth germanate (Bi4Ge3O12)," *Applied Optics,* vol. 35, pp. 3562-3569, 1996/07/01 1996.

[68] O. Masanori, N. Taneo, and H. Yoshihiro, "Thermal and Electric Field Broadening in Electro-Optical Effect," *Japanese Journal of Applied Physics,* vol. 11, p. 1002, 1972.

[69] C. Li and T. Yoshino, "Simultaneous measurement of current and voltage by use of one bismuth germanate crystal," *Applied Optics,* vol. 41, pp. 5391-5397, 2002/09/01 2002.

[70] S. Takeshita and T. Sasano, "Measurement of impulse current by laser current transformer," *Proceedings of the IEEE,* vol. 56, pp. 1404-1405, 1968.

[71] A. Braun and J. Zinkernagel, "Optoelectronic Electricity Meter for High-Voltage Lines," *IEEE Transactions on Instrumentation and Measurement,* vol. 22, pp. 394-399, 1973.

[72] A. J. Rogers, "Optical technique for measurement of current at high voltage," *Electrical Engineers, Proceedings of the Institution of,* vol. 120, pp. 261-267, 1973.

[73] T. W. MacDougall, D. R. Lutz, and R. A. Wandmacher, "Development of a fiber optic current sensor for power systems," *Power Delivery, IEEE Transactions on,* vol. 7, pp. 848-852, 1992.

[74] R. M. Silva, H. Martins, I. Nascimento, J. M. Baptista, A. L. Ribeiro, J. L. Santos, P. Jorge, and O. Frazão, "Optical Current Sensors for High Power Systems: A Review," *Applied Sciences,* vol. 2, p. 602, 2012.

[75] M. H. Samimi, A. A. S. Akmal, and H. Mohseni, "Optical Current Transducers and Error Sources in Them: A Review," *IEEE Sensors Journal,* vol. 15, pp. 4721-4728, 2015.

[76]   Y. Shen, Y. Lu, Z. Liu, X. Yu, G. Zhang, and W. Yu, "Performance of magneto-optical glass in optical current transducer application," *Journal of Magnetism and Magnetic Materials,* vol. 389, pp. 180-185, 2015.

[77]   A. J. Rogers, "Method for simultaneous measurement of current and voltage on high-voltage lines using optical techniques," *Electrical Engineers, Proceedings of the Institution of,* vol. 123, pp. 957-960, 1976.

[78]   A. J. Rogers, "Optical Measurement of Current and Voltage on Power Systems," *Electric Power Applications, IEE Journal on,* vol. 2, pp. 120-124, 1979.

[79]   IEEE, "Optical current transducers for power systems: a review," *Power Delivery, IEEE Transactions on,* vol. 9, pp. 1778-1788, 1994.

[80]   K. Kyuma, S. Tai, M. Nunoshita, T. Takioka, and Y. Ida, "Fiber optic measuring system for electric current by using a magnetooptic sensor," *Quantum Electronics, IEEE Journal of,* vol. 18, pp. 1619-1623, 1982.

[81]   A. Cruden, J. R. McDonald, I. Andonovic, D. Uttamchandani, R. Porrelli, and K. Allan, "Current measurement device based on the Faraday effect," in *1993 Fifth International Conference on Developments in Power System Protection*, 1993, pp. 69-72.

[82]   T. W. Cease and P. Johnston, "A magneto-optic current transducer," *Power Delivery, IEEE Transactions on,* vol. 5, pp. 548-555, 1990.

[83]   E. Khazanov, N. Andreev, A. Babin, A. Kiselev, and O. Palashov, "Measurements of thermooptic characteristics of magnetoactive glasses," in *Lasers and Electro-Optics, 1999. CLEO '99. Summaries of Papers Presented at the Conference on*, 1999, pp. 499-500.

[84]   A. E. Petersen, "Portable optical AC- and proposed DC-current sensor for high voltage applications," *IEEE Transactions on Power Delivery,* vol. 10, pp. 595-599, 1995.

[85]   N. Grumman. (2015). *Terbium Gallium Garnet (TGG)* Available: http://www.northropgrumman.com/BusinessVentures/SYNOPTICS/Products/SpecialtyCrystals/pages/TGG.aspx

[86]   A. Cruden, J. R. McDonald, I. Andonovic, D. Uttamchandani, R. Porrelli, and K. Allan, "A magneto-optic crystal based current measurement device," in

Advances in Power System Control, Operation and Management, 1993. APSCOM-93., 2nd International Conference on, 1993, pp. 725-728 vol.2.

[87]   E. Hecht, *Physics*: Brooks/Cole Pub., 1994.

[88]   M. H. Samimi, A. A. S. Akmal, H. Mohseni, and J. Jadidian, "Open-Core Optical Current Transducer: Modeling and Experiment," *IEEE Transactions on Power Delivery,* vol. 31, pp. 2028-2035, 2016.

[89]   P. Niewczas, "Implementation of a Faraday Effect based Optical Current Transducer using digital signal processing techniques," Thesis [Ph. D.] -- University of Strathclyde, 2000., 2000.

[90]   L. Shen-Wang, Z. Guo-Qing, Y. Wen-Bin, G. Zhi-Zhong, S. Yan, Z. Yi-Nan, C. Song, and L. Hong-Kai, "Optimization Design of Optical Current Sensor with Magnetic Concentrator Ring for Gas Insulated Switchgear," in *2012 Second International Conference on Instrumentation, Measurement, Computer, Communication and Control*, 2012, pp. 926-930.

[91]   T. Sato, G. Takahashi, and Y. Inui, "Method and apparatus for optically measuring a current," ed: Google Patents, 1986.

[92]   B. Yi., A. Cruden, I. Madden, J. R. McDonald, and I. Andonovic, "A novel bulk-glass optical current transducer having an adjustable multiring closed-optical-path," *Instrumentation and Measurement, IEEE Transactions on,* vol. 47, pp. 240-243, 1998.

[93]   K. Bohnert, A. Frank, L. Yang, G. M. Mueller, M. Lenner, T. Roininen, B. Guelenaltin, P. Gabus, S. V. Marchese, and A. Vujanic, "Fiber-optic current sensor in 420 kV circuit breaker," in *2016 Conference on Lasers and Electro-Optics (CLEO)*, 2016, pp. 1-2.

[94]   K. Bohnert, R. Wuest, A. Frank, P. Gabus, S. Wiesendanger, J. Nehring, and H. Brandle, "Experimental and theoretical investigations of the high current regime of an interferometric fiber-optic current sensor," in *2008 IEEE Sensors*, 2008, pp. 926-929.

[95]   N. Peng, Y. Huang, S. Wang, T. Wen, W. Liu, Q. Zuo, and L. Wang, "Fiber Optic Current Sensor Based on Special Spun Highly Birefringent Fiber," *IEEE Photonics Technology Letters,* vol. 25, pp. 1668-1671, 2013.

[96] M. Abdel-Baki and F. El-Diasty, "Glasses for photonic technologies," *International Journal of Optics and Applications,* vol. 3, pp. 125-137, 2013.

[97] M. J. Weber, *Optical materials*. Boca Raton, Fla.: Boca Raton, Fla. : CRC Press, 1986.

[98] R. B. Wagreich and C. C. Davis, "Accurate magneto-optic sensitivity measurements of some diamagnetic glasses and ferrimagnetic bulk crystals using small applied AC magnetic fields," *IEEE Transactions on Magnetics,* vol. 33, pp. 2356-2361, 1997.

[99] J. A. Davis and R. M. Bunch, "Temperature dependence of the Faraday rotation of Hoya FR-5 glass," *Applied Optics,* vol. 23, pp. 633-636, 1984/02/15 1984.

[100] Y. Shen, Y. Lu, X. Yu, Z. Liu, G. Zhang, and W. Yu, "Characteristics of rare-earth-doped glass in optical current transducers," *Optik - International Journal for Light and Electron Optics,* vol. 127, pp. 2069-2073, 2016.

[101] K. B. Rochford, A. H. Rose, and G. W. Day, "Magneto-optic sensors based on iron garnets," *IEEE Transactions on Magnetics,* vol. 32, pp. 4113-4117, 1996.

[102] E. J. J. Mallmann, A. S. B. Sombra, J. C. Goes, and P. B. A. Fechine, "Yttrium Iron Garnet: Properties and Applications Review," *Solid State Phenomena,* vol. 202, pp. 65-96, 2013.

[103] M. Imaeda and Y. Kozuka, "Optical Magnetic Field Sensors Using Iron Garnet Crystals," in *8th Optical Fiber Sensors Conference*, 1992, pp. 386-389.

[104] K. Tsushima and N. Koshizuka, "Research activities on magneto-optical devices in Japan," *IEEE Transactions on Magnetics,* vol. 23, pp. 3473-3478, 1987.

[105] S. Kahl, "Bismuth iron garnet films for magneto-optical photonic crystals," 5292 Doctoral thesis, comprehensive summary, Trita-FYS, Mikroelektronik och informationsteknik, Kista, 2004.

[106] K. Okubo and O. Kamada, "Magnetic field optical sensors using (TbY) IG crystals with stripe magnetic domain structure," in *INTERMAG Asia 2005. Digests of the IEEE International Magnetics Conference, 2005.*, 2005, pp. 431-432.

[107] L. Sun, S. Jiang, J. D. Zuegel, and J. R. Marciante, "Effective Verdet constant in a terbium-doped-core phosphate fiber," *Optics Letters,* vol. 34, pp. 1699-1701, 2009/06/01 2009.

[108] J. N. Damask, *Polarization optics in telecommunications [internet resource]*. New York: New York : Springer, 2004.

[109] N. Grumman. (2012). *TGG (Terbium Gallium Garnet)*. Available: http://www.northropgrumman.com/BusinessVentures/SYNOPTICS/Products/SpecialtyCrystals/Pages/TGG.aspx

[110] N. Grumman. (2015). *Advantages of Terbium Gallium Garnet (TGG)*. Available:
http://www.northropgrumman.com/BusinessVentures/SYNOPTICS/Products/SpecialtyCrystals/Documents/pageDocs/TGG.pdf

[111] A. J. S. d. Oliveira, "Optical fibre pilot differential relaying for a 138 kV Eletrosul short transmission line," in *1993 Fifth International Conference on Developments in Power System Protection*, 1993, pp. 248-251.

[112] J. Wang, F. Viawan, and T. Werner, "Effects of sensor technology on differential protection," in *10th IET International Conference on Developments in Power System Protection (DPSP 2010). Managing the Change*, 2010, pp. 1-5.

[113] L. Yiqing, H. Gao, G. Weicong, L. Naiyong, and X. Mingjiang, "A design scheme of line current differential protection based on IEC61850," in *2011 IEEE Power Engineering and Automation Conference*, 2011, pp. 520-523.

[114] H. Y. Li and P. A. Crossly, "Design and evaluation of a current differential protection scheme incorporating a fiber optical current sensor," in *Power Engineering Society Summer Meeting, 2000. IEEE*, 2000, pp. 1396-1400 vol. 3.

[115] G. Fusiek, P. Orr, H. Wang, and P. Niewczas, "All-optical differential current detection technique for unit protection applications," in *2013 IEEE International Instrumentation and Measurement Technology Conference (I2MTC)*, 2013, pp. 1214-1217.

[116] G. Fusiek, P. Orr, and P. Niewczas, "Reliability of an all-optical differential current detection technique during environmental temperature perturbations," in *IEEE SENSORS 2014 Proceedings*, 2014, pp. 1121-1124.

[117] M. Nasir, A. Dysko, P. Niewczas, C. Booth, P. Orr, and G. Fusiek, "Development of Power System Differential Protection Based on Optical Current Measurement," in *48th International Universities' Power Engineering Conference*, Dublin, 2013.

[118] D. Tzelepis, A. Dyśko, G. Fusiek, J. Nelson, P. Niewczas, D. Vozikis, P. Orr, N. Gordon, and C. D. Booth, "Single-Ended Differential Protection in MTDC Networks Using Optical Sensors," *IEEE Transactions on Power Delivery,* vol. 32, pp. 1605-1615, 2017.

Chapter 4. All-optical Configuration of Busbar Differential Protection Scheme

Following the detailed review of the optical method for current and voltage measurement, the Faraday magneto-optic rotation is proposed as a method which not only overcomes the limitations of the existing current transformers but also facilitates the core functionality of a proposed optical busbar differential protection scheme. A new configuration concept of a differential-type protection scheme incorporating a series of Faraday magneto optical current sensors (termed Faraday optical current sensor) is presented. This novel configuration of an all-optical differential protection scheme is developed by utilizing optical devices configured to perform a function analogous to circulating current differential protection. This chapter started with an overview of design, modelling and the generic steps of problem formulation and followed by basic processes and operation of the all-optical differential busbar protection scheme. Then, the basic processes and operation of the proposed all-optical busbar differential protection scheme is explained and followed by the design of optical current sensor based on the Faraday magneto optic rotation. The concept and configuration guidelines including operating time for the proposed protection scheme are also presented. Furthermore, extended configuration of the proposed protection scheme using simple Jones matrix representation are revealed. Finally, a theoretical proof regarding the proposed configuration of all-optical busbar differential protection scheme is also demonstrated.

4.1. Design, modelling and problem formulation

4.1.1. Introduction to design and modelling

In the dictionary, design has several meanings which are the general arrangement of the different parts of something that is made; the process of deciding how something

will work by drawing plans or making models; a drawing or plan from which something may be made [1].

Many statements about design have been documented in literatures. Design can be used to mean all the creative processes of conceiving, developing, and realizing products that requires understanding of logic, basic science and knowledge, as well as experiences [2-4]. In addition, design is an iterative process that is triggered by a new idea. This iterative process is conducted that implies analysing several trial designs one by one until an acceptable design is obtained [5].

Design in engineering is an interesting activity that requires the laws, knowledge and experience to provide the prerequisites for the physical realisation of ideas. Both the understanding and knowledge of the principles are essential when design decisions are used to produce desirable results. The desirable result is expected to be a useful physical entity or a system, valuable in meeting some needs and improving the quality of life [6, 7].

Based on dictionary, modelling has several meanings such as the work of making a simple description of a system or a process that can be used to explain it; the activity of making model which is a copy of something or object that usually smaller than the original object; the activity of making a simple description of a system, used for explaining how something works or calculating what might happen. [8].

Modelling can also be defined as a representation of a system state or condition in real world for observation purposes in order to investigate relationship of each variable. Therefore, the purpose of the model is usually to represent a complex set of behaviours and to help design of experiments as part of the process of hypothesis testing [9, 10],[11]. There are many ways to realize the model such as statement list, drawing, mathematical models, virtual models and physical model. In order to choose the best representation of the model, the selection criteria are depended on circumstance where the model will be applied.

The mathematical modelling has many benefits because it can be used to predict system behaviour, assessment of performance within and beyond the normal operating conditions, and therefore, helps to prevent time wasting [9].

4.1.2. Design and modelling process

Input of design process is the recognition of needs or ideas and objectives that become an ignition or stimulation of the design process. Developing a design or model requires careful examination of information about the real system. The concept generation (generation of ideas) is ignited with a defined problem statement that includes the needs and design specifications and end result with several product concepts. Meanwhile, output of design process is a set of drawing that provides detail of the system along with calculation, analysis, survey, and reports to support the selection of a particular design.

Design process is not merely a single or stand-alone task but could comprise many steps such as: problem definition, design synthesis, parameterization, analysis, ranking and selection, prototype and testing [3],[12]. This multi-step process should be conducted in iterative manner to create a better output as shown in Figure 4.1 [3].
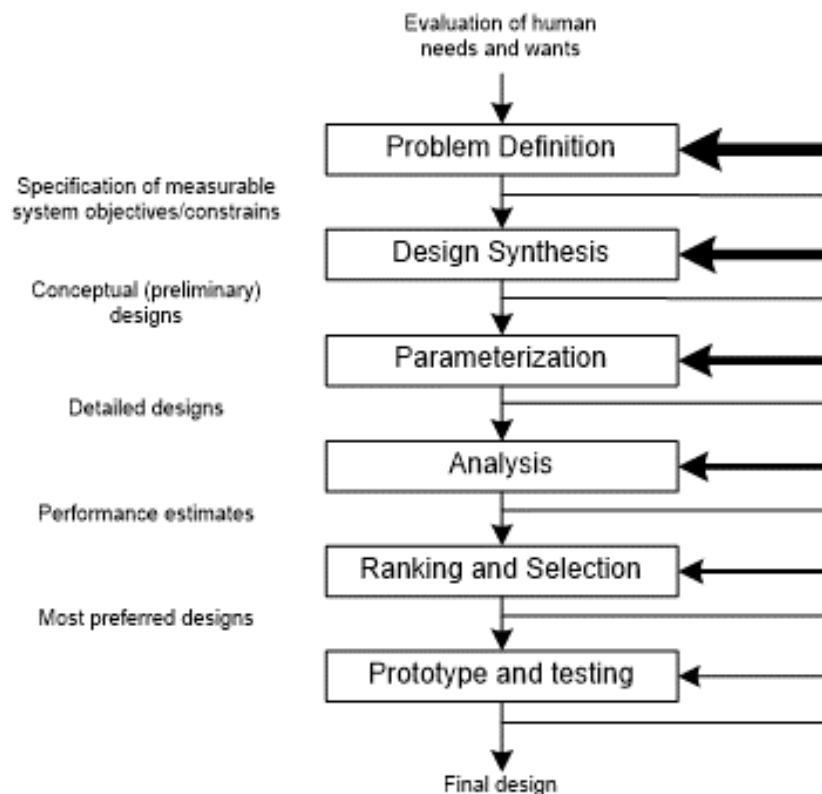
Figure 4.1 Iterative design process [3]

These steps of design process are used in this thesis where the sections and chapters are indicated as follows

- Problem definition: chapter 1 (section 1.2), chapter 2 (section 2.6), and chapter 3 (section 3.2).
- Design synthesis: chapter 3 (section 3.2, and 3.3), and chapter 4 (section 4.2 and 4.3).
- Parameterization: chapter 3 (section 3.4), chapter 4 (section 4.4), and chapter 5 (section 5.1).
- Analysis: chapter 4 (section 4.6), and chapter 5 (section 5.2).
- Ranking and selection: chapter 5 (section 5.3),
- Prototype and testing: chapter 6 (section 6.1, and 6.3)

The modelling process is also documented in [13] that starts with understanding a task or a problem in the real world in order to create a proper problem definition. Then it is followed by an effort to complete the design and modelling process which can have a number of stages undertaken iteratively as listed below:

1. Understand the real situation to create problem definition. This first step was presented at section 2.6 in chapter 2 and section 3.2 in chapter 3.
2. If possible, simplify the problem to obtain a simplified (but representative) version. This step relates to section 4.3.1
3. Find or develop a mathematical model. This step corresponds to chapter 3 (section 3.4 and 3.5), chapter 4 (section 4.4 and 4.5), and chapter 5 (section 5.1).
4. Solve the mathematical model to generate a solution to mathematical description of the problem. This step corresponds to chapter 4 (section 4.3.2 and 4.6), and section 5.2 in chapter 5.
5. Translate the solution in order to obtain a simplified practical solution. This step links to section 5.3 in chapter 5 and section 6.2 in chapter 6.
6. Check feasibility. This step correlates to section 5.3 in chapter 5 and section 6.4 in chapter 6.
7. Decide whether the solution meets the assumed performance criteria; if yes go later steps or a certain step that correlates to the performance criteria.
8. Done.

Furthermore, a similar design process could be found in the operation research/ management science process that consists of three phases and 11 steps and is illustrated in Figure 4.2 [10].
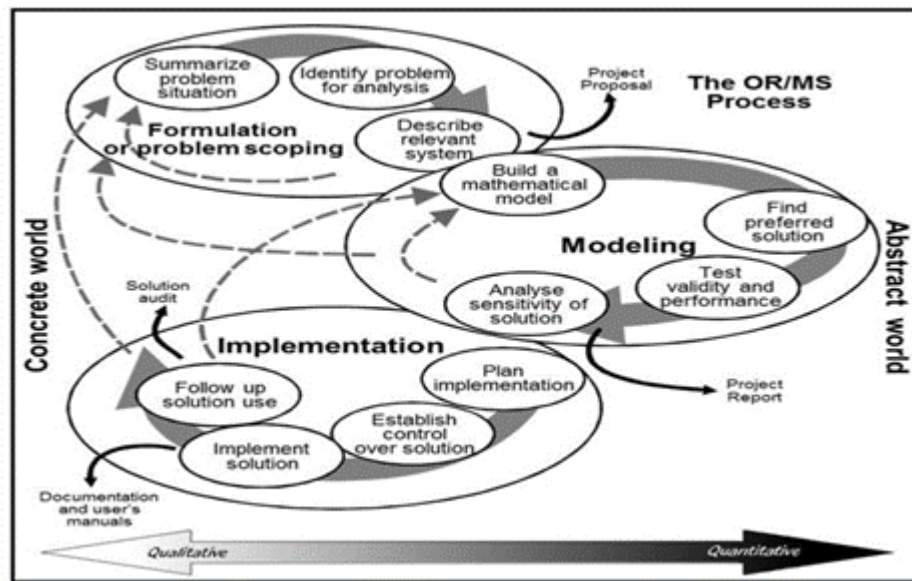
Figure 4.2   A typical research process [10]

4.2. Basic development of optical differential protection scheme

The modelling and design process approaches mentioned above will be applied in this chapter to develop a configuration of fully-optical differential protection scheme which is the main objective of this thesis. The intended protection takes the operation of circulating current differential protection scheme as a guiding principle. The analogy is applied to "translate" the conventional circulating current differential method (used in analogue relays) into optical differential protection (i.e. using optical–based circuits to achieve similar functionality). In this approach, each feature of the circulating current differential relay scheme including the relationships, equations, and key operating function, are converted into optical form.

Firstly, using the analogy in the development of the optical differential protection scheme, the primary line current needs to be translated into optical quantity using a suitable optical transducer. Secondly, the optical relaying quantities have to be defined and differential protection principle implemented by facilitating suitable interaction between the relaying quantities. These two stages (analogous to the conventional protection) have to be defined in the design process of the optical differential protection scheme.

Since the proposed all-optical differential protection scheme is developed based on circulating current differential protection principles. Therefore it is generally accepted that the proposed all-optical differential protection scheme (optical type) has similar operation principles to the electromagnetic relay type of circulating current differential protection (analogue type). The difference among them is only on the media of execution process of the differential quantity where in the analogue type is conducted by current and in the optical type is executed by the polarized light.

In order to develop an optical differential protection scheme using this approach, three basics subject areas of knowledge are utilised in this thesis, i.e. principle of Faraday magneto-optic effect (as a basic element of optical current sensor), circulating current differential protection, and Jones principles (as a convenient tool for optical signal analysis).

4.2.1. Basic processes in the proposed optical configuration of all-optical differential protection scheme

The proposed all-optical differential protection scheme consists of six basic operations which can be listed below:

1. Translating current into a polarization state or a signature (by optical current sensors).
2. Conveying the signature (by polarization state).
3. Summing process (by optical differential arrangement)
4. Converting polarization state to intensity modulation (by the combination of polariser-analyser pair)
5. Photon receiving (by photo-receiver or photo-detector)

6. Comparison and decision-making process (by optical threshold detector).

4.2.1.1. Translating current into a polarization state (signature)

The first basic operation process is translating process. This process is conducted by optical current sensors which are specially designed according to requirements of the proposed all-optical differential protection scheme. Regarding the translating current to optical state modulation, the Faraday optical current sensor has a function to translate the measured current quantities into the polarization state (the light state) quantities. Thus, the input of the Faraday optical current sensor is current, whereas the output is the polarization state as the signatures. The polarization state signatures are proportional to the magnetic fields that are caused by the measured currents in the electric power system.

4.2.1.2. Conveying information (signatures)

The second basic operation process is transmitting information (signatures). The polarized light also has a role as a carrier wave because every status of the measured current that is detected by the Faraday optical current sensor is signed in the polarized light as a piece of information. While the polarized light propagates, it brings sequence information of the measured current. In other words, the polarized light contains a chain of the signatures of the measured current. As consequences, while the polarized light propagates, every status of the measured current quantities in the Faraday optical current sensors always has a unique relationship with the polarization states as the signatures along with its propagation.

4.2.1.3. Summing process

The summing process can be called the optical differential process because output of this process is an optical difference in degree between input and output. The optical differential arrangement is aimed to obtain the difference of polarization state due to the current difference in the protected section.

The optical differential process is inherent process to obtain the optical polarization state difference that automatically accomplished by the optical devices arrangement.

The reason is that while the polarized light propagates, it always updates its polarization state every time. By using a continuous polarized light source, the updating process of polarization state is also a continuous process that always gives the recent status of the polarization state. Since the frequency of polarized light is very much greater than the frequency of the electric current, therefore the variations of polarization state can represent the variations of the measured current.

4.2.1.4. Converting polarization state to intensity modulation

The fourth basic operation process is optical state to intensity modulation conversion process. The optical state to intensity modulation conversion is needed to convert the optical state output of the optical differential arrangement in order to comply with current differential protection principles. Since the final polarization state quantity is actually a modulation state quantity, it cannot be directly applied into the optical differential protection scheme without further processing.

4.2.1.5. Photon receiving (by photo-receiver or photo-detector)

The photon receiving device has to detect amount of photon that contains in the polarized light exiting from the analyser. In this process, the photon that is directed to the surface of optical receiver will be caught and the photon energy will be transferred to other energy form such as current, or voltage. Thus, there are actually two processes in the fifth basic operation process which are photon catching and energy transferring process.

4.2.1.6. Comparison and decision making process

Sixth basic operation process is comparison process. This comparison process compares the energy outputs from photon detector with the threshold setting (reference setting). Since the output of the comparison process is decision signal, therefore the comparison process is also known the decision process because it generates a decision signal. The output of decision process has only two option outputs which are a trip signal or no-trip signal. The output signals correspond to the fault occurrence in the protected zone of electric power system. Thus, the trip signal is generated if the internal fault occurs and vice versa, no-trip signal if no fault exists or the external fault happens.

4.2.2. Basic operation of the proposed all-optical differential protection scheme as the busbar differential protection scheme

The proposed all-optical differential protection scheme utilises the polarized light as the operating quantity. The polarized light incorporating with the optical current sensor is used to translate the measured current. After the polarized light travelling in the proposed optical differential protection configuration, the light states at the exit of the protection scheme configuration are then monitored by a single photo-detector which measures the optical state intensity (power). Afterwards, comparison process is carried out through optical power comparison using a simple optoelectronic threshold detector. The optoelectronic threshold comparison is used to compare the optical power modulation outputs with a threshold quantity in order to determine a fault occurrence. Then, output of the optical threshold comparison is a decision signal which is a trip or no-trip signals which are send to the CB tripping coil as part of the optical protection relaying operation.

The first decision output is a trip signal which is generated by the proposed all-optical differential protection scheme when the optical power modulation is greater than the threshold setting. This condition occurs when an internal fault occurs at the protected circuit which cause both outputs of the Faraday optical current sensors have different polarization states. Therefore, the cumulative result of polarization states is greater than zero at the internal fault situation.

In the other hand, the second decision output is a no-trip signal which is generated by the proposed all-optical differential protection scheme when the optical power modulation is less than the threshold setting. This condition takes place when a fault occurs at outside of the protected circuit (external fault) which cause both outputs of the Faraday optical current sensors (rotators) have the same of polarization states but in opposite direction. Therefore, the cumulative result of light rotations is zero at the external fault condition.

4.2.3. Optical current sensor application and modelling for optical busbar differential protection scheme

Following the detailed review of optical current sensor based on Faraday magneto-optic rotation in section 3.5.2.2, this section utilises the generic Faraday optical current sensor for applying in this thesis. As part of the optical busbar differential protection scheme, the optical sensors for current measurement are used to translate the electric current into optical form [14], [15],[16],[17]. The optical current sensor principle is based on Faraday magneto-optic rotation as displayed in Figure. 4.3.
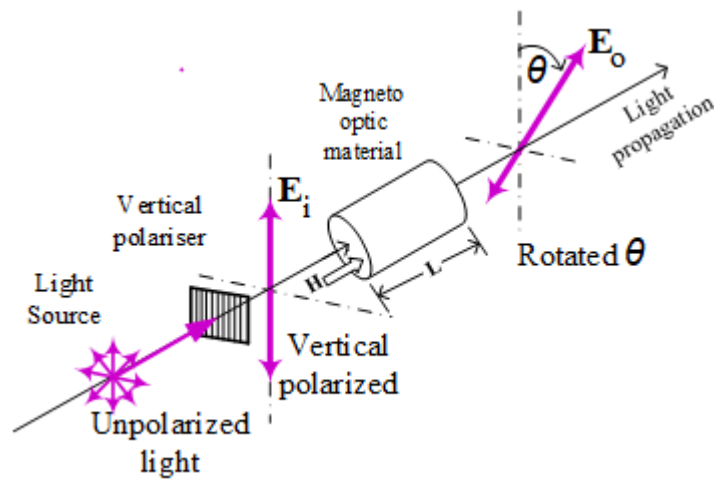
Figure 4.3   Rotation of the polarization plane of a linearly polarized light due to Faraday effect.

The equation (3.66) is rewritten here as a basic representation of a current measuring device as expressed in equation (4.1) [14, 18],[19].

$$\theta \;=\; V\,\boldsymbol{B}\,L \qquad\qquad (4.1)$$

When the magnetic field $\boldsymbol{B}$ in equation (4.1) is generated by the electric current $\boldsymbol{I}$ that flows in a conductor with a certain geometric form, the magnetic field $\boldsymbol{B}$ at any point can be calculated using Biot-Savart formula [20],[21],[22]. The magnetic field $\boldsymbol{B}$ at the centre of a single circular loop with radius R is expressed in (4.2)

$$B = \frac{\mu I}{2R} \qquad (4.2)$$

If the electric current I flows in a solenoid (coil) which has a number of turns per unit length of the solenoid n', the magnetic field B at the centre of solenoid is determined by (4.3)

$$B = \mu n' I \qquad (4.3)$$

Equation (4.3) can be used as guidance for a conceptual design of a coil to generate the magnetic field B as needed in the equation (4.1). Substituting equation (4.3) into (4.1) gives

$$\theta = V \mu n' I L \qquad (4.4)$$

In this equation, V is a Verdet constant of the optical medium that is related to material characteristics, wavelength, and temperature, L is the distance of the polarized light traversing the Faraday magneto-optic material, μ is the permeability of the magneto-optic material, n' is the number of turns per unit length of the coil, and I is the electric current.

According to the equation (4.4), a conceptual design of optical current sensor based on the Faraday magneto optic principle can be developed as shown in Figure 4.4 [23]. It is important to note that the magneto-optic (anisotropic) material is situated at the centre of the coil and positioned perpendicular to the coiled flow of the measured current.

FR sensor

a. Compact FR design

B

b. FR and Coil design as current sensor
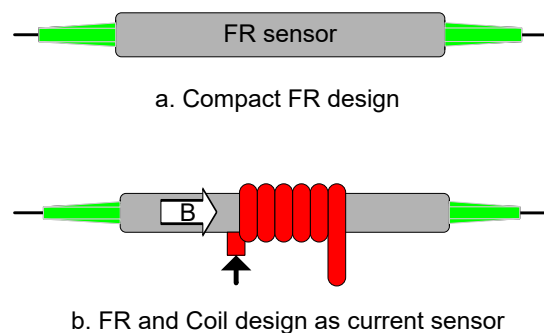
Figure 4.4   FR based optical current sensor prototype

A simple optical current sensor prototype can be realized by constructing each component of the sensor in a proper manner. As a result, the rotation of light state θ in such optical construction could be expressed as

$$\theta = (V\,L\,\mu\,n')\,I \qquad (4.5)$$

This equation means that the angle of rotation is proportional to the measured current on the primary side when polarized light travelled away from the sensor. Thus, overall output of the optical current sensor prototype is characterized by the measured current when other variables in equation (4.5) are constant.

Since the variables in the bracket will be in turn fixed at the final step of design, therefore, the value of those variables are constant and could be changed into a coefficient k as expressed in equation (4.6) and (4.7)

$$\theta = k\,I \qquad (4.6)$$

$$I = K\,\theta \qquad (4.7)$$

where $k = V\,L\,\mu\,n'$ is a coefficient of the optical current sensor and $K = 1/k$.

Since this optical current sensor is based on Faraday magneto optic rotation principle, therefore it could be called Faraday magneto optic rotation-based current sensor (FRCS).

In order to measure current at certain point in the electric power system without saturation problems, the Faraday magneto optic rotation-based current sensor (FRCS) is proposed to substitute the ferrous-core CT [17],[24],[25],[26].

4.3. Concept of optical differential protection scheme

Basic optical differential protection scheme using optical devices can be realized by combining the circulating current differential principle with optical current sensor equation and related optical principles using analogy approach. Let us recall the fundamental differential protection in the equation (2.3).

$$I_{diff} = \Delta I = \left| \sum_{p=1}^{n} I_p \right|$$

The electric current I can be substituted by the rotation angle of polarized light θ using equation (4.7). As a result, it would produce an equation as written in (4.8).

$$I_{diff} = \Delta I = \left| K \sum_{p=1}^{n} \theta_p \right| \qquad (4.8)$$

where θ_p is the optical rotation angle produced by the electric current I_p in the p-th branch, p is branch number, n is total number of branches (circuits) connected to the protected element (e.g. busbar).

For the optical design development and validation, a simple busbar with one incoming and one outgoing circuit is used. Thus, in equation (4.8) I_{diff} is equal (or very close) to zero for the external fault and normal operation because both θ_1 and θ_2 have the same magnitude but opposite direction. Solving equation (4.8) results equation (4.9) and (4.10)

$$|I_1 + I_2| = \left| K \sum_{p=1}^{n} \theta_p \right| \qquad (4.9)$$

$$\theta_{diff} = \left| \sum_{p=1}^{n} \theta_p \right| = k\,|I_1 + I_2| \qquad (4.10)$$

Assuming that all related variables such as verdet constant, length of Faraday material, geometric of coil and number of coil turns in both the proposed optical current sensors FRCS 1 and FRCS 2 [17],[23],[26], are the same (or very similar), the value of $V_1\,L_1\,\mu_1\,n_1'$ is equal to $V_2\,L_2\,\mu_2\,n_2'$. As a result, equation (4.10) could be rewritten as (4.11)

$$\theta_{diff} = V\,L\,\mu\,n'\,|I_1 + I_2| \qquad (4.11a)$$

$$\theta_{diff} = k_{FRCS}\,|I_1 + I_2| \qquad (4.11b)$$

where k_{FRCS} is a constant value of the FRCSs which equal to $V\,L\,\mu\,n'$.

Equation (4.11) shows a simple linear equation where the difference of the angles is caused by difference of the measured currents by the two optical current sensors. Equation (4.11) consists of two terms which are: summation processes (right hand side, RHS, of equation (4.11)), and optical modulation state, θ_{diff} (left hand side, LHS, of equation (4.11)).

Although the RHS of equation (4.11) is seen as a simple summation process of the two currents, it is actually an optical summation which is the basic principle of the proposed novel differential protection scheme. The resulting angle θ_{diff} is the total cumulative polarization state. Since θ_{diff} is an instantaneous modulation state quantity, it is not possible to use it directly in the optical differential protection scheme without further processing.

4.4. Design requirements for a configuration of optical busbar differential protection scheme

Although equation (4.11) is only a simple equation and may not provide immediate solution for the full implementation of optical protection, it contains a key principle on which optical devices can be arranged. All efforts and treatments to realize an optical protection concept have to conform to equations (4.10) and (4.11), and should always consider the simplicity of the optical framework.

In addressing these potentialities, there are three conditions that have to be fulfilled to implement the RHS and the LHS of equation (4.11) as a concept of the optical differential protection scheme:

1) The polarized light is needed for optical current sensor operation. This light is intended to travel along inside fibre optic and the optical current sensors in order to collect the measured currents information through its polarization state.

2) The RHS of equation (4.11) should be conducted using an optical devices arrangement to perform a summing process of the light propagation angle. This

116

summing process should comply with the optical differential process as in equation (4.11).

3) The LHS of equation (4.11) must be transformed to perform the operation principles of the optical differential protection scheme.

4.4.1. First condition: the polarized light

First requirement is straightforward to be fulfilled because there are many simple methods to generate a polarized light as shown in Figure 4.5.

a. Schematic model   b. Devices arrangement

c. Linearly polarized light
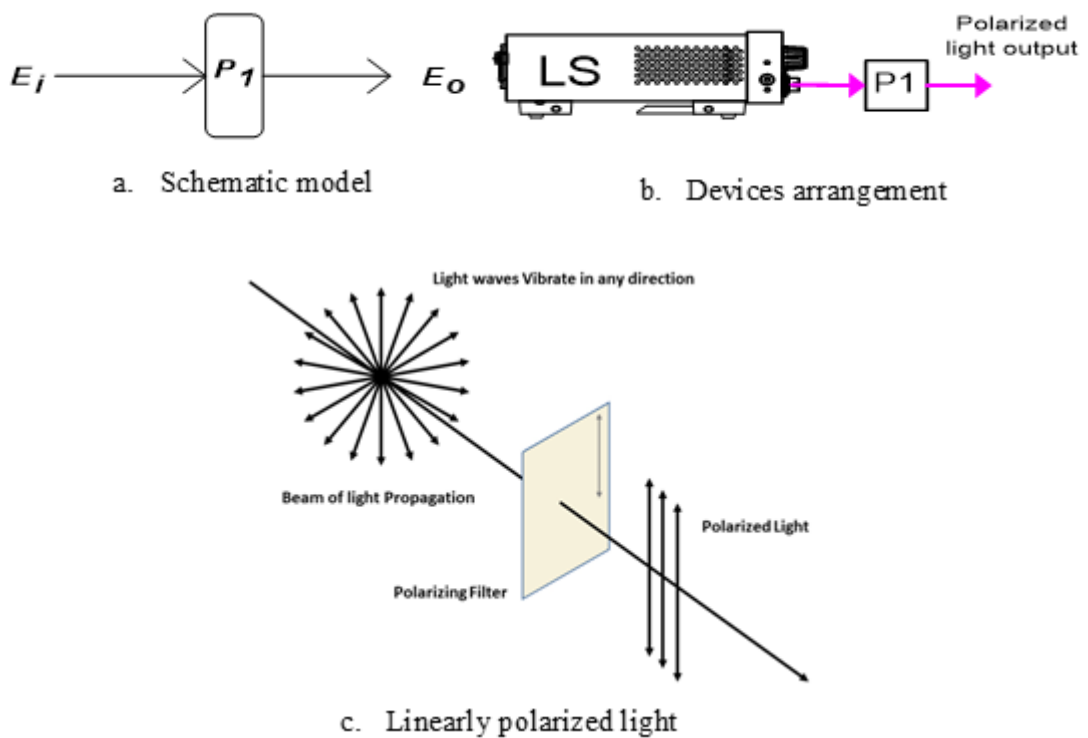
Figure 4.5   Generating polarized light

A polarized light can be generated by applying an optical devices such as a linear polariser on a laser beam [27-30]. Therefore, the first requirement is easily met by using a simple linear polariser and a laser source.

Moreover, the main role of the polarized light is to convey an optical information from optical current sensors by interrogating process when the light passes through them.

The purpose of interrogation process is to collect information of the measured currents from optical current sensors based on its polarization state.

4.4.2. Second condition: optical differential arrangement

A core of second condition is an optical differential arrangement that can perform optical summing processes in the RHS. Although, the summing processes can be basically breakdown into two processes either addition or subtraction process, these processes will appear when direction or orientation of the measured currents is taken into account.

4.4.2.1. The summing process (optical differential process) in the second condition

The optical summing process could be achieved by two option methods which are a direct and an indirect optical summing methods. First, the indirect method is a method to achieve the optical summing process based on the RHS of equation (4.11). Second, the direct method uses only the optical domain processes or devices (pure optical process) to perform the optical summing process.

The indirect method by optical summing process can be conducted by a numerical method process. To achieve this numerical process, outputs of optical current sensors have to be translate from optical form to digital form by electronic conversion devices. Then, the measured currents in digital form are processed in digital summation algorithm to achieve a digital differential process. Thus, the indirect method for optical summation process relies on a contribution of the non-optical domain process or electronic device (mixed optical and non-optical process) such as the involvement of digital processing and digital algorithm.

Selection of these two methods should consider its benefits and drawbacks. The indirect method may need a simple arrangement of optical system. However, the indirect method involves both a signal processing and digital processing as well as requires a digital summing algorithm to carry out the differential process in the RHS of equation (4.11). Therefore, the indirect method could also avoid the optical differential processing that is the aim of this research. Moreover, the indirect method

unfavourable due to the involving many devices and time-consuming process that potentially could contribute a noise, an error and a protection operation delay.

In contrary, the direct method may require a complex arrangement of optical devices, but it does not involve with the non-optical domain devices i.e. digital summing algorithms, signal processing, or digital processing.

Although both methods are potential to be implemented, the direct method is preferred over the indirect method because it offers some promising features i.e. simplicity and speed of process. The direct method requires all optical differential arrangement to execute the optical summing process in order to meet the rule of the RHS of equation (4.11). Thus, the realization of the all optical differential arrangement using the direct method is the focus of discussion in next paragraph.

The realization of all optical differential arrangement could be achieved by developing a proper arrangement of optical devices that can carry out the optical summing process. The summing process can be called the optical differential process because it actually a differential process of electric current in digital form. The output of this process is an optical difference between input and output. The equation (4.11) shows an existence summing operator as part of the summing process. The summing operator can be used as a guidance to develop all optical differential arrangement to meet the rule of the RHS of equation (4.11). In addition, the summing operator in the RHS of equation (4.11) has a meaning the cumulative processes of the light propagation angle.

4.4.2.2. Optical devices arrangement for the second condition

To achieve the optical summing process, an analogue summing process in current transformer (CT) summation method could be referred because it is very similar to the direct summation of optical current sensors [31]. The direct summation of optical current sensors may a simple way to achieve the optical differential arrangement according to a pattern of the RHS of equation (4.11). The direct optical summation method is conducted through summation of the whole optical current sensors by utilizing the polarized light that passes only from one direction through a successive of the optical current sensors in series.

It is also important to be mentioned that the polarity of optical current sensors have to be carefully considered in order to meet requirements in equation (4.10). The polarity of optical current sensor is directly determined by the direction of the magnetic field in the optical current sensor. However, direction of the magnetic field in the optical current sensor depends on the current flow direction into the coil of optical current sensor. Thus, it is required to determine the current flow direction into the coil of optical current sensor. An example for two optical current sensors connection is displayed in Figure. 4.6, where the optical differential arrangement is a consecutively arrangement of FRCS-1 and FRCS-2 with series connection [23].
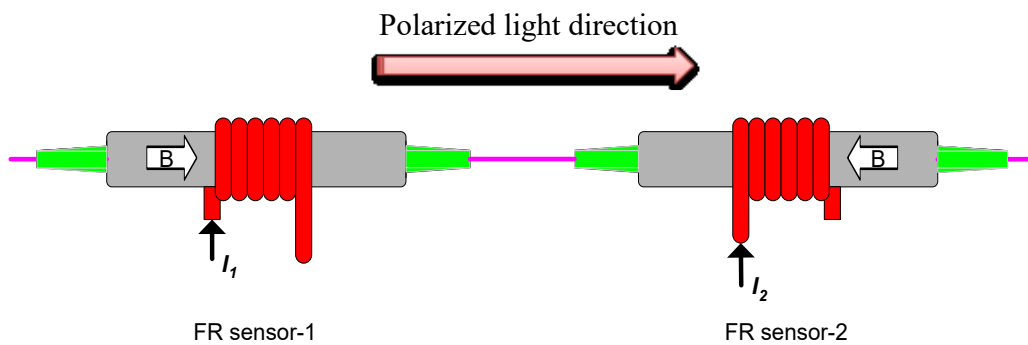
Figure 4.6   The FRCS-1 and the FRCS-2 in series connection

The direct summation method is carried out, firstly, by connecting two optical current sensors in series and reversing current flow into a certain coil of the optical current sensor with respect to other coil (refer to Figure 4.6). This connection type is required in order to cancel a FRCS-1's modulation signal by FRCS-2's modulation signal when the external fault occurs. In the external fault, FRCS-1 produces a certain modulation signal that is cancelled by FRCS-2 which produces the similar modulation signal in the same magnitude but opposite direction. Thus, this connection type could be termed cancellation method. Lastly, the polarized light has to be travelled one direction in the optical differential arrangement.

4.4.2.3. Inherent process in the FRCS-1 and FRCS-2 arrangement

An optical differential process is inherently and automatically performed by the optical devices arrangement. The reason is that while the polarized light propagates, it always updates its polarization state (signature) every time. Therefore, the updating process of polarization state is a continuous process and always gives the recent status of the polarization state where the variations of polarization state are proportionally equivalent to the variations of the measured current. Thus, the optical differential arrangement conducts the inherent summing up process of the polarization state as displayed in Figure 4.7 and Figure 4.8.
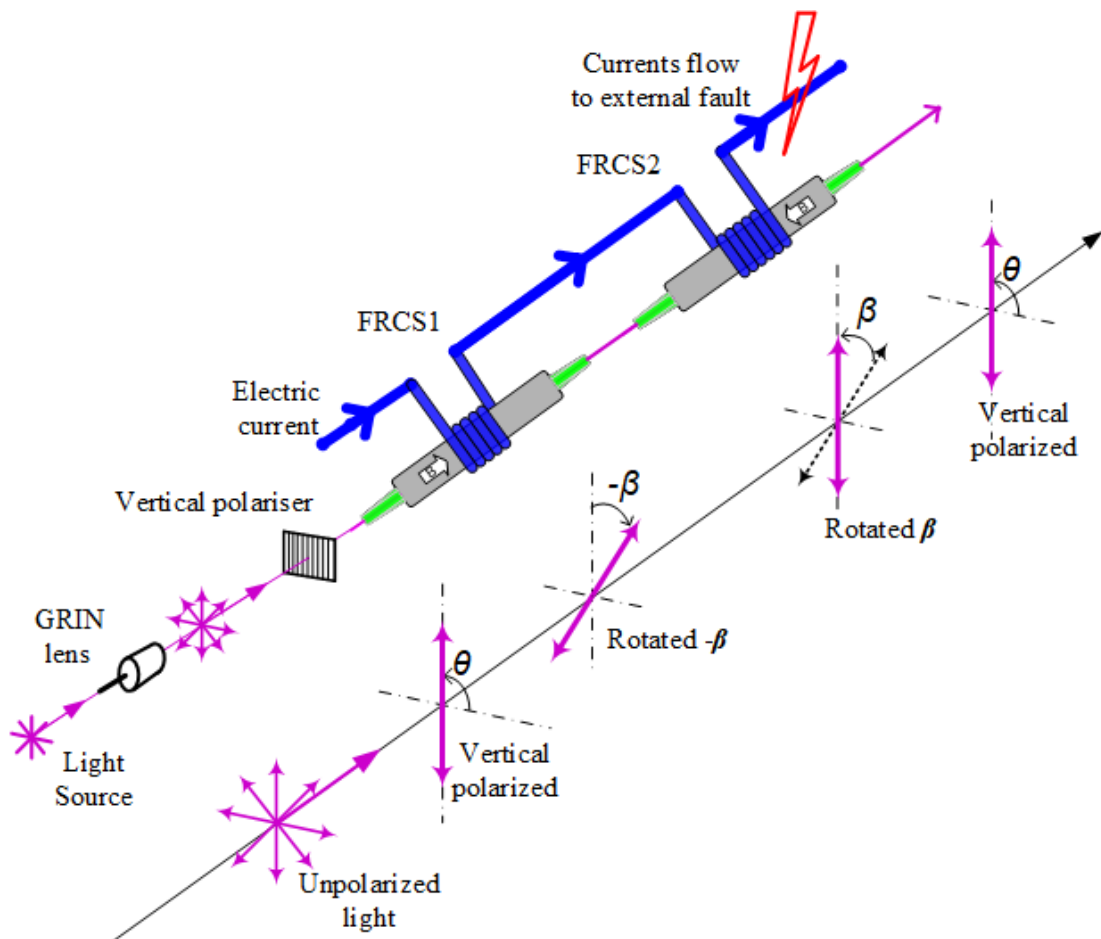
Figure 4.7   An example of the inherent processes in the optical differential arrangement for the external fault

As an output of the inherent process, the signature emitting from the last FRCS is the polarization state difference of the polarized light in the optical differential arrangement. Thus, the final polarization state is the polarization state emerging from the last of consecutive FRCSs. The inherent processes in the optical differential arrangement for the external fault could be seen in Figure 4.7. In this figure, the sensors are put in the coil conductor in order to provide a high electric current in ampere-turns for laboratory experiments. For an example, if current is 5A and a number of coil turns are 400, it will generate 2000 ampere-turns. In the actual power system, the sensors would be putting in the magnetic field round on nearby or very close to busbar conductor.

As a conclusion for the external fault as in Figure 4.7, the final state output of the proposed all-optical differential protection scheme is a vertical polarized light which similar to the input state when the external fault happen. Thus, this final state is actually same with the input state to the optical differential arrangement which is in vertical polarized as well.

The inherent processes in the optical differential arrangement for the internal faults is depicted in Figure 4.8. In this figure, the final state when the internal fault happen is different position of the polarization comparing to the input state.
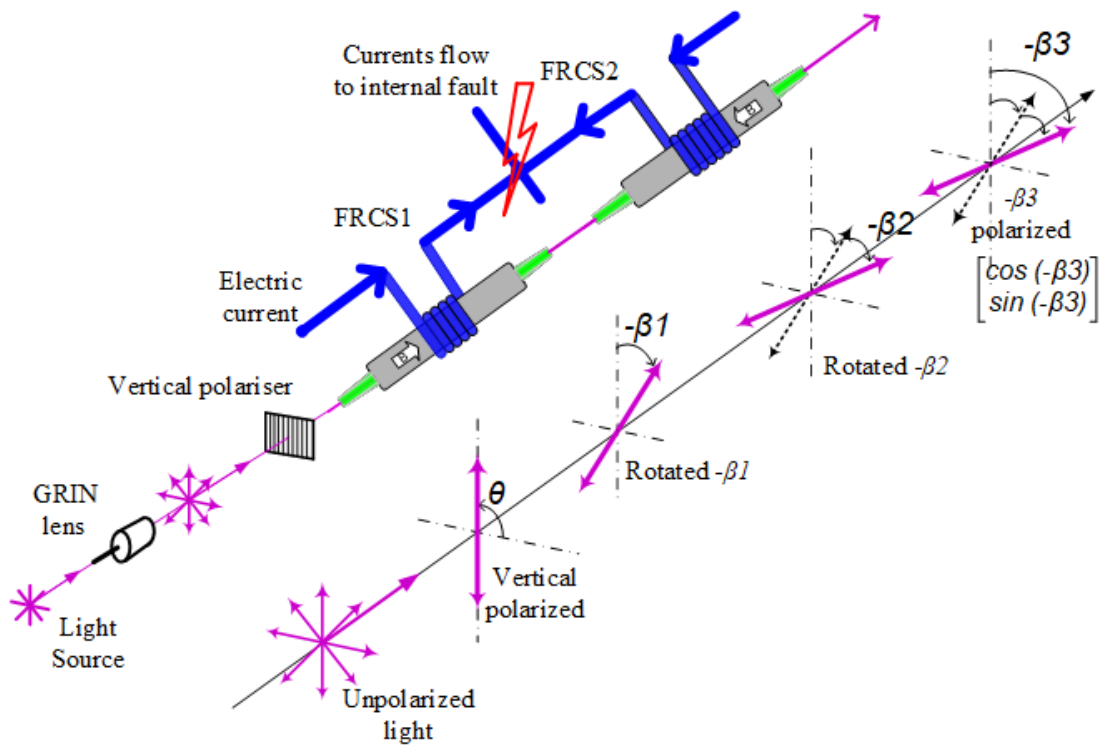
Figure 4.8 An example of the inherent processes in the optical differential arrangement for the internal fault

4.4.2.4. Function of a polariser in the FRCS-1 – FRCS-2 arrangement

Since a FRCS output is a polarization state of polarized light that is referred to the polarization state of the light input, the FRCS output is a relative deviation of the polarization state.

The relative deviation of the polarization state from single or multiple devices can be directly determined if both input and output of the FRCSs polarization state are known. Measuring the polarization state is the key to solve the problems. However it is a very difficult because it will need a precise measurement devices and the device may not available. Therefore, finding the relative deviation of the polarization state by measurement method is unfeasible approach.

The aim of optical differential arrangement is to get the differences of polarization state due to the measured current in the protected section. The summing process is performed by the optical differential arrangement where the whole FRCS is located.

Moreover, the optical differential arrangement is intended to obtain the cumulative change of polarization state output referred to the polarization state input. The cumulative change of polarization state output is derived from summing process in this optical differential arrangement. Since this optical differential arrangement provides a method to obtain total relative deviation of the polarization state, therefore, it is required a reference axis such as the polarization state input or a global reference if it exists.

The lack of the reference axis can be solved by utilising a polariser before the FRCS-1 – FRCS-2 arrangement. This solution is also in line with the first requirement. Due to the use of a polariser, the transmission axis (TA) of the polariser can be used as the reference axis or global reference axis. Therefore, the polarization state input can be easily determined based on orientation of the TA polariser.

As a result, the polarization state output of FRCS either in single or multiple arrangements such as the FRCS-1 – FRCS-2 arrangement can also be determined by referring to the polarization state input.

4.4.2.5. Summary of the optical differential arrangement

In summary, the best practice of the optical summation method is performed by series connection of two optical current sensors where the other sensor must be in reverse magnetic field direction. Propagation of the polarized light in the optical differential arrangement is in one direction and it has function as an executable of the summing process in the RHS of equation (4.11).

The final polarization state output in the optical differential arrangement is directly derived from the polarization state exiting the last FRCSs. In other word, the final polarization state of the polarized light can be also stated as the total cumulative of the output of the whole FRCSs when the polarized light has travelled across them in the optical differential arrangement.

The optical differential process is inherent process to obtain the optical polarization state difference that is automatically accomplished by the optical devices arrangement. While the polarized light propagates, it always updates its polarization state based on

the measured current. Using a continuous polarized light source, the updating process of polarization state is also a continuous process that always gives the recent status of the polarization state. Since the frequency of polarized light is much higher than the frequency of the electric current, therefore the variations of polarization state can represent the variations of the measured current.

Moreover, the final polarization state output of the optical differential arrangement is resulted from the inherent summing up process of the FRCSs. Obviously, the final polarization state has a direct linear relationship with optical modulation difference (optical differential), θ_{diff} and current differential, I_{diff} in the protected circuit of the electric power system.

Furthermore, an inference can be stated that the final polarization state which is actually the differences between the polarization state exiting and entering the optical differential arrangement is equivalent to current differential in the circulating current differential protection.

4.4.3. Third requirement: polarisers arrangement

4.4.3.1. Converting polarization state to intensity (power) modulation

The last requirement is to translate the LHS quantity of equation (4.11) into other quantity that complies with differential protection principles and also meets both of the previous requirements. The LHS quantity of equation (4.11) is an angle difference or cumulative polarization state (termed the final polarization state) quantity. Since the final polarization state quantity is actually a modulation state quantity, it is unable to be directly applied into the optical differential protection scheme without further treatment. Therefore, the final polarization state have to be translated into a suitable quantity that requires further optical treatment for operation of the optical differential protection.

Moreover, the LHS of equation (4.11) should be carefully considered because it is a core design of operating principles of the optical differential protection scheme. The intended LHS quantity of equation (4.11) must be translated into a quantity which at least is similar with a magnitude quantity of differential protection analogue type (an electromagnetic relay type). Since the final polarization state quantity has to be

converted to a magnitude quantity, therefore, the final quantity of θ_{diff} must be converted into optical power modulation that is either probably similar or exactly similar to the i_{diff} quantity in equation (2.4).

Some available options of optical conversion process could be selected from a simple to complex device arrangement in order to achieve the third requirement. However, a simple optical devices arrangement is preferred over the complex device arrangement because it may contribute to faster operating time and simplicity.

Furthermore, since polariser has been applied to meet the first requirement, therefore, the option criteria are now bounded and limited to the polariser arrangement. As result, the polariser arrangement should be a preferred option for a potential solution. The polariser arrangement should be also used as simple as possible methods in order to prevent the use of a complex digital signal processing that may contribute to an additional of significant operation time.

As a consequence of an applied polariser, the polarisers arrangement has to be utilized in order to convert the final polarization state quantity of θ_{diff} to optical power modulation quantity ($|S_{mod}|$) which is known as an optical intensity modulation.

To find out the polariser-based optical converter, Malus law [29, 30] could be referred to understand how the polariser configuration works as the converter unit in order to meet third requirement. Two linear polarisers in series are used to proof the Malus theorem. Moreover, many researchers had basically applied a similar two pieces of linear polariser method which is known as a polariser – analyser set [16, 32, 33]. The simple device arrangement that meets this condition at the same time is a successive two pieces of linear polariser arrangement. These two pieces of linear polariser must be placed with the transmission axis (TA) in perpendicular (crossed) position with respect each other polariser as shown in Figure 4.9. As a result, the use of the crossed TA polariser pair arrangement can convert the final polarization state quantity of θ_{diff} to optical power modulation quantity ($|S_{mod}|$). The crossed TA position of two polarisers meet also the required characteristic of the differential relay.
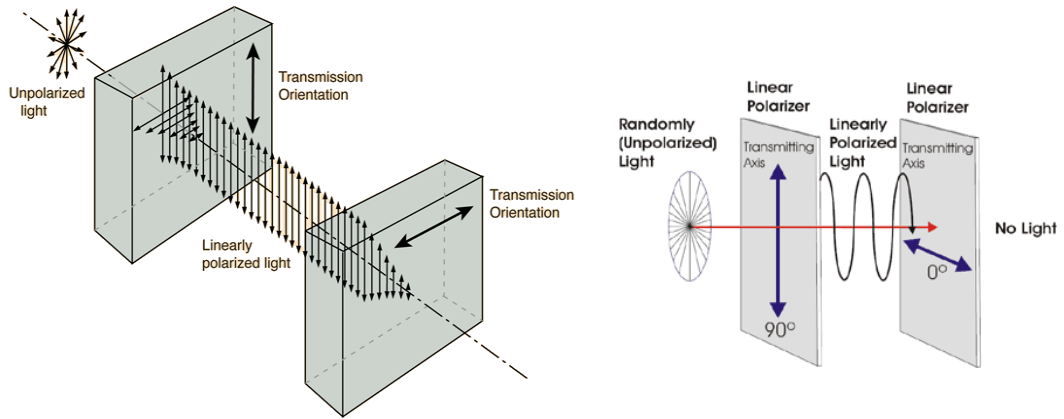
Figure 4.9 Crossed transmission axes arrangement of two polarisers

The use of polariser pairs to meet the third requirement is also in line with the first and second requirements. Therefore, a total number of the needed first polariser is three polarisers based on the requirements and excluding the second polariser in the third requirement. However, it is also sufficient if only using a piece of polariser as a first polariser instead of three polarisers.

4.4.3.2. Function of the crossed transmission axis P1-P2 pairs

Although the need of polarization state reference has been solved by using a polariser in second requirement, it is a benefit for using the P1-P2 pairs because determining any changes in the oscillation direction without the need of polarization state reference can be resolved.

The P1-P2 pairs are needed in order to omit the reference in polarization state by converting the polarization state deviations (differences) into optical modulations. Therefore, the role of this arrangement is to convert the differences of polarization state between FRCS1 and FRCS2 into optical modulations. A pairs of crossed TA polariser arrangement has a function as a converter unit which converts the final polarization state quantity of θ_{diff} to optical power modulation quantity ($|S_{mod}|$).

As consequences, if there is a deviation the polarization state, then an output of optical modulation will occur. Otherwise, if there is no polarization state deviation, hence

there is also no optical modulation output. Thus, a P1-P2 arrangement can substitute the function of the polarization state reference by transforming into the optical modulation. Therefore, the output of the configuration can be easily monitored.

As a summary, the FRCS1-FRCS2 optical differential arrangement can be utilized to obtain the differences of polarization state, but it needs the polarization state reference. In order to detect any differences of the polarization state output without that constrains, the crossed TA P1-P2 pairs have to be added into the FRCS1-FRCS2 arrangement. The crossed TA P1-P2 pairs in the P1-FRCS1-FRCS2-P2 configuration can resolve the reference problem in relation with the differences of polarization state by converting it to the optical modulation.

4.4.4. Final arrangement of the all-optical differential scheme

After completing the three requirements of the optical differential protection conceptual design, a step by step development design including a final design of the optical differential arrangement could be shown in Figure 4.10.a – Figure 4.10.e.
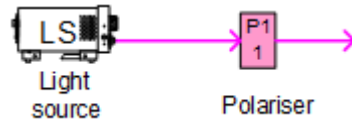
a)   A design results for the first requirement
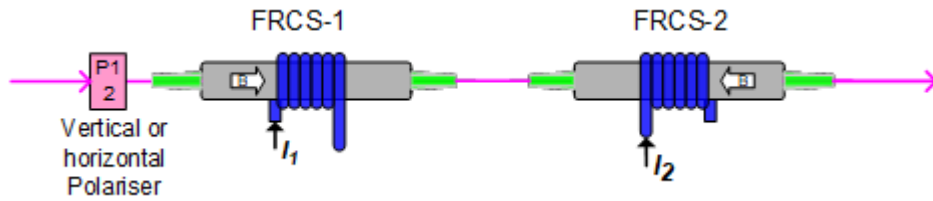
b)   A design result for the second requirement
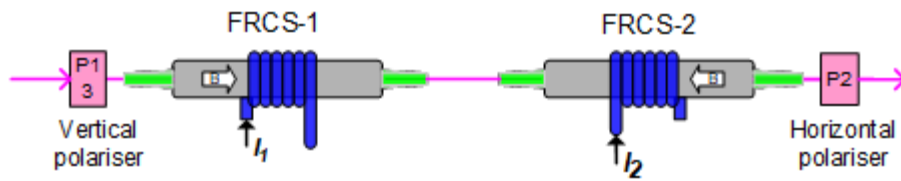
c)   A design result for the third requirement
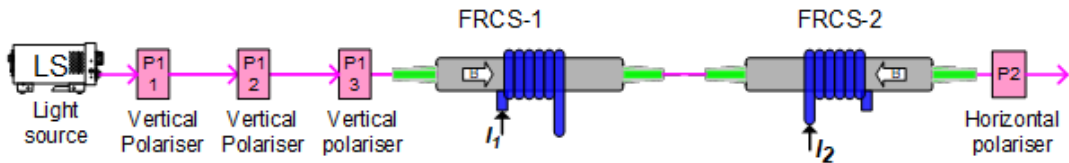
d)   A preliminary design
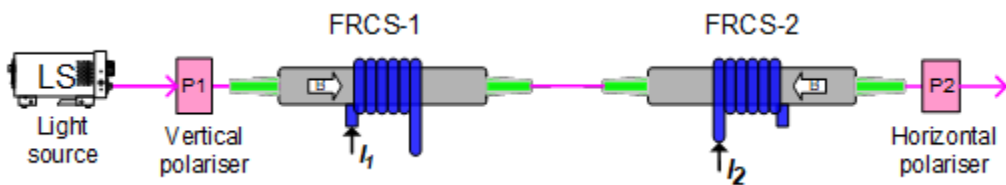
e)   A final design after reducing two polarisers

Figure 4.10 A step by step arrangement of the all-optical differential scheme

129

The final design of the optical differential arrangement as shown in Figure 4.11 is a simple optical devices arrangement which consists of a light source, two polarisers, and two FRCSs. Due to the use of all optical devices in the optical differential arrangement, therefore, this arrangement can be termed all-optical differential arrangement. It provides a simple design because it applies a direct method of optical differential without using non-optical domain devices i.e. a digital summing algorithm.
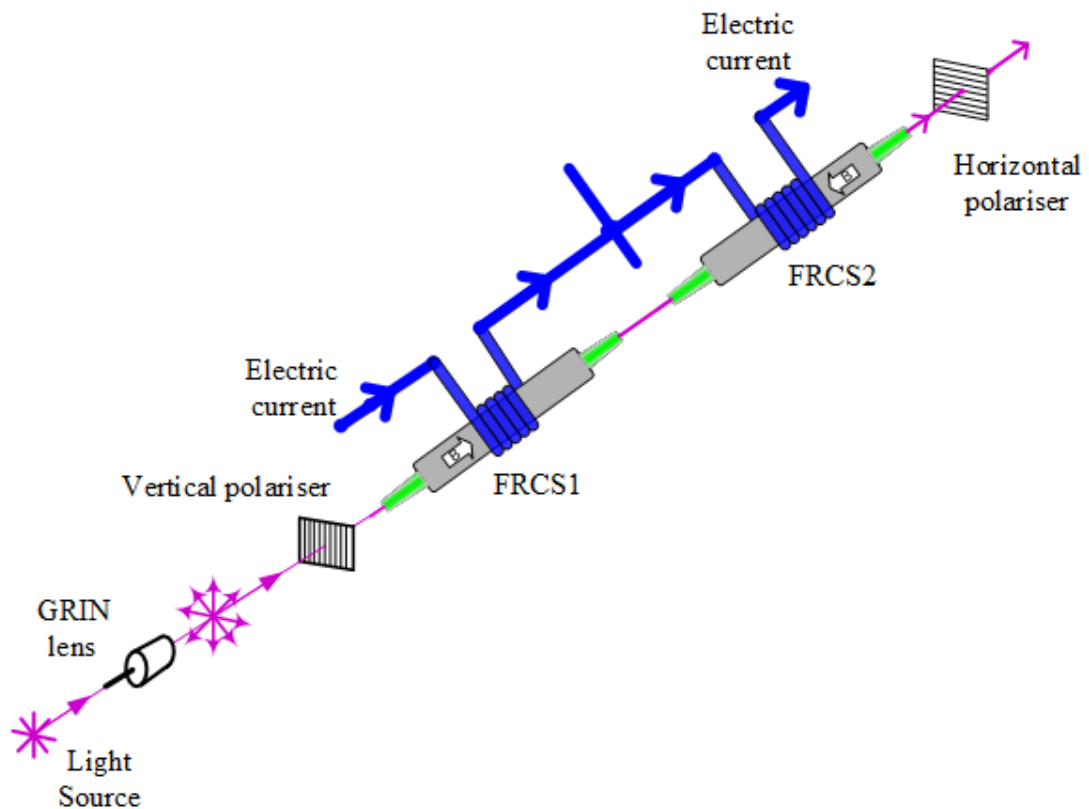
Figure 4.11 An optical layout including orientation of TA polarisers and electrical connection in the optical differential arrangement

In summary, this final optical differential arrangement is a preliminary configuration of the optical differential protection scheme because it needs a photon detection and a threshold comparison devices.

Another summary, the connection pattern of the circulating current differential

130

protection has been maintained during development of the optical differential arrangement. The purpose of the maintained connection pattern is to retain the similarity of operation principle and the simplicity of differential protection scheme. In addition, this action has generated an analogous process from analogue type to optical type of differential protection scheme. Therefore, it could be said that the optical differential arrangement is an analogy of the electromagnetic relay type of circulating current differential protection.

There are some possible outcomes that rise from the proposed all-optical differential arrangement. Firstly, inherent operations functionality of differential protection is conducted by proper arrangement of optical current sensors and the crossed TA polariser pair. These are intended to have a direct contribution to minimize complexity of the optical differential protection configuration, thus gives simplicity to this model. Secondly, an indirect contribution may have an influence to reduce the total operating time through a simple design and optical devices arrangement.

4.4.5. Optical detector (photo-detector / photo-receiver)

Optical detector is required in the configuration of the all-optical differential protection scheme to measure the optical modulation output. Since polariser P2 is the last sequence of optical devices in the optical differential arrangement, an output of P2 must be connected to the photon detection unit. The photon detection is performed by a photo-receiver which consists of photodiode such as Si and InGaAs, to measure amount of receiving photon that arrive at surface of photon receiver. Due to low optical power levels, the photo-diode is followed by trans-impedance amplifier ($1k\Omega$ to $100M\Omega$) to increase the output power. The amount of photon is then translated into optical intensity (power). The optical power output at detector unit can be expressed in equation (4.12) [34, 35].

$$I = |S| = \frac{(E_0 . E_0^*)}{Z} \tag{4.12}$$

where E_o is electric field component of the transverse wave, E_o^* is transpose of the complex conjugate E_o and Z is total impedance of the medium which is the ratio of the electric field to the magnetic field.

Another expression to calculate the incident light power (P) is written in equation (4.13).

$$P = \frac{I_{PD}}{R(\lambda)} \tag{4.13}$$

where, I_{PD} is a generated photo-current, and $R(\lambda)$ is responsivity of a photo-diode at given wavelength.

The photo-detector output which is optical intensity (power) is then passed to a threshold comparison unit.

4.4.6. Optical threshold comparator

The main function of an optical threshold comparison is to compare the photo-receiver's power modulation output to a certain optical power level or a threshold setting (a reference setting). The threshold relies on sensitivity of detector components including photo-receiver. When threshold and photo-receiver are made from a high quality material, these devices can convert the whole received photon on its surface. It could be said that those devices have high sensitivity.

The optical threshold setting have to be increased when the power modulation output consists of white noise or some unintended signals. As a comparison to the role of a high impedance resistor in the circulating current differential protection, the high impedance resistor in series with the relay could decrease the relay sensitivity because the differential current is forced to flow away from the relay branch to the saturated CT impedance.

The comparison process in this unit is carried out by a simple optoelectronic threshold detector through optical comparison. Since the output of the comparison process is a decision signal, therefore the comparison process is also known the decision process because it generates a decision signal.

The output of comparison process is either a trip signal or no-trip signal. A trip signal is generated when power modulation level is greater than the threshold setting. Otherwise, no-trip signal is happen if power modulation level is less than or equal to the threshold setting.

The optical threshold comparator can be utilized as fault detector to detect an occurrence of fault in the protected zone of power system. Thus, it is needed in the configuration of the all-optical differential protection scheme as fault detector. The comparator output of the all-optical differential protection which is either a trip signal or no-trip signal depends on the existence of faults.

The threshold setting is determined by considering simulation outputs of the electric power system in two significant different situations which are high resistance internal fault and zero resistance (solid) external fault. After determining the threshold setting, the simulation is performed to evaluate and assess the protection attributes i.e. sensitivity, stability and dependability.

In relation with the all-optical differential protection and the power system faults, the decision output of the comparison task could be interpreted as follows. First condition, a trip signal is generated by the comparison device if the optical intensity modulation is greater than the threshold setting. This condition happens when an internal fault occurs in the protected circuit. Second condition, no-trip signal is generated by the comparison device when the optical intensity modulation is less than or equal to the threshold setting. This condition takes place when an external fault occurs.

4.5. Operating time of the proposed all-optical differential protection scheme

In general, there are three group processes of the proposed optical differential protection scheme which are optical differential, optical detection and decision processes. These processes are respectively carried out in optical differentiator (optical differential arrangement), optical detector and optical comparator. As consequence, the total operating time of the proposed optical differential protection scheme also consists of three consecutive time intervals which are: the optical differentiator time, optical detection time and intensity comparison including decision processing time.

The optical differential process is a combination of translating the measured currents, conveying the unique information (signature) and summing up processing.

Although the optical differential consist of some processes, the total processing time in the whole Faraday optical current sensors configuration is conducted in very short interval time (in microsecond) because it uses the polarized light to execute the sum up process in whole optical devices.

The optical differential processing time can be calculated using a formula which will be explained as follows. Suppose that c is the light constant and n is refractive index of optical medium. The light speed in the optical medium v_n is expressed (4.14)

$$v_n = \frac{c}{n} \tag{4.14}$$

The total time (t) that is needed by an object (such as the polarized light in this case) to travel in the optical medium with total distance (s) and the speed v_n is written as

$$t = \frac{total\ distance\ (s)}{v_n} \tag{4.15}$$

Substituting equation (4.14) into (4.15), the optical differential processing time is calculated as

$$t = \frac{total\ distance\ (s)}{c/n} \tag{4.16a}$$

$$t = \frac{n}{c}\ x\ s \tag{4.16b}$$

For the remaining processes, which are the photo-detection and comparison of the optical power modulation and decision making processes, their processing time are very difficult to be directly determined because it has no theoretical equation. These difficulties can be overcome by using the similar processing time from the relay manufacturer's data [36-39]. Therefore, the typical numerical relay processing time is reasonably used because these processes in both relay types are approximately similar.

4.6. Optical busbar differential protection scheme configuration

An optical differential protection scheme can be established by combining the final all-optical differential arrangement with a photo receiver and an optical threshold comparator as displayed in Figure 4.12. Since the all-optical differential arrangement is utilised in the optical differential protection scheme, therefore, it can be termed as an all-optical differential protection scheme. In the first development step including prototype and laboratory experiment activities, the all-optical differential protection scheme will be simulated and assessed for busbar protection application. Therefore, it is named as an all-optical busbar differential protection scheme.

a. Schematic diagram

b. The proposed all-optical differential protection scheme
(analogous to the circulating current differential)
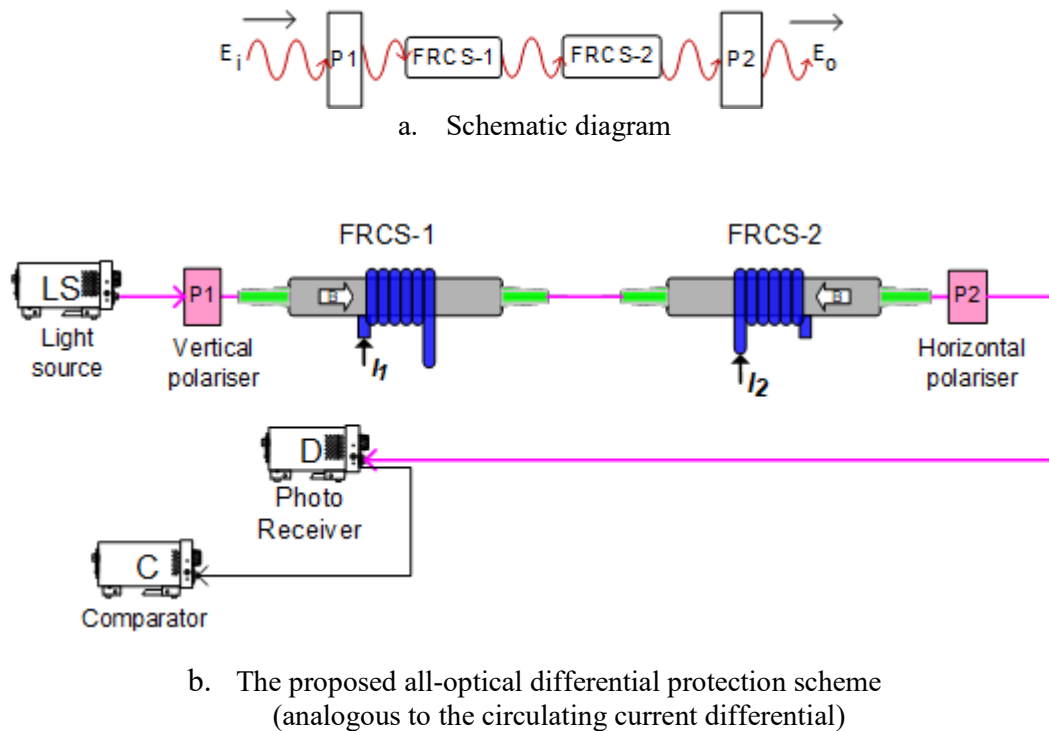
Figure 4.12 Configuration of proposed all-optical busbar differential protection scheme

In the Figure 4.12, there are 4 optical devices model which are $P1$ as J_1, FRCS1 as J_2, FRCS2 as J_3 and the last $P2$ as J_4. Following Jones principle in equation (2.50), the

proposed all-optical differential protection scheme in Jones formalization that states a relationship between input and output of polarized light could be expressed in equation (4.17) [40].

$$E_o = J_{P2} \, J_{FRCS2} \, J_{FRCS1} \, J_{P1} \, E_i \qquad (4.17)$$

where J_{P1} and J_{P2} are matrices representation of polarisers 1 and 2 with crossed TA position, J_{FRCS1} and J_{FRCS2} are matrices representation of optical current sensor 1 and 2, and E_i is matrices representation of the polarized light input.

In this complete configuration of the proposed all-optical differential protection scheme, the transmission media are considered to be an ideal transmission medium. As a result, the polarized light wave could propagate freely in the transmission media without affected by them in such condition that any losses and disturbances are supposed to be zero. Since the absence of the effect of the transmission media, therefore, either it could be constituted by an identity matrix J_I in equation (4.17) or it may be just neglected their existence.

In order to present the configuration of the proposed all-optical differential protection scheme using perfect optical devices model, all optical model symbols in section 2.8.2 should be properly substituted into equation (4.17). In addition, it should be remembered that both polarisers must have the TA difference 90 degrees each other. It means that when TA of polariser P1 is in vertical position, TA of polariser P2 must be in horizontal position. As a consequence, the rule in equation (2.53) should be applied to equation (4.17) and, therefore, this effort would yield

$$E_o = R(90) \, J_{P1} \, R(-90) \, J_{FRCS2(\theta_2)} \, J_{FRCS1(\theta_1)} \, J_{P1} \, E_i \qquad (4.18)$$

At this point, the complete configuration of the proposed all-optical differential protection scheme with perfect Jones matrices representation could be obtained by substituting the representation symbols in equation (4.18). The Jones matrix configuration of the proposed method would be written as

$$E_o = \begin{bmatrix} 0 & 0 \\ 0 & 1 \end{bmatrix} \begin{bmatrix} \cos\theta_2 & -\sin\theta_2 \\ \sin\theta_2 & \cos\theta_2 \end{bmatrix} \begin{bmatrix} \cos\theta_1 & -\sin\theta_1 \\ \sin\theta_1 & \cos\theta_1 \end{bmatrix} \begin{bmatrix} 1 & 0 \\ 0 & 0 \end{bmatrix} \begin{bmatrix} E_x \\ E_y \end{bmatrix} \qquad (4.19)$$

4.7. Extended configuration of the proposed all-optical differential protection scheme

Configuration of the proposed all-optical differential protection scheme that has been explained earlier is only for the electric power system that has busbar with one incoming and one outgoing feeder. However, the configuration of the proposed all-optical differential protection scheme can be extended in order to fit with the number of busbar circuits for application on a multi-terminal busbar.

In order to adapt the busbar topology extension, an example of extended configuration of the all-optical differential protection scheme is provided here. Suppose that the number of feeders in the busbar section have been extended to 5 circuits ($n = 5$) which consist of 2 incoming (i_1 and i_2) and 3 outgoing (i_3, i_4 and i_5) circuits. For these five circuits, the optical differential output in equation (4.10) is rewritten as

$$\theta_{diff} = \left| \sum_{p=1}^{n=5} \theta_p \right|$$

Also, a number of optical current sensors must be added accordingly based on Kirchhoff Current Law into the proposed configuration as in Figure 4.12 and the equation (4.17). Therefore, modifying the equation (4.17), a new equation is generated in order to accommodate the addition of 3 optical current sensors into the existing configuration that could be expressed as

$$\boldsymbol{E_o} = J_{PV} \, J_{FRCS5} \, J_{FRCS4} \, J_{FRCS3} \, J_{FRCS2} \, J_{FRCS1} \, J_{PH} \, \boldsymbol{E_i} \qquad (4.20)$$

The configuration of the proposed scheme can be extended to adapt an implementation in the multi-terminal busbar. In other word, the configuration must be changed to comply with the number of optical current sensor in the busbar.

Regarding the increasing number of busbar circuit, this result shows also that the extended configuration of the all-optical differential protection scheme amends only the number of optical current sensor J_{FRCS-n}. The augmentation of optical current sensors may still be feasible because this action probably will not cause a serious

problem as long as the optical transmission links are considered to be an ideal transmission medium.

However, when the transmission media are viewed as an imperfect optical link, their effect to the polarized light such as absorption, reflection and refraction should be taken into account. Therefore, providing an augmentation of the equation (4.20) by including the fibre optic features as imperfect optical transmission link could be become critical issues because of the birefringence (double refraction) effect and attenuation of the optical fibre medium. Both the birefringence effect and attenuation of the optical fibre medium can distort optical modulation and also increase losses of the optical modulation. Therefore, utilization of a computer programme could be very useful in order to simulate, to predict, and to validate the model [41].

Although existence of the birefringence effect and attenuation in the optical fibre cannot be neglected and have to be considered in equation (4.20), the extended configuration of the proposed all-optical differential protection scheme may still give a satisfied output when the requirements are fulfilled [40]. The requirements are that a relatively short length of fibre optic sections is used for the optical link in the proposed all-optical configuration and an extra concern should be delivered in order to choose a suitable fibre optic characteristic that gives a small birefringence effect and as well as lower attenuation.

4.8. Demonstrating the proposed all-optical configuration using the theoretical method

In order to demonstrate the proposed configuration of all-optical differential protection scheme, the Jones matrix configuration in equation (4.19) has to be solved by substituting some related variables. It should be noted that the equation (4.19) have to be equal to zero for the external faults and non-zero values for the internal faults. Therefore, by solving this equation through matrix multiplication, the result could be written as

$$E_o = \begin{bmatrix} 0 \\ (\sin\theta_2 \, \cos\theta_1 \, + \, \sin\theta_1 \, \cos\theta_2) \, E_x \end{bmatrix} \qquad (4.21a)$$

$$E_o = (\sin\theta_2 \, \cos\theta_1 \, + \, \sin\theta_1 \, \cos\theta_2) \, E_x \qquad (4.21b)$$

In order to solve equation (4.21b), there are two ways which are using flow direction of the current in FRCS coil and the rotation angle.

4.8.1. The external fault conditions

4.8.1.1. The theoretical demonstration method 1: using the current flow direction in the coil

From equation (4.7a) and (4.11), It is noted that

$$\theta_1 = k_{FRCS1} . i_1 = k_1 i_1$$

and

$$\theta_2 = k_{FRCS2} . i_2 = k_2 i_2.$$

By substituting these two variables into equation (4.21b), the complete relationship between input and output of polarized light in the configuration can be written as

$$E_o = (\sin k_2 i_2 \, \cos k_1 i_1 + \sin k_1 i_1 \, \cos k_2 i_2 \,) \, E_x \qquad (4.22)$$

As mentioned in equation (4.10) above, the variable k_1 is treated to have similar value with k_2 and will be a constant value at the final design, so thus $k_1 = k_2 = k$

$$E_o = (\sin (k.i_2) \, \cos (k.i_1) + \sin (k.i_1) \, \cos (k.i_2) \,) \, E_x \qquad (4.23)$$

By design, the coil turn direction of FRCS2 is in opposite with respect to FRCS1. Therefore, it is clear that $i_2 = -i_1$ for an external fault case. Substituting this value into equation (4.23) above would create

$$E_o = (-\sin (k.i_1) \, \cos (k.i_1) + \sin(k.i_1) \, \cos(k.i_1) \,) \, E_x \qquad (4.24)$$

Note that the entities in the bracket {} are equal and in opposite sign hence

$$\{ -\sin (k.i_1) \, \cos (k.i_1) + \sin(k.i_1) \, \cos(k.i_1) \} = 0$$

Therefore, the result is

$$E_o = 0 \qquad (4.25)$$

$$\therefore \quad E_o = 0 \qquad (\because \text{q. e. d})$$

4.8.1.2. The theoretical demonstration method 2: using rotation angle

By design the direction of magnetic field in FRCS-2 is opposite with respect to the direction of magnetic field in FRCS-1 and since for the external fault both the magnitude and direction of the flow current is equal. Therefore, the magnetic field can be rewritten

$$B_{OCS2} = -B_{OCS1}$$

As consequences, from equation (4.3) and (4.10), it is clear that

$$\theta_2 = -\theta_1$$

Substituting this value into equation (4.21b) would yield

$$E_o = (\sin(-\theta_1) \; \cos\theta_1 \; + \; \sin\theta_1 \; \cos(-\theta_1)) \; E_x \qquad (4.26a)$$
$$E_o = (-\sin\theta_1 . \cos\theta_1 \; + \; \sin\theta_1 . \cos\theta_1 \,) \; E_x \qquad (4.26b)$$
$$E_o = 0 \qquad (4.26c)$$

$$\therefore \quad E_o = 0 \qquad (\because \text{q. e. d})$$

4.8.2. The internal fault conditions

4.8.2.1. The theoretical demonstration method 1: using the current flow direction in the coil

It is needed to choose two arbitrarily values for example i_1 and i_2 for an internal fault case. Due to the design condition, $i_2 = i_1$ are obtained. Substituting this value into equation (4.23) above would create

$$E_o = (\; \sin(k.i_1) \; \cos(k.i_1) + \sin(k.i_1) \; \cos(k.i_1) \,) \; E_x \qquad (4.27a)$$
$$E_o = (2(\; \sin(k.i_1) \; \cos(k.i_1)) \; E_x \qquad (4.27b)$$

Therefore, the result is non-zero values and written as

$$E_o \neq 0 \qquad\qquad (4.28)$$

$$\therefore \quad \boldsymbol{E_o} \neq 0 \qquad (\because \mathrm{q.e.d})$$

4.8.2.2. The theoretical demonstration method 2: using rotation angle

The similar assumption is made that an arbitrarily value for example $\boldsymbol{i}_1$ and $\boldsymbol{i}_2$ for an internal fault case. Due to the design condition, $\boldsymbol{i}_2 = \boldsymbol{i}_1$ are obtained. Therefore, the magnetic field can be rewritten

$$B_{OCS2} = B_{OCS1}$$

As consequences, from equation (4.3) and (4.10), it is clear that

$$\theta_2 = \theta_1$$

Substituting this value into equation (4.21b) would yield

$$\boldsymbol{E_o} = (\sin(\theta_1)\ \cos\theta_1\ +\ \sin\theta_1\ \cos(\theta_1))\ E_x \qquad\qquad (4.29a)$$
$$\boldsymbol{E_o} = 2(\ \sin\theta_1 . \cos\ \theta_1\ )\ E_x \qquad\qquad (4.29b)$$

Therefore, the result is non-zero values and written as

$$\boldsymbol{E_o} \neq 0 \qquad\qquad (4.30)$$

$$\therefore \quad \boldsymbol{E_o} \neq 0 \qquad (\because \mathrm{q.e.d})$$

Both final results of the polarized light output for the external fault cases $\boldsymbol{E_o}$ are zero, whereas for the internal fault cases are non-zero values. Since the proposed all-optical configuration of differential protection scheme generates a similar result with the circulating current differential protection, two simple conclusion can be made.

First, the results provide a theoretical proof that the proposed configuration of all-optical differential protection scheme is correct. Therefore, this proposed all-optical configuration is valid and the optical device models in this configuration are also correct.

Second, it can give an inference that representation of the mentioned configuration in the optical domain as stated by equation (4.17) is similar to the representation of

circulating current differential protection in the electrical domain as expressed by equation (2.3).

4.9. Conclusions

Design, modelling and basic processes of the proposed configuration of all-optical busbar differential protection scheme have been presented. A conceptual design of the Faraday rotation optical current sensor (FRCS) and the all-optical busbar differential protection scheme have been developed by solving the design requirements. The developed FRCSs incorporating with optical devices arrangement i.e. polarisers have been directly applied to invent a novel configuration of all-optical busbar differential protection scheme. As part of the optical protection scheme modelling, the optical devices representations using Jones formalization were also applied in the extended configuration of all-optical busbar differential protection scheme.

Finally, theoretical proof methods have been conducted to verify the correctness of the proposed configuration of all-optical protection scheme.

Next chapter will present simulation of the proposed all-optical busbar differential protection scheme.

4.10. References for chapter 4

[1]   Oxford.   (2016).   *Oxford   Learner's   Dictionaries*.   Available: http://www.oxfordlearnersdictionaries.com/definition/english/design_1?q=design

[2]   P. R. N. Childs, "Chapter 1 - Design," in *Mechanical Design Engineering Handbook*, ed Oxford: Butterworth-Heinemann, 2014, pp. 1-24.

[3]   *Handbook of systems engineering and management*: New York : Wiley, 1999.

[4]   G. Pahl, K. Wallace, L. n. Blessing, and Springerlink, *Engineering design : a systematic approach*, 3rd ed.. ed. London: London : Springer, 2007.

[5]   *Engineering Design [internet resource] : Representation and Reasoning*: Cambridge : Cambridge University Press, 2012.

[6]   J. Armstrong, *Design matters [internet resource] : the organisation and principles of engineering design*. London: London : Springer, 2008.

[7]   J. S. Arora, "Chapter 1 - Introduction to Design Optimization," in *Introduction to Optimum Design (Third Edition)*, ed Boston: Academic Press, 2012, pp. 1-15.

[8]   O. University. (2016). *Oxford Learner's Dictionaries*. Available: http://www.oxfordlearnersdictionaries.com/definition/english/modelling?q=modelling

[9]   D. J. Murray-Smith, *Modelling and simulation of integrated systems in engineering [internet resource] issues of methodology, quality, testing and application*. Oxford; Philadelphia: Woodhead Publishing, 2012.

[10]   H. G. Daellenbach, *Management science : decision making through systems thinking*, 2nd ed.: New York : Palgrave Macmillan, 2012.

[11]   A. Dysko, "A dynamic modelling methodology for protection system performance assessment," Thesis [M. Sc.] -- University of Strathclyde, 1998., 1998.

[12]   A. M. Law, "How to Build Valid and Credible Simulation Models," in *the IEEE Winter Simulation Conference*, 2008, p. 9.

[13]   M. M. Meerschaert, *Mathematical modeling [internet resource]*, Fourth edition.. ed. Waltham, MA: Waltham, MA : Academic Press/Elsevier, 2013.

[14]   A. Cruden, J. R. McDonald, I. Andonovic, D. Uttamchandani, R. Porrelli, and K. Allan, "Current measurement device based on the Faraday effect," in *1993 Fifth International Conference on Developments in Power System Protection*, 1993, pp. 69-72.

[15]   P. Niewczas, "Implementation of a Faraday Effect based Optical Current Transducer using digital signal processing techniques," Thesis [Ph. D.] -- University of Strathclyde, 2000., 2000.

[16]   M. H. Samimi, S. Bahrami, A. A. S. Akmal, and H. Mohseni, "Effect of Nonideal Linear Polarizers, Stray Magnetic Field, and Vibration on the Accuracy of Open-Core Optical Current Transducers," *IEEE Sensors Journal,* vol. 14, pp. 3508-3515, 2014.

[17] IEEE, "Optical current transducers for power systems: a review," *Power Delivery, IEEE Transactions on,* vol. 9, pp. 1778-1788, 1994.

[18] K. Kyuma, S. Tai, M. Nunoshita, T. Takioka, and Y. Ida, "Fiber optic measuring system for electric current by using a magnetooptic sensor," *Quantum Electronics, IEEE Journal of,* vol. 18, pp. 1619-1623, 1982.

[19] M. Aerssens, A. Gusarov, B. Brichard, V. Massaut, Me, x, P. gret, and M. Wuilpart, "Faraday effect based optical fiber current sensor for tokamaks," in *Advancements in Nuclear Instrumentation Measurement Methods and their Applications (ANIMMA), 2011 2nd International Conference on*, 2011, pp. 1-6.

[20] U. Krey, *Basic theoretical physics [internet resource] : a concise overview*, 1st ed.. ed. Berlin, New York: Berlin, New York : Springer, 2007.

[21] D. Jiles, *Introduction to magnetism and magnetic materials*: London : Chapman and Hall, 1991.

[22] H. J. El-Khozondar, M. S. Muller, R. J. El-Khozondar, and A. W. Koch, "Magnetic field inhomogeneity induced on the magneto-optical current sensors," in *Information Photonics (IP), 2011 ICO International Conference on*, 2011, pp. 1-2.

[23] M. Nasir, A. Dysko, P. Niewczas, and G. Fusiek, "All-optical busbar differential protection scheme for electric power systems," in *The 13rd IET International Conference on Development in Power System Protection*, Edinburgh, 2016.

[24] J. D. P. Hrabluik, "Optical current sensors eliminate CT saturation," in *Power Engineering Society Winter Meeting, 2002. IEEE*, 2002, pp. 1478-1481 vol.2.

[25] S. Kucuksari and G. G. Karady, "Experimental Comparison of Conventional and Optical Current Transformers," *Power Delivery, IEEE Transactions on,* vol. 25, pp. 2455-2463, 2010.

[26] K. Bohnert, P. Gabus, and B. H, "Fiber-Optic Current and Voltage Sensor for High-Voltage Substations," in *16th International conference on Optical Fiber Sensors*, 2003, p. 3.

[27] E. Hecht, *Physics*: Brooks/Cole Pub., 1994.

[28] E. Hecht, *Optics*: Harlow : Pearson Education Limited, 2013.

[29]   R. D. Guenther, *Modern optics*: New York : Wiley, 1990.

[30]   A. Lipson, *Optical physics*: Cambridge : Cambridge University Press, 2011.

[31]   A. Hobson, "Current summations with current transformers," *Electrical Engineers, Journal of the Institution of,* vol. 1, pp. 231-232, 1955.

[32]   T. Sawa, K. Kurosawa, T. Kaminishi, and T. Yokota, "Development of optical instrument transformers," *Power Delivery, IEEE Transactions on,* vol. 5, pp. 884-891, 1990.

[33]   K. Kurosawa, S. Yoshida, and K. Sakamoto, "Polarization properties of the flint glass fiber," *Lightwave Technology, Journal of,* vol. 13, pp. 1378-1384, 1995.

[34]   F. L. Pedrotti, L. S. Pedrotti, and L. M. Pedrotti, *Introduction to Optics*: Pearson Prentice Hall, 2007.

[35]   C. A. Dimarzio, *Optics for engineers*: Boca Raton, FL : CRC Press, 2012.

[36]   ABB. (2015). *ABB Busbar Protection Document 611 Series*. Available: http://new.abb.com/medium-voltage/distribution-automation/numerical-relays/busbar-protection

[37]   Siemens. (2015). *Siemens Centralized Busbar Protection Document SIPROTEC 7SS85*. Available: http://w3.siemens.com/smartgrid/global/en/products-systems-solutions/Protection/busbar-protection/Pages/7SS85.aspx

[38]   Toshiba. (2015). *Toshiba Busbar Protection Document GRB 200*. Available: http://www.toshiba-tds.com/tandd/products/pcsystems/en/grb200.htm

[39]   GE-Alstom. (2015). *GE Busbar Protection Document Multilin B90*. Available: https://www.gegridsolutions.com/multilin/catalog/b90.htm

[40]   M. Nasir, A. Dysko, P. Niewczas, and G. Fusiek, "All-optical Busbar Differential Protection Scheme for Electric Power Systems," in *The 13th IET DPSP™ International Conference on Developments in Power System Protection - 2016*, Edinburgh - UK, 2016, p. 6.

[41]   I. Mathwork. (2016). *Simulation and model-based design*. Available: https://www.mathworks.com/products/simulink.html?s_tid=hp_ff_p_simulink

Chapter 5. Simulation of the Proposed All-optical Configuration of Busbar Differential Protection Scheme

Following the detailed discussion of the concept development and design requirements of the Faraday optical current sensor and the optical differential protection scheme, a novel configuration of the all-optical differential protection scheme has been proposed. This chapter aims to perform a systematic simulation model based evaluation of the protection scheme performance.

The chapter begins with an optical device model using a complex function for representing optical components such as: polarisers, Faraday rotation current sensors, and fibre optics. For simulation purposes, the power system faults and optical systems simulation scenarios are explained. Moreover, based on two types of polariser component model and six different types of fibre optic model including a proposed model of polarization-maintaining optical fibre, five different configurations of the optical devices are simulated for the evaluation purposes of the all-optical differential protection scheme. All five configurations are simulated using Matlab simulation environment.

The simulation of the proposed optical protection scheme is carried out in order to quantify the ability of the protection scheme to fulfil the key objectives of a protection system, i.e. sensitivity/dependability, stability/security and speed of operation. The simulation results are analysed according to these objectives. Validation of the simulation models are discussed using sensitivity analysis technique.

5.1. Models of optical components included in the all-optical differential protection scheme

Optical devices such as polariser, Faraday rotator current sensor (FRCS) and fibre optic (FO) should be modelled using the ideal medium and non-perfect medium to perform computer simulations of the proposed scheme. These models utilize the basic functional optical blocks described in section 3.4.

The representation of perfect polariser, perfect optical current sensor and free propagation were expressed in the equation (3.46) to equation (3.49).

There are three typical optical transmission wavelengths λ, which are 850 nm, 1310 nm and 1550 nm. The wavelength of 1550 nm is chosen because it has low-loss optical fibre [1],[2]. Therefore, this wavelength will be used in the Matlab simulation and laboratory experiment.

5.1.1. Non-perfect polariser component model

Polariser component model using Jones matrix representation ($\boldsymbol{J_P}$) [3] as displayed in Figure 3.10 is derived from equation (3.54). Polarisers that will be used in experiments are from Thorlabs and available in the market. Polariser material is nanoparticles linear film polarisers which consist of spherical ellipsoid nanoparticles that have been embedded in the sodium-silicate glass. Thickness d of this material is 250 μm as dictated in the Thorlabs product specifications [4] and also explained in [5]. Due to unavailability data of refractive index n and extraordinary extinction coefficient k_e of the nanoparticles linear film polarisers, SCHOTT Optical Glass Datasheets, which are a standard reference for the properties of many optical glasses, are used. Using one of the popular optical glasses BK7 (N-BK7 SCHOTT), the corresponding value at wavelength 1550 nm for the refractive index n and extinction coefficient k_e are 1.5007 and $1.4361x10^{-7}$ respectively [6],[7],[8]. The selected wavelength of 1550 nm has been decided, whereas the ordinary extinction coefficient k_o is arbitrarily chosen 0.01.

After substituting the corresponding values, the polariser model (J_P) is

$$J_P = \begin{bmatrix} 0.954 - j\,0.2993 & 0 \\ 0 & 3.788 \times 10^{-5} + j\,1.188\,x\,10^{-5} \end{bmatrix}.$$

This polariser representation will be used in the next section for the simulations.

A perfect polariser representation could be created when substituting k_e with a very small value ($k_e \cong 0$) and $k_o \cong 1$. An example perfect polariser is obtained when $k_e = 10^{-20}$ and $k_o = 0.975$.

$$J_{P\,perfect} = \begin{bmatrix} 0.9541 - j\,0.2994 & 0 \\ 0 & 0 \end{bmatrix}.$$

5.1.2. Faraday rotation current sensor component model

Faraday rotation current sensor (FRCS) component model that utilizes Jones matrix representation (J_{FR}) as depicted in Figure 3.11 is derived from equation (3.55). In this equation, the length of the Faraday optic material for the sensor head d is similar with L in the Faraday equation (3.66). Since the terbium gallium garnet (TGG) is applied for the FRCs sensor head, the corresponding values of the refractive index n and Verdet constant V at a wavelength of 1550 nm, respectively, are 1.95 and 16 rad/(T.m) [9]. The detailed FRCS design for simulation involves two parameters [10] i.e. number of the coil turn N, and the coil radius R. The designed value of these two parameters respectively which are N is equal to 1 and R is equal to 2 mm. The orientation of magnetization relative to the plane of incidence and the surface of the sensor head medium is considered in the polar orientation [10],[11],[12]. Other required FRCS data is the length of the TGG material for the sensor head d which is 28 mm in this design that considers the available TGG dimension in the market. These data of optical sensors was given from the manufacturer that made this sensor based on model requirements. As a result, the FRCS model (J_{FR}) after substituting the parameters is

$$J_{FR} = 0.04759 - j0.9989 \begin{bmatrix} \cos\,(1.43\,x\,10^{-6}\,i) & -\sin\,(1.43\,x\,10^{-6}\,i) \\ \sin\,(1.43\,x\,10^{-6}\,i) & \cos(1.43\,x\,10^{-6}\,i) \end{bmatrix},$$

where i is a current flowing into the FRCS' coil. This representation will be used in the simulation of the proposed all-optical differential configuration.

5.1.3. Fibre optic component model

Optical transmission component models using non-perfect medium are fibre optic models which could be represented in equation (3.52), and (3.53). Other representations of optical fibre will be explained in the next few paragraphs using equation (5.1), (5.2) and (5.3).

The first fibre optic model J_{FO1} in the equation (3.52) seems to have a reasonable representation because it has the retardation and attenuation components. In this model, a linearly polarized plane wave is isotropic retarded and attenuated after travelling a distance d which is a very tiny slab, for example 1 μm. Two common materials for glass optical fibre are fused silica and fused quartz. The silica can have extremely low absorption and scattering losses of the order of 0.2 dB/km around the wavelength of 1550 nm. However, fused quartz has low birefringence due to a small difference between the ordinary refractive index n_o and the extraordinary refractive index n_e [13]. Therefore, a single mode fibre optic that is made from fused silica and fused quartz are used in the simulation models, whereas Corning® single mode fibre which made from fused silica will be used for laboratory experiment.

For the silica material, the refractive index n is 1.4440 [14],[15] which also similar in [7],[8]. However, in [7],[14],[15] the extinction coefficient k is not be provided except in [8] that stated the coefficient is zero. As a consequence if the extinction coefficient k is zero, the fibre optic model in (3.51) and (3.52) are similar. Therefore, it should be better to provide the extinction coefficient k in the simulation model by a nearly zero value, for an example, 10^{-10}.

Substituting the fused silica parameters into equation (3.52), the first fibre optic model J_{FO1} is represented by

$$J_{FO1} = \begin{bmatrix} 0.9091 + j0.4166 & 0 \\ 0 & 0.9091 + j0.4166 \end{bmatrix}.$$

However, this model neglects the linier and circular birefringence effects which exist in the fibre optic cable.

Another fibre optic model in the second group is based on equation (3.53) and considers the linear birefringence effect. However, it ignores the circular birefringence effect. After substitution of the similar parameter at the previous model and the extraordinary refractive index n_e which is 1.4679 [13], [16], the numerical model is represented as follows

$$J_{FO2} = \begin{bmatrix} 0.7231 + j0.6907 & 0 \\ 0 & 0.7231 + j0.6907 \end{bmatrix}$$

These two fibre optic models, which are J_{FO1} and J_{FO2}, will be used to check and compare with the other fibre optic model in the section 5.6.

The third group component models of fibre optic provide more realistic representation because it consists of a simple linear and circular birefringence effect. This model considers both birefringence effects at the same time as expressed in (5.1) [17],[18],[19].

$$J_{FO3} = \begin{bmatrix} e^{j\frac{\pi}{\lambda}(n_y - n_x)d} & \frac{\pi}{\lambda}(n_r - n_l)d \\ -\frac{\pi}{\lambda}(n_r - n_l)d & e^{-j\frac{\pi}{\lambda}(n_y - n_x)d} \end{bmatrix} \tag{5.1}$$

It is assumed that the refractive index of fast axis n_y and slow axis n_x is equal to the refractive index of ordinary n_o and extraordinary n_e [19]. The similar assumptions are also made for refractive index of the right n_r and left n_l circularly polarized light which corresponds to the refractive index of ordinary n_o and extraordinary n_e [17],[18]. After substitution of the parameters, equation (5.1) becomes

$$J_{FO3} = \begin{bmatrix} 0.9988 - j0.04842 & -0.04844 \\ 0.04844 & -0.9988 + j0.04842 \end{bmatrix}.$$

Another fibre optic model is a more complex model of fibre optic with the linear and circular birefringence as in equation (5.2) which includes its fast axis orientation [20],[21],[22],[23]. In this equation, the linear birefringence is δ per unit length, the circular birefringence is 2ρ per unit length, and the axis Ox and Oy coincide with the fast and slow axis of the linear birefringence.

$$J_{FO4} = \begin{bmatrix} \alpha + j\beta & -\gamma \\ \gamma & \alpha - j\beta \end{bmatrix} \tag{5.2}$$

where,

$\alpha = cos\,\Delta$

$\beta = j\dfrac{\delta}{2}z_0 \cdot (sin\,\Delta)/\Delta$

$\gamma = \rho z_0 \cdot (sin\,\Delta)/\Delta$

With

$\Delta = z_0 \left(\rho^2 + \dfrac{\delta^2}{4} \right)^{\frac{1}{2}}$

The corresponding value of the fibre optic parameters which are the linear birefringence δ, the circular birefringence ρ, and the slab thickness z_0 respectively are 0.0239, 0.0002086 rad, and 1 μm. After substituting the corresponding parameters, the fibre optic model in Jones matrix representation is

$$J_{FO4} = \begin{bmatrix} 1 + j1.195x10^{-8} & -2.086x10^{-10} \\ 2.086x10^{-10} & 1 - j1.195x10^{-8} \end{bmatrix}$$

When the linear birefringence fast axis lies at an angle of q (towards Y) with respect to the chosen axis, the matrix becomes [20],[21],[11]

$$J_{FO5} = \begin{bmatrix} \alpha + j\beta\,cos(2q) & -\gamma + j\beta\,sin(2q) \\ \gamma + j\beta\,sin(2q) & \alpha - j\beta\,cos(2q) \end{bmatrix} \tag{5.3}$$

This fibre optic model was used in the simulation by two different values of angle q which are zero and non-zero values. For q is equal to zero degree, the equation (5.3) is similar to equation (5.2) which is the fibre optic model J_{FO4} and for an arbitrarily value as an example, $q = 2^o$, the matrix J_{FO5} becomes

$$J_{FO5} = \begin{bmatrix} 1 + j1.192x10^{-8} & -2.086x10^{-10} + j8.336x10^{-10} \\ 2.086x10^{-10} + j8.336x10^{-10} & 1 - j1.192x10^{-8} \end{bmatrix}.$$

The equation (5.3) could be referred as a general equation of the fibre optic model because many models of fibre optic could be derived from this equation. The equation

(5.3) becomes equation (5.2) when q is equal to zero degree. Other model using the equation (5.3) will be examined and exploited in depth in the section 5.6.

5.2. Modelling of the proposed all-optical configuration of busbar differential protection scheme

Mathematical modelling and simulation is an approach widely used by power systems engineers to understand the behaviour of the system before new solutions are implemented. It helps to identify potential design issues in the early stages, and thus reduces, the overall development time. It can also be used for evaluating various strategies for the operation of the system.

Computer simulation is an important tool for predicting and assessing the system characteristics such as performance, reliability, and various operational modes. The simulation based predictions are used to guide decisions regarding the system design, construction, and operation and also to verify its acceptability. The application of computer simulation to the proposed all-optical differential protection scheme will be performed in order to gain these benefits.

In order to simulate the polarized light behaviour in the optical devices arrangement, especially in the proposed configuration of all-optical differential protection scheme, the Matlab simulation programs were written based on the equation (5.4) and (5.5)

$$E_o = R(\alpha) J_{P1} R(-\alpha) J_{FO-3} J_{FR2(\theta_2)} J_{FO-2} J_{FR1(\theta_1)} J_{FO-1} J_{P1} E_i \qquad (5.4)$$

For the proposed configuration of all-optical differential protection scheme, $\alpha = 90$, and equation (5.4) becomes

$$E_o = R(90) J_{P1} R(-90) J_{FO-3} J_{FR2(\theta_2)} J_{FO-2} J_{FR1(\theta_1)} J_{FO-1} J_{P1} E_i \qquad (5.5)$$

Equation (5.5) can be termed as the general formula of all-optical differential protection scheme because all alternative configurations of the proposed optical differential protection considered in this thesis utilise this equation.

Computer simulation utilised in this work consists of a power system model and the proposed all-optical differential protection model for busbar protection [24]. All models are developed within the Matlab®/Simulink environment. In Matlab®, some required power system elements exist as part of the Simulink library (SimPowerSystems toolbox). However, the optical device models are unavailable in the Simulink library. Therefore, the models had to be created using function blocks, mathematical operators and equations.

5.2.1. Model of the test power system

The power system model employed for testing and assessment of the proposed all-optical differential protection performance is shown in Figure 5.1.
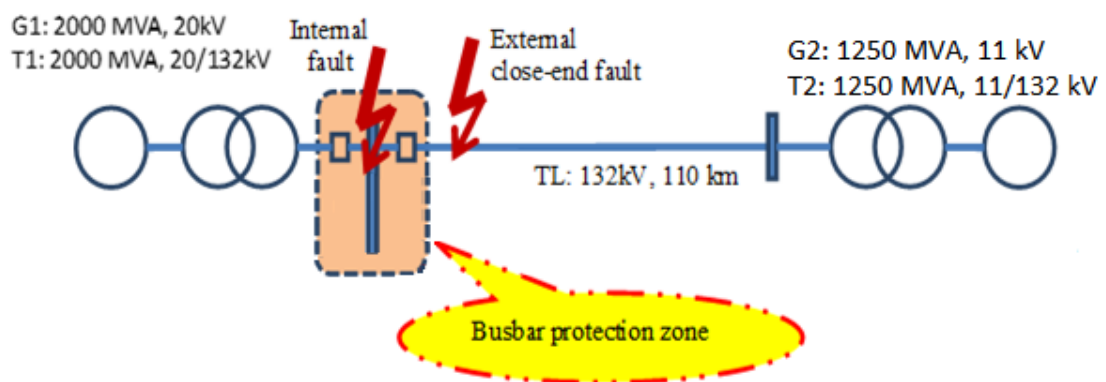
Figure 5.1 Test power system 1 (Busbar with 2 circuits)

In general, two main fault conditions are taken into account, i.e. internal and external close-up faults with respect to the protected zone. The internal faults with different fault resistances are considered including a high resistive fault with R_f=200 Ω. The fault scenarios are summarised in Table 5-1. In the simulation scenarios, the time of fault inception is assumed to be 0.020 seconds (20 ms) which is equivalent to 1 cycle of the power system frequency (50 Hz).

Table 5-1 Location, type and resistance of simulated faults

Case	Fault location	Fault type	Fault resistance
1.a	Internal	L-G	$R_f = 0\ \Omega$ (solid)
1.b	Internal	L-L-L	$R_f = 0\ \Omega$ (solid)
1.c	Internal	L-G	$R_f = 200\ \Omega$
2.a	external	L-G	$R_f = 0\ \Omega$ (solid)
2.b	external	L-L-L	$R_f = 0\ \Omega$ (solid)

5.2.2. Various optical configuration

In order to simulate the protection scheme, the busbar highlighted in Figure 5.1 is equipped with the proposed configuration of all-optical busbar differential protection scheme. There are five possible options of series optical configuration to realize the proposed all-optical configuration of differential protection scheme. These five options of the series configurations are:

1. Series optical configuration 1: laser source – fibre optic – polariser – FRCS1 – fibre optic – FRCS2 – analyser – fibre optic – photo detector (termed as fibre optic outside the polariser-analyser pair) as shown in Figure 5.2.

2. Series optical configuration 2: laser source – polariser – fibre optic – FRCS1 – fibre optic – FRCS2 – fibre optic – analyser – photo detector (termed as fibre optic inside the polariser-analyser pair).

3. Series optical configuration 3: laser source – fibre optic – polariser– FRCS1 – fibre optic – FRCS2 – fibre optic – analyser – photo detector (termed as fibre optic before polariser and before analyser).

4. Series optical configuration 4: laser source – polariser – fibre optic – FRCS1 – fibre optic – FRCS2 –analyser – fibre optic – photo detector (termed as fibre optic after polariser and after analyser).

5. Series optical configuration 5: laser source – fibre optic – polariser – fibre optic – FRCS1 – fibre optic – FRCS2 – fibre optic – analyser – fibre optic – photo detector (termed as fibre optic between two optical devices).
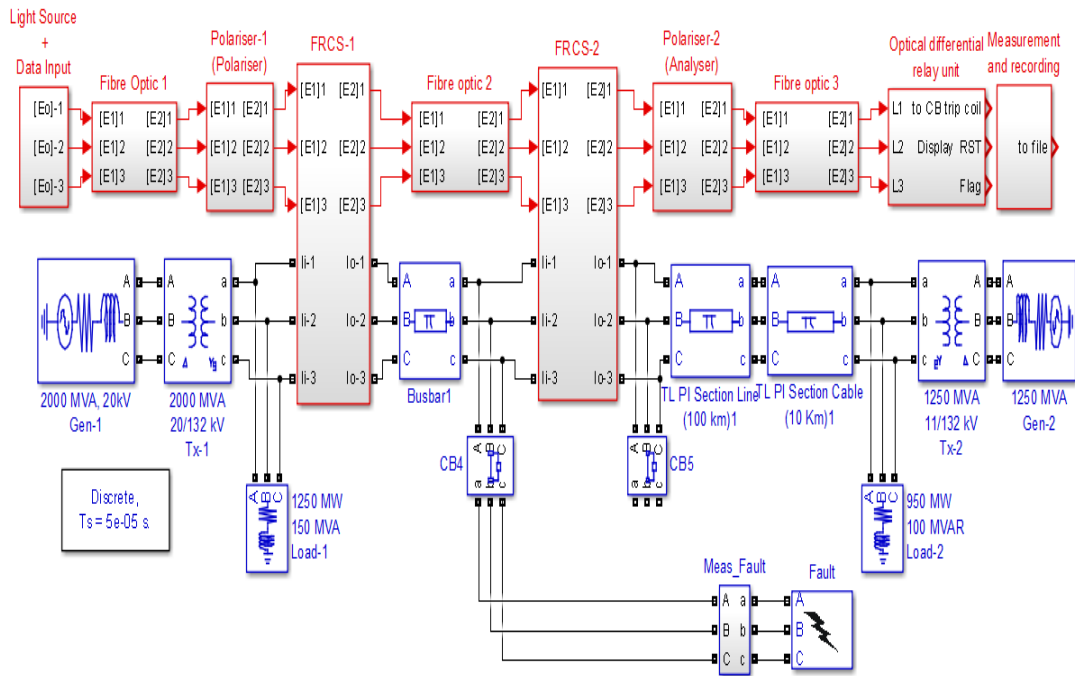
Figure 5.2 Optical configuration 1

Although the configurations 1, 2, 3, and 4 use the same number of fibre optic section which three sections, these optical configurations are different on the position of fibre optic that links to optical devices. Fox example, there is a fibre optic link between laser source and polariser in the optical configuration 1 as shown in Figure 5.2, whereas in the configuration 2, the fibre optic do not use to link those optical devices. The length of the three sections of fibre optic in these two optical configurations can be changed in the simulation for performance assessment.

Unlike the previous four optical configurations, the optical configuration 5 uses a section of optical fibre to link between two optical devices. The length of these five sections of optical fibre in this configuration can also be changed in the simulation for the protection performance assessment of the proposed all-optical configuration.

5.2.3. Various optical system components

The arranged optical system that represents the proposed configuration of all-optical differential protection scheme implements the general formula as in the equation (5.5).

It covers six simulation types for both perfect (only one type) and non-perfect optical media (5 options).

For the perfect optical medium, a single type of simulation is simulated using representation of the perfect polarisers, the perfect optical current sensors and the ideal transmission media. This simulation type can be termed as an ideal simulation type. The ideal simulation type was carried out in order to provide reference data for proving the concept of all-optical configuration by simulation.

For the non-perfect optical medium, there are five simulation fibre types as follows:

1) Simulation fibre type I: using representation of the non-perfect polarisers, the non-perfect optical current sensors, and the first fibre optic model J_{FO1}.

2) Simulation fibre type II: using model of the non-perfect polarisers, the non-perfect optical current sensors, and the second fibre optic model J_{FO2}.

3) Simulation fibre type III: using representation of the non-perfect polarisers, the non-perfect optical current sensors, and the third fibre optic model J_{FO3}.

4) Simulation fibre type IV: using model of the non-perfect polarisers, the non-perfect optical current sensors, and the fourth fibre optic model J_{FO4}.

5) Simulation fibre type V: using model of the non-perfect polarisers, the non-perfect optical current sensors, and the fifth fibre optic model J_{FO5}.

Simulation fibre types I to V have the increasing level of model complexity, where the simulation fibre type V may represent the most realistic conditions for a non-polarization maintaining single mode optical fibre.

It is worth to be mentioned that laser source wavelength of 1550 nm was used in simulation model of the all-optical configuration of differential protection scheme. The laser source in the simulation is also set to provide optical power output 1 mW at wavelength of 1550 nm. The fibre optic attenuation, connector's insertion loss, and other losses such as Fresnel reflection is inherently calculated by the programme in the optical model [25],[26],[27].

5.3. Verification and validation of the simulation model

5.3.1. Initial verification of the simulation model

Verification is a process of determining that a (simulation) model accurately represents the developer's conceptual description and specification [28],[29],[30]. In short, verification addresses to answer key question: ''have we build the simulation model right?'' [31],[32].

The computerized simulation model has been created based on the mathematical representation (conceptual model) using the Matlab software environment. Although the optical devices have been modelled and configured according to the specifications and requirements, the models should still undergo a verification process. A computerized model verification is aimed to assure that computer programming and implementation of the conceptual model are correct [33]. Verification and comparison procedures of the simulation model as depicted in Figure 5.3 are started with power system simulations in order to generate electric current waveforms. Then, the waveforms are applied to provide optical angles. Next, the optical angles are proceed to provide optical powers.

One of the verification techniques which is dynamic verification technique [32] could be used to verify the simulation of the proposed all-optical configuration. This technique looks at the execution results of the simulation model and compares the simulated value by Matlab at certain point to the expected values (observed value by other software). To achieve this outcome, the simulated data need to be generated at various points by the insertion of code into the Matlab's simulation program to collect or monitor model behaviour during execution.

The verification of the simulation model used two independent software to obtain the expected value by two steps model verification. First step, the verification of the fault current simulations were conducted using the DIgSILENT power factory software. The second step, the verification of the optical system model was carried out by comparing the Matlab's simulation output to the Microsoft spreadsheet application.

Two generated data which were the Faraday rotation θ and the optical power from the Matlab simulations were compared to the Microsoft spreadsheet calculation.
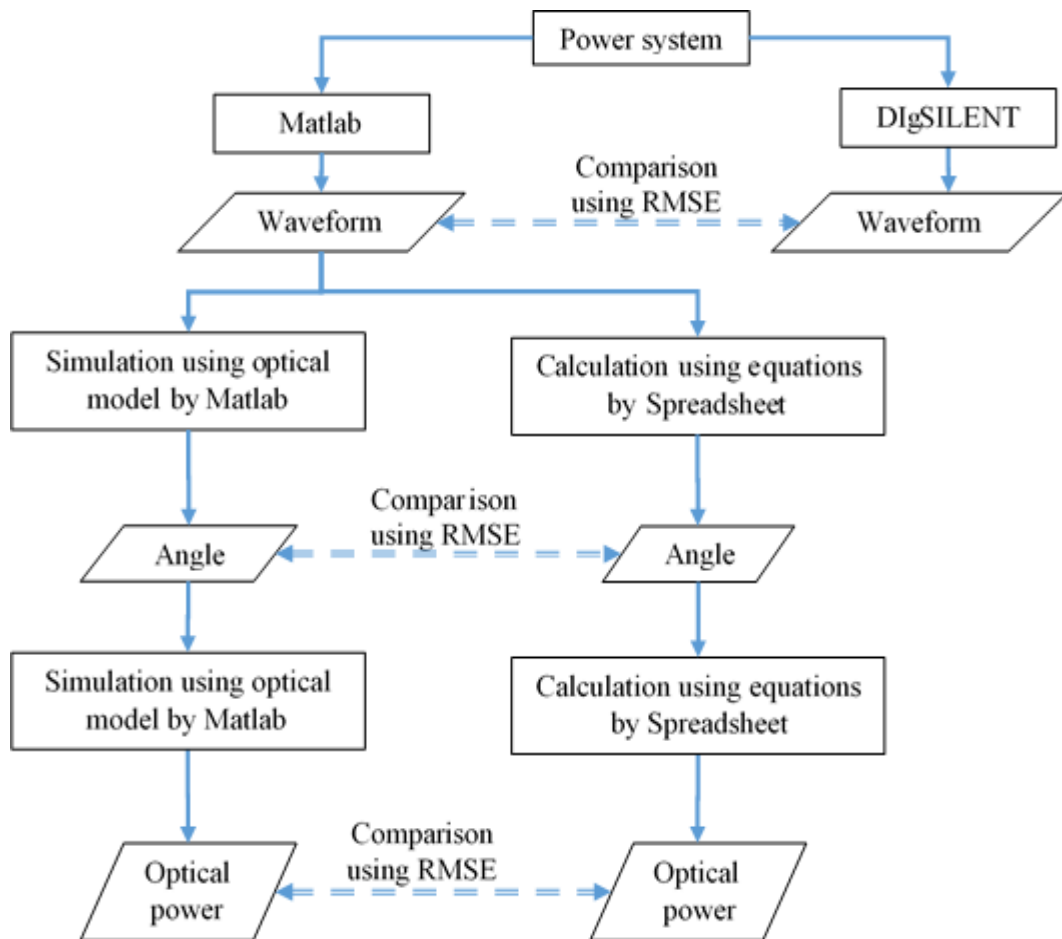
Figure 5.3 Verification and comparison procedures of the simulation model

In order to quantify the differences of a set of values in the verification steps, the root mean square error (RMSE) was used. The smaller an RMSE value means the closer Matlab's simulation value to the calculated values (by independent software application). Thus the RMSE value could be used as dissimilarity index between the simulated values and the calculated values.

As for the fault current verification, the fault current data from the matlab and the DIgSILENT simulations were compared to obtain the dissimilarity index as shown in Table 5-2. The RMSE value (dissimilarity index) for L-L-L and L-G faults are 10 and

10 respectively. This dissimilarity index is high because only a single value is compared.

Table 5-2 Fault current comparison of the power system simulation

Fault current type	Maximum fault current (kA)		RMSE (dissimilarity index)
	Matlab	DIgSILENT	
L - G	25.5	24.49	10
L-L-L	18.29	18.28	10

Applying the similar procedure as in the first step, the comparison results of the Faraday rotation θ_1 and θ_2 are respectively displayed in Figure 5.4 and Figure 5.5.
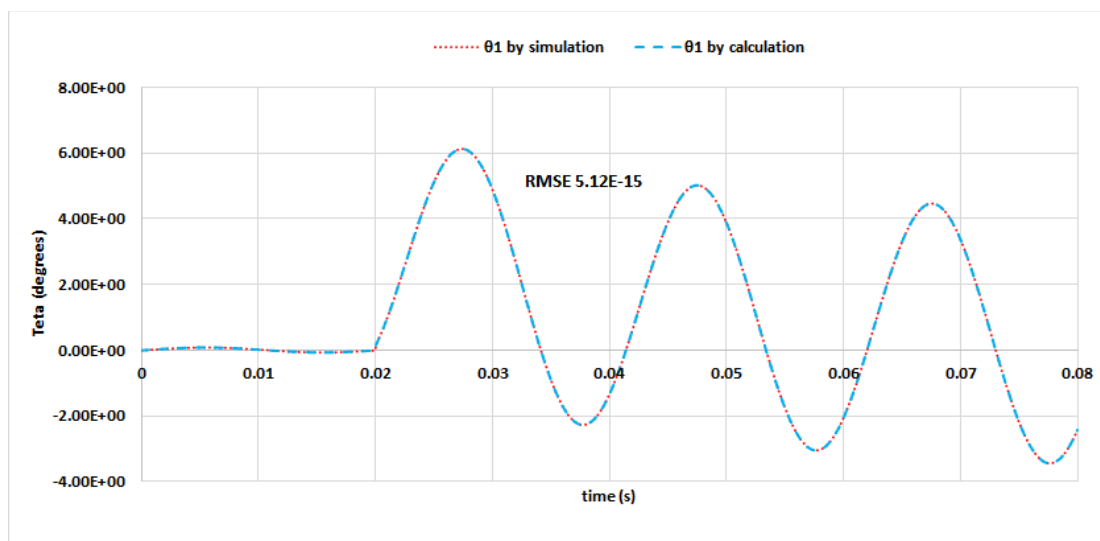
Figure 5.4 Comparison of the Faraday rotation θ_1: the simulation against calculation

The dissimilarity index of the Faraday rotation θ_1 in Figure 5.4 is 5.12E-15 which is a very small value. This value means that results of both the simulation and the calculation are very similar.
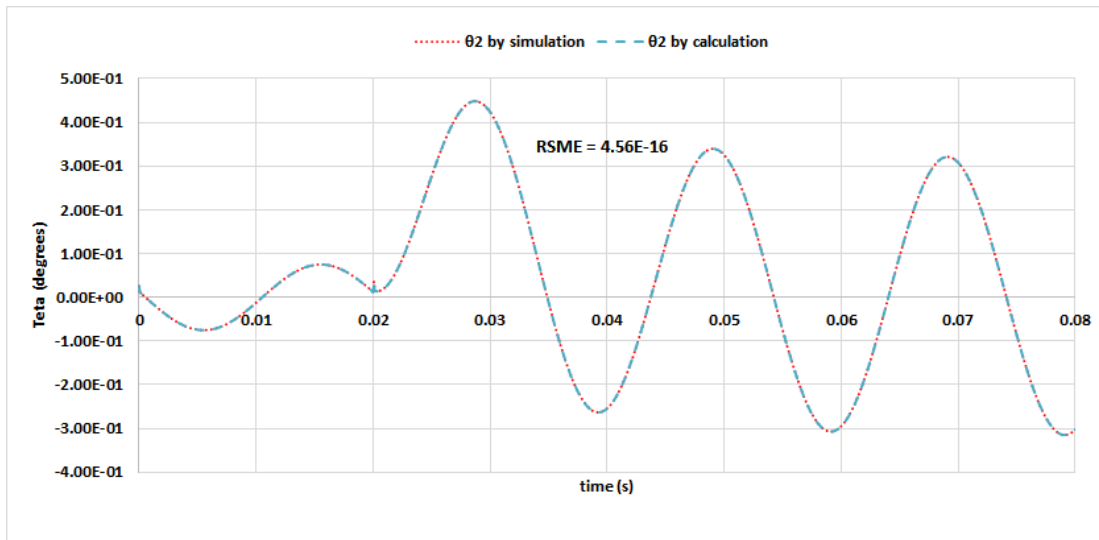
Figure 5.5 Comparison of the Faraday rotation θ₂: between the simulation and calculation

For the Faraday rotation θ_2 as shown in Figure 5.5 the dissimilarity index is 4.56E-16 which is less than the dissimilarity index of the Faraday rotation θ_1. This value indicates that both value from the simulation and the calculation are similar.
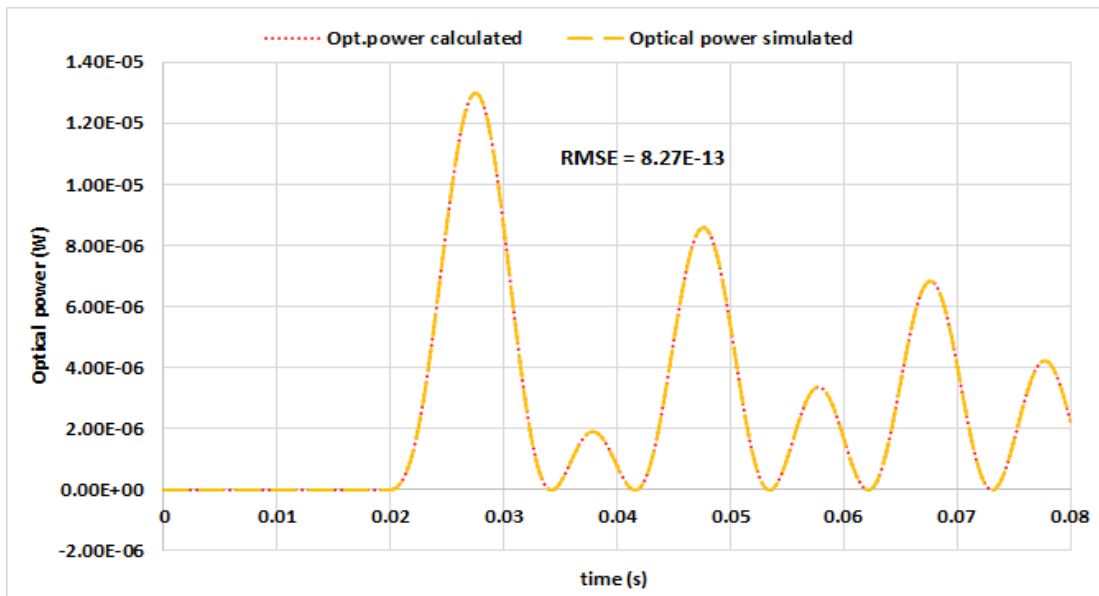
Figure 5.6 Comparison between the simulated and the calculated of optical powers

The optical power comparison is depicted and Figure 5.6. The dissimilarity index of the optical power between the Matlab simulation and the Spreadsheet calculation is 8.27E-13 that means very similar.

5.3.2. Initial validation of the simulation model

Validation addresses to answer a key question: ''have we build the right simulation model?'' [31],[32]. Validation of a simulation model provides a degree of confidence to the simulation results. This action is needed in order to examine the correct representation of the simulation models that have been made. Several methods could be used to validate the simulation models as described in [34],[35],[36],[37], however parameter variability (sensitivity analysis) method is chosen to be used in this thesis.

Since the sensitivity analysis technique explains that changing the input values including the internal parameters of a simulation model will change the output of the simulation in relatively the same magnitude as input change [38],[39],[40]. Therefore, the same relations should occur in the model as in the real system.

Another validation technique which use an independent data from the laboratory experiment data will be presented in chapter 6.

5.4. Demonstrating the concept of all-optical configuration by simulations

5.4.1. Fault simulations, fault current and current differential

Fault simulations of the test power system were conducted to determine two kinds of fault current i.e. the total fault currents on faulted point, fault current contribution including the flow of fault current to the faulted point. For the protection purposes, two fault types which are a line to ground (L-G) and a three phase (L-L-L) faults should be considered because they could contribute the maximum fault current. Comparing these two faults, the solid line to ground fault in the protection zone provides the maximum fault current is approximately 25.5 kA, whereas the solid three phase fault is 18.29 kA as shown in Figure 5.7.
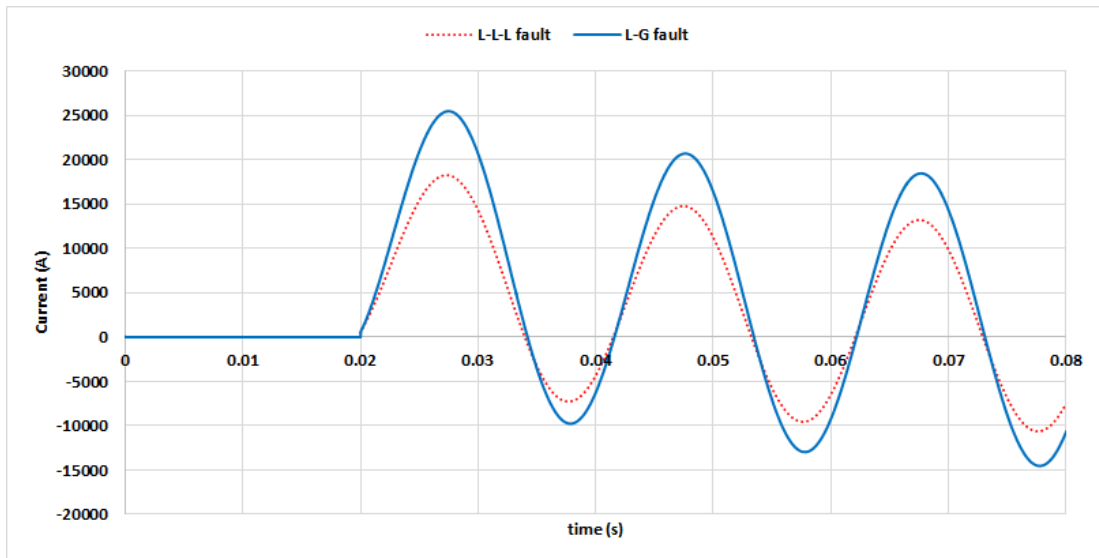
Figure 5.7 Comparison of fault current between the line to ground and three phase faults.

These fault results are different than the common short circuit results due to the system grounding. In this power system test 1, all generators connection types are star connection with solid grounding and all transformers winding connection are delta-star with solid grounding. This connection type causes a reduction in zero sequence impedance, hence, it increases the all ground fault currents especially a line to ground fault current. Due to this fact, the solid line to ground fault becomes the tested fault for internal and external fault to examine performance of the protection scheme in this course.

The current differential protection scheme works on the principle of comparison between the phase angle and magnitude of current quantities. Term "current differential" is similar with "current difference". It means the difference between the current entering a protected zone and the current leaving that zone.

A fault outside the zone as displayed in Figure 5.8 gives the same fault current at the entry and exit of the zone, but faults within the zone as depicted in Figure 5.9 show up as a difference in current (termed current differential). This current differential flows into the protection relay and the relay operates if the differential current is greater than a threshold setting.
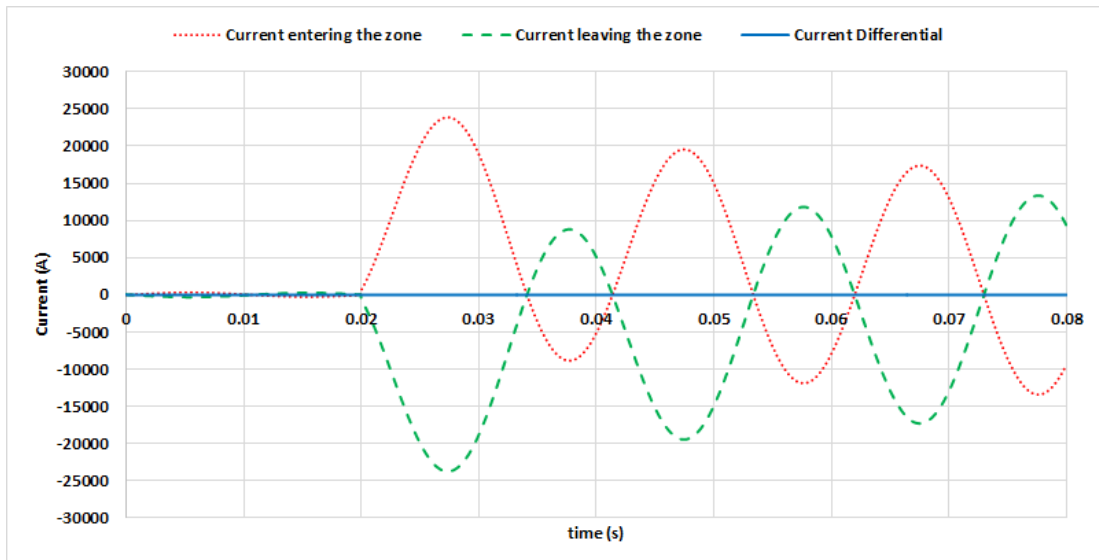
Figure 5.8 Fault current simulation for an external fault
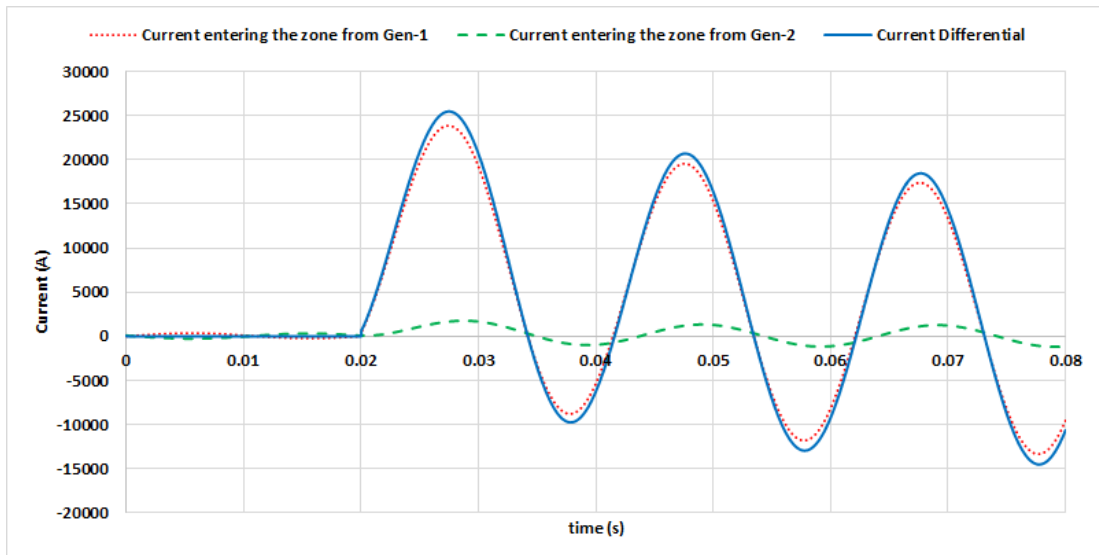
Figure 5.9 Fault current simulation for an internal fault

5.4.2. Demonstrating the concept of all-optical configuration by simulations

Although the concept of the all-optical configuration had been demonstrated by theoretical method in section 4.8 using the equation (4.19), this section is presented to

163

give another demonstration method by simulations. The ideal simulation type of the proposed all-optical configuration for both external and internal faults were performed to provide simulation data. Results of optical power against current differential for external and internal faults are displayed in Figure 5.10 and Figure 5.11, respectively.
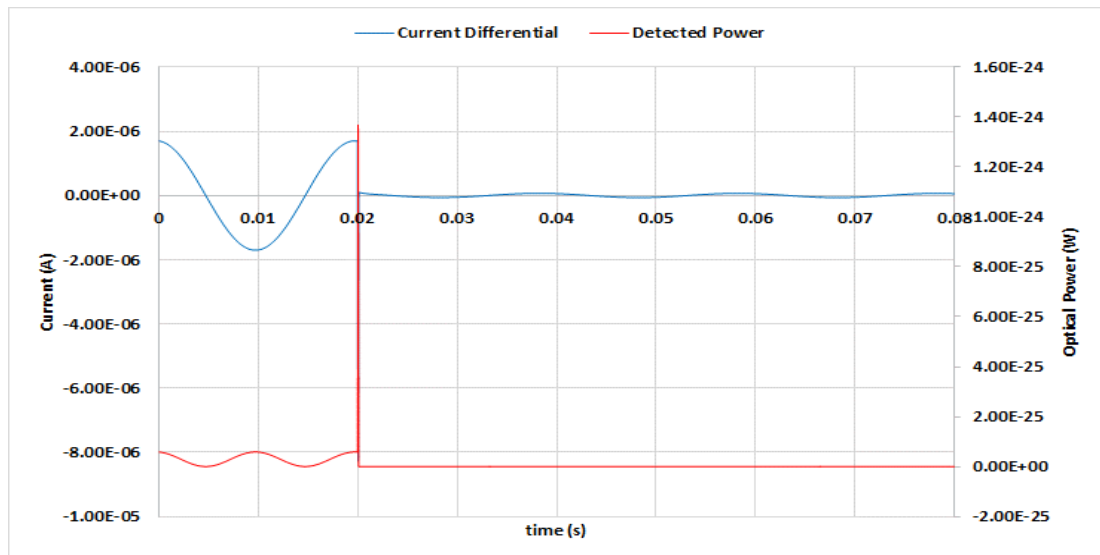
Figure 5.10 Results of the ideal simulation type for an external fault

These simulation results demonstrate that the polarized light outputs E_O at photo-receiver (optical power) for the external faults as in Figure 5.10 are zero, whereas the outputs E_O for the internal faults as in Figure 5.11 are non-zero. These simulation results also give the same conclusion as the conclusion of the theoretical demonstration method was presented in section 4.8. Therefore, the proposed configuration of all-optical busbar differential protection scheme is valid.

164
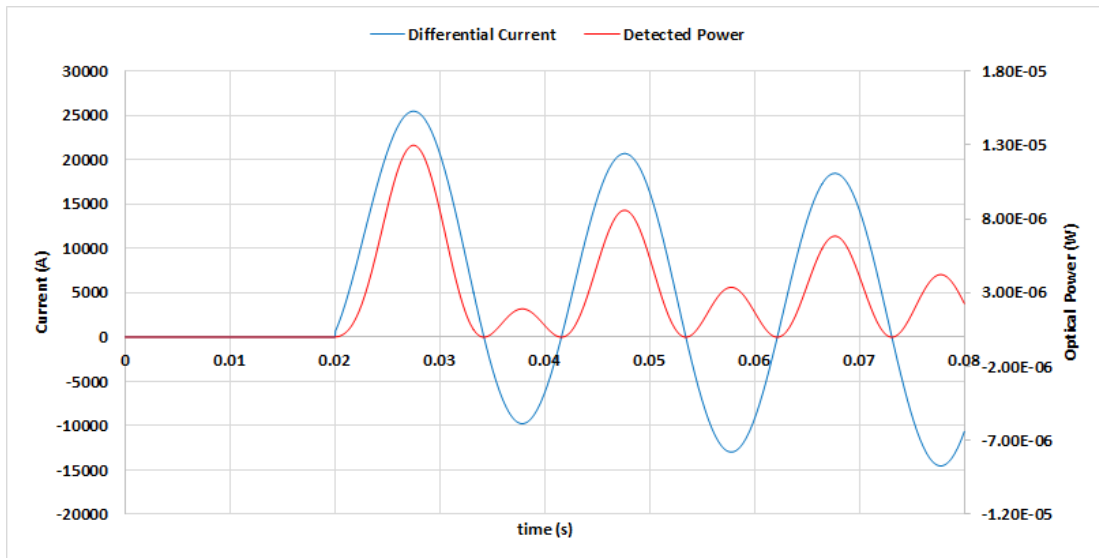
Figure 5.11 Results of the ideal simulation type for an internal fault

Although the simulation results show that the polarized light outputs E_O (the optical power) for an external fault as in Figure 5.10 are not exactly zero, these optical power outputs are almost zero (10^{-26} to 10^{-28}). Maximum current differential when fault occurred at 0.02 second is $8x10^{-6}$ A that corresponds to optical power output $1.4x10^{-24}$ W, whereas the current differential at 0.03 second (first half-cycle) decreases to be $7x10^{-8}$ A that relates to the optical power output $1x10^{-28}$ W.

5.5. Current measurement range

5.5.1. Current measurement range of the proposed prototype

Due to the use optical phase modulation method in the FRCSs, the maximum and minimum rotation phase angle of polarized light are -90^0 and $+90^0$. Hence, the possible operation interval is in between -90^0 and $+90^0$. However, the use of a polariser pair causes the proposed configuration response is limited to be only a few degrees which are in the interval 0^0 to $+90^0$. Therefore, the current linear measurement region of the proposed configuration is also in the same interval, 0^0 to 90^0.

The current linear measurement region corresponds to the FRCS design parameters which are measured current I, number of turn N, length of sensor head L, and Verdet constant. Using a simulation, the maximum linear measurement region of the designed FRCS coil prototype is 13 turns when the solid line to ground fault occurs at the busbar in the power system test. This value is equivalent to 331.5 kA when the FRCS coil has a single turn. This current measurement range of the proposed configuration will limit its application to the power systems that have higher fault current level. The maximum current measurement ranges against number of coil turns N in the proposed configuration are listed in Table 5-3.

Table 5-3 Current measurement range of the proposed all-optical configuration

Number of coil turns N	Maximum current range (kA)
1	331.50
2	165.75
5	66.30
10	33.15
30	11.05

It is clear that although the proposed all-optical configuration does not cause saturation problems, it could introduce a non-linear output due to the number of coil turn and the measured current parameters are exceeded the design specification. As a consequence, the non-linear output have to be considered when the proposed all-optical configuration is applied to power system protection. Responses of the proposed configuration to an internal fault for different coil turns which are a single turn and 15 turns are shown in Figure 5.12 and Figure 5.13 respectively.
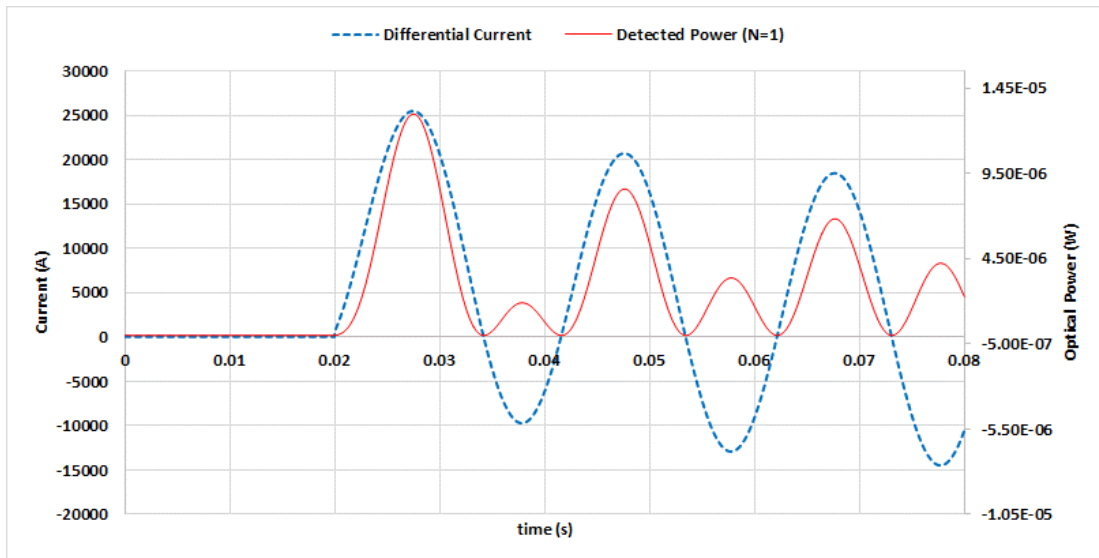
Figure 5.12 Response of the proposed configuration with a single coil turn (N=1)

It can be seen that Figure 5.13 is significantly more distorted than Figure 5.12. This is because number of coil turns *N* is higher in Figure 5.13 than Figure 5.12 and consequently the FRCS in Figure 5.13 has a smaller current measurement range than the FRCS in Figure 5.12.
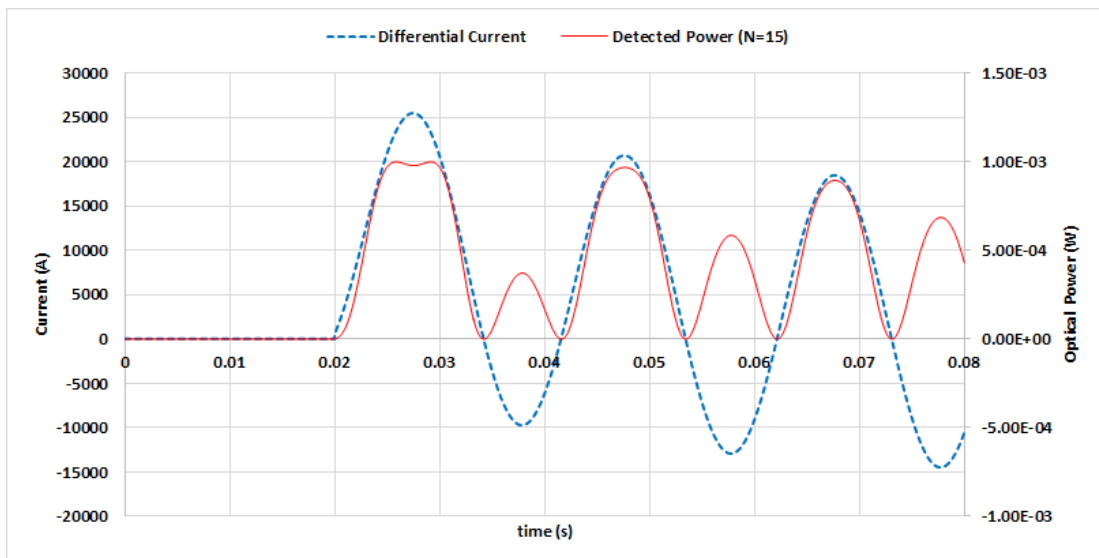
Figure 5.13 Response of the proposed configuration with 15 coil turns (N=15)

Another illustration regarding the number of coil turns, which are N=15 and N=20, is depicted in Figure 5.14.
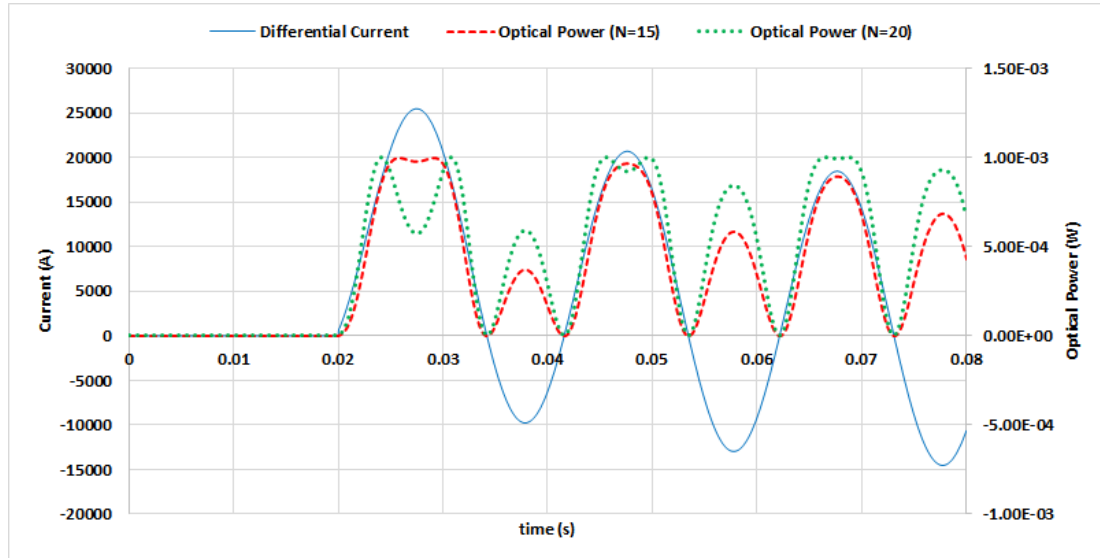
Figure 5.14 Response of the configuration for two different coil turns (N=15 and N=20)

The optical power for two different number of coil turns (*N*=15 and *N*=20) have been simulated. The optical power for the FRCS coil turns *N*=20 is significantly more distorted comparing when the FRCS coil turns *N*=15. Thus, in a protection application, it is necessary to select the number of FRCS coil turn that is appropriate for the maximum magnitude of the fault current that can occur. Hence, the simulation is needed to obtain the maximum simulated fault current and to select the appropriate parameters for the proposed all-optical configuration.

5.5.2. Increasing the current measurement range

The current linear measurement region could be expanded by changing the corresponding FRCS design parameters such as the length of sensor head *L*, coil radius *R*, and Verdet constant. However the Verdet constant parameter is very difficult to be changed because the terbium gallium garnet was chosen for the sensor head material. Therefore, the most preferred parameter for improvement the linear measurement region is the length of sensor head *L* and the coil radius *R*.

Expanding the current measurement range could be achieved by either increasing the coil radius R or decreasing the length of sensor head L, and also by simultaneously changing the both parameters. The simulations with different FRCS parameters were carried out and the maximum current measurement ranges were improved as listed in Table 5-4.

Table 5-4 Improved current measurement ranges

Coil radius R	Length of sensor head L	Number of coil turns N	Maximum current range (kA)
Initial R value Based on the FRCS prototype (R=2 cm)	Initial L value Based on the FRCS prototype (L=28 mm)	1	331.5
2.5 R	L	1	867.0
10 R	L	1	3,493.5
R	0.1 L	1	3,493.5
2.5 R	0.25 L	1	3,493.5
10 R	L	2	1,746.7

When changing the both parameters are still not meet the current measurement range, the last alternative is to replace the sensor head material that has small Verdet constant and should have the most similar characteristics. However, this last alternative should be carefully considered because it will change the sensor characteristics. For the future work, the sensors installation on the busbar should consider practical aspect of sensor installation and integration to other substation hardware and components.

5.6. Comparison of simulation for the busbar with 2 circuits

5.6.1. Base case simulations and optical configuration 1

Base case simulations were aimed to become a reference for assessing other simulation cases. Due to unavailability of a base case simulation, results of the simulation fibre

type I to V using optical configuration 1 as described in section 5.2.2, could be decided to become the base case simulation. This base case simulation was referred as a relative reference because this role will be taken by another optical configuration with or without the parameters changes that had a better performance.

The optical models were substituted according to the configuration and the simulation type, as well as the fault scenarios as in the Table 5-1 which were applied to the simulation. Moreover, for the base case simulations, it was assumed that the fibre optic is made from fused quartz. Thus, the corresponding parameters in [13] are substituted to the fibre optic models. The length of fibre optic from polariser to FRCS1 is 2 meters, from FRCS2 to analyser is 2 meters, and from FRCS1 to FRCS2 is 4 meters. These fibre optic lengths are referred to as the base case of fibre optic length as listed in Table 5-5.

Table 5-5 Base case data for the length of optical fibre in the simulation

From	To	Label designation	Base case (m)
Polariser	FRCS1	FO1	2
FRCS1	FRCS2	FO12	4
FRCS2	Analyser	FO2	2

The proposed configuration was built based on the optical configuration 1 and the simulation fibre type I – V were performed. The simulation results present that modulated optical power of the five simulations for the internal fault provide almost similar outputs in terms of magnitude and modulation form as depicted in Figure 5.15.
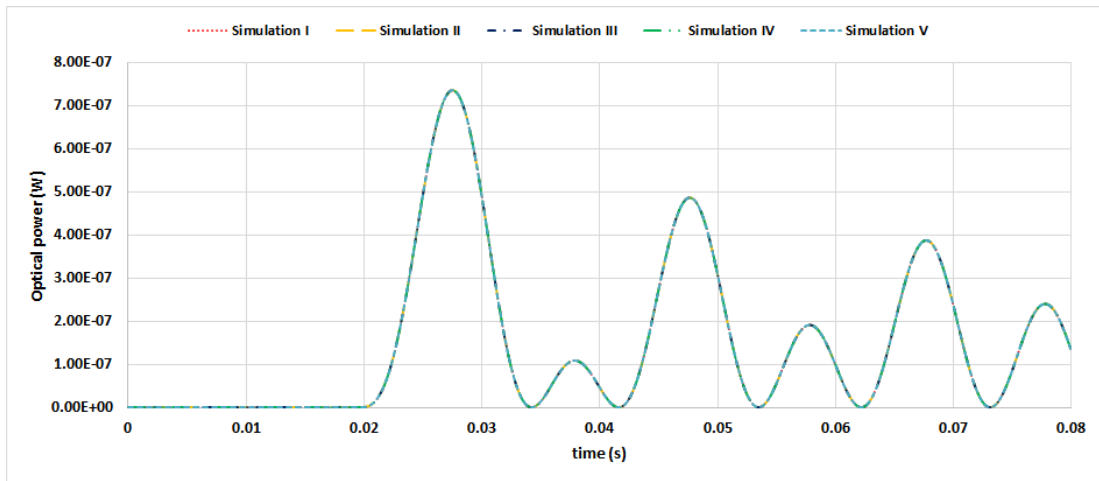
Figure 5.15 Response of the configuration 1 simulation fibre type I to V for internal fault

Different results of the simulation for the external fault are obtained. Three simulation types which were simulation fibre type I, II and III provided optical power of near zero watts as depicted in Figure 5.16, whereas two fibre type simulations which were simulation fibre type IV and V generated non-zero value of the optical power (Figure 5.17).
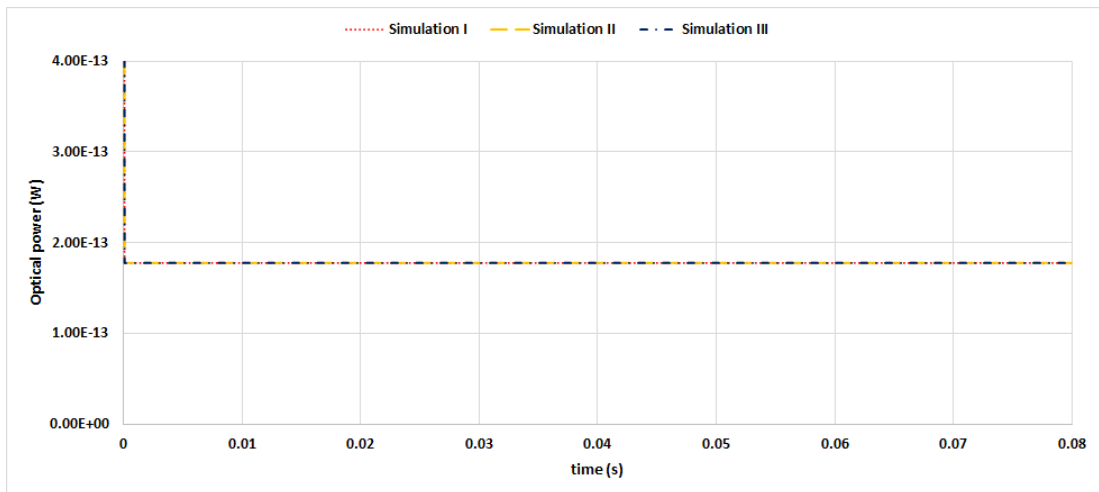
Figure 5.16 Simulation fibre type I to III for external fault using optical configuration 1

171

Results of the simulation fibre type I, II and III that generated the optical power of near zero watts correspond to their fibre optic model. The simulation fibre type I only uses the retardation and attenuation components in the first fibre optic model. Likewise the simulation fibre type I, the simulation fibre type II also comprises the same components but added the linear birefringence effect and ignore the circular birefringence effect in the model. The simulation fibre type III includes both the linear and circular birefringence effect with the same components in the simulation fibre type I and II. Therefore, the simulation fibre type I, II and III provided the optical power of near zero watts.

Different results of the optical power were shown by the simulation fibre type IV and V that generated non-zero value of the optical power as in Figure 5.17. These results were caused by the birefringence effect that is represented by a more complex model of the fibre optic including the fast and slow axis orientation. These fibre optic behaviours will be discussed in more detail in the next section.
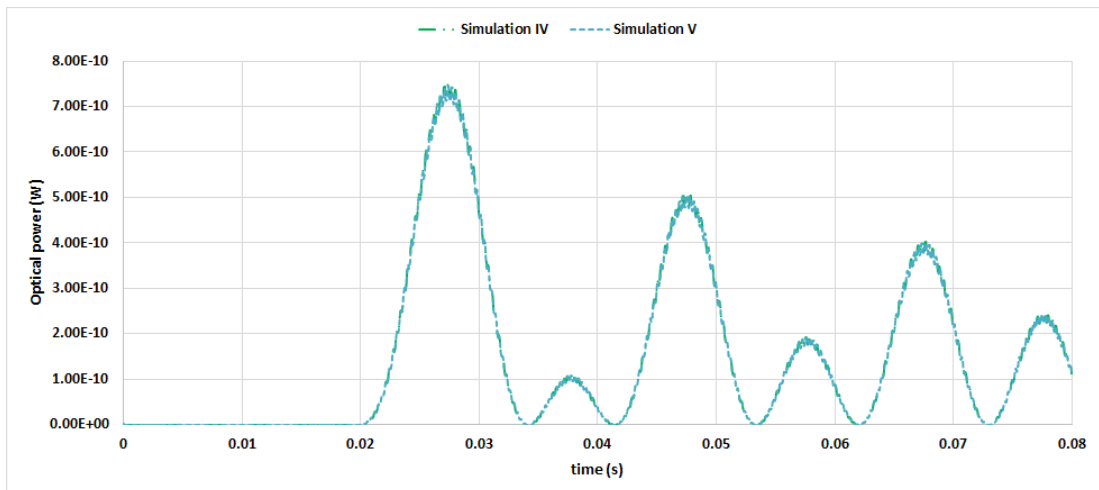
Figure 5.17 Simulation fibre type IV and V for external fault using optical configuration 1

Comparison of the maximum optical power between internal and external faults at first half-cycle for simulation fibre type I to V using the optical configuration 1 are listed in Table 5-6.

172

Table 5-6 Comparison of the maximum optical power for internal and external faults using various fibre types

Fibre Type	Maximum optical power (W)		
	Internal fault	External fault	Power ratio of the internal to external fault
I	7.34E-7	1.78E-13	4.12E+6
II	7.34E-7	1.78E-13	4.12E+6
III	7.34E-7	1.78E-13	4.12E+6
IV	7.34E-7	7.49E-10	9.81E+2
V	7.34E-7	7.45E-10	9.85E+2

This table shows that simulation using fibre type I, II and III could meet the condition of differential protection scheme where the maximum output power for internal are 7.34E-7 W, whereas for external fault are 1.78E-13 W. Thus, the optical power ratio of the internal to external faults for simulation fibre type I, II, and III are 4.12E+6 which is a significant value for a fault discrimination.

Different results have been presented by the simulation fibre type IV and V. Although these simulations provided the same optical power of 7.34E-7 W for internal fault as previous simulation types, they presented optical power of 7.49E-10 and 7.45E-10 W for external fault which are different than the previous simulation types. As consequences, the simulation fibre type IV and V give the optical power ratio of approximately 9.81E+2 and 9.85E+2 respectively. These optical power ratio are less significant values for the fault discrimination. Although these values are less significant for the fault discrimination, it could be used for a fault indication.

In summary, the fibre type III and V will be applied for the next step simulation. The fibre type IV and V have same representation except for q parameter where q = 0 for fibre type IV and q = 2 for fibre type V.

Other finding in the simulations which are the optical power output is modulated in every half-cycle of the current differential cycle. Thus, the polarized light output is

modulated at twice of the current frequency.

5.6.2. Changing the optical configuration

Changing the optical configuration is aimed to determine a better option for the proposed all-optical configuration by comparing its performance to the base case simulations (optical configuration 1).

Using the same manners, the simulation fibre type I to V using the optical configuration 2 to 5 (as in section 5.2.2) were performed. The simulation results have been tabulated as in Table 5-7.

Table 5-7 Comparison of various optical configurations using the simulation fibre types III and V

Configuration	Maximum optical power (W)				Optical power ratio	
	Internal fault		External fault		Internal Fault	External fault
	Fibre type III	Fibre type V	Fibre type III	Fibre type V	Fibre type III	Fibre type V
1	7.34E-7	7.34E-7	1.78E-13	7.45E-10	4.12E+6	9.85E+2
2	7.34E-7	7.34E-7	1.78E-13	7.45E-10	4.12E+6	9.85E+2
3	7.34E-7	7.34E-7	1.78E-13	7.45E-10	4.12E+6	9.85E+2
4	7.34E-7	7.34E-7	1.78E-13	7.45E-10	4.12E+6	9.85E+2
5	7.30E-7	7.30E-7	1.77E-13	7.41E-10	4.12E+6	9.85E+2

It could be concluded that the configuration 1 to 5 have the same opportunity to be implemented because there is no significant difference in the optical power at the photo receiver. However, the configuration 2 and 5 have practical consideration for implementation. The configuration 2 has a benefit in term of practical consideration due to the position of polariser and analyser. In this configuration, the polariser and laser source could be put in a single case and placed in substation's building. The same

layout is for the analyser and photo receiver where they are put in the same case and the same place.

The configuration 5 has also a benefit for laboratory experiments because it is easy in detail design, prototype development and laboratory experimental steps. Therefore, the configuration 5 will be used in this thesis. Although, the optical configuration 5 results a slightly lower optical power than the other configurations, it is reasonable due to the increasing losses that are caused by the increasing number section of fibre optic (length) and fibre optic connectors. Thus, optical configuration 2 and 5 will be implemented in the next section and the next chapter.

The optical power ratio of the internal to external faults for simulation fibre type III and optical configuration 1 to 5 have also the same value which is 4.12E+6 W. Although the simulation fibre type V for external fault provide result of the optical power ratio (9.85E+2 W) which is different than other simulation type, these values of the optical power are same as the base case simulation. A different result which is the configuration 5 has a slightly lower optical power than the other configurations for simulation fibre types III and V, however they still have the same optical power ratio as listed in Table 5-7.

For the internal and external faults, the simulations generated data that modulated optical power of the four simulation types and the four optical configurations provide the same output of the optical power in terms of magnitude and modulation form as the base case (simulation type I) except for the optical configuration 5.

5.6.3. Changing the angle q in the fibre optic model J_{FO5}

The previous simulation case used the angle q in the fibre optic model J_{FO5} which was 2 degrees. In these cases, the simulations have been conducted with different of angle q using simulation fibre type V. The simulation results which are the maximum optical power for the simulation fibre type V with different angle q are tabulated in Table 5-8.

An interesting finding from Table 5-8 is a unique behaviour of the fibre optic model J_{FO5} for external fault that the increasing of the angle q causes the decreasing of optical

power modulation until it reaches 45 degrees. A conclusion from this finding which is optical fibre type V with q = 45 degrees provides the highest optical power ratio. Such optical power ratio would give a good discrimination when this fibre type is implemented for the proposed all-optical differential protection scheme.

Table 5-8 Optical power comparison for simulation fibre type V at different angle q

| | configuration | Maximum optical power (W) for the simulation type V with different angle q in degrees | | | | | |
		q=0	q=2	q=10	q=30	q=45	q=60
Internal fault	2	7.34E-07	7.34E-07	7.34E-07	7.34E-07	7.34E-07	7.34E-07
	5	7.30E-07	7.30E-07	7.30E-07	7.30E-07	7.30E-07	7.30E-07
External fault	2	7.49E-10	7.45E-10	6.62E-10	1.91E-10	1.78E-13	1.91E-10
	5	7.45E-10	7.41E-10	6.59E-10	1.90E-10	1.77E-13	1.90E-10
Optical power ratio	2	9.81E+02	9.85E+02	1.11E+03	3.84E+03	4.12E+06	3.84E+03
	5	9.81E+02	9.85E+02	1.11E+03	3.84E+03	4.12E+06	3.84E+03

This table gives a description that the angle of 45 degrees generates the best ratio of the optical power when it uses the non-polarization-maintaining single mode optical fibre. Therefore, the best performance of the non-PM single mode optical fibre could be achieve as long as the orientation angle of fast and slow axis can be determined. However, it is difficult to find the angle of 45 degrees when using the non-polarization-maintaining single mode optical fibre because it has no marking for the degree identification.

Figure 5.18 provides a good description about the optical fibre type V at different q parameters. It is shown that at q = 45 degrees gives the minimum optical power for the external and becomes a turning point because after this point (45 degrees) the unique behaviour is reversed.
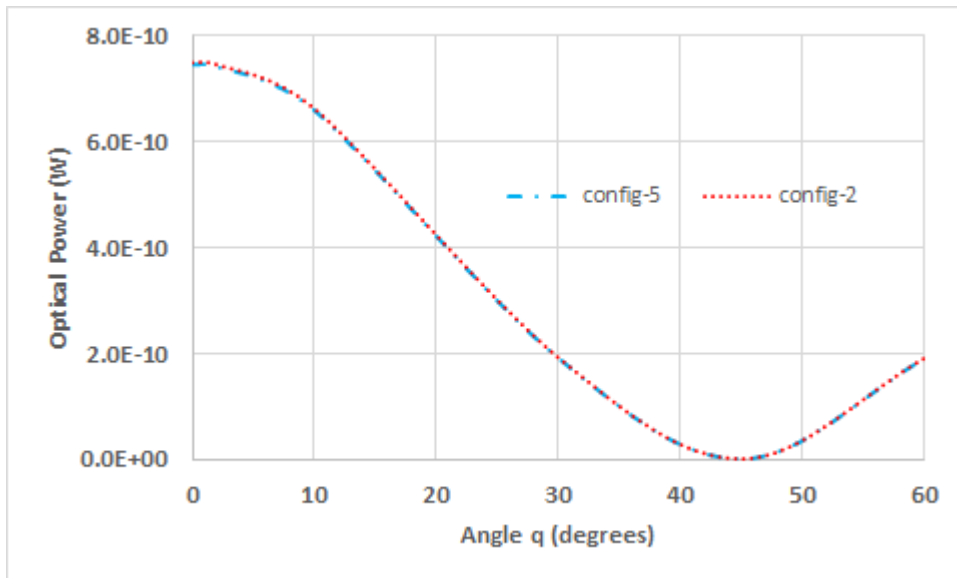
Figure 5.18 A unique behaviour of the simulation fibre type V at different angle q when the external fault happen

5.6.4. Changing the material and type of the fibre optic

5.6.4.1. Changing the material of fibre optic

The previous simulation has used the single mode optical fibre that is made from fused quartz. When the fibre optic material is changed from fused quartz to fused silica, the simulation results are listed in Table 5-9. This table concludes that the fused silica has lower optical power comparing to the fused quartz. These differences are caused by the birefringence of fused silica is higher than the fused quartz. Thus, the fused quartz material of fibre optic provides a higher optical power ratio that is suitable for a fault discrimination. Therefore, this fibre type could be applied as optical links in the proposed all-optical differential protection scheme.

Table 5-9 Optical power for the changing material of fibre optic

	Configuration	Maximum optical power (W)			
		Fibre type III		Fibre type V	
		Fused quartz	Fused silica	Fused quartz	Fused silica
Internal fault	2	7.34E-07	7.26E-07	7.34E-07	7.26E-07
	5	7.30E-07	7.26E-07	7.30E-07	7.25E-07
External fault	2	1.78E-13	1.76E-13	7.45E-10	5.74E-09
	5	1.77E-13	1.76E-13	7.41E-10	5.74E-09
Optical power ratio	2	4.12E+06	4.12E+06	9.85E+02	1.26E+02
	5	4.12E+06	4.12E+06	9.85E+02	1.26E+02

The ratio of optical power in the fused silica are lower than the fused quartz as tabulated in table 5-9. Therefore, in term of power modulation, the fibre optic that is made from fused quartz has better performance compare to fused silica.

5.6.4.2. Changing the type of fibre optic

The previous simulation has used a non-polarization maintaining single mode optical fibre type. A different fibre optic type which has low birefringence was applied in the simulation. The birefringence in the fibre optic can be reduced by using a special fabricated material or special designed fibre optic which is a polarization-maintaining (PM) optical fibre type [41]. For example, the birefringence B in [42] and [43] is 3.3E-4, whereas birefringence B for the Panda fibre is 3.5E-4 as documented in the Thorlabs website [44].

A proposed representation of the PM optical fibre is developed utilizing the fifth optical fibre model (J_{FO5}) with some changes in parameters such as birefringence B and the angle q. This model is proposed as the PM optical fibre model (J_{FO6}). After substituting the corresponding parameters such as birefringence of 3.4E-4 and the specified angle q (45 degree), the results are tabulated in Table 5-10. In this table, there is no significant difference of power modulation between each simulation when the

internal fault applied in the simulation. However, significant difference of power modulations appear for the external faults. Therefore, the use of PM single mode optical fibre type provides better performance of power modulation comparing to the non-PM optical fibre.

It is also seen in the Table 5-10 that the optical fibre type VI as a PM optical fibre and the optical fibre type III has approximately the same optical power. These results indicate that the third optical fibre model could be used to express the model of polarization-maintaining single mode optical fibre (the sixth optical fibre model) in the simple way. In addition, the optical fibre type III uses the proposed model that was developed by Jones.

Table 5-10 Comparison optical power between a non-PM and a PM type of optical fibre

	configuration	Maximum optical power (W)		
		Fibre type III (PM fibre)	Fibre type V (non-PM fibre)	Fibre type VI (PM fibre)
Internal fault	2	7.34E-07	7.34E-07	7.34E-07
	5	7.30E-07	7.30E-07	7.30E-07
External fault	2	1.78E-13	7.45E-10	1.78E-13
	5	1.77E-13	7.41E-10	1.77E-13
Optical power ratio	2	4.12E+06	9.85E+02	4.12E+06
	5	4.12E+06	9.85E+02	4.12E+06

Moreover, this table also shows that the optical power ratio of the PM single mode optical fibres have very high values which are approximately 4.12E+06, whereas for the non-PM single mode optical fibre are roughly 1.0E+03. Therefore, the use of the PM single mode optical fibre in the proposed all-optical configuration is recommended in order to achieve a very significant value for the fault discrimination. Other

consequence of using the PM single mode optical fibre type is an introduction of the sixth optical fibre model which is the PM single mode optical fibre. The sixth model of optical fibre is actually based on the fifth model of optical fibre. Thus, the sixth model is derived from the fifth model by substituting the related parameters of optical fibre which is the birefringence parameter.

5.6.5. Changing the length of fibre optic

Changing the length of optical fibre in the simulation of the proposed all-optical configuration were carried out. Variations of the optical fibre length are tabulated in the Table 5-11.

Table 5-11 Variation of the optical fibre length for the power system with 2 circuits

From	To	Label	Base case (m)	Case 1 (m)	Case 2 (m)
Polariser	FRCS1	FO1	2	100	200
FRCS1	FRCS2	FO12	4	30	60
FRCS2	Analyser	FO2	2	100	200
FO total length (m)			8	230	460

Due to the practical consideration, only the configuration 2 was selected to be performed with certain optical fibre models in the next simulation. The simulation results for different length of optical fibre are tabulated in Table 5-12. This table also concludes that the simulation fibre type III and VI generate very significant values of the optical power ratio. These value are very consistent results of optical power against the change of optical fibre length, whereas the simulation fibre type V gives inconsistent results. Therefore, this result provide a recommendation that the proposed all-optical configuration should use the PM optical fibre to link each optical device in the configuration in order to obtain the best performance.

Table 5-12 Comparison optical power for various fibre types using the configuration 2

	Fibre type (according to the fibre optic model)	Maximum optical power (W)			
		Base case (8 m)	Case 1 (230 m)	Case 2 (460 m)	optical fibre type
Internal fault	Fibre type III	7.34E-07	7.29E-07	7.24E-07	PM Fibre
	Fibre type V	7.34E-07	7.27E-07	7.13E-07	Non-PM Fibre
	Fibre type VI	7.34E-07	7.29E-07	7.24E-07	PM Fibre
External fault	Fibre type III	1.78E-13	1.77E-13	1.76E-13	PM Fibre
	Fibre type V	7.45E-10	4.06E-08	1.58E-07	Non-PM Fibre
	Fibre type VI	1.78E-13	1.77E-13	1.76E-13	PM Fibre
Optical power ratio	Fibre type III	4.12E+06	4.12E+06	4.12E+06	PM Fibre
	Fibre type V	9.85E+02	1.79E+01	4.50E+00	Non-PM Fibre
	Fibre type VI	4.12E+06	4.12E+06	4.12E+06	PM Fibre

First conclusion that could be derived from this table is the simulation fibre type V provides an acceptable optical power ratio only when it uses a very short length of optical fibre which is 8 meters. This conclusion is supported by a very high optical power ratio of 9.85E+02. However, increasing the length of optical fibre to be 460 metres in total as in the case-2 causes the decreasing optical power ratio to a very small value which is 4.5. Thus, the non-PM single mode optical fibre is not recommended to be used in the proposed all-optical configuration of the protection scheme.

Moreover, it is also seen that the simulation type III gives the same results with the simulation type VI. This fact also supports the previous statement in the section 5.6.4 that the third optical fibre model could be used to represent the model of PM optical fibre (the sixth optical fibre model) in the simple way.

Furthermore, the simulation fibre type V which used the non-PM single mode optical fibre provides an acceptable fault discrimination (a high value of optical power ratio) only when it uses a very short length of optical fibre. However, the fibre type V will loss of a fault discrimination when the fault is not a solid fault and the optical fibre length of approximately 250 metres in total.

In contrast, the simulation type III and VI provide a better fault discrimination (ratio of optical power) due to the use of PM single mode optical fibre. This result support previous recommendation that the PM single mode optical fibre should be used in the proposed all-optical configuration of the protection scheme.

5.7. Power system with busbar more than 2 circuits

5.7.1. Busbar with 3 circuits with generators

Other models of the test power system is a busbar of power system that has 3 circuits which is named the test power system 2 as shown in Figure 5.19. This test power system 2 is based on the test power system 1 with the addition of a generator (G3), a transformer (T3) and a transmission line (TL 132 kV, 10 km). As a consequence of the addition of these power system elements, the fault current increases to be 30.55 kA.
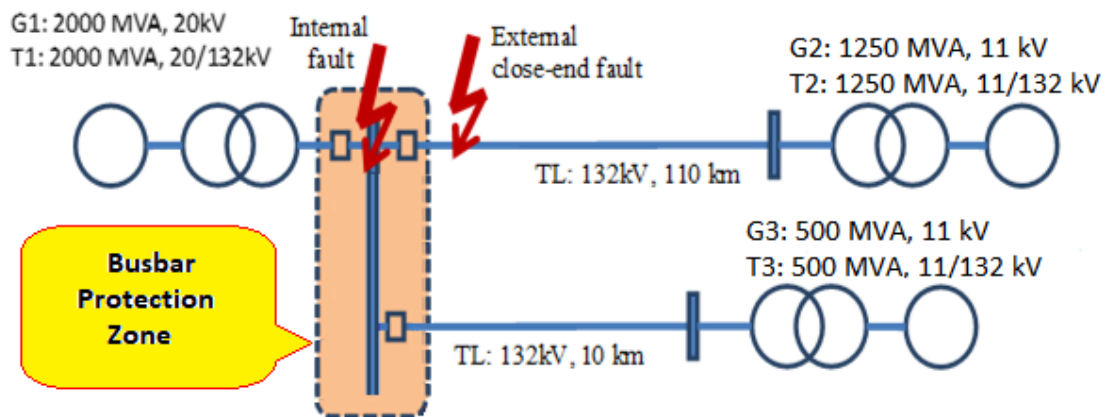
Figure 5.19 The test power system 2 (Busbar with 3 circuits)

Following the change of the number of busbar circuits in the test power system 2, the proposed all-optical configuration is also altered accordingly which is an addition of the optical current sensor (FRCS 3) including optical fibre. The optical fibre length are listed in the table 5-13.

Table 5-13 Variation of the optical fibre length for the power system with 3 circuits

From	To	Label designation	Fibre optic Length (m)
Polariser	FRCS1	FO1	200
FRCS1	FRCS2	FO12	30
FRCS2	FRCS3	FO23	30
FRCS2	Analyser	FO2	200
FO total length (m)			460

Implementing the proposed all-optical differential protection scheme into the power system busbar with 3 circuits as in the figure above has produced a complete power system with the proposed all-optical configuration that is shown in Figure 5.20. This figure of the proposed all optical differential protection scheme consists of two schematic diagrams, which are schematic optical components connection (upper graph) and the polarised light status in the optical components (bottom graph).

To describe the optical principle of the proposed method in that power systems, the fault current magnitude of $I1$, $I2$, and $I3$ are assumed to be equal in order to simplify the optical rotations as displayed in Figure 5.20. For an example of the external fault, the polarised light output after the analyser (the horizontal polariser) is an extinct polarised light ($E=0$) because the light status is in a vertical polarised light that is passed into the horizontal polariser as on the bottom graph in Figure 5.20.
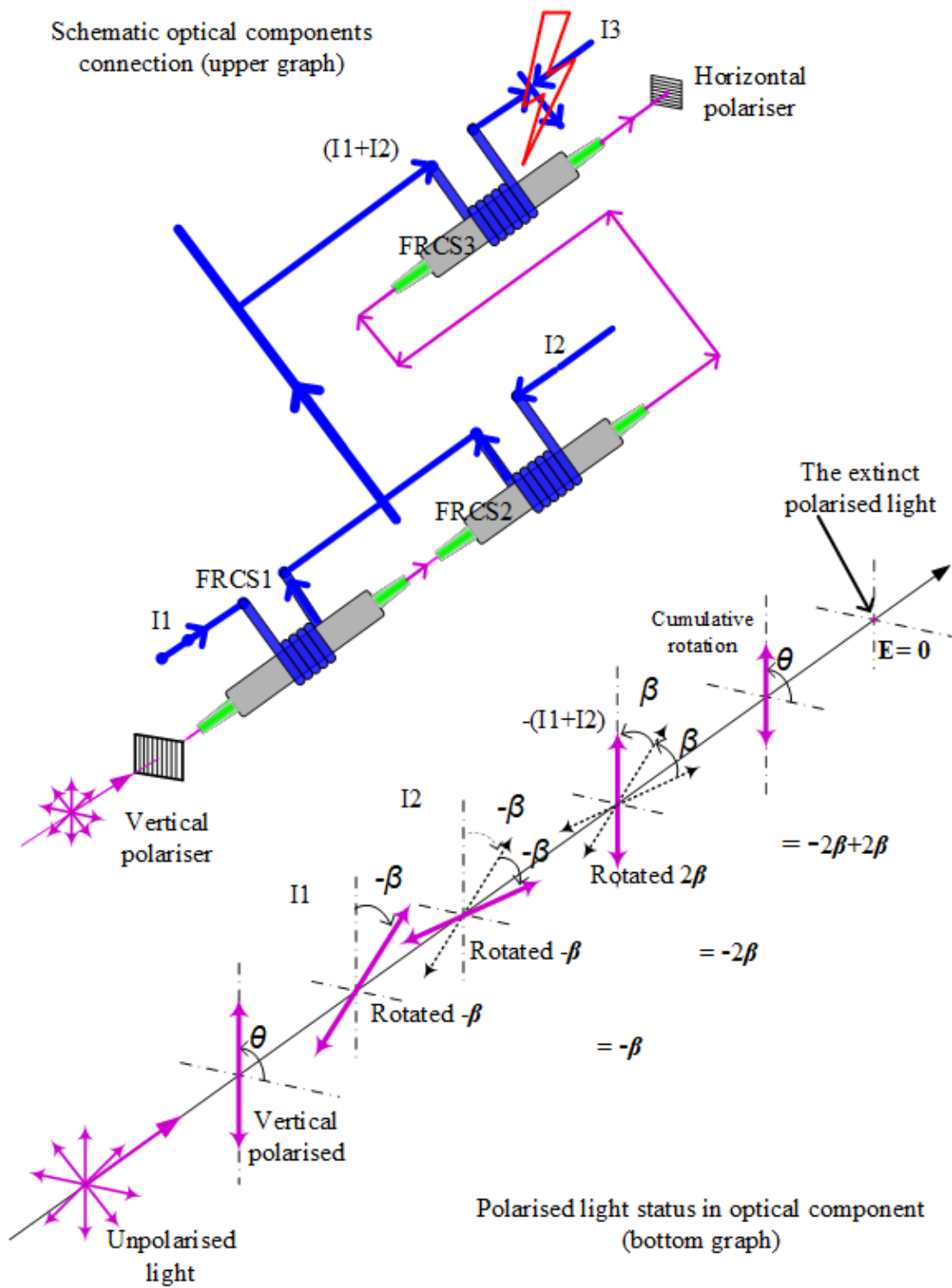
Figure 5.20 Schematic diagrams of the proposed optical configuration on the busbar with 3 circuits for the external fault.

Contrary to the external fault, applying the same procedures as in the previous paragraph, an optical status has been resulted for the internal fault as in Figure 5.21.
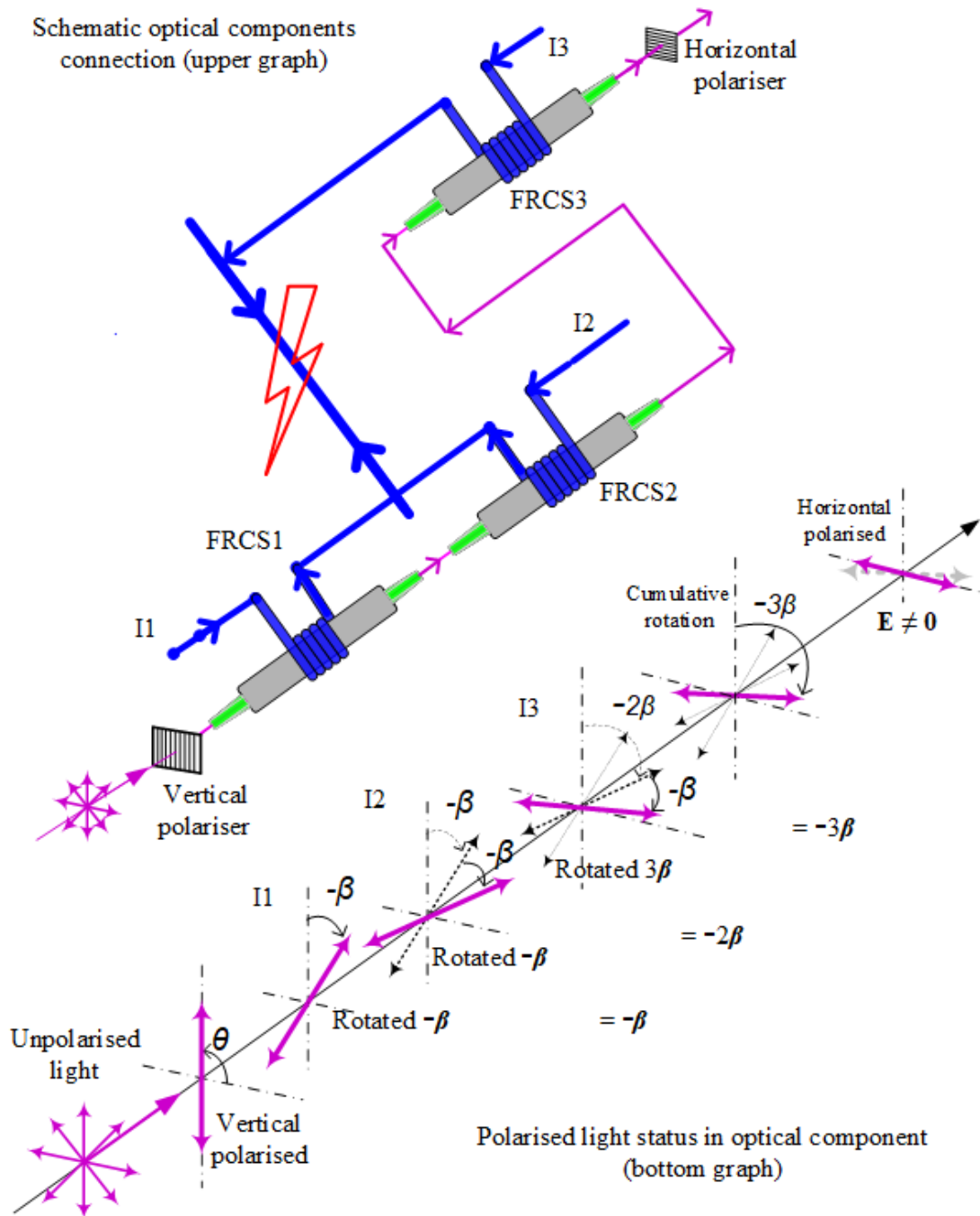
Figure 5.21 Schematic diagrams of the proposed optical configuration on the busbar with 3 circuits for the internal fault.

It could be resumed that the polarised light output after the analyser (the horizontal polariser) is a horizontal polarised light (E≠0) that is smaller than the polarised light before the analyser as shown on the bottom graph in Figure 5.21 above.

5.7.2. Busbar with 4 circuits with generators

The same procedure as the previous section was used to develop the test power system 3 which was based on the test power system 2 with the addition of a generator (G4), a transformer (T4) and a transmission line (TL 132 kV, 100 km). These addition of elements caused an increasing of a fault current to be 33.2 kA. This test power system 3 as shown in Figure 5.22 has a busbar with 4 circuits that was used to assess the proposed all-optical configuration of the protection scheme.
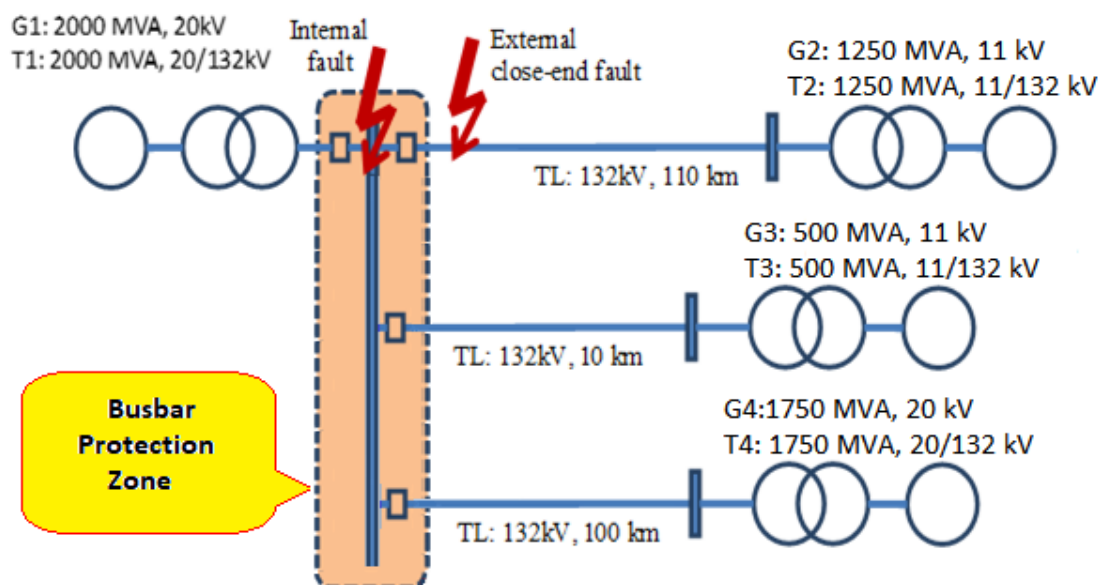
Figure 5.22 The test power system type 3 (Busbar with 4 circuits)

Following the change of the number of busbar circuits in the test power system 3, the proposed configuration is also modified accordingly which is an insertion of optical current sensor (FRCS 4) including a section of the optical fibre. It is worthy to be mentioned that the addition and connection of optical sensors into the system have to be conducted in proper way based on Kirchhoff's Current Law (KCL). As a

consequence of optical sensor addition, variation of the optical fibre length are listed in Table 5-14.

Table 5-14 Variation of the optical fibre length for the power system with 4 circuits

From	To	Label designation	Fibre optic Length (m)
Polariser	FRCS1	FO1	200
FRCS1	FRCS2	FO12	30
FRCS2	FRCS3	FO23	30
FRCS3	FRCS4	FO34	30
FRCS2	Analyser	FO2	200
FO total length (m)			490

A justification could be made by employing the same techniques of the all optical configuration as for the previous test power system 2 that has busbar with 3 circuits. The extinct polarised light (E=0) is also resulted as the polarised light outputs after the analyser when the external fault occurs in the power system busbar that has either 4 circuits or more. Thus, using an inference method, the same results would be obtained either for the busbar with 4 circuits or more circuits.

Contrary to the previous result, for the internal faults, the optical rotations have been resulted which are horizontal polarised lights (E≠0) that are smaller than the polarised light before the analyser.

Simulations of the proposed all-optical configuration were performed using these two power system models and the results of optical power responses are tabulated in Table 5-15. The optical power ratio for various number of circuits in the busbar are listed in Table 5-15. This table shows that simulation fibre type III and VI provide a better fault discrimination because it has extremely high value of the optical power ratio, whereas the simulation fibre type V could not generate a significant fault discrimination due to a very low value of the optical power ratio. Thus, this conclusion provides the same statement as the previous conclusion regarding the change of fibre length and fibre type as in the section 5.6.4 and section 5.6.5.

Table 5-15 Comparison of the optical power response between three power system models

	Fibre type (according to the fibre optic model)	Maximum optical power (W)			
		Busbar 2 circuits (FO length 460 m)	Busbar 3 circuits (FO length 460 m)	Busbar 4 circuits (FO length 490 m)	optical fibre type
internal	Fibre type III	7.24E-07	4.84E-07	2.66E-07	PM Fibre
	Fibre type V	7.13E-07	4.68E-07	2.52E-07	Non-PM Fibre
	Fibre type VI	7.24E-07	4.84E-07	2.66E-07	PM Fibre
external	Fibre type III	1.76E-13	8.20E-14	3.82E-14	PM Fibre
	Fibre type V	1.58E-07	1.35E-08	4.57E-09	Non-PM Fibre
	Fibre type VI	1.76E-13	8.20E-14	3.82E-14	PM Fibre
Optical power ratio	Fibre type III	4.12E+06	5.90E+06	6.97E+06	PM Fibre
	Fibre type V	4.50E+00	3.47E+01	5.51E+01	Non-PM Fibre
	Fibre type VI	4.12E+06	5.90E+06	6.97E+06	PM Fibre

This table shows that there are differences of optical power between the busbar 2 circuits and the busbar 3 circuits. Although the optical fibre in these cases have the same length, these differences are caused by insertion loss of the FRCS3 and connectors.

5.8. Performance evaluation of the all-optical configuration of busbar differential protection scheme using simulations

The selected configuration of all-optical busbar differential protection scheme was decided based on the practical applications in the previous simulation that it uses the configuration 2. Therefore, this configuration is also implemented in the simulation for the protection performance evaluation. Only two simulations fibre types (type V and VI) of the proposed all optical configuration of busbar differential protection

scheme will be analysed because they are the most realistic optical fibre representation. The simulation fibre type V used the non-PM single mode optical fibre model, whereas the simulation fibre type VI applied the PM single mode optical fibre model.

In these simulations, the faults inception time was occurred at 0.02 second. Additionally, a small stabilising delay of 0.1 ms has been applied inherently in the simulation of the protection tripping logic to prevent spurious tripping on random noise.

Implementation of the all-optical configuration of the busbar differential protection scheme in the electric power system requires a threshold optical power setting for the relay operation. The threshold setting of the optical power modulation is determined as an average value of the optical power modulations between a solid external fault and a high resistance internal fault. The chosen value is intended to ensure a comfortable margin for both sensitivity and stability attributes of the protection scheme.

In the simulation, there are two requirements for generating a trip signal. Firstly, the power level of optical modulation must be greater than the threshold setting. Secondly, the duration of the optical power modulation must be greater than an intended additional time delay which was assumed to be 0.1 ms. Thus, the trip signal is generated when both of the requirements are fulfilled.

5.8.1. Sensitivity and dependability: simulation fibre type V and VI

This section consists of two analyses, which are the determination of protection sensitivity, and verification of sensitivity and dependability for two sets of optical fibre. These two sets of the optical fibre are fibre type V as a model of non-PM fibre and fibre type V as a model of PM fibre.

The first analysis is for determining the protection sensitivity. Two types of faults which are internal and external faults will be considered. Two internal fault types i.e. a solid internal fault and a high resistance internal fault of 200 Ω and a solid external fault were applied in the simulation. The simulation results are shown in Table 5-16.

189

Table 5-16 Optical power modulation response at different fibre types and fault scenarios

	Fibre type (according to the fibre optic model)	Maximum optical power (W)		
		(0 Ω)	(200 Ω)	optical fibre type
Internal faults	Fibre type V	7.13E-07	2.33E-10	Non-PM Fibre
	Fibre type VI	7.24E-07	1.78E-10	PM Fibre
External Faults	Fibre type V	1.58E-07	1.58E-07 (0 Ω)	Non-PM Fibre
	Fibre type VI	1.76E-13	1.76E-13 (0 Ω)	PM Fibre
Ratio of the internal to external faults	Fibre type V	4.5	1.47E-03	Non-PM Fibre
	Fibre type VI	4.12E+06	1.02E+03	PM Fibre

In table 5-16, for a resistive external fault of 200 Ω, no tests are needed to obtain the fault currents because those cells are only needed the fault current for solid external fault just outside the busbar zone (the solid external close-end fault), which is the external fault of 0 Ω. Thus, the corresponding data to fill that cells are optical power at the external fault of 0 Ω (a solid external close-end fault). As a result, the corresponding data to fill that cells for the optical fibre type V and VI respectively are 1.58E-07 (0 Ω) and 1.76E-13 (0 Ω).

Based on the simulation, the threshold setting for the test power system 1 is obtained to be 7.93E-10 W (equivalent to 0.793 nW) for simulation fibre type V and 9.17E-11 W (equivalent to 0.092 nW) for simulation fibre type VI as tabulated in Table 5-17.

In Table 5-17, an anomaly is occurred in the simulation type V as supported by data in Table 5-16. Although the current differential of the solid external fault is smaller than the current differential of the high resistance internal fault of 200 Ω, the optical power modulation at the external fault is greater than the optical power modulation at the internal fault as well as the threshold setting. This problem could be arisen from the existence of circular birefringence in optical fibre which causes the distortion in the polarized light that has an amplification effect on the optical power modulation. As a consequence, this problem can cause unwanted operation of the optical protection scheme which operates when the solid external fault happens and not operate when

high resistive internal fault occurs.

Table 5-17 Sensitivity attribute of the optical protection scheme

Fibre type	Case	Maximum optical power (W)	Threshold setting (W)	Generated trip signal	Required signal	Remarks
Fibre type V	Internal fault 1.c	2.33E-10	7.93E-08	No	**Yes**	N
	External fault 2.a	1.58E-07		Yes	**No**	N
Fibre type VI	Internal fault 1.c	1.83E-10	9.17E-11	Yes	**Yes**	M
	External fault 2.a	1.76E-13		No	**No**	M

Note:

N = Not meet the differential protection principle (because it is no trip when internal fault happens)

M = Meet the differential protection principle (because it trips when internal fault happens)

Solving this problem could be achieved with two possible solutions. The first solution is by increasing the threshold setting value to be greater than 1.58E-07 W. However, this solution has an impact to the optical protection scheme because it could not detect the fault if the fault resistance is greater than 3.7 Ω (equivalent to a current fault of less than 12 kA).

Another solution is replacing the non-PM optical fibre type with the polarization maintaining fibre type because this type provides better performance of the protection scheme as shown in Table 5-17. Therefore, the use of non-PM optical fibre to link the optical devices in the all-optical configuration of the protection scheme is not recommended.

The second analysis is for verifying protection sensitivity and dependability. The same simulation with high resistance of 200 Ω internal fault was applied and the threshold setting was embedded in the simulation programme. The simulation result shows that the all-optical configuration of the differential protection scheme could detect an

occurrence of a fault that provides power modulation with a peak value of 1.83E-10 W for simulation fibre type VI at the first cycle of the faulted current. The fault occurrence are indicated by an existence of the trip signal as illustrated in Figure 5.23.
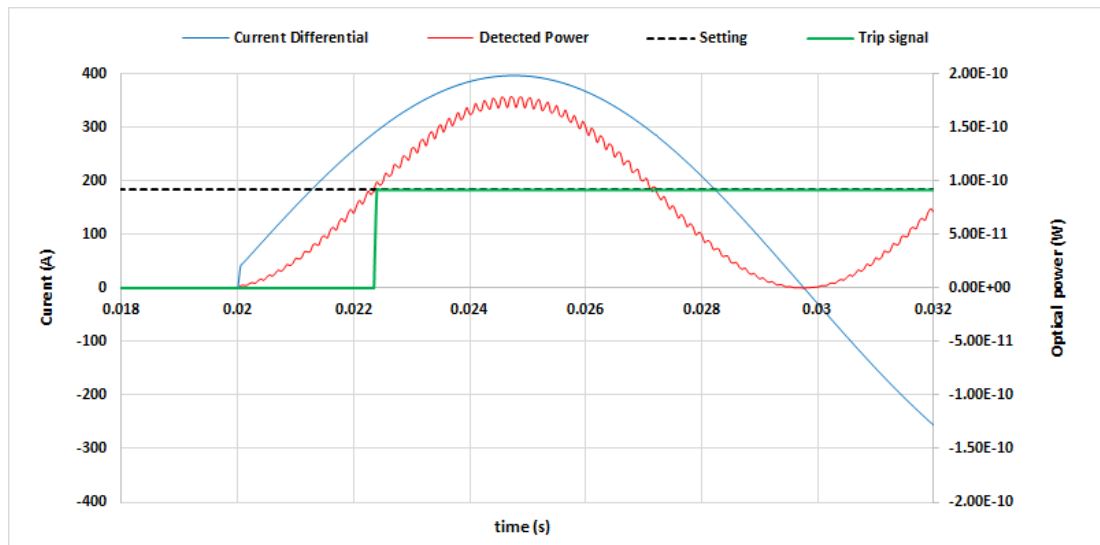
Figure 5.23 Simulated trip signal using the optical fibre type VI for resistive internal fault of 200 Ω.

The optical power modulations in Figure 5-23 are generated by the fault current of 400 A peak due to a high resistive internal fault of 200 Ω. These high fault currents generate the corresponding high optical power modulations that are a cumulative result from both optical current sensors 1 and 2.

Moreover, verifying the protection sensitivity can be also checked by increasing the internal fault resistance. Using the same setting in the simulation type VI, the optical protection scheme is still able to detect the high resistance internal fault of 250 Ω (equivalent to 1.15E-10 W) that is designated by the trip signal at 0.0233 seconds.

As considerations to the selected setting for performance verification, some optical power modulation data from the simulation are tabulated in Table 5-18. This table is also intended to provide the verification results of the selected protection setting for internal and external faults. It is becoming clear that the selected settings are met the

protection performances which generate a trip signal on the internal fault and no trip signals are generated at the external fault and at both pre-faults conditions.

Table 5-18 Verification results of the simulation fibre type VI

	Pre-fault or fault conditions	Differential Current (A)	Optical power (W)	Threshold setting (W)	Generated trip signal	Required signal	Remarks
Internal faults	Pre-fault condition (Rf = 0 Ω)	0.08	1.76E-13	9.17E-11	No	No	Meet the differential protection principle (Trip when internal fault happens)
	Fault condition (Rf = 0 Ω)	25,500	7.24E-7	9.17E-11	Yes	Yes	
	Fault condition (Rf = 200 Ω)	400	1.83E-10	9.17E-11	Yes	Yes	
	Fault condition (Rf = 250 Ω)	318	1.15E-10	9.17E-11	Yes	Yes	
External fault	Pre-fault condition (Rf = 0 Ω)	0.08	1.76E-13	9.17E-11	No	No	
	Fault condition (Rf = 0 Ω)	0	1.76E-13	9.17E-11	No	No	

As part of protection performance verification, several data in Table 5-18 could be analysed in more detail by combining several enlarged images that are derived from Figure 5.23 at two exact cases. The two exact cases of the enlarged images are, first, at the pre-fault condition of the internal fault of 0 Ω and, second, at fault condition of the external fault of 0 Ω.

The detailed analyses are explained in two group comparisons which are the magnitude of the optical power modulation and the modulation signal comparisons as follows.

The first comparison is the magnitude of the optical power modulation. This comparison would use optical power from two simulation results. The first and the second cases are actually the same conditions which are similar to the external fault

condition where the differential protection should not operate in these cases because both cases are through current which the differential current is equal to zero or approximately close to zero. Thus, the first case is through current in normal condition (through normal current) and the second case is through fault current. Moreover, the first case is at the pre-fault condition of the internal fault of 0 Ω (through normal current), whereas the second case is at fault condition of the external fault of 0 Ω (through fault current). Thus, the differential current for a peak value is 0.08 A in the first case as shown in Figure 5.24 and 0 A in the second case as displayed in Figure 5.25. In addition, the differential current in the second case has been enlarged 1E+07 times in order to make a clear plot.

For the magnitude of optical power comparison, the optical power modulation in the first case is approximately 1.76E-13 W as listed at row 1 in Table 5-18, while in the second case is also roughly 1.76E-13 W as listed at row 6 in Table 5-18. It is reasonable that the small values of the optical power modulations are caused by small differential currents. Thus, both values of optical power generate no trip signal because it is smaller than the threshold setting (9.17E-11 W). The reason of the small differential current at the first case and the second case are based on Kirchhoff's Current Law that the total sum up of electric current in a junction point is equal to zero. Therefore, the differential current is also equal to zero.

The second comparison is the modulation signal. This comparison would use optical modulation from two simulation results. Looking carefully at Figure 5.24 as an enlarged image in the first case and Figure 5.25 as an enlarged image in the second case. Both images show that modulation signals of the optical power in the proposed all-optical configuration with two patterns which are high-frequency oscillation and AC system frequency modulation. However, they have differences in the magnitude of optical power. The optical power magnitudes in Figure 5.24 fluctuate between 1.7721E-13 W (maximum) and 1.7407 W (minimum) which have a different value of 3.15E-15 W, whereas in Figure 5.25 has value of 1.7565E-13 W (maximum) and 1.7565 W (minimum) which have a different value of 6.64E-20 W. These optical magnitude differences are caused by the differences of differential current as listed in Table 5-18.
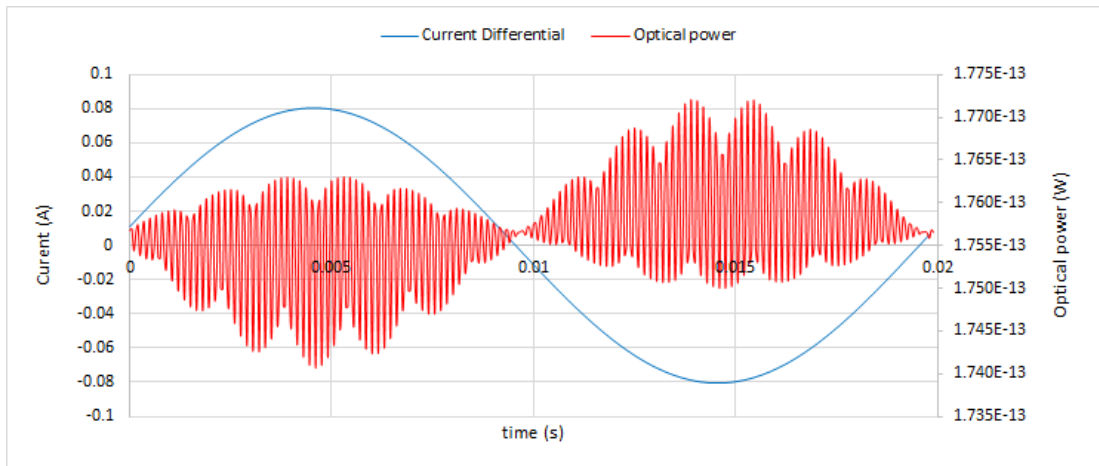
Figure 5.24 The simulation fibre type VI at pre-fault condition for an internal fault of 0 Ω.
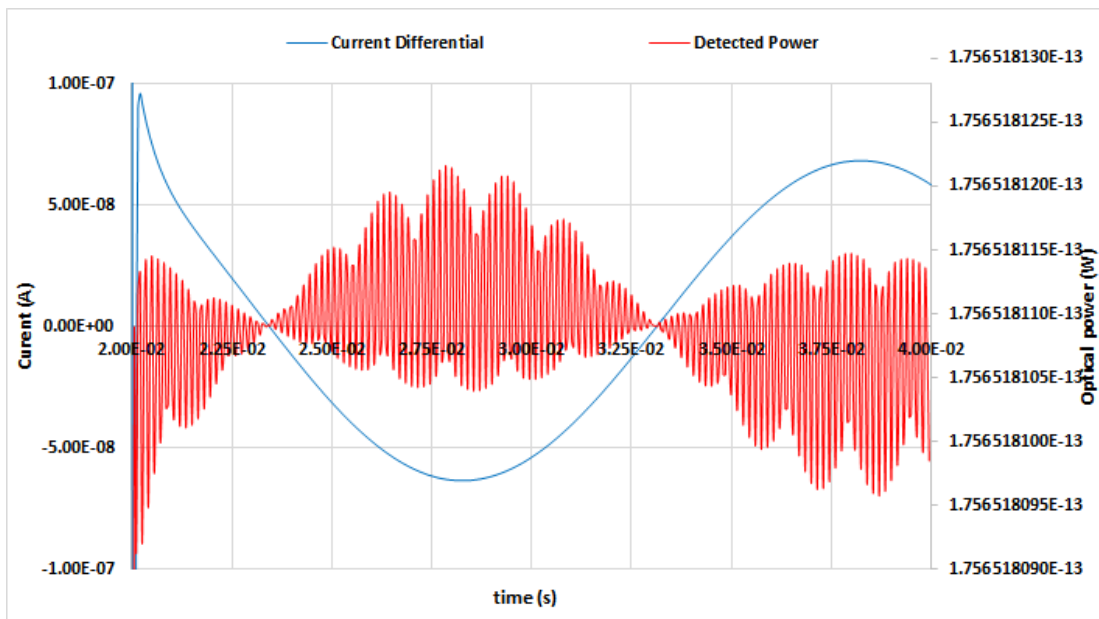
Figure 5.25 The simulation fibre type VI for a solid external fault

To discuss the sources of high-frequency oscillation and AC system frequency modulation in both images, it is noted that there are two existed frequencies in the proposed all-optical configuration that will be useful in order to explain the optical modulation frequencies and their characteristics. The first frequency is a very high frequency of 193.55 THz for a centre wavelength of 1550 nm. This frequency is from

the electromagnetic wave source which is actually from laser source as in this case. The second frequency is a frequency of 50 Hz which is from an AC electric source.

Moreover, it is important to explain a generating principle of optical signal modulation in the proposed all-optical differential configuration. An optical signal in the proposed all-optical differential configuration is generated from a polarised light source such as a laser source. Then, this polarised light travels in two optical components which are the optical fibre and the optical current sensor. While the polarised light traveling, the polarised light interacts with the optical fibre (first interaction) and then it continues to interact with optical current sensors (second interaction). Thus, the polarised light interacts with the optical components along its journey in the proposed all-optical differential configuration. Therefore, the polarised light is modulated in magnitude and frequency along the trip.

Furthermore, based on both images, the optical modulations with different magnitudes and frequencies are derived from the accumulation of the first and the second interactions that depend on their magnitude to suppress each other. As an example, the total sum up of electric current (the differential current) for the first case is 7.2E-08 (very close to zero). Due to a very small differential current effect in the proposed optical system, the electromagnetic wave effect appears more significant as the polarised light interaction in the optical fibre that generates modulation signal with higher frequency as depicted in Figure 5.25. Thus, it is the reason for optical modulation with a higher frequency appears more dominant.

As a consequence from the first interaction, the polarised light interacts with the optical fibre, that has birefringence characteristics (a linear and a circular effect), to produce a high-frequency optical modulation with linear and circular effects. Thus, from the first interaction, the polarised light obtains birefringence effects that seem to be a twisted optical modulation with a non-uniform pattern as depicted in both images.

As a consequence from the second interaction, the polarised light interacts with the optical current sensors that have the differential current effect to generate the magnitude and 50 Hz frequency of optical modulations. Higher differential currents have also the higher magnitude with 50 Hz optical modulations as shown in Figure

196

5.23 as a resistive internal fault of 200 Ohm. When the differential currents exist, the magnitude and 50 Hz modulations are dominant than the second interaction effect. In addition, the method that applied into a series arrangement of the optical current sensors is the cancellation method that has been explained in the section 4.4.2.2. The cancellation method means that a modulation effect of the current in the optical current sensor 1 is cancelled by the modulation effect of the current in the optical current sensor 2. The series arrangement of the optical current sensors (cancellation method) work properly for the electric current. However, the birefringence effect could not be cancelled in the sensors arrangement because it applies the Faraday rotation principle. In contrary, the Faraday rotation principle amplify the birefringence effect, therefore, it enforces optical modulations that have both the linear and circular component in the first interaction above.

To conclude, it is seen from both Figure 5.24 and Figure 5.25 that both images have the same high-frequency oscillation and the same AC system frequency modulation. The differences are only in the magnitude of modulation due to the differences in differential current. The optical signal modulation is an accumulation of the frequency from the polarised light source and the AC electric source including polarised light interaction with optical fibre and optical current sensors either with or without differential current effect. The cancellation method works properly in the optical sensors for the current differential. However, it amplifies the birefringence effects. The birefringence effects become significant only when the differential current is zero or close to zero. Otherwise, the birefringence effect is suppressed when the differential current increases significantly as a result of the internal fault.

The protection dependability is checked by the solid internal fault simulation as shown in Figure 5.26.
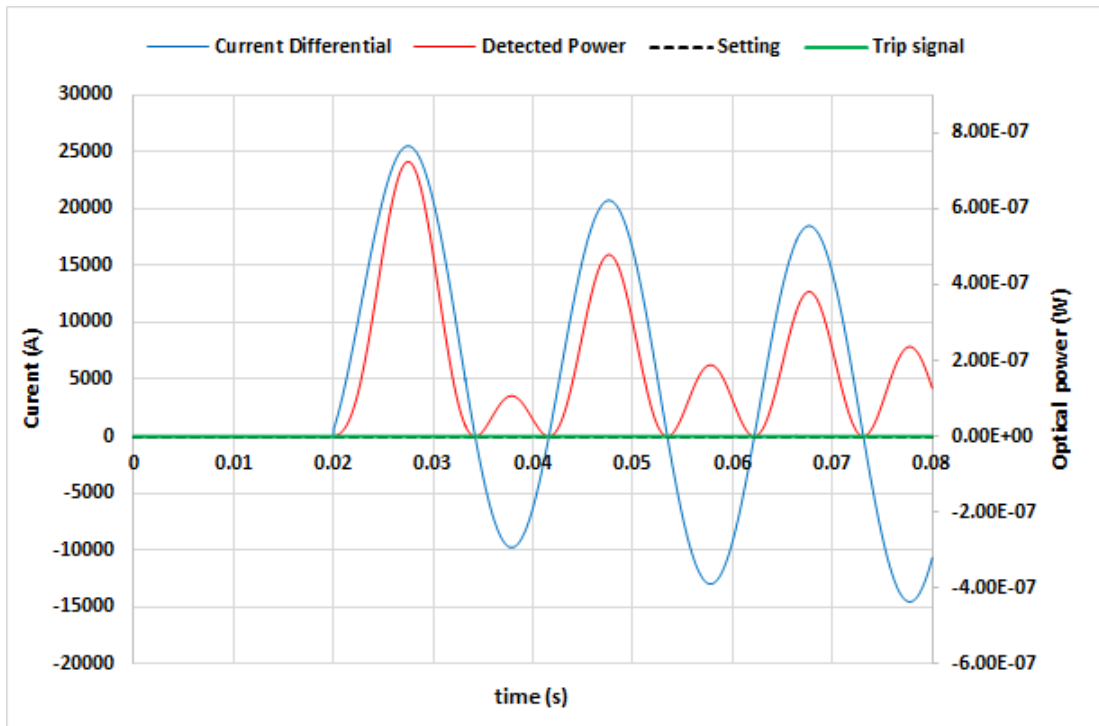
Figure 5.26 Simulation type VI on the solid internal fault

The zooming view of Figure 5.26 is shown in Figure 5.27. The solid internal fault produces the optical power modulation as tabulated in Table 5-19 is much higher than the assumed threshold (7,893 times) which demonstrates very good level of dependability (7.24E-7 W) compared to the threshold setting (9.17E-11 W). In this case, the optical protection scheme generates the simulated trip signal at 0.0201 seconds as displayed in Figure 5.27 as a zooming view of Figure 5.26.

Table 5-19 Dependability attributes of the simulation fibre type VI

attribute	Fault case	Maximum optical power (W)	Threshold setting (W)	Remarks
Dependability	Solid internal fault	7.24E-7	9.17E-11	Meet the requirement
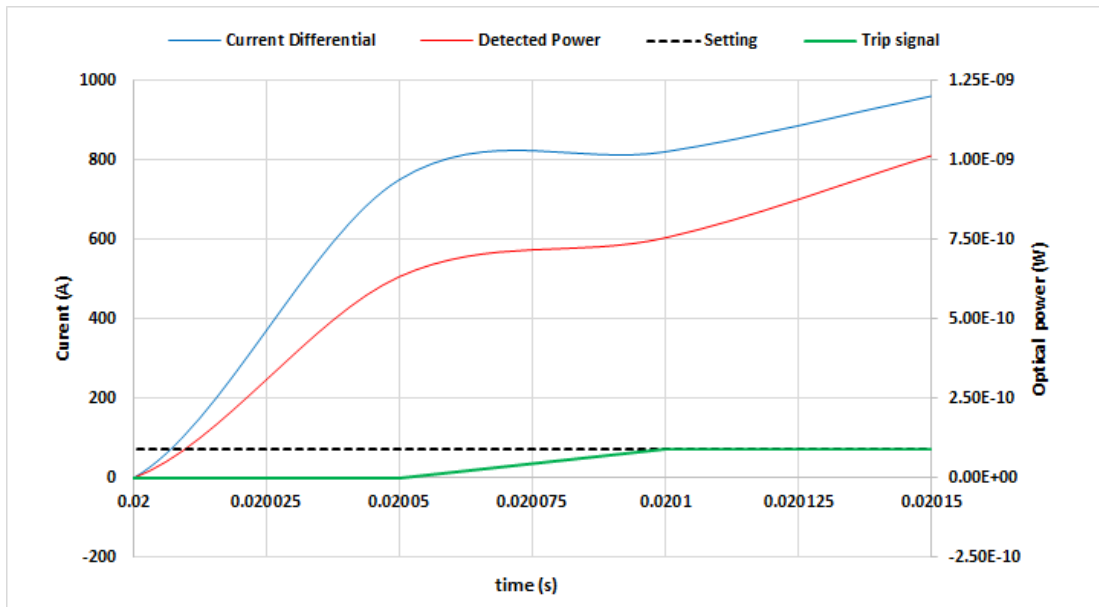
Figure 5.27 Trip signal of simulation fibre type VI on the solid internal fault (zooming view Figure 5.26)

A conclusion can be derived from the simulation fibre type VI that it meets the sensitivity and dependability requirements of the optical protection scheme, whereas the simulation fibre type V is not meet the requirements. Therefore, the non-PM optical fibre is not recommended to link the optical devices in the all-optical configuration of the protection scheme.

5.8.2. Stability / security: simulation fibre type VI

Since result of the simulation fibre type V in previous section does not meet the protection requirements, this simulation type does not considered in this and the following sections.

Stability / security attribute of the all-optical differential protection is tested by external solid fault (Case 2.a). In this case the optical power modulation level is 1.76E-13 W which is 522 times below the assumed threshold setting (9.17E-10 W). Hence, the trip signal is not generated. This result provides a conclusion that the simulation fibre type VI meets the stability/ security requirement.

5.8.3. Protection operation time: simulation fibre type VI

The differential output processing time in this optical differential protection scheme can be determined using equation (4.16). Since the optical fibre has a big portion of length in the series configuration of optical devices in the optical protection scheme, the optical fibre parameters such as length and refractive index are used to calculate the processing time in this equation. The optical differential processing time is tabulated in Table 5-20.

Table 5-20   Optical differential processing time

Length of optical fibre (m)	The optical differential processing time (s)
8	4.17E-8
460	2.36E-6
1,000	5.12E-6
2,000	1.02E-5

It is seen that the processing time is very short (in microseconds) because it uses polarized light to conduct the summing up process. In the presented case in the previous section, it is approximately 2.36 μs with optical fibre length around 460 m.

Using the Matlab simulation software, the protection operation time was conducted and the simulation results are listed in Table 5-21.

Table 5-21   Protection operation time

attribute	Case	Fault inception at (s)	Trip status	Trip Signal at (s)	Protection operation time (s)
sensitivity	Internal fault 200 Ω	0.02	Trip	0.0224	0.0024
	Internal fault 250 Ω	0.02	Trip	0.0233	0.0033
dependability	Internal fault 0 Ω	0.02	Trip	0.0201	0.0001
Stability/ security	External fault 0 Ω	0.02	No trip	NA	NA

5.8.4. Speed of operation in practical applications

It is understandable that in practical applications the total protection operation time would be longer than the one indicated by the simulation model. Total operating time of the all-optical differential protection consists of three consecutive time intervals which are: the differential output, optical power comparison, and decision processing time (including any stabilising time delays and tripping logic).

In practical applications, operating time for the photo-detection, comparison to the threshold setting, and decision making processes could be determined by direct measurement or indirect method. Other approach is by using a benchmarking data of similar processing time from the relay manufacturer which in this case could be achieved in less than 2 ms [45-48].

As calculated in the previous section, the differential output processing time is approximately 2.36 μs with optical fibre length around 460 m. The simulated protection operation time is vary from 3.3 ms to 0.1 ms (from slowest to fastest time) and average time of the protection operation is 1.7 miliseconds.

5.9. Conclusion

The proposed all-optical configuration of busbar differential protection scheme has been simulated using six simulation models and five configurations, i.e. from the ideal model to the complex, the most realistic models. The results of simulation fibre type

VI show that the proposed optical configuration has success to be implemented as a busbar differential protection . The protection is sensitive to a high resistive internal fault (up to 250 Ohm), and stable during an external solid close-up fault. The differential output processing time is relatively very fast, i.e. 5.12 μs with optical fibre length of 1 km. The simulated protection operation time is vary from 3.3 ms to 0.1 ms and average time of the protection operation is 1.7 miliseconds.

The proposed protection has been subsequently validated through prototype experiment in the Advanced Sensor Laboratory within EEE Department at the University of Strathclyde. The experiment and the test results are presented in the next chapter.

5.10. References for Chapter 5

[1]   B. E. A. Saleh, *Fundamentals of photonics*, 2nd ed.. ed. Hoboken, N.J.: Hoboken, N.J. : Wiley-Interscience, 2007.

[2]   A. Lipson, *Optical physics*: Cambridge : Cambridge University Press, 2011.

[3]   R. M. A. Azzam, Bashara, N. M, *Ellipsometry and Polarized Light*. Amsterdam: Elsevier Science BV, 1987.

[4]   Thorlabs, "Nanoparticle Linear Film Polarizer," vol. 2015, Thorlabs, Ed., ed: Thorlabs, 2015.

[5]   D. S. Kliger, *Polarized light in optics and spectroscopy*. Boston: Boston : Academic Press, 1990.

[6]   SCHOTT.   (2017).   *SCHOTT   Products*   Available: https://www.us.schott.com/english/index.html

[7]   M. N. Polyanskiy. (2008). *Refractive index database*. Available: https://refractiveindex.info

[8]   Filmetrics.   (1995).   *Refractive   index   database*.   Available: https://www.filmetrics.com/refractive-index-database

[9]   N. Grumman. (2012). *TGG (Terbium Gallium Garnet)*. Available: http://www.northropgrumman.com/BusinessVentures/SYNOPTICS/Products/SpecialtyCrystals/Pages/TGG.aspx

[10] D. Jiles, *Introduction to magnetism and magnetic materials*: London : Chapman and Hall, 1991.

[11] M. Gaugitsch and H. Hauser, "Optimization of a magneto-optical light modulator-Part I: modeling of birefringence and Faraday effect," *Journal of Lightwave Technology,* vol. 17, pp. 2633-2644, 1999.

[12] R. P. Hunt, "Magneto-Optic Scattering from Thin Solid Films," *Journal of Applied Physics,* vol. 38, pp. 1652-1671, 1967.

[13] G. Ghosh, "Dispersion-equation coefficients for the refractive index and birefringence of calcite and quartz crystals," *Optics Communications,* vol. 163, pp. 95-102, 1999/05/01/ 1999.

[14] I. H. Malitson, "Interspecimen Comparison of the Refractive Index of Fused Silica*,†," *Journal of the Optical Society of America,* vol. 55, pp. 1205-1209, 1965/10/01 1965.

[15] C. Z. Tan, "Determination of refractive index of silica glass for infrared wavelengths by IR spectroscopy," *Journal of Non-Crystalline Solids,* vol. 223, pp. 158-163, 1998/01/01/ 1998.

[16] Corning. (2015). *Corning Products* Available: https://www.corning.com/worldwide/en.html

[17] R. C. Jones, "A New Calculus for the Treatment of Optical Systems. VII. Properties of the N-Matrices," *Journal of the Optical Society of America,* vol. 38, pp. 671-685, 1948/08/01 1948.

[18] R. C. Jones, "A New Calculus for the Treatment of Optical Systems. IV," *Journal of the Optical Society of America,* vol. 32, pp. 486-493, 1942/08/01 1942.

[19] P. Yeh, "Electromagnetic propagation in birefringent layered media," *Journal of the Optical Society of America,* vol. 69, pp. 742-756, 1979/05/01 1979.

[20] A. J. Rogers, *Polarization in optical fibers*: Norwood, MA : Artech House, 2008.

[21] M. Aerssens, A. Gusarov, B. Brichard, V. Massaut, Me, x, P. gret, and M. Wuilpart, "Faraday effect based optical fiber current sensor for tokamaks," in *Advancements in Nuclear Instrumentation Measurement Methods and their*

Applications (ANIMMA), 2011 2nd International Conference on, 2011, pp. 1-6.

[22]   P. Yeh, *Optical waves in layered media*. New York: New York : Wiley, 1988.

[23]   S. C. Rashleigh, "Origins and control of polarization effects in single-mode fibers," *Lightwave Technology, Journal of,* vol. 1, pp. 312-331, 1983.

[24]   M. Nasir, A. Dysko, P. Niewczas, and G. Fusiek, "All-optical busbar differential protection scheme for electric power systems," in *The 13rd IET International Conference on Development in Power System Protection*, Edinburgh, 2016.

[25]   A. R. Zakharian, E. B. Marin, C. Fiebig, H. V. Tran, L. Hepburn, and A. Kobyakov, "Predicting insertion loss in multi-fiber multimode connectors," in *2015 European Conference on Optical Communication (ECOC)*, 2015, pp. 1-3.

[26]   W. C. Young, V. Shah, and L. Curtis, "Loss and reflectance of standard cylindrical-ferrule single-mode connectors modified by polishing a 10 degrees oblique endface angles," *IEEE Photonics Technology Letters,* vol. 1, pp. 461-463, 1989.

[27]   J. Allington-Smith, G. Murray, and U. Lemke, "Simulation of complex phenomena in optical fibres," *Monthly Notices of the Royal Astronomical Society,* vol. 427, pp. 919-933, 2012.

[28]   IEEE, "IEEE Draft Guide: Adoption of the Project Management Institute (PMI) Standard: A Guide to the Project Management Body of Knowledge (PMBOK Guide)-2008 (4th edition)," *IEEE P1490/D1, May 2011,* pp. 1-505, 2011.

[29]   R. G. Sargent, "Verification and validation of simulation models," in *2007 Winter Simulation Conference*, 2007, pp. 124-137.

[30]   B. H. Thacker, S. W. Doebling, F. M. Hemez, M. C. Anderson, J. E. Pepin, E. A. Rodríguez, and D. 2004, "Concepts of Model Verification and Validation," 2004.

[31]   B. Boehm, "Software Engineering Economics," *IEEE Transactions on Software Engineering,* vol. SE-10, p. 18, January 1984 1981.

[32] D. A. Cook and J. M. Skinner. (2005). *How to Perform Credible Verification, Validation, and Accreditation for modeling and Simulation*. Available: https://pdfs.semanticscholar.org/c76f/f966a1c00696c39bd476a6e657f7a24f7 468.pdf

[33] R. G. Sargent, "Verification and validation of simulation models," presented at the Proceedings of the Winter Simulation Conference, Phoenix, Arizona, 2011.

[34] A. M. Law, "How to Build Valid and Credible Simulation Models," in *the IEEE Winter Simulation Conference*, 2008, p. 9.

[35] A. M. Law and M. G. McComas, "How to build valid and credible simulation models," in *Proceeding of the 2001 Winter Simulation Conference (Cat. No.01CH37304)*, 2001, pp. 22-29 vol.1.

[36] MITRE. (2017). *Verification and Validation of Simulation Models*. Available: https://www.mitre.org/publications/systems-engineering-guide/se-lifecycle-building-blocks/other-se-lifecycle-building-blocks-articles/verification-and-validation-of-simulation-models

[37] B. Jones, I. Jenkinson, Z. Yang, and J. Wang, "The use of Bayesian network modelling for maintenance planning in a manufacturing industry," *Reliability Engineering & System Safety,* vol. 95, pp. 267-277, 2010/03/01/ 2010.

[38] A. Saltelli and Dawsonera, *Global sensitivity analysis [internet resource] : the primer*. Chichester: Chichester : John Wiley & Sons, Ltd., 2008.

[39] A. Saltelli, *Sensitivity analysis in practice : a guide to assessing scientific models*. Hoboken, NJ: Hoboken, NJ : Wiley, 2004.

[40] D. Fitzpatrick, "Chapter 24 - Sensitivity Analysis," in *Analog Design and Simulation Using OrCAD Capture and PSpice (Second Edition)*, ed: Newnes, 2018, pp. 351-365.

[41] K. Suzuki, H. Kubota, S. Kawanishi, M. Tanaka, and M. Fujita, "Optical properties of a low-loss polarization-maintaining photonic crystal fiber," *Optics Express,* vol. 9, pp. 676-680, 2001/12/17 2001.

[42] W. Zou, Z. He, and K. Hotate, "Complete discrimination of strain and temperature using Brillouin frequency shift and birefringence in a polarization-maintaining fiber," *Optics Express,* vol. 17, pp. 1248-1255, 2009/02/02 2009.

[43]   C. Li, J. Yang, Z. Yu, Y. Yuan, J. Zhang, B. Wu, F. Peng, and L. Yuan, "High-Order Interference Effect Introduced by Polarization Mode Coupling in Polarization—Maintaining Fiber and Its Identification," *Sensors,* vol. 16, p. 419, 2016.

[44]   Thorlabs. (2015). *Polarization-Maintaining Single Mode Optical Fiber*. Available:
https://www.thorlabs.de/newgrouppage9.cfm?objectgroup_id=1596&pn=PM1550-XP

[45]   ABB. (2015). *ABB Busbar Protection Document 611 Series*. Available:
http://new.abb.com/medium-voltage/distribution-automation/numerical-relays/busbar-protection

[46]   Siemens. (2015). *Siemens Centralized Busbar Protection Document SIPROTEC 7SS85*. Available:
http://w3.siemens.com/smartgrid/global/en/products-systems-solutions/Protection/busbar-protection/Pages/7SS85.aspx

[47]   Toshiba. (2015). *Toshiba Busbar Protection Document GRB 200*. Available:
http://www.toshiba-tds.com/tandd/products/pcsystems/en/grb200.htm

[48]   GE-Alstom. (2015). *GE Busbar Protection Document Multilin B90*. Available:
https://www.gegridsolutions.com/multilin/catalog/b90.htm

Chapter 6. Prototype Development and Laboratory Testing of the Proposed All-Optical Configuration of Busbar Differential Protection Scheme

A simulation which is based on validation and performance assessment of the proposed all-optical configuration of busbar differential protection scheme has been presented in chapter 5. The simulation results have shown that the proposed scheme can be successfully applied as a busbar differential protection. This chapter is focused on two development steps which are the physical prototype development process, including laboratory work, and laboratory experimentation. Thus, the chapter is started with the prototype design, followed by the selection of the required components and tools for laboratory testing of the proposed all-optical busbar differential protection scheme. Then, setting up the experiment's equipment are revealed. The experiment outcomes are utilised for the validation of the simulation results.

6.1. Prototype design of the all-optical configuration of a differential protection scheme

The proposed all-optical busbar differential protection scheme is a series arrangement of optical components that consist of two polarisers, two optical current sensors (Faraday rotation current sensor, FRCS) and optical fibre (FO), as depicted in Figure 6.1 [1]. Several optical components with specific characteristics have to be prepared to create a prototype of the proposed all-optical busbar differential protection configuration. There are two possible options for these optical components, either available or not available in the market.
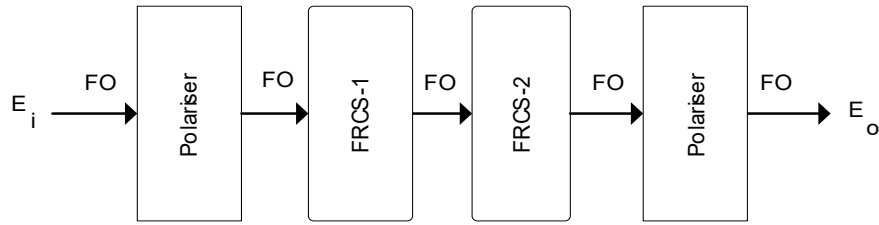
Figure 6.1 A series arrangement of optical components in the proposed all-optical differential busbar protection scheme.

For the optical components that are available on the market, a selection process which consists of several steps, i.e. detailing component specification, gathering price information, and decision making are needed. Some optical components of the proposed all-optical busbar differential protection scheme, i.e. polariser and fibre optic, including connection types, are available on the market.

In contrast, for the optical components that are not readily available on the market, it should be created/custom made. Thus, the five steps effort in the design process including (1) system specification, (2) preliminary design, (3) detailed design, (4) prototype, and (5) testing will be conducted to realise the component [2],[3],[4]. For example, the FRCSs are not available on the market. Therefore, the FRCS prototype must be designed and developed either in the EEE laboratory or requested to a manufacturer to prepare it.

The wavelength that will be used for the protection prototype is 1550 nm. There are several reasons for this chosen wavelength. Firstly, it is due to the absorption characteristics of the glass material used in fibre optic. For short wavelengths region, Rayleigh scattering of non-homogeneities becomes essential. Towards the UV wavelengths region, electronic absorption starts to take effect. For a larger wavelengths region, infrared absorption starts to increase. Secondly, the loss of any optical fibres is minimum (0.2dB/km) at the wavelength 1550 nm. Thirdly, eye safety and compatibility with the current and future all-optical networks for the next generation [5]. Another reason is based on available equipment at the Advanced Sensor Laboratory within the EEE department.

The required components for developing the protection prototype are:

a. FRCS
b. Fibre bench and polarisation kit
c. The light source, photodetector and PXI for a real-time data acquisition and processing unit. The PXI (Peripheral component interconnect extensions for instrumentation) is a modular electronic instrumentation platform. This platform is used as a basis for building electronic test equipment, automation systems and modular laboratory instruments. PXI is based on industry-standard computer buses. PXI modules providing the instrument functions are plugged into a PXI chassis which may include its controller and running with a standard operating system such as Windows.

The design and selection process for each component of the proposed all-optical configuration of the busbar differential protection scheme will be described in the following sections.

6.1.1. Faraday rotation current sensor (FRCS) design and the prototype developing process

The FRCS consist of two components which are a Faraday rotator and a coil, as shown in Figure 6.2.
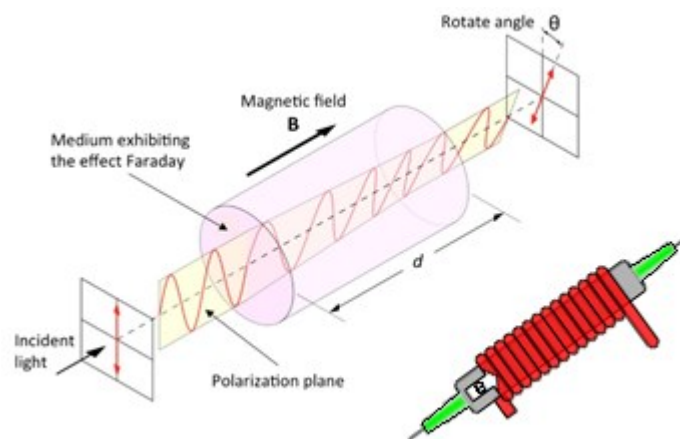
Figure 6.2 Principle of the Faraday Effect in an optical medium with a magnetic field (above), FRCS preliminary design (below)

Due to the unique specifications and unavailability of the FRCS on the market, it is essential to be noted that the FRCS needs to be built. Some factors should be carefully considered in the FRCS design such as optical material, wavelength, collimator, non-magnetic frame, and also connection types. Therefore, the step by step design process will be implemented to realize the Faraday rotators and coils for the laboratory experimentation purposes.

6.1.1.1. FRCS specifications

Since the FRCS consists of two components, i.e. Faraday rotator and coil, the specification of these components will be detailed in separate tables. Overall specifications of the Faraday rotator for the required FRCS is described in Table 6-1.

Table 6-1 Faraday rotator specifications

• Faraday rotator medium	:	Terbium gallium garnet (TGG) [6]
• Wavelength	:	1550 nm
• Power	:	Less than 100 mW
• Incident light orientation	:	Normal (perpendicular) to the TGG surface [7]
• Input type	:	Fibre type
• Fibre connection type	:	Ferrule connector / physical contact (FC/PC) or Ferrule connector / angle-polished connector (FC/APC)
• Fibre type	:	Single-mode fibre (SMF) or polarization-maintaining fibre (PMF) with maximum length of 1 metre
• Output type	:	Fibre type
• Fibre connection type	:	FC/PC or FC/APC
• Fibre type	:	SM or PM (max. 1 meter length)
• Housing type	:	Non-magnetic material

As a guidance for next step design process which is preliminary design, the Faraday rotator design could be depicted in Figure 6.3
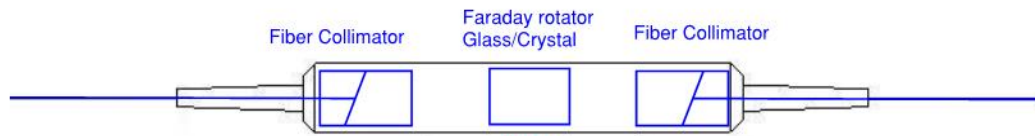
Figure 6.3 Faraday rotator in the first step design

Together with Faraday rotator, a current coil is needed as a magnetic field source. The coil requirements are relatively simple, and it can be implemented as a coiled wire in a symmetrical cylindrical shape that has ampere rating (current carrying capacity) of 10 A. The coil specifications are listed in Table 6-2.

Table 6-2 Coil specifications

• Number of turn	:	150 (coil-1) and 400 (coil-2)
• Wire material	:	Copper (Cu), 1 mm^2
• Shape	:	tubular form
• Inner diameter	:	10 mm
• Coil length	:	40 mm

Due to the simplicity of the coil design and availability of the wire and toolset, these coils were built in the Advanced Sensor Laboratory. The final coil design is shown in Figure 6.4.
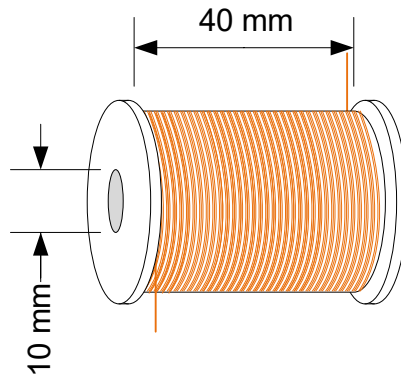
Figure 6.4 A final coil design

6.1.1.2. FRCS preliminary design

The Faraday rotator preliminary design is built according to the available TGG dimension on the market which had diameter (Ø) of 2.8 mm and length of 14 mm. As the measured currents in the laboratory experiments are relatively small (in the region of 5 A), a minimum length of 20 mm of the TGG is required to achieve a sufficient rotation signal. Therefore, a series arrangement of two TGGs is required inside one FRCS, as shown in Figure 6.5.
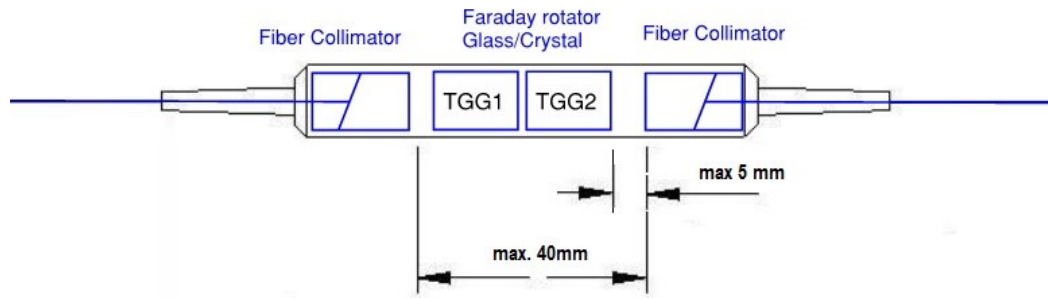
a.   Two dimensions (2D) drawing
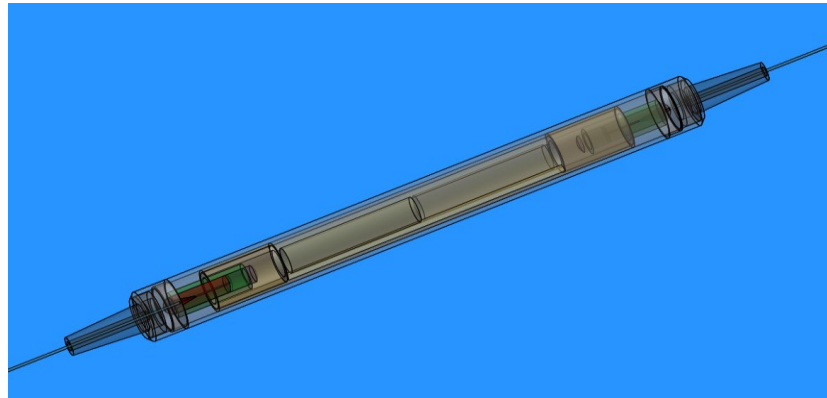
b.   Isometric view (3D drawing)

Figure 6.5 Faraday rotator in the preliminary design

6.1.1.3. FRCS detailed design

Detailed engineering design of the Faraday rotator as presented in Figure 6.6 is needed for sensor prototype developing step. Some details have been updated, such as connector type using FC/APC, single-mode (SM) fibre optic, and collimator type. Two identical FRCS prototypes are needed for the proposed configuration of the all-optical protection scheme.
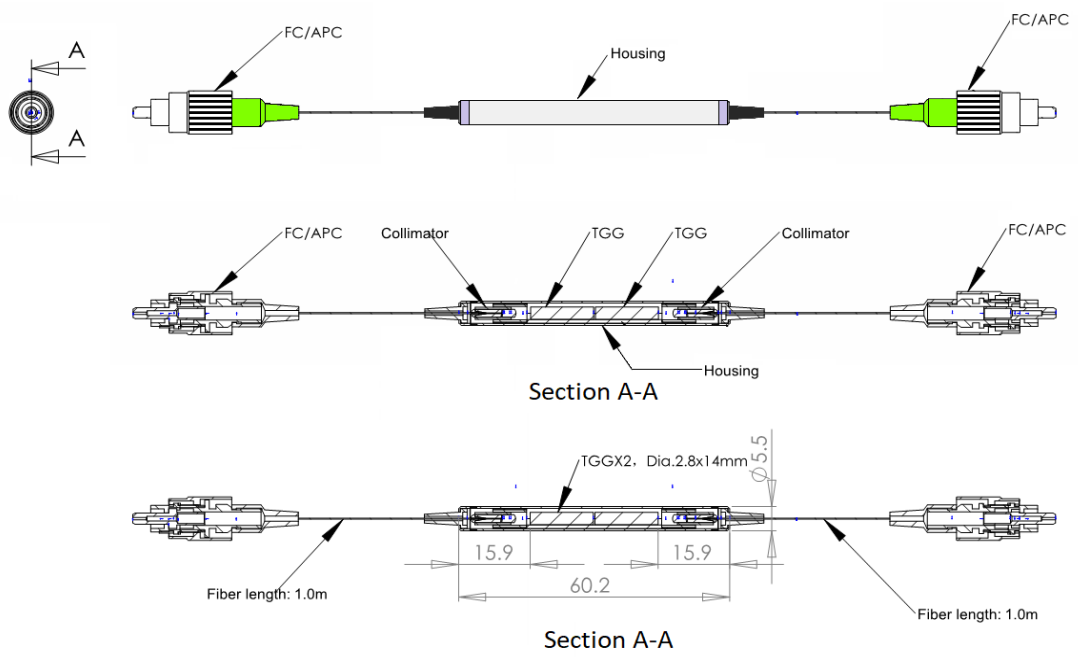
Figure 6.6 Detailed engineering design of the Faraday rotator

An isometric view of the Faraday rotator in Figure 6.7 in conjunction with detailed engineering design could help operators in the constructing step of the Faraday rotator prototype.

Figure 6.7 An isometric view of the Faraday rotator

6.1.1.4. Prototype of FRCS

In total, two sets of the Faraday rotator prototype are used in the experiment, including optical fibre cable (1 metre for each collimator), and connectors, as shown in Figure 6.8. As mentioned earlier, these Faraday rotators are custom made based on the above specifications.
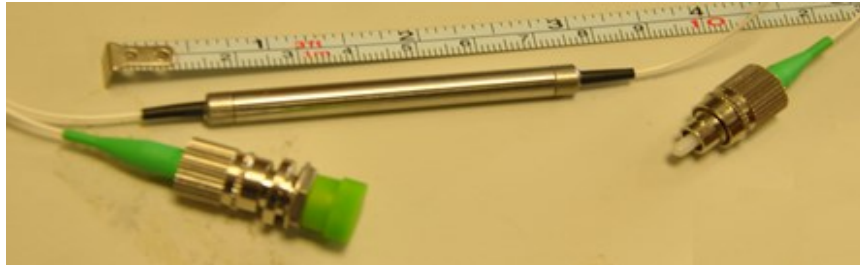
Figure 6.8 An isometric view of the Faraday rotator

An actual FRCS prototype is the Faraday rotator prototype that is symmetrically located in the centre of the coil as depicted in Figure 6.9.

a. Design
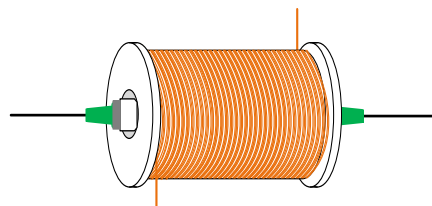
b. Prototype
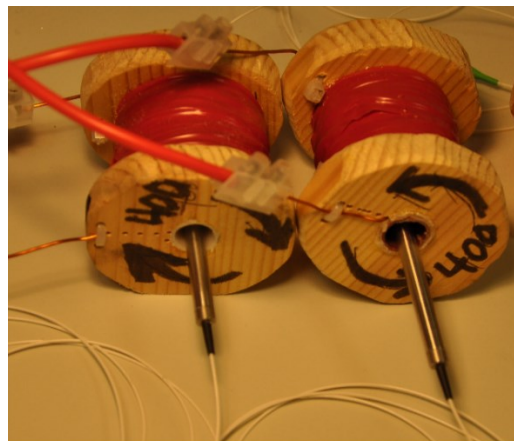
Figure 6.9 A set of FRCS: a. design, b. prototype

6.1.1.5. FRCS testing

Testing of FRCS as the final step of the design process will be discussed in section 6.3. (Laboratory experiment).

6.1.2. Fibre bench and polarization modules selection

The polarisers application for the proposed all-optical differential busbar protection scheme requires higher flexibilities in rotation and position adjustments. It is also intended to facilitate the insertion of a polariser. Therefore, it is vital to utilise a fibre bench and polarization kit. The fibre bench and polarization kit consist of:

1. Fibre bench
2. Collimator
3. Optic mounts
4. Polariser

Based on several considerations and technical requirements, it was decided to use the fibre bench and polarization modules made by Thorlabs Inc. [8].

6.1.2.1. Fibre bench, collimator, and optic mounts

There are two fibre benches that are used in the proposed optical protection scheme. The first fibre bench is a fixed fibre to fibre U-bench (part number FBC-1550-APC) that is a complete unit with wall plate mounts, collimators, and a single mode fibre with FC/APC connectors as shown in Figure 6.10 [9].

Figure 6.10 Fixed fibre to fibre U-bench (FBC-1550-APC)

The second fibre bench utilised in the proposed optical protection scheme is a single axis fibre bench (part number FB-51) [10]. This fibre bench is simple and has to be combined with pigtailed GRIN collimators (part number 50-1550A-APC), optical mounts (FT-SM05) and adapter (SM05PT) to have a similar function to the first fibre bench [11],[12]. This arrangement can be seen in Figure 6.11 (one side is shown only). The complete arrangement, including polarisers, is displayed in Figure 6.13.

Figure 6.11 An arrangement of single-axis fibre bench, wall mount, adapter and collimator

6.1.2.2. Optical polariser

The optical polarisers for the proposed all-optical configuration are from Thorlabs. This polarisers type are the fibre bench rotating linear polariser modules (FBR-LPNIR), as seen in Figure 6.12 [13]. These polarisers utilise a thin layer of sodium-silicate glass. The polariser module absorbs light that is not aligned to the transmission axis of the polariser and is also designed for the wavelength range of 650 - 2000 nm.

Figure 6.12 A rotating linear polariser module

A complete arrangement of the polarisers on both of the two fibre benches is displayed in Figure 6.13. In this figure, two different benches were used due to these benches had available in the laboratory.
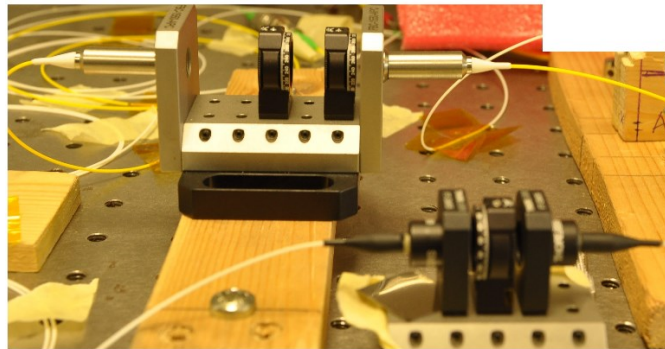
Figure 6.13 The complete arrangement of polarisers on the fibre benches

6.1.3. Light source, photodetector and PXI real-time processing platform

Optical components such laser beam source, photodetector and PXI are also required to support operation of the proposed all-optical configuration of the busbar differential protection scheme. These devices were available in the Advanced Sensor Laboratory.

A light beam source is a benchtop unit that has an integrated super-luminescent diode (SLD) with emission centred at 1550 nm manufactured by Thorlabs [8]. Other features of this unit are the availability of the SLD output power adjustment and temperature controller. This unit is displayed in Figure 6.14.
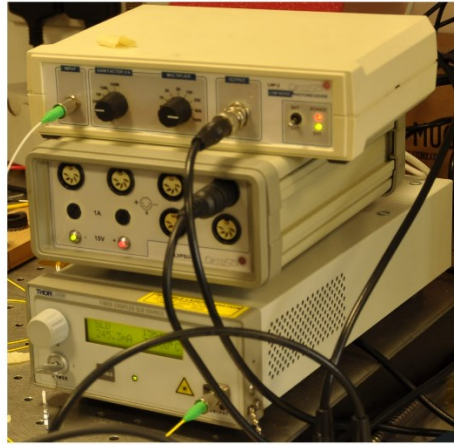
Figure 6.14 A laser beam source (**bottom**) and a photodetector (**top**) with a power supply unit (**middle**)

A photodetector (photo-receiver) is utilized to detect the power level of the light modulation output from the all-optical configuration. The photodetector that is available in the Advanced Sensor Laboratory is a low noise photo-receiver LNP-2, as shown in Figure 6.14 [14]. It has a high gain and low noise equivalent power (NEP) that provides very high sensitivity front-end for an optical system. Therefore, it is suitable for use in the proposed configuration of the all-optical busbar differential protection scheme that has very low power modulations.

PXI is a PC-based generic platform for laboratory prototyping, manufacturing, industrial testing, measurement and monitoring of automation systems. Due to high performance, it is suitable for applications that require rapid access to hardware and data. The available PXI unit (Figure 6.15) is NI PXI-8106 which is combined with a multifunction IO module (PXI-6259) and chassis (PXI-1031) manufactured by National Instruments [15]. The PXI is operated by systems engineering software LabVIEW [16]. In this work, the PXI is utilised as a processing unit for the prototyping and testing of the all-optical differential protection scheme.
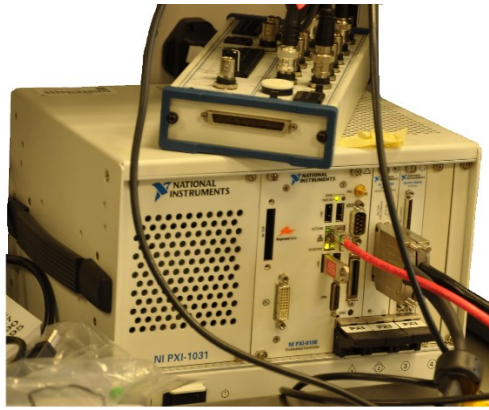
Figure 6.15 The PXI for data acquisition

6.2. Configuration of the proposed all-optical differential protection scheme

The prototype configuration of the all-optical differential protection scheme is a combination of several devices such as a light beam source, detector and PXI. A complete optical configuration of the scheme is depicted in Figure 6.16.
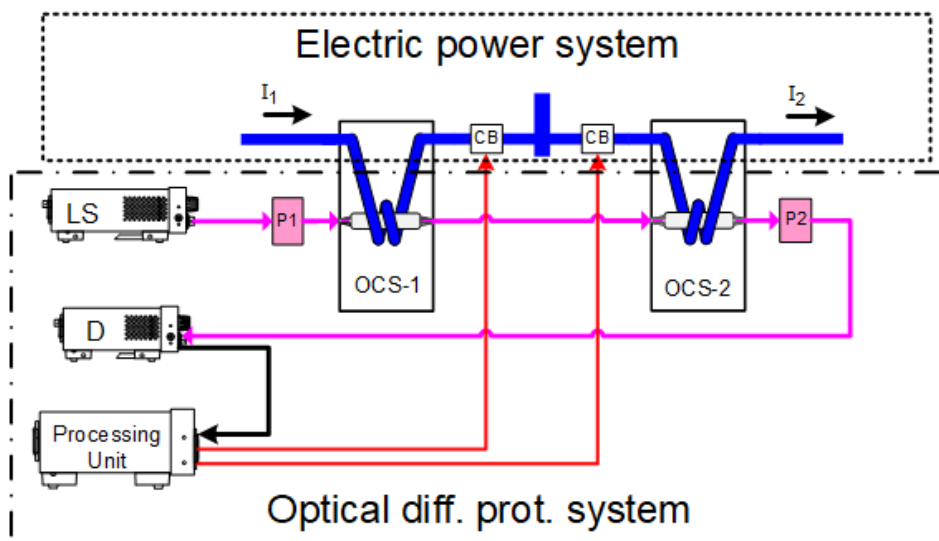
Figure 6.16 The proposed configuration of all-optical differential protection scheme

6.3. Laboratory experiment

6.3.1. The experiment set up and tools

To conduct a laboratory experiment of the all-optical busbar differential protection scheme, two fault conditions which are internal and external faults have to be physically replicated using APTS protection relay test set.

Due to difficulties of implementing these two simulated fault currents into the experiment circuitry in Figure 6.16, it was decided to configure two different circuits for injecting the replica fault current. One circuit is for representing the internal fault conditions, as shown in Figure 6.17a, and the other is for emulating the external fault conditions during the experiment (Figure 6.17b).
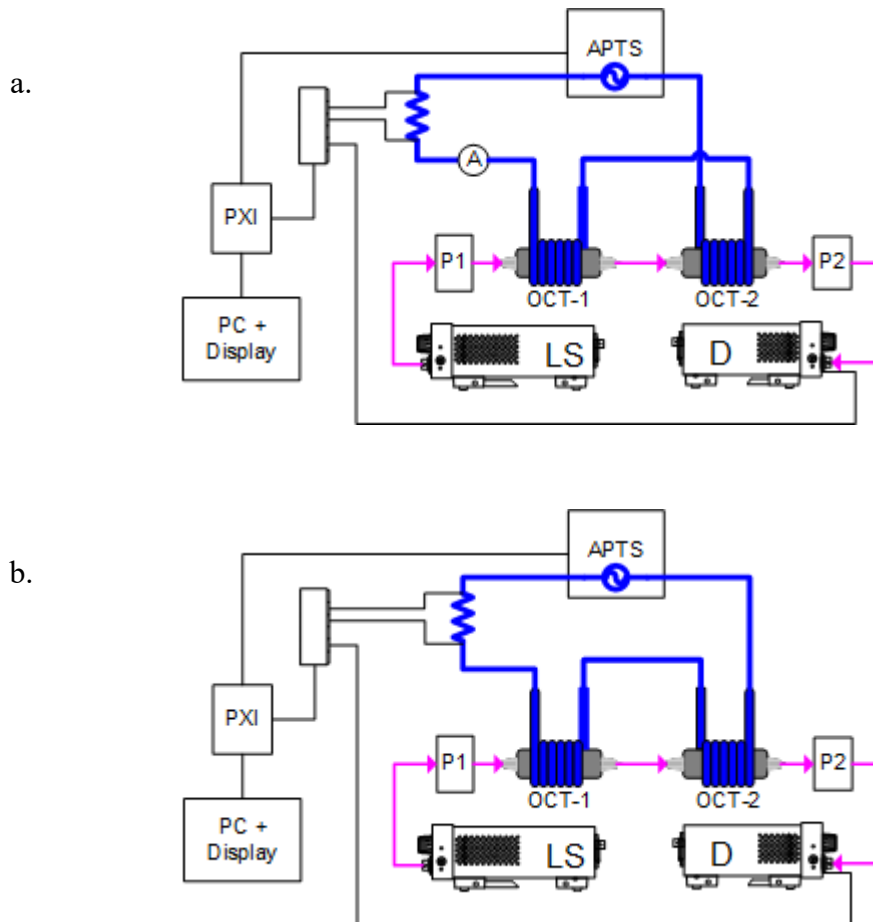
Figure 6.17 The experiment circuitry for investigating: a. the simulated internal fault, and b. the simulated external fault.

Based on these figures, besides devices in the proposed configuration of the all-optical busbar differential protection scheme, several additional equipments are needed to conduct experiments for testing of the proposed protection scheme configuration. These equipment are:

1. APTS protection relay test set [17],[18] including analogue current amplifier
2. Standard resistor 0.1 Ohm, 22 Ampere
3. Personal computer (PC)

6.3.2. Experiment results

6.3.2.1. Results for the internal fault

After setting up all devices and equipment, the experiment was conducted in several stages as follows.

First stage, the investigation is started with internal fault condition, and the circuitry is set up by following Figure 6.17 (a). The light source is adjusted to provide a power output around 1 mW, and the APTS current output is set to 1 A or 5A. When the injected current from the APTS is 1 A, it could give 400 ampere-turns when using a coil with 400 turns or 150 ampere-turns for 150 turns of coil in the circuit. When the injected current is increased to 5 A, it means the circuit is equivalent to 2000 ampere-turns for the coil of 400 turns.

The second stage, both polariser and analyser should be adjusted in order to get cross-polarization. The angle of cross-polarization is theoretically 90 degrees between polariser and analyser. In the first effort of the experiment, the polariser is adjusted to 0 degrees and analyser is fixed at 90 degrees. When the current differential is zero, the modulated power level should also be zero. On the contrary, when the current differential is not zero, the modulated power level should exist and should be easily detectable. However, with the existing laboratory set up of polariser and analyser it was not possible to achieve a near-zero power output modulation on the photo-detector (photo-receiver).

Due to the fact that polariser was placed on the fixed fibre to fibre U-bench and analyser was on a single axis fibre bench, it was preferable to perform fine adjustments

of the polariser experimentally in order to obtain the angle of cross-polarization. As a result, the cross-polarization angle is achieved when the polariser angle is at 32 degrees and the analyser, which is fixed at 90 degrees. This result gives evidence that the birefringence effect in the optical fibre does exist.

The proof of the existence of birefringence in the optical fibre can also be explained as follows.

Both the polariser and analyser are placed on the same fixed U-bench with cross-polarization angle 90 degrees and spacing between them is greater than 10 mm (refer to Figure 6.18). The similar results (i.e. non-zero power modulation) are obtained even when there is no current flow in the circuit. However, when the spacing between polariser and analyser is less than 10 mm, the power modulation extinction occurs. Therefore, this fact could also be used to justify that the optical models which utilize birefringence model in the simulation are valid.

Figure 6.18 The experiment setup for investigating the simulated internal fault.

Due to the fact that birefringence consists of two components which are linear and circular birefringences, it is difficult to investigate these components independently by only using this experimental setup.

The third stage, when the cross-polarization angle has been obtained in the previous stage, the experiment is conducted for determining the power modulation output by increasing the injected simulated current for the internal fault condition. This experiment should be very carefully conducted because the fibre optic links are very sensitive to vibration, which could disturb the measurement of modulation signal output.

In this experiment, the Faraday rotators are combined with a coil of 400 turns in order to perform a functionality of an optical current sensors (FRCS). The laser source generates wavelength of 1550 nm with power level of around 1 mW. When the photodetector's trans-impedance gain (gain factor) of $1x10^8$ V/A and additional gain stage (multiplier) of 20 have been selected, the signal modulation data for the simulated internal fault were collected utilising the PXI unit. The data are depicted in Figure 6.19.
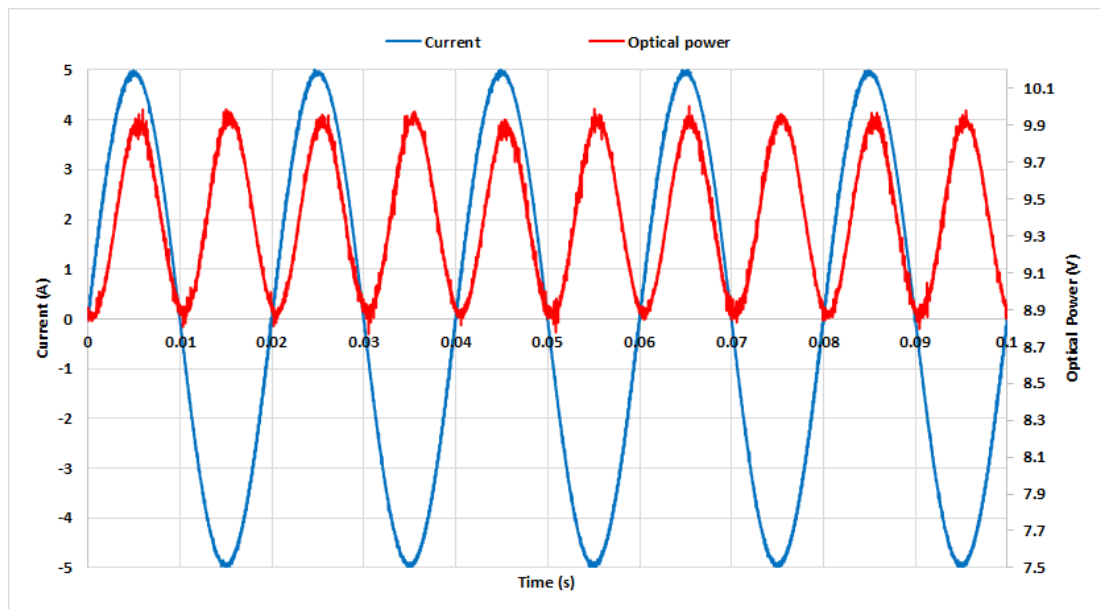
Figure 6.19 Experiment result for investigating the simulated internal fault.

It is seen from Figure 6.19 that frequency of the modulation signal is 100 Hz, whereas the AC frequency is 50 Hz. It means that the frequency of the modulation signal is twice the AC frequency. This result had been predicted on the simulation in chapter 5.

Another significant finding, the optical power modulation signal is delayed by a few milliseconds relating to the AC plot. It means that there is "a time lag" in the optical power modulation signal. This "time lag" will be discussed in more details on section 6.4.1.

Using a spreadsheet programme, i.e. MS Excel, the maximum, minimum and average value of the signal modulation outputs are obtained from experimental data as 10.00 V, 8.77 V, and 9.41 V, respectively. Since the output values of the optical signal modulation at the photodetector is in voltage unit (volt, V), these values should be converted to the power unit, i.e. watt (W).

The photodetector output can be converted from volt to watt by following two calculation procedures. These calculation procedures are by the Ohm's Law and the photodetector's responsivity at a given wavelength. The power level of light incident at the LNP-2's photo-receiver (which is the active area of the photodetector) can be derived using an example of the average value of the signal modulation output as follows:

The generated current due to the receiving photon at the LNP-2's active area is

$$I = \frac{9.41 \text{ V}}{2x10^9 \text{ V}/\text{A}} = 4.71 \ x \ 10^{-9} \text{ A}$$

Then, this current is converted into watt using the corresponding responsivity value of the LNP-2. The photodetector responsivity of the LNP-2 at 1550 nm is 0.95 A/W, which is based on the datasheets of the responsivity curve contained in the Indium Gallium Arsenide Photodetector's (InGaAs photodetector) [19]. Therefore, the incident power at photodetector can be calculated as:

$$\text{calculated incident power} = \frac{4.71 \ x \ 10^{-9} \text{ A}}{0.95 \text{ A}/\text{W}} = 4.95 \ x \ 10^{-9} \text{ W}$$

calculated incident power = 4.95 nW

Hence, the converted power level, the value of 9.41 V at LNP-2 photodetector as the average value of optical power output is equivalent to 4.95 nW.

It is worth mentioning that this value is the amount of incident power on the photo-receiver, not necessarily the actual power of the beam as not all of the beam may be falling on the photo-receiver (photodetector).

Using a similar method, the converted optical power modulation from volts to the power level in watts can be displayed in Figure 6.20.
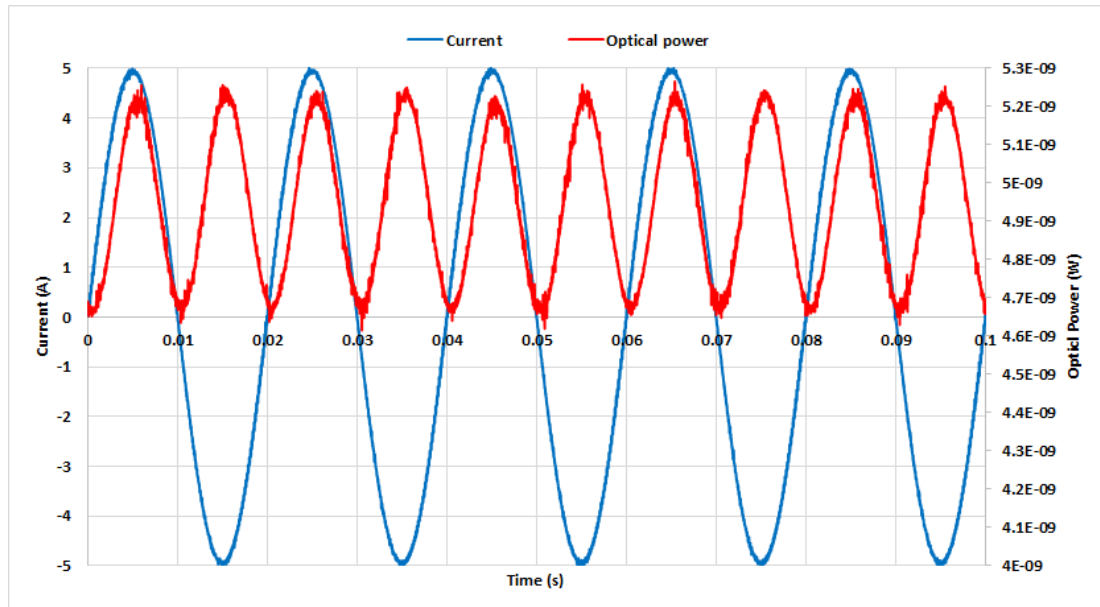
Figure 6.20 The converted optical power modulation for the simulated internal fault.

6.3.2.2. Results for the external fault

In general, the same procedures were applied to investigate the external fault experiment, but the current circuit had to be reconfigured according to Figure 6.17 (b) to emulate the external fault condition. Again, it is essential to be mentioned that changing the circuit has to be done very carefully to maintain the optical link in the same position as in the previous experiment.

The external fault experiment was conducted using the same laser source, which has the wavelength of 1550 nm and the power level at one mW. The signal modulation data for the simulated external fault were collected using the PXI unit. The experiment data had recorded using the trans-impedance gain of $1x10^8$ V/A and the multiplier gain of 200 as depicted in Figure 6.21. Using a spreadsheet programme, the average of signal modulation output is at the level of 0.06 V.
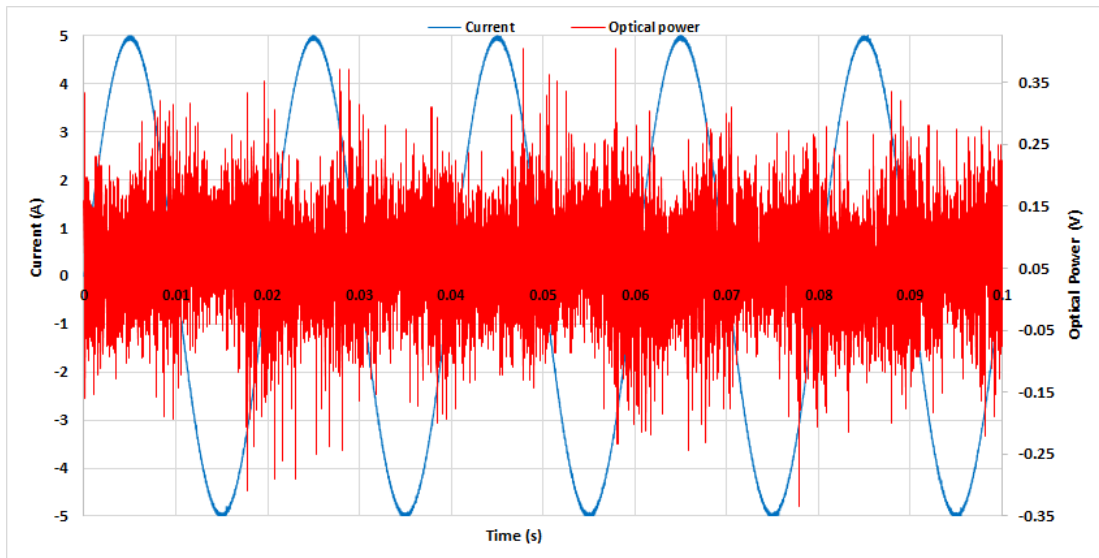
Figure 6.21 Experiment result for investigating the simulated external fault.

Conversion of the average signal modulation output 0.06 V can be conducted using a similar conversion procedure as previous. The generated current due to the receiving photon at the LNP-2's active area is

$$I = \frac{0.06 \text{ V}}{2x10^{10} \text{ V}/_\text{A}} = 3.0 \ x \ 10^{-12} \text{ A}$$

Based on the responsivity curve contained in the InGaAs Photodetector datasheet, the responsivity of the LNP-2 at 1550 nm is 0.95 A/W [19]. Therefore, the incident power at photodetector can be calculated as:

$$\text{calculated incident power} = \frac{3.0x10^{-12} \text{ A}}{0.95 \ ^\text{A}/_\text{W}} = 3.1579 \ x \ 10^{-12} \text{ W}$$

Thus, the calculated incident power is 3.158 pW, or equivalent to 0.003158 nW. As a result of the converted power level, the value 0.06 V at LNP-2 photodetector is equivalent to 0.003158 nW.

Using the similar procedure, the converted signal modulation from volts to power level in watts can be displayed in Figure 6.22.

227
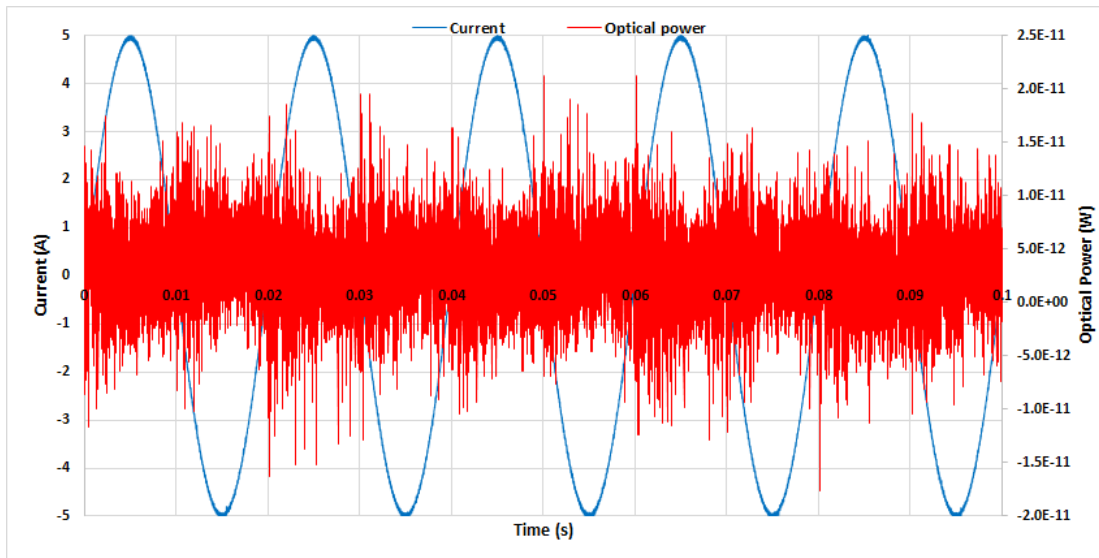
Figure 6.22 The converted optical power modulation for the simulated external fault.

It is seen in this figure that it is challenging to determine the frequency and the time lag of the modulation signal. Therefore, a clear conclusion is also difficult to be made.

6.3.2.3. Summary of the experiment results

The key findings from the laboratory experiments are:

a) Existence of the birefringence
b) Frequency of the optical modulation signal being twice that of the AC current frequency
c) The maximum, minimum and average value of the optical power modulation.
d) "Time lag" in the optical modulation.

6.4. Validation of the simulation model using empirical data

Although the prototypes have been designed and constructed that comply with the specifications and requirements, it is required to pass a validation process.

Predictive validation [20] is a method that could be used to validate simulation models. The system's data may come from an operational system or be obtained by conducting experiments on the system, e.g., laboratory tests. In general, the experiments are

performed to obtain high-quality data in order to improve fundamental understanding of physical behaviour, to improve mathematical models, to estimate values of model parameters, and to assess component or system performance.

The common test for the validity of a simulation is established by comparing to the actual system data. The simulation data are collected from the computer simulations, whereas the actual system data are collected from the laboratory experiments. The two sets of data are compared in order to obtain a validation result. The simulation models are considered "valid" if the output data of the simulation closely resembles the output data from the actual system. The degree of the commonality between the actual and the proposed optical system configuration can be used as the degree of confidence in the model of the proposed configuration. Thus, the greater commonality means the greater confidence.

According to the experiment data, the existence of birefringence can be utilised for validating the simulation models. The simulation type I and II cannot pass on the validation step because these simulation models do not have birefringence representation in their optical fibre models.

Moreover, the simulation type VI also cannot go to the validation step because the simulation type VI contains a PM optical fibre model in its representation. In contrast, the non-PM optical fibre sections had used in the experiment that is contradicted to these simulation models.

Furthermore, the simulation type III also cannot reach the validation step because this simulation model gives the same results with the simulation type VI for both internal and external faults. These results indicate that simulation type III may contain the same representation with the simulation type VI but it is in a simple way. Therefore, the simulation type III could be assumed that it has the PM optical fibre model in its representation that prevents this model goes to the validation step.

As for the simulation type IV and V could go to the validation step because both simulation models have the same representation in their models which uses the non-PM optical fibre model. These simulation models are fitted to the experiment setup that had used several sections of the non-PM optical fibre. The difference between the

simulation type IV and V is only on the angle of q. The simulation type IV is designed for the angle of q that is equal to zero degree, whereas the simulation type V is for q other than zero degree.

6.4.1. Validation of the simulation type IV and V for internal fault using the experiment data

Due to the experiment was conducted using several sections of the non-PM optical fibre, the experiment's data are related to the simulation type IV and V. Therefore, both results of the experimental and the simulation models are compared to validate the model of the proposed all-optical differential protection configuration.

For validation, a simulation model of the proposed all-optical protection scheme was conducted using simulation type V, where the parameters were substituted according to the experimental data. The main parameter is the fault current. The fault current, which is the differential current, in this case, is set to have the same magnitude to the one in the laboratory experiment. Since the amount of current in the FRCS is 2000 ampere-turns which is equivalent to the injected current of 5 A at the coil of 400 turns, the power system model have to be tuned in order to provide a current flow of 2000 ampere-turns in the FRCS model. This could be achieved by a fault simulation with fault resistance of 37.2 Ω.

Other parameters in the laboratory testing stage such as fibre bench insertion loss, refractive index of optical media, temperature, optical fibre attenuation, length of optical fibre are taken into account in the simulation for validation purposes. The first fibre bench insertion loss is 0.97 dB (equivalent to power ratio of 80 percent) and the second fibre bench insertion loss is 7.7 dB (equivalent to power ratio of 17 percent).

Several comparative results of the laboratory experiment and the simulation type V for the internal fault using these parameters are explained as follows.

Firstly, the comparison results confirm that the experiment results (refer to Figure 6.20) and the simulation type V (refer to Figure 6.23) produce the same result in terms of the frequency of modulation signal. The result shows that the frequency of the

optically modulated signal is twice the AC frequency. This result also conforms to the Malus law, which used a set of polariser and analyser to prove his theorem.
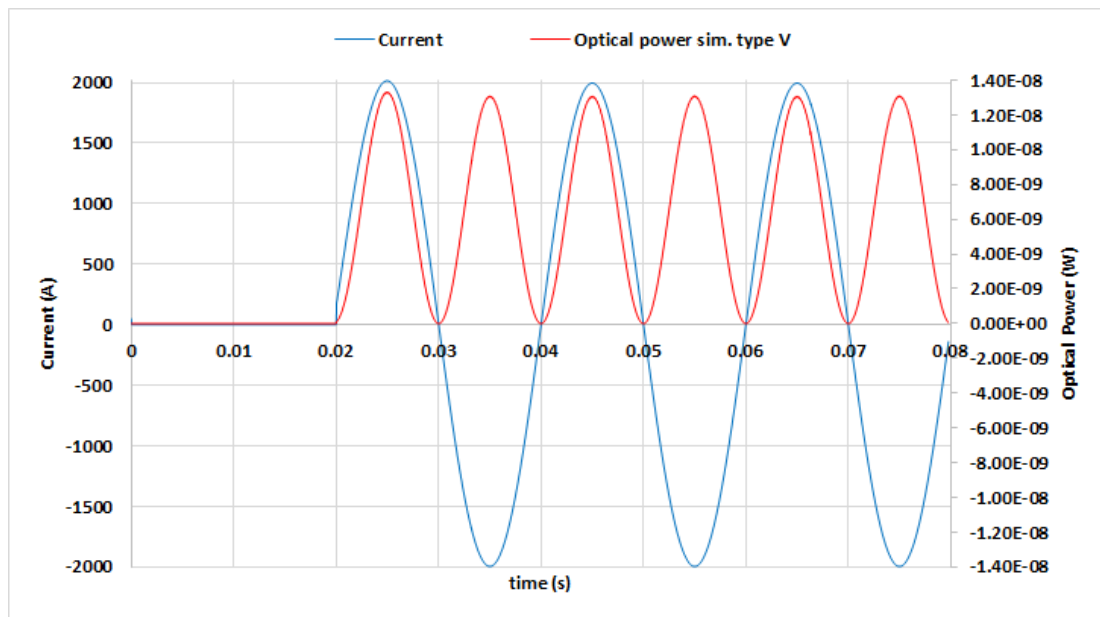
Figure 6.23 The simulation type V for the resistive internal fault of 37.2 Ω

Secondly, it can be seen from Figure 6.24 that, in general, both the laboratory experiment plot (refer to Figure 6.20) and the simulation plot (refer to Figure 6.23) has a similar shape of the optical power modulations for internal fault. In this figure, it is also provided with a small square window for zooming view that will be used in Figure 6.27 in the following paragraph.
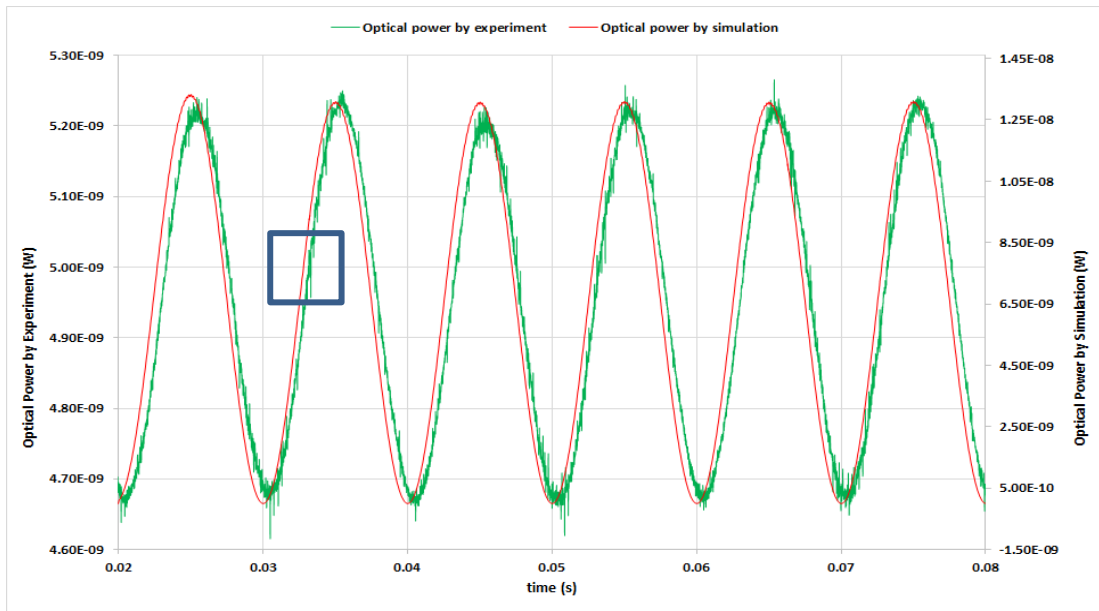
Figure 6.24 Comparison of the signal modulation shape and level between the simulation type V and the laboratory experiment for the internal fault.

Moreover, it is seen from Figure 6.25 that the optical power modulation of the simulation has oscillated between a minimum value ($1.48x10^{-13}$ W) and a maximum amount ($1.33x10^{-8}$ W). The experiment plot also shows the same oscillation in optical power but different in the magnitude. The experiment data spread in the interval $4.62x10^{-9}$ W (the minimum value) to $5.27x10^{-9}$ W (the maximum amount).

Furthermore, the root mean square error (RMSE) could be used as a dissimilarity index in order to quantify how different (dissimilarity) a set of the simulation values to the experiment values. The smaller a RMSE value means the closer simulation values to the experimental values and vice versa. Thus the RMSE value is a dissimilarity index between the simulated values and the experimental values.

After the RMSE calculation, the dissimilarity index of the optical modulation signals between the simulation and the experiment value is $4.73x10^{-9}$. The dissimilarity index for the average value of optical power modulation level between the simulation and the experiment is $1.61x10^{-9}$.
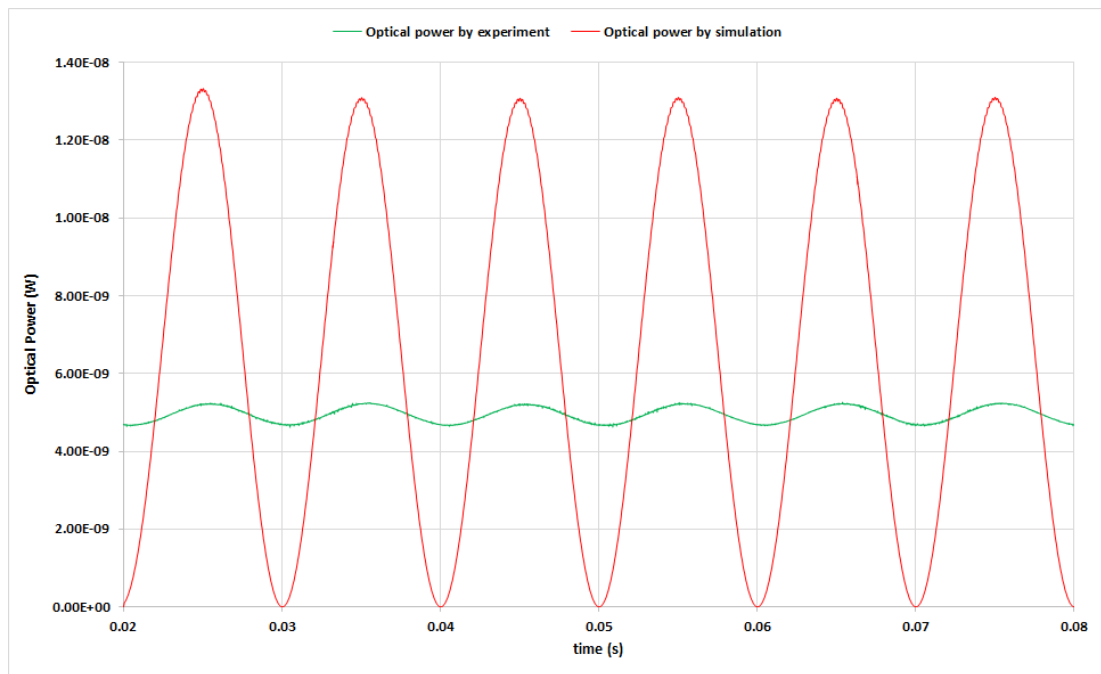
Figure 6.25 Comparison of the optical power modulation level between the simulation type V and the laboratory experiment for the simulated internal fault.

Thirdly, the optical power modulation for internal fault is different in terms of the maximum and minimum of optical power level, as shown in Figure 6.25. However, the average optical power level is approximately the same which the average power level of the modulation signal of the laboratory experiment and the simulation type V are $4.95x10^{-9}$ W and $6.57x10^{-9}$ W, respectively. It means there is a difference in the power level around $1.61x10^{-9}$ W, which is similar to the dissimilarity index (RSME) of the average value of optical power modulation. Two causative factors may generate this difference value. The first causative factor is from the second fibre bench type (refer to Figure 6.11) that is prone to misalignment, and it can cause an increase in the insertion loss. This insertion loss may not precisely be represented in the simulation due to the change of insertion losses at the experiment, and the insertion loss was only measured at the first time of the tests. Another causative factor, it may be triggered by some amount of the beam that does not fall on the photo-receiver (photodetector).

Fourthly, both current and optical power modulation data of the laboratory experiment were collected in voltage quantities (volts) and using time synchronisation in the PXI.

233

However, it is seen that the optical power modulation signal for the internal fault is delayed by a few milliseconds to the AC plot as in Figure 6.26.
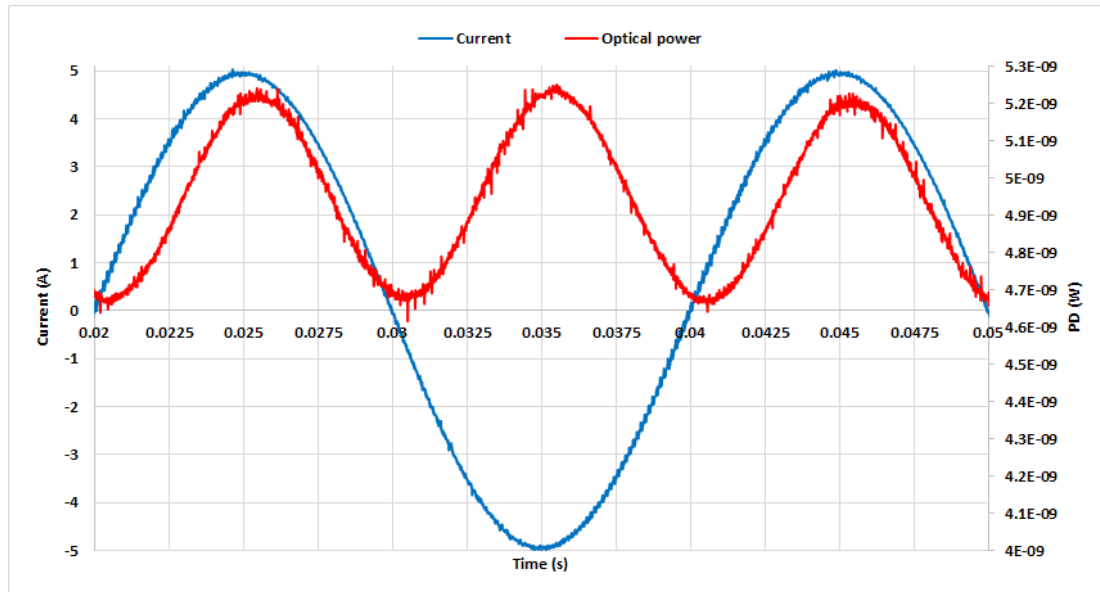
Figure 6.26 Experiment results: the optical power modulation and the internal fault.

In this figure, there is "a time lag" on the optical power modulation of the experiment. This "time lag" is real and caused by three consecutive processing times which are photon-receiving, converting the photon to the generated photocurrent and converting the generated photocurrent into voltage (in volts). Therefore, this "time lag" is a duration of the optical conversion time of the polarized light modulation into the optical power. Thus, it is reasonable when the duration of this processing time is longer than the duration of direct measurement of AC voltage by PXI due to the flowing AC current from the APTS circuitry.

Although the two sets of data (simulation and experiment) did not be collected at the same time, both the simulation and experiment have AC current data and the corresponding optical power data. Both the data could be plotted against a time axis, and this time axis could be used as a standard time frame. Since both simulation and experiment have the same AC current data, therefore the intended optical power plot (Figure 6.24) is obtained by superimposing both AC current data (AC plots) on the

same axis. Using this approach, a simple way to identify the duration of the optical conversion time, which is started from optical modulation to optical power, is by calculating a horizontal distance between the simulated optical power and experimental optical power. The result of superimposing the experiment plot (Figure 6.20) and the simulation plot (Figure 6.23) with zooming view at a small window (0.032-0.034 s) as shown in Figure 6.27.
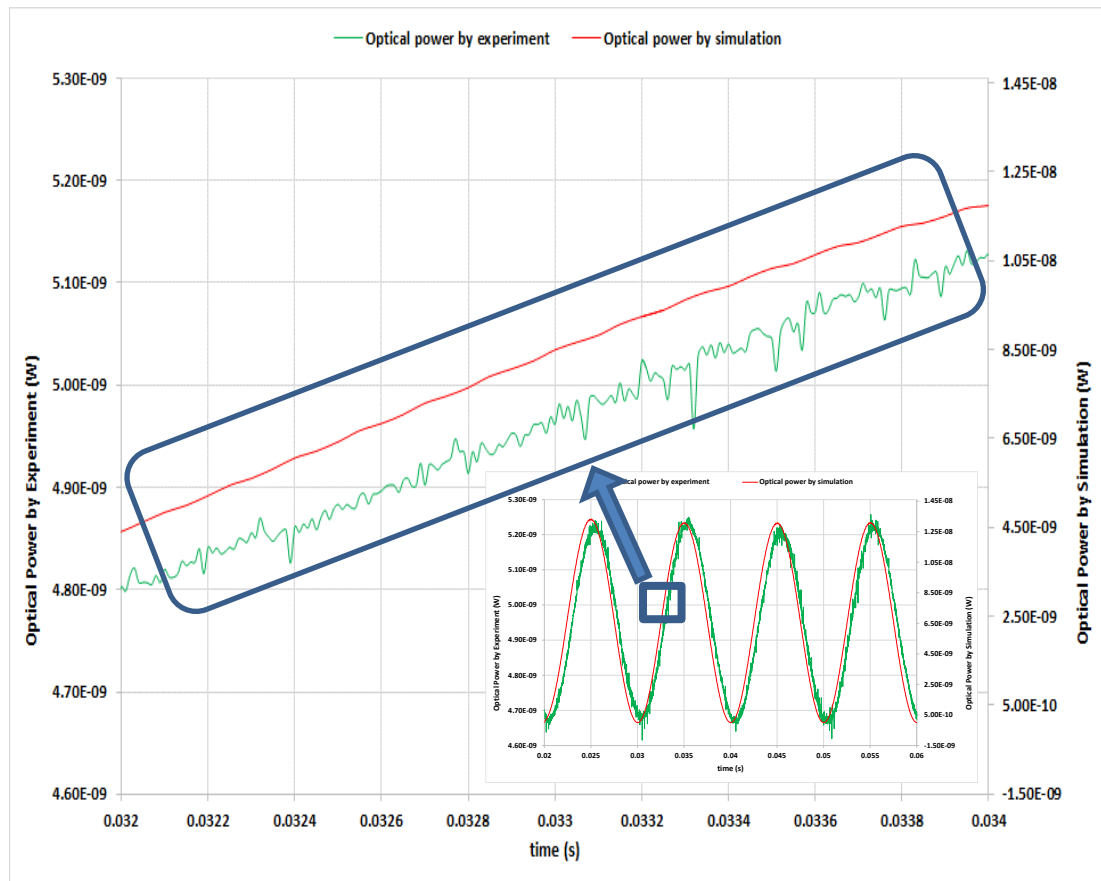
Figure 6.27 Time lag of the optical power modulation between the simulation type V and the laboratory experiment for the internal fault (zooming view of Figure 6.24).

This approach may not be entirely appropriate in determining the time duration of the optical conversion processes. However, this approach could be beneficial in estimating the time duration of the optical conversion processes. The estimated time of the optical conversion processes, in this case, is approximate $4.0x10^{-4}$ seconds (0.40 ms) by

calculating the horizontal difference between the two plots in Figure 6.27. Thus, the five consecutive processing times of the optical modulation is $4.0x10^{-4}$.

The time duration of the optical conversion processes from the first process to the fifth process as explained in section 4.2.1 is a part of the total operation time of the optical protection scheme. Therefore, this time duration would be used for determining the optical protection operation time when it will be implemented in the power system. An illustration is provided to describe the optical protection operation time for this purpose. If the proposed optical protection scheme utilises the non-PM optical fibre length of 460 m, the optical differential processing time is approximately 2.36 μs. Then, the time duration of optical conversion processes is 0.4 ms. Thus, the estimated total operation time of the proposed optical protection scheme is $4.0236x10^{-4}$ seconds (or approximately equivalent to 0.402 ms). This entire operation time is very fast when it compares to other relay manufacturer's data which is around 2 ms [21-24].

As for the comparison of the laboratory experiment and the simulation type IV for the internal fault, the results are approximately similar with the simulation type V as tabulated in Table 6-3.

Due the experiment used several sections of the non-PM optical fibre, it is difficult to determine the values of the angle q (in degree) in these optical fibre sections whether it is same or different in each section. These angle values should be exactly substituted in the simulation model in order to obtain the reasonable results.

This validation step provides a conclusion that the simulation and the experiment have closer values between them. This conclusion is indicated by a small amount of the dissimilarity index. Therefore, it could be concluded that the optical representation in the simulation type IV and V for internal fault is to provide credibility of the developed simulation model.

Table 6-3 Several comparative results for the internal fault in the validation stage

No	Compared Items	Experiment	simulation type IV	simulation type V (q=2º)	simulation type V (q=15º)	simulation type V (q=30º)
1	Frequency of the AC current (Hz)	50 Hz	50 Hz	50 Hz	50 Hz	50 Hz
2	Frequency of the modulation signal (Hz)	100 Hz	100 Hz	100 Hz	100 Hz	100 Hz
3	The dissimilarity index of the simulated optical modulation plot to the experiment plot (using 1601 points)	reference	$4.73x10^{-9}$	$4.73x10^{-9}$	$4.73x10^{-9}$	$4.73x10^{-9}$
4	Average power of the optical modulation (W)	$4.95x10^{-9}$	$6.85x10^{-9}$	$6.57x10^{-9}$	$6.58x10^{-9}$	$6.60x10^{-9}$
5	The dissimilarity index for the average value of optical power modulation	reference	$1.62x10^{-10}$	$1.61x10^{-9}$	$1.62x10^{-9}$	$1.65x10^{-9}$
6	Optical Differential processing time (s)	$4.0x10^{-4}$	reference	reference	reference	reference

6.4.2. Validation of the simulation type IV and V for external fault using the experiment data

Using the same procedure in the previous section, both the experimental results and the simulation type V for the external fault condition are compared to validate the model of the proposed all-optical differential protection configuration. Several comparative results of the laboratory experiment and the simulation type V for the external fault are explained as follows.

Firstly, the experiment results (refer to Figure 6.22) could not provide a piece of clear information regarding a number of the signal modulation frequency, whereas the simulation type V (refer to Figure 6.28) gives a clear appearance of the plot that shows the frequency of the modulation signal being twice the AC current frequency.
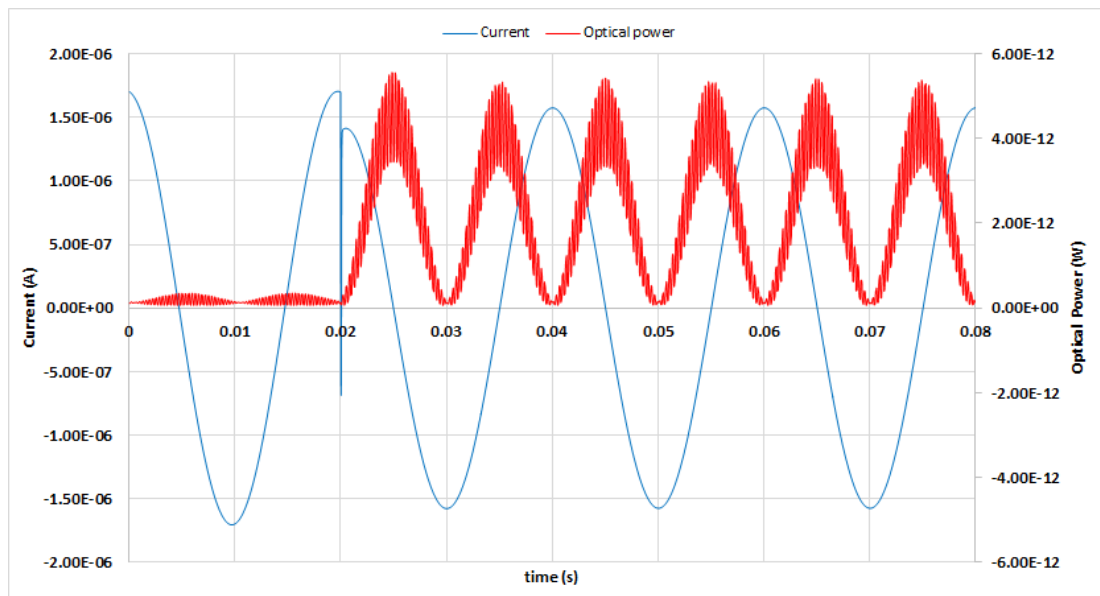
Figure 6.28 The simulation type V for the resistive external fault of 37.2 Ω

Secondly, superimposing both the laboratory experiment and the simulation plots as shown in Figure 6.29 are performed in order to know the similarity shape of the modulation. From this figure, it is difficult to determine that both the laboratory

experiment and the simulation plots have a similar shape of the optical power modulation because the experiment plot show no clear shape.
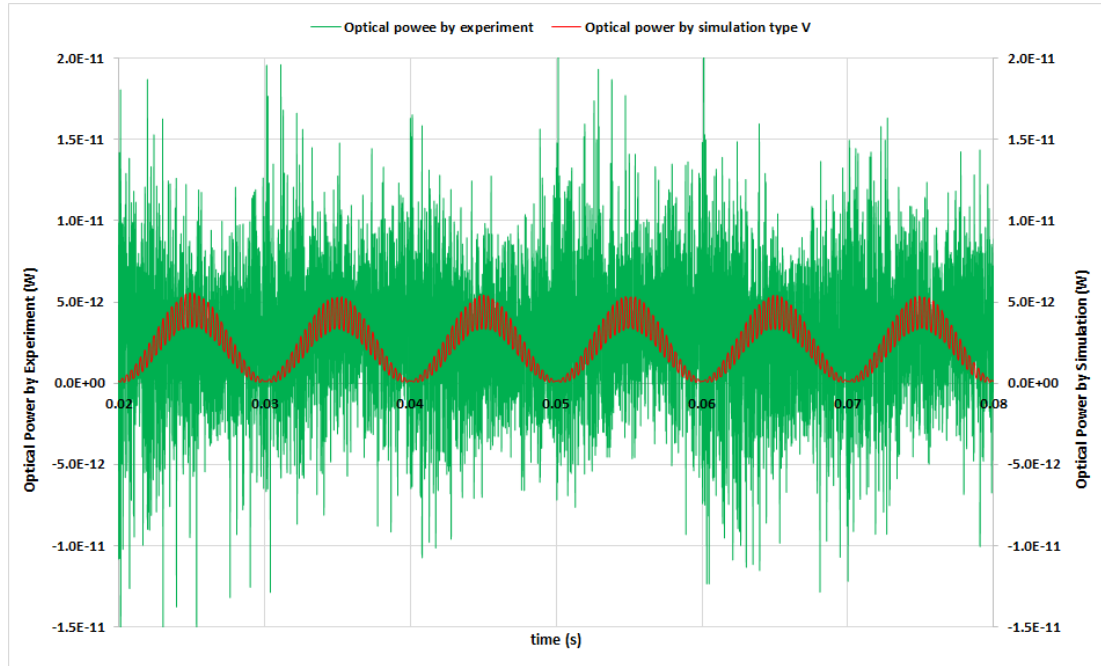
Figure 6.29 Comparison of the signal modulation level between the simulation type V and the laboratory experiment for the external fault.

The dissimilarity index calculation was obtained that value of the optical modulation signals between the simulation and the experiment is $4.60x10^{-12}$. The dissimilarity index for the average value of optical power modulation level between the simulation ($2.26x10^{-12}$ W) and the experiment ($3.13x10^{-12}$ W) is $8.67x10^{-13}$.

Thirdly, the optical power modulation for external fault is different in terms of the maximum and minimum of optical power level as shown in Figure 3.29. However, the average of optical power level is approximately same which the average power level of the laboratory experiment and the simulation type V are $3.13x10^{-12}$ W and $2.26x10^{-12}$ W, respectively. The difference of the average power level is $8.67x10^{-13}$ W which is a very small number. This difference value is reasonable because two main reasons as explained in the internal fault case.

As a summary, comparison results between the experiment and the simulation type IV and V for an external fault are listed in Table 6-4.

It is worth to be mention in Table 6-4 that the average power of optical modulation from the experiment is higher than the average power by simulation. These results indicate the existence of birefringence in the non-PM optical fibre that gives inconsistent result for protection application. These results also support a conclusion that the non-PM optical fibre is not suitable to be implemented as the fibre link between optical devices in the proposed optical differential protection scheme.

Table 6-4 Validation results for the external fault

No	Compared Items	Experiment	simulation type IV	simulation type V (q=2º)	simulation type V (q=15º)	simulation type V (q=30º)
1	Frequency of the AC current (Hz)	50 Hz	50 Hz	50 Hz	50 Hz	50 Hz
2	Frequency of the modulation signal (Hz)	No data	100 Hz	100 Hz	100 Hz	100 Hz
3	The dissimilarity index of the simulated optical modulation plot to the experiment plot (using 1601 points)	reference	$4.60x10^{-12}$	$4.60x10^{-12}$	$4.60x10^{-12}$	$4.88x10^{-12}$
4	Average power of the optical modulation (W)	$3.13x10^{-12}$	$2.27x10^{-12}$	$2.26x10^{-12}$	$1.73x10^{-12}$	$6.64x10^{-13}$
5	The dissimilarity index for the average value of optical power modulation	reference	$8.57x10^{-13}$	$8.67x10^{-13}$	$1.39x10^{-12}$	$2.46x10^{-12}$
6	Optical Differential processing time (s)	No data	reference	reference	reference	reference

6.4.3. Experiment results comparison: the internal versus external

An experimental result comparison between the average optical power level of the modulation signal for both the internal and external faults when the resistive fault of 37.2 Ω involved can be plotted as in Figure 6.30.
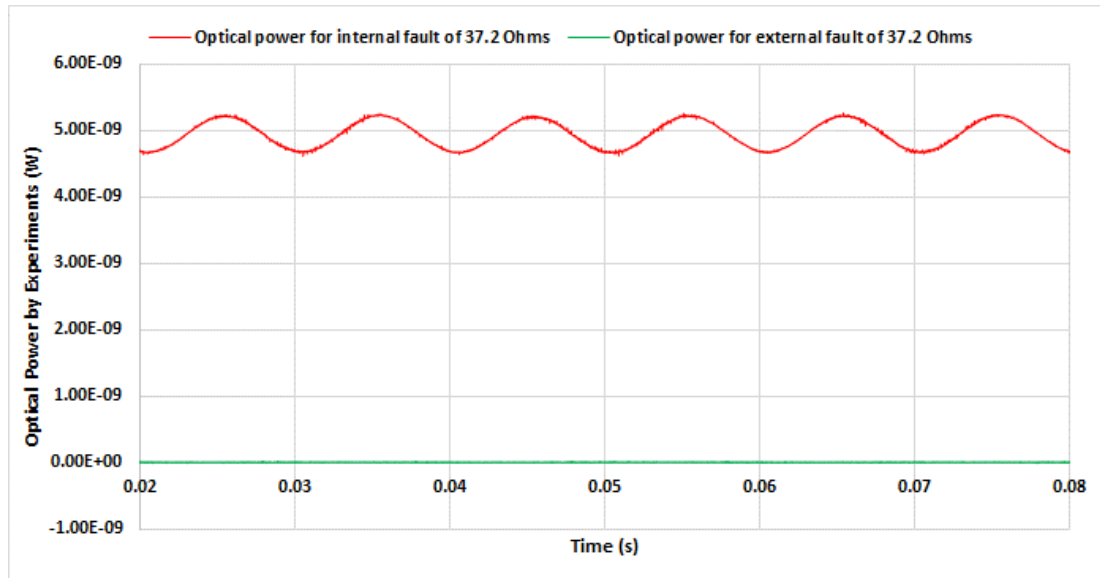
Figure 6.30 Experimental comparison of the optical power level between the internal of 37.2 Ω and external fault of 37.2 Ω

The ratio of the optical power modulation output for the resistive internal fault of 37.2 Ω to the resistive external fault of 37.2 Ω based on the experiment is approximately 1583. This ratio should be no problem with achieving good discrimination of external and internal faults for the protection purposes when the resistive fault is involved.

As a comparison based on simulation, a ratio of the optical power modulation output for the resistive internal fault of 37.2 Ω to the resistive external fault of 37.2 Ω based on the simulation as shown in Figure 6.31 is 2900. This value is approximate twice the experiment data.
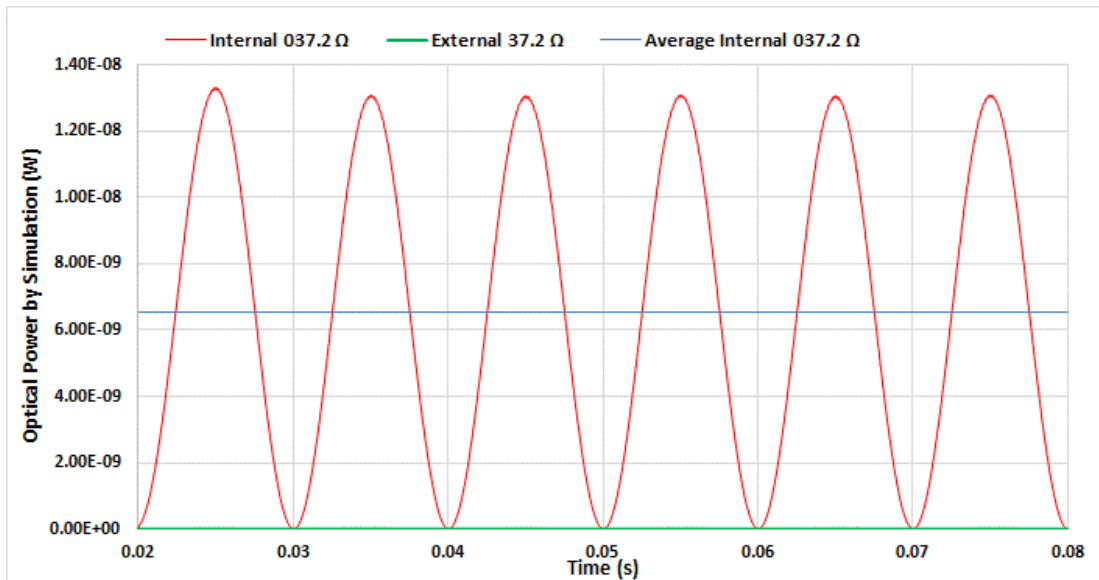
Figure 6.31 Simulation comparison of the optical power level between the internal of 37.2 Ω and external fault of 37.2 Ω

Both Figure 6.30 and Figure 6.31 from the experiment results provide a conclusion that the simulation model of the proposed all-optical configuration of the busbar differential protection scheme is valid. The inference of this conclusion is the models of the optical components such as polariser, optical current sensor (FRCS), optical fibre also are properly represented.

6.5. Conclusion

The experiment of the all-optical differential protection prototype has been conducted. Several vital observations are explained as follows.

The birefringence effect does exist in the optical fibre that used in the experiment. This fact has been supported by two different tests to demonstrate the birefringence effect. Thus, the use of birefringence model in the optical fibre for the simulation is valid.

A number of the optical modulation frequency in the proposed all-optical busbar differential protection scheme between simulations and experiments are the same

which is 100 Hz. This result has been precisely presented by the simulation models in the previous chapter.

The optical power modulations of the experiments data were collected, including the maximum and minimum value. The plot shape of optical modulation between the experiments and the simulation are very similar. This statement is supported by the dissimilarity index of the optical modulation between both plots that have a small index. Moreover, the dissimilarity index for the average value of optical power modulation level between the experiment and the simulation has also a smaller index than the previous index.

The time duration of the optical conversion process for electric currents from an optical domain in the first step process to the digital form in the fifth step process based on the experimental data has been calculated by the indirect approach which is approximate $4.0x10^{-4}$ seconds (0.40 milliseconds). The calculated optical differential processing time when the proposed optical protection scheme utilises the non-PM optical fibre length of 460 meters is approximately 2.36 µs. Thus, the total operation time of the proposed optical differential protection scheme is about 0.402 ms.

The configuration of the proposed optical differential protection scheme that utilises all-optical devices, including a short section of the non-PM optical fibre has been tested in the laboratory. The experiment data have been fitted to simulation data, and the results have confirmed that the simulation models are valid. Consequentially, the arrangement of the optical devices are correctly configured, and the optical device models are correctly represented.

Another benefit of the successful comparison between the experimental data and the simulation data of the proposed all-optical protection configuration is to provide credibility of the developed simulation models.

It is essential to be mentioned that the experimental data have successfully predicted by the simulation models. Therefore, the simulation model could be used to predict the system behaviour with different parameters, to assess performance within and beyond the normal operating conditions, and to enhance the performance of the system.

The experiment shows that the prototype of the proposed all-optical differential protection scheme could perform its primary function as expected. Therefore, it could be physically implemented as a busbar differential protection scheme. However, the use of the non-PM optical fibre as optical transmission links in the proposed configuration could not provide good discrimination due to the birefringence effect. According to the simulation results, as explained in chapter 5, this issue can be resolved by utilising a uniquely designed optical fibre either with the angle q of 45 degrees or using the PM optical fibre.

The optical power modulation levels in the experiments were very low due to the high insertion loss of the second fibre bench, which is 7.7 dB (approximately equivalent to a power ratio of 17 percent). Replacing the second fibre bench with a fixed U-bench according to the simulation could increase the optical power modulation to a significant level from $5.15x10^{-7}$ W to $1.14x10^{-5}$ W for internal faults. This effort could increase the performance of the proposed all-optical differential protection scheme.

6.6. References for Chapter 6

[1] M. Nasir, A. Dysko, P. Niewczas, and G. Fusiek, "All-optical busbar differential protection scheme for electric power systems," in *The 13rd IET International Conference on Development in Power System Protection*, Edinburgh, 2016.

[2] J. S. Arora, "Chapter 1 - Introduction to Design Optimization," in *Introduction to optimum design [internet resource]*, Elsevier, Ed., 3rd ed.. ed. Boston, MA: Boston, MA : Academic Press, 2011.

[3] A. K. Kamrani, *Engineering design and rapid prototyping [internet resource]*. New York, London: Springer, 2010.

[4] A. P. Sage and W. B. Rouse, *Handbook of systems engineering and management*. New York: New York : Wiley, 1999.

[5] E. Leitgeb, T. Plank, M. S. Awan, P. Brandl, W. Popoola, Z. Ghassemlooy, F. Ozek, and M. Wittig, "Analysis and evaluation of optimum wavelengths for

free-space optical transceivers," in *2010 12th International Conference on Transparent Optical Networks*, 2010, pp. 1-7.

[6] N. Grumman. (2012). *TGG (Terbium Gallium Garnet)*. Available: http://www.northropgrumman.com/BusinessVentures/SYNOPTICS/Products/SpecialtyCrystals/Pages/TGG.aspx

[7] M. Gaugitsch and H. Hauser, "Optimization of a magneto-optical light modulator-Part I: modeling of birefringence and Faraday effect," *Journal of Lightwave Technology,* vol. 17, pp. 2633-2644, 1999.

[8] Thorlabs. (2015). *Thorlabs Product*. Available: https://www.thorlabs.de/navigation.cfm

[9] Thorlabs. (2015). *Fiber-to-Fiber U-Benches*. Available: https://www.thorlabs.de/newgrouppage9.cfm?objectgroup_id=3160

[10] Thorlabs. (2015). *Single-Axis Fiber Benches*. Available: https://www.thorlabs.de/newgrouppage9.cfm?objectgroup_id=3092

[11] Thorlabs. (2015). *Optic Mounts & Wall plates*. Available: https://www.thorlabs.de/newgrouppage9.cfm?objectgroup_id=3146

[12] Thorlabs. (2015). *Fixed Collimator Mounting Adapters*. Available: https://www.thorlabs.de/newgrouppage9.cfm?objectgroup_id=219&pn=SM05PT#2533

[13] Thorlabs. (2015). *Rotating Linear Polarizer Modules*. Available: https://www.thorlabs.de/newgrouppage9.cfm?objectgroup_id=3101

[14] Optosci. (2015). *Photoreceivers*. Available: http://www.optosci.com/photoreceivers/

[15] NI. (2015). *NI Product and Support*. Available: http://www.ni.com/en-id/shop.html

[16] NI. (2015). *NI LabVIEW*. Available: http://www.ni.com/en-id/shop/labview.html

[17] R. L. Relay Engineering Service. *APTS3 Protection Relay Test Set*. Available: http://www.reptame.com/files/RES_APTS3.pdf

[18] RES. *APTS3 Protection Relay Test Set*. Available: http://www.invirotech.co.uk/data-sheets/APTS3.PDF

[19]   A.   P.   I.   API.   (2015).   *LNP-2   Data   sheet*.   Available:
        http://www.advancedphotonicsintl.com/specsheets/lnphotoreceiver.pdf

[20]   MITRE. (2017). *Verification and Validation of Simulation Models*. Available:
        https://www.mitre.org/publications/systems-engineering-guide/se-lifecycle-
        building-blocks/other-se-lifecycle-building-blocks-articles/verification-and-
        validation-of-simulation-models

[21]   ABB. (2015). *ABB Busbar Protection Document 611 Series*. Available:
        http://new.abb.com/medium-voltage/distribution-automation/numerical-
        relays/busbar-protection

[22]   Siemens. (2015). *Siemens Centralized Busbar Protection Document
        SIPROTEC   7SS85*.   Available:
        http://w3.siemens.com/smartgrid/global/en/products-systems-
        solutions/Protection/busbar-protection/Pages/7SS85.aspx

[23]   Toshiba. (2015). *Toshiba Busbar Protection Document GRB 200*. Available:
        http://www.toshiba-tds.com/tandd/products/pcsystems/en/grb200.htm

[24]   GE-Alstom. (2015). *GE Busbar Protection Document Multilin B90*. Available:
        https://www.gegridsolutions.com/multilin/catalog/b90.htm

Chapter 7. General conclusions and future work

7.1. Principal results and contributions

The primary objective of this thesis was to design, demonstrate and validate the all-optical differential protection scheme built on the principle analogous to the current differential protection. The design process was carried out in two steps. Firstly, polarimetric optical current sensors were designed to provide the measurement of electric currents. Secondly, a novel configuration of the proposed all-optical differential protection scheme was created by utilising a series arrangement of optical devices. The research work presented in this thesis had resulted in successful modelling, computer simulations, detailed design, physical prototype construction, and laboratory testing of the all-optical busbar protection. The laboratory testing provided additional empirical validation of the proposed optical protection scheme and also demonstrated the practical applicability of the Faraday magneto-optic principle.

On the way to the final result, several outcomes had been obtained by completing a few stages. The first outcome had been achieved by producing the reformulated Jones formalization with considering the optical model and orientation of optical material position, including the polariser's axis orientation. These reformulated Jones formalizations had been used to facilitate the computer-aided simulation programmes.

The second stage was the theoretical evaluation of optical techniques for measuring current and voltage. The second outcome, which was optical sensing techniques, including system requirements and crystal material for the head of the optical current sensor, were defined. A polarimetric optical current sensor which utilises a terbium gallium garnet (TGG) crystal as the sensor head was determined.

Third outcome, the proposed all-optical busbar differential protection scheme incorporating the optical current sensors was developed. New design requirements of the all-optical protection scheme were created, and a configuration of the all-optical

busbar protection scheme was proposed. Then, a theoretical approach to demonstrate the correctness of proposed all-optical busbar protection configuration was written. The results have shown that the configuration correctness has been clarified. Based on the inference method, the first outcome was also correct because the third outcome was built using the first outcome.

Fourth, the main outcome was the optical models and computer simulation results of the proposed all-optical differential protection scheme. Optical devices model using complex function based on Jones Formalization for simulation purposes were represented. Six simulation types and five configurations as the proposed all-optical differential protection scheme utilising two polariser models, a Faraday optical current sensor model and six fibre optic models were developed. Then, translation of the six simulations of optical fibre types and five optical configurations into computer simulation programmes using Matlab® software have also been completed.

Fifth, an initial verification procedure to check the correctness of the simulation programme had been conducted. The results had shown that RSME of fault currents were 10. However, the dissimilarity index of the Faraday rotation θ_1 and θ_2 between Matlab simulation and calculation by spreadsheet application which were very small values had been obtained. These indexes indicate that both values from the simulation and the calculation are very similar. Another verification was optical power modulation. The dissimilarity index of the optical power between the Matlab simulation and the spreadsheet calculation, which was also a small value that means very similar, had been determined.

Moreover, a proving method using simulations had been verified, and the result demonstrated that the configuration is correct. Thus, the statement result, which was the same conclusion as the conclusion of the theoretical proving method had been clearly stated.

Furthermore, the six simulation types and five configurations were conducted in order to assess the performance of the proposed optical protection configuration. The simulation results confirmed that the model and configuration of the proposed all-optical differential protection scheme was valid.

Sixth, the simulation results had confirmed that the configuration 1 to 5 have the same opportunity to be implemented because there is no significant difference in the optical power at the photo receiver. However, the optical configuration 2 had a benefit in term of practical consideration due to the placement of polariser and analyser. In this optical configuration, the polariser and a laser source could be put in a single case and placed at substation's building. The same layout is for the analyser and photo receiver where they are put in the same case and at the same place as well.

Seventh, a complete simulation programme of the proposed optical busbar protection scheme was created to accommodate the change of parameters and variables such as the angle q in the fibre optic model $\boldsymbol{J_{FO5}}$, optical fibre material (refractive index), optical fibre type (a non-polarization or polarization-maintaining fibre), optical fibre length, optical configuration, the number of busbar circuit (optical current sensors), temperature and insertion loss. These simulation results had been documented in chapter 5.

Moreover, the simulations type V (using the non-PM fibre model) and VI (using the PM fibre model) have to be passed into performance evaluation because they are most realistic of optical fibre representation. Results of simulation type V with the optical fibre length of 8 meters give some acceptable results for the resistive internal fault up to 50 Ω. However, over that value, it does not meet the protection requirements because the optical power of the external faults is going to be higher values. This problem could have arisen from the existence of circular birefringence in the optical fibre, which distorts the polarized light that has an amplification effect on the optical power modulation. As a consequence, this problem can cause undesired operation of the optical protection scheme which operates when the solid external fault happens and not operate when the high resistive internal fault occurs. Therefore, the non-PM optical fibre does not suitable to be used as the fibre link in the proposed optical differential protection scheme.

Furthermore, results of simulation type VI had given acceptable results for protection purpose. Surprisingly, the simulation type VI is still able to detect the high resistance internal fault of 250 Ω.

Eighth, the prototype of the all-optical busbar differential protection had been developed, and the laboratory testing of the proposed all-optical busbar protection scheme had also been performed. The optical current sensors were built, and the proposed all-optical busbar protection scheme was configured for laboratory testing. The novel configuration of the all-optical busbar protection scheme was validated by the laboratory testing, and the results confirm that the prototype has generated a good power modulation ratio between internal and external faults. This ratio can be used for achieving good discrimination for the protection purposes when the resistive fault is involved.

The benefits of successful data comparison between the laboratory testing and the simulation of the proposed optical busbar protection configuration is to validate the simulation models. Another benefits are to provide credibility of the developed simulation models because it has successful predict the laboratory testing data with small dissimilarity index. Therefore, the validated simulation model could be applied in the extended use for predicting the system behaviour with different parameters, assessing performance within and beyond the normal operating conditions, assisting the system design and helping to prevent time-wasting.

Ninth, the validated simulation model, as in the seventh outcome confirmed that results of the simulations type V (using the non-PM fibre model) were correct. These results also support the conclusion that the non-PM optical fibre does not suitable to be used as the fibre link for the total length more than 10 meters in the proposed optical differential protection scheme. Moreover, the simulations type VI (using the PM fibre model) had provided acceptable results for protection purpose. Therefore, the use of PM fibre to link optical devices in the proposed configuration of the all-optical busbar differential protection scheme is recommended.

The features of the proposed all-optical busbar differential protection scheme can be summarised as follows:
- Simple configuration.
- Utilise entire optical components for its configuration, i.e. two polarisers, two pieces of terbium gallium garnet as sensor head, eight collimators, and fibre optic cables.

In summary, the main contribution of the work was described in this thesis is the novel configuration of the all-optical busbar protection scheme. The novel configuration is a simple series arrangement of optical components, i.e. polarisers, the Faraday magneto optic-based current sensors, collimators and optical fibre link.

7.2. Future work

The research and development work in this thesis excludes vibration and temperature effect on the novel configuration of all-optical differential protection scheme and their test under adverse environmental conditions such as high temperature, high vibration level, and strong electromagnetic interference. The presented configuration of the all-optical busbar protection scheme, including the optical current sensors, which were developed for the laboratory testing, were only tested at room temperature due to the use of low-temperature fibre optic cable. Moreover, extensive examination for completing the full characterisation of the proposed configuration of the all-optical busbar differential protection scheme should be included in the future work.

According to those statements, the future research and development work of the proposed all-optical busbar protection scheme including the Faraday magneto optic-based current sensors should focus on:

- Vibration and temperature effect and their test under real environment condition.
- Repeating experiments with a different number of coil turns and some variations in material type (PM optical fibre) and length of fibre optic to investigate sensitivity.
- Changing some different position of polariser pairs to obtain optimal power output. Some options of polarisers positions will be selected from section 5.2.2, including some variations of the optical fibre length.
- The increasing number of busbar circuit to be protected and validate with prototype tests
- Optical sensor configuration for installation in the power system busbar should also be considered and completed optical system integration with practical busbar hardware.

Moreover, several laboratory equipment's such as the Thorlabs laser source, the LNP-2 photo-receiver and the NI PXI processing unit for using in the configuration of optical busbar protection scheme were available in the advanced sensor laboratory. However, the equipment was used in this work was not dedicated to the proposed configuration of the all-optical busbar differential protection scheme. Therefore, the optical busbar protection prototype would be beneficial when those components are dedicated as an integrated unit of the optical protection configuration in a single box.

Another area of research and development work should be concentrated on the application of the novel configuration of the all-optical differential protection scheme for a short transmission line protection. The critical element in this configuration is the optical fibre link that should maintain polarisation state of the polarised light which travels inside the optical fibre link. As long as the polarisation states are well maintained in the fibre optic link, the achieved performance of the all-optical differential protection scheme for a short transmission line protection can also be obtained.

Finally, lifetime tests of the protection scheme and the protection scheme behaviour evaluation at high vibration levels and strong electromagnetic interference will complete the full characterisation of the proposed all-optical differential protection scheme.